ISSN: 2153-1196 Volume 9, Number 8, July 2018

Scientific Research Publishing

Journal of Modern Physics

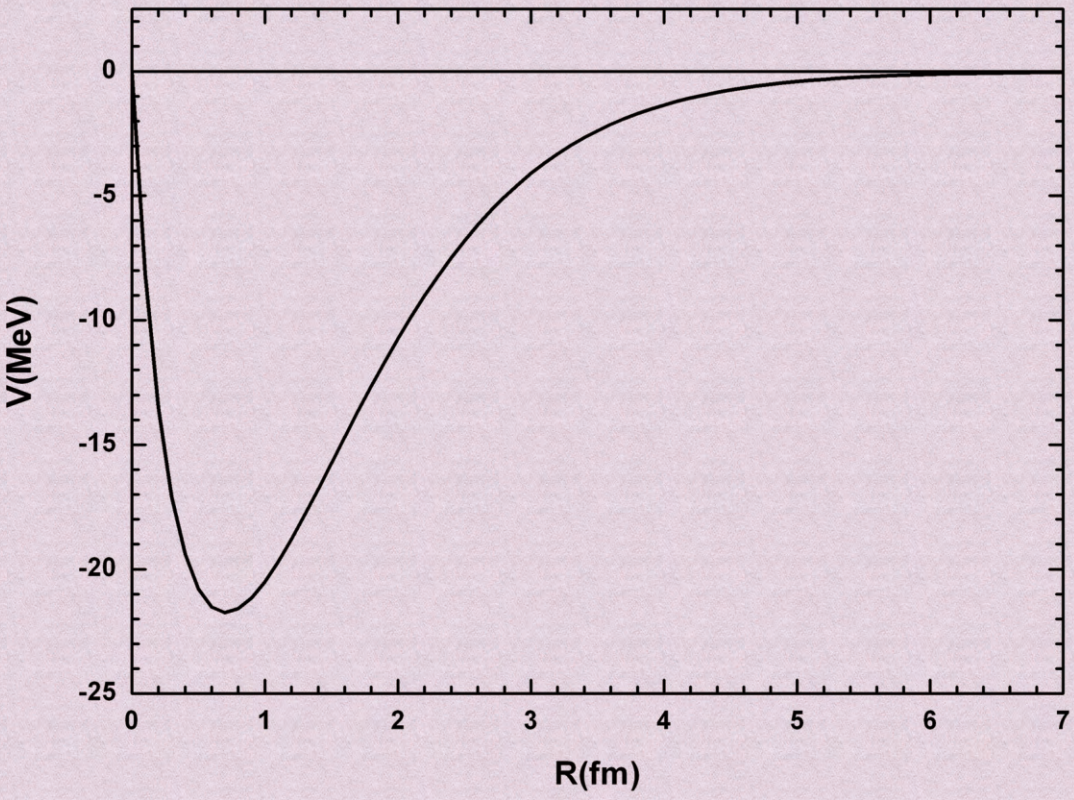

ISSN: 2153-1196
9 772153 119007 08

www.scirp.org/journal/jmp

Journal Editorial Board

ISSN: 2153-1196 (Print) ISSN: 2153-120X (Online)
http://www.scirp.org/journal/jmp

Editor-in-Chief

Prof. Yang-Hui He City University, UK

Executive Editor-in-Chief

Prof. Marko Markov Research International, Buffalo Office, USA

Editorial Board

Prof. Nikolai A. Sobolev Universidade de Aveiro, Portugal
Dr. Mohamed Abu-Shady Menoufia University, Egypt
Dr. Hamid Alemohammad Advanced Test and Automation Inc., Canada
Prof. Emad K. Al-Shakarchi Al-Nahrain University, Iraq
Prof. Tsao Chang Fudan University, China
Prof. Changle Chen University of Science and Technology of China, China
Prof. Stephen Robert Cotanch NC State University, USA
Prof. Peter Chin Wan Fung University of Hong Kong, China
Prof. Ju Gao The University of Hong Kong, China
Prof. Sachin Goyal University of California, USA
Dr. Wei Guo Florida State University, USA
Prof. Cosmin Ilie Los Alamos National Laboratory, USA
Prof. Haikel Jelassi National Center for Nuclear Science and Technology, Tunisia
Prof. Christophe J. Muller University of Provence, France
Prof. Ambarish Nag National Renewable Energy Laboratory, USA
Dr. Rada Novakovic National Research Council, Italy
Prof. Tongfei Qi University of Kentucky, USA
Prof. Mohammad Mehdi Rashidi University of Birmingham, UK
Prof. Alejandro Crespo Sosa Universidad Nacional Autónoma de México, Mexico
Dr. A. L. Roy Vellaisamy City University of Hong Kong, China
Prof. Yuan Wang University of California, Berkeley, USA
Prof. Fan Yang Fermi National Accelerator Laboratory, USA
Prof. Peter H. Yoon University of Maryland, USA
Prof. Meishan Zhao University of Chicago, USA
Prof. Pavel Zhuravlev University of Maryland at College Park, USA

Scientific Research Publishing

Journal of Modern Physics, 2018, 9, 1459-1711
http://www.scirp.org/journal/jmp
ISSN Online: 2153-120X
ISSN Print: 2153-1196

Table of Contents

Volume 9 Number 8 July 2018

Journal of Modern Physics, 2018, 9, 1459-1711
http://www.scirp.org/journal/jmp
ISSN Online: 2153-120X
ISSN Print: 2153-1196

The figure on the front cover is from the article published in Journal of Modern Physics, 2018, Vol. 9, No. 8, pp. 1459-1468 by Nicolae Bogdan Mandache and Dragos Iustin Palade.

Journal of Modern Physics (JMP)
Journal Information

SUBSCRIPTIONS

The *Journal of Modern Physics* (Online at Scientific Research Publishing, www.SciRP.org) is published monthly by Scientific Research Publishing, Inc., USA.

Subscription rates:
Print: $89 per issue.
To subscribe, please contact Journals Subscriptions Department, E-mail: sub@scirp.org

SERVICES

Advertisements
Advertisement Sales Department, E-mail: service@scirp.org

Reprints (minimum quantity 100 copies)
Reprints Co-ordinator, Scientific Research Publishing, Inc., USA.
E-mail: sub@scirp.org

COPYRIGHT

Copyright and reuse rights for the front matter of the journal:
Copyright © 2018 by Scientific Research Publishing Inc.
This work is licensed under the Creative Commons Attribution International License (CC BY).
http://creativecommons.org/licenses/by/4.0/

Copyright for individual papers of the journal:
Copyright © 2018 by author(s) and Scientific Research Publishing Inc.

Reuse rights for individual papers:
Note: At SCIRP authors can choose between CC BY and CC BY-NC. Please consult each paper for its reuse rights.

Disclaimer of liability
Statements and opinions expressed in the articles and communications are those of the individual contributors and not the statements and opinion of Scientific Research Publishing, Inc. We assume no responsibility or liability for any damage or injury to persons or property arising out of the use of any materials, instructions, methods or ideas contained herein. We expressly disclaim any implied warranties of merchantability or fitness for a particular purpose. If expert assistance is required, the services of a competent professional person should be sought.

PRODUCTION INFORMATION

For manuscripts that have been accepted for publication, please contact:
E-mail: jmp@scirp.org

Journal of Modern Physics, 2018, 9, 1459-1468
http://www.scirp.org/journal/jmp
ISSN Online: 2153-120X
ISSN Print: 2153-1196

On the Mechanism of Nucleon-Nucleon Attraction by Pion Exchange

Nicolae Bogdan Mandache, Dragos Iustin Palade

Plasma Physics and Nuclear Fusion Laboratory, National Institute for Laser, Plasma and Radiation Physics, Bucharest-Magurele, Romania
Email: mandache@infim.ro, dragos.palade@inflpr.ro

How to cite this paper: Mandache, N.B. and Palade, D.I. (2018) On the Mechanism of Nucleon-Nucleon Attraction by Pion Exchange. *Journal of Modern Physics*, **9**, 1459-1468.
https://doi.org/10.4236/jmp.2018.98090

Received: June 7, 2018
Accepted: June 28, 2018
Published: July 3, 2018

Copyright © 2018 by authors and Scientific Research Publishing Inc.
This work is licensed under the Creative Commons Attribution International License (CC BY 4.0).
http://creativecommons.org/licenses/by/4.0/
Open Access

Abstract

A formula is derived for the central nucleon-nucleon potential, based on an analysis of the physical origin of the nucleon-nucleon attraction by pion exchange. The decrease of the dynamical mass of the interaction field, exchanged pion in this case, is the principal mechanism responsible for the nuclear attraction in a similar way that the decrease of the kinetic energy of the exchange electron in the diatomic molecule is directly responsible for the covalent molecular attraction. The minimum value of this central nucleon-nucleon potential and the position of the minimum are similar with the values reported in literature for a potential calculated by lattice QCD, which shares the features of the phenomenological nucleon-nucleon potentials. The Schrodinger equation with this central nucleon-nucleon potential was solved numerically for different values of the pion mass. The binding energy increases with the decrease of the pion mass. For masses higher than the real pion mass the nucleon-nucleon system is unbound. We discuss on the two pion exchange and hard core repulsion. The minimum value of the potential for two pion exchange is comparable with the minimum value of the CD Bonn potential. For a hard core radius of 0.5 fm the binding energy is equal to the deuteron binding energy.

Keywords

Pion Exchange, Dynamical Mass, Central Nucleon-Nucleon Potential, Bound State

1. Introduction

The effective degrees of freedom in the nuclear interaction at low energy, in particular in the nuclear bound state, are the nucleons and the pions. The pion ex-

change is the basic mechanism of nucleon-nucleon (NN) attraction at low energy [1]-[6].

As it is well known the current masses of quarks (antiquarks) u (ū) and d (đ) are very small; the nucleon and pion masses are mainly of dynamical origin ("kinetic" energy). The confinement of the quarks into nucleon and pion associate an energy, given by the Heisenberg uncertainty relation, which is just the dynamical mass.

The long range structure of the nucleon is given roughly by the pion [7] [8], which also gives the range of nuclear forces. In particular, the Compton wavelength of the pion $\lambda\!\!\!^{-}_{\pi} = \hbar/m_{\pi}c$, which has a value of 1.41 fm for the charged pion, gives the range r_N of the nucleon extension. The pion in nucleon can be represented by a degree of freedom of current mass $\cong$ 0, localized into a region of radius $r_N = \lambda\!\!\!^{-}_{\pi}$. This localization into the nucleon associates an energy (dynamical mass) $E \cong pc = \hbar c/\lambda\!\!\!^{-}_{\pi} = m_{\pi}c^2$, given by the uncertainty relation, which is just the mass of the pion.

At the formation of a nuclear bound state this dynamical mass decreases, which determines a mass defect and consequently a binding energy for the nucleon-nucleon state [9] [10]. Indeed, when two nucleons approach each other to form a bound state, in particular the deuteron, they put in common their pion degrees of freedom (pion exchange). This is equivalent with a slight de-localization of the pion degree of freedom from a region of radius $r_N \cong \lambda\!\!\!^{-}_{\pi}$ to a region of radius $r_N + \Delta(R) = \lambda\!\!\!^{-}_{\pi} + \Delta(R)$, where $\Delta(R)$ is direct proportional to the distance R between the two bound nucleons and is strongly dependent on the probability of the pion to penetrate the potential barrier between the two nucleons [10]. The dynamical mass gets:

$$E_{\Delta} \cong \frac{\hbar c}{\lambda\!\!\!^{-}_{\pi} + \Delta(R)} \tag{1}$$

and is lower than the initial one (that in the free nucleon). To form a bound state, the decrease of the dynamical mass of the pion degree of freedom:

$$\Delta E = \frac{\hbar c}{\lambda\!\!\!^{-}_{\pi}} - \frac{\hbar c}{\lambda\!\!\!^{-}_{\pi} + \Delta(R)} \tag{2}$$

must be larger than the kinetic energy acquired by the system of two nucleons due to their localization at a distance R each other:

This mechanism of nuclear binding has similarities with the mechanism of molecular binding of diatomic molecules [11]. In fact Heisenberg was the first who presented the attractive force between proton and neutron in analogy to that in the hydrogen molecular ion H_2^+, where the electron is the particle exchanged between the two protons [2].

2. Feynman Approach to the Molecular and Nuclear Exchange Interactions

Let's start with the physical interpretation of the mechanism of H_2^+ ion binding

presented by Feynman in [11].

In the H_2^+ ion, since there are two protons, there is more space where the electron can have a low potential energy than in the case of hydrogen atom. The exchanged electron spreads out lowering its kinetic energy, in accord with uncertainty relation. This kinetic energy decrease is at the origin of the molecular attraction in covalent bond, in particular in the H_2^+ ion [11] [12] [13] [14].

For large distances between the two protons of the H_2^+ ion the electrostatic potential energy of the exchanged electron is nearly zero over most of the space between the protons and the electron moves nearly like a free particle in empty space but with a negative energy [11]:

$$\frac{p^2}{2m_e} = -W_H \tag{3}$$

where W_H is the binding energy (+13.6 eV) of the hydrogen atom. This means that p is an imaginary number:

$$p = i\sqrt{2m_e W_H} \tag{4}$$

The probability amplitude A for a particle of definite energy to get from one place to another a distance R away is proportional to [11]:

$$A \sim \frac{e^{(i/\hbar)pR}}{R} \tag{5}$$

where p is the momentum corresponding to the definite energy. Replacing p one obtains that the amplitude of jumping of electron from one proton to the other, for large separation R between the two protons, will vary as [11]:

$$A \sim \frac{e^{-\left(\sqrt{2m_e W_H}/\hbar\right)R}}{R} = \frac{e^{-R/a_0}}{R} \tag{6}$$

where a_0 is the Bohr radius.

If the particle goes in one direction the amplitude is [11]:

$$A \sim e^{-R/a_0} \tag{7}$$

One can note that this exponential function limits drastically the amplitude of electron exchange for large separation.

The nuclear interaction which takes place between a neutron and a proton by pion exchange is described by Feynman with similar arguments [11]. Since in the nuclear process the proton and the neutron have almost equal masses, the exchanged pion will have zero total energy. But for a pion of mass m_π:

$$E^2 = p^2c^2 + m_\pi^2 c^4 \tag{8}$$

where E and p are the total energy and the momentum of the pion.

Since the exchanged pion have practically zero total energy the momentum is again imaginary [11]:

$$p = im_\pi c \tag{9}$$

This means the amplitude for the pion to jump from one nucleon to another is for large R:

$$A \sim \mathrm{e}^{-(m_\pi c/\hbar)R} = \mathrm{e}^{-R/\lambda\!\!\!^{-}_\pi} \tag{10}$$

The exponential function is typical for a Yukawa potential or exponential potential, and again it limits drastically the exchange for large R.

3. The Central Nucleon-Nucleon Potential Due to Pion Exchange

In fact, the exponential factor is well known from the tunneling of a potential barrier of width R by a particle with an energy much lower than the barrier height. The probability of transmission is the (absolute) square of the amplitude [11], this means in our case:

$$P \sim \mathrm{e}^{-2R/\lambda\!\!\!^{-}_\pi} \tag{11}$$

The increase $\Delta(R)$ of the radius of localization region of the pion degree of freedom, which appears in formulae (1) and (2), is strongly limited by this exponential function (11), *i.e.* the probability for the exchanged pion to penetrate (tunnel) the potential barrier between the two nucleons. From a physical point of view one expects that this probability of transmission is 1 for a barrier width $R \to 0$. Therefore $\Delta(R)$, which is proportional both to the distance R between the nucleons and to the probability of transmission of the exchanged pion, is equal to:

$$\Delta(R) = R\mathrm{e}^{-2R/\lambda\!\!\!^{-}_\pi} \tag{12}$$

By replacing (12) in formula (2), we obtain the decrease of the dynamical mass of the pion degree of freedom, which is at the origin of nuclear attraction. In fact with sign minus this decrease is just the NN potential due to pion exchange [10]:

$$V(R) = -\Delta E = \frac{\hbar c}{\lambda\!\!\!^{-}_\pi + R\mathrm{e}^{-2R/\lambda\!\!\!^{-}_\pi}} - \frac{\hbar c}{\lambda\!\!\!^{-}_\pi} = -\frac{\hbar c}{\lambda\!\!\!^{-}_\pi} * \frac{R\mathrm{e}^{-2R/\lambda\!\!\!^{-}_\pi}}{\lambda\!\!\!^{-}_\pi + R\mathrm{e}^{-2R/\lambda\!\!\!^{-}_\pi}} \tag{13}$$

where $\hbar c/\lambda\!\!\!^{-}_\pi = m_\pi c^2$.

The NN potential $V(R)$ as a function of inter-nucleon distance R is shown in **Figure 1** for a charged pion exchange between the two nucleons $(\lambda\!\!\!^{-}_\pi = 1.41\,\mathrm{fm})$. This potential has some similarities with that obtained by lattice QCD [15] [16], which shares the features of the phenomenological NN potentials: an attractive well at intermediate and larger distances and a hard core repulsion at small range, with the maximum depth of the potential in the intermediate range [1] [2] [3] [4] [5]. The minimum value of the potential (−22 MeV) and the position of the minimum (0.7 fm) in **Figure 1**, are comparable with the values shown in **Figure 3** from [15]: about −25 MeV and 0.7 fm. The fall of the potential towards zero value in **Figure 1** for small R ($R < 0.6$ fm) is compatible with the beginning of the hard core repulsion region [1] [2] [3] [4] [5] [15] which gets dominant at short range.

The potential in **Figure 1** is a little larger, in particular the fall towards higher values of R is slower than in the case of potential obtained in [15]. But the results in [15] were obtained for a pion mass (530 MeV) higher than the real pion mass.

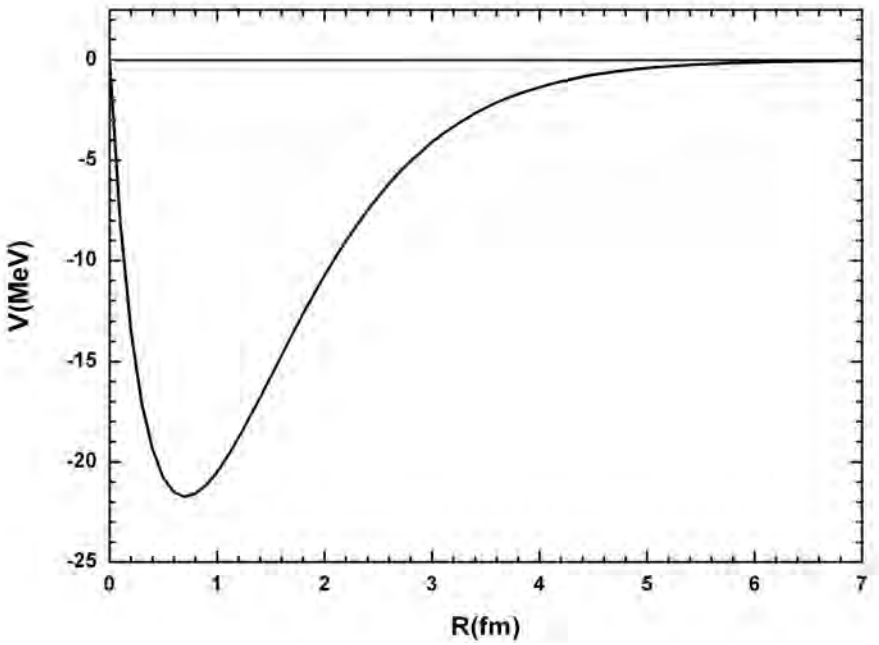

Figure 1. The NN potential in the case of charged pion exchange.

For a lower pion mass (360 MeV) the range of the potential gets wider also [15].

We solved numerically the Schrodinger equation for the potential $V(R)$ given in relation (13), for different values of the pion mass m_π:

$$-\frac{\hbar^2}{2\mu}\Delta\psi(R)+V(R)\psi(R)=E\psi(R) \tag{14}$$

where μ is the reduced mass of the two nucleons.

From a numerical point of view, the Schrodinger equation in central potential has been solved using the substitution: $\psi(R)=\phi(R)/R$ which, in turn, gives a standard Sturm-Liouville eigenvalue problem with a constant coefficient for the second order derivative:

$$-\frac{\hbar^2}{2\mu}\frac{\mathrm{d}^2\phi(R)}{\mathrm{d}R^2}+V(R)\phi(R)=E\phi(R) \tag{15}$$

We look for the ground state, this means zero centrifugal energy ($l=0$).

The spatial dimension has been truncated as $R\in[0,20]\text{fm}$ with a standard discretization in equal intervals of $\Delta R=10^{-3}$ fm. Such large radial extension is needed in order to resolve properly the states lying closely to the continuum ($E<\cong 0$). The eigenvalue problem is solved by means of a finite difference method with the boundary values $\phi(0)=\phi'(0)=0$ and imposing an exponential decay at large radius. The resulting Hamiltonian is diagonalized and the eigenvalues (energy) are obtained.

In **Figure 2** is given the dependence of the total energy of the two nucleons in function of the exchanged pion mass m_π. For the real pion mass corresponds about −0.1 MeV, this means a very small binding energy.

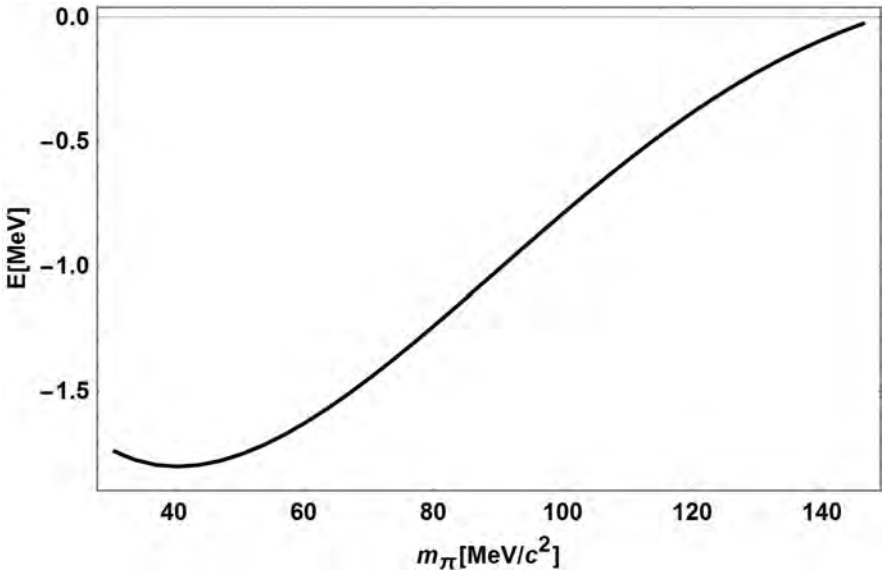

Figure 2. The total energy of the two nucleons as a function of the pion mass m_π.

The total energy of the two nucleons decreases, this means the binding energy increases with the decrease of the pion mass. For masses higher than the real pion mass the total energy gets positive (unbound state). This underline the central role of the pion as main player in the production of nuclear attraction, as largely accepted in literature [1]-[6].

4. The Two Pion Exchange and the Hard Core Repulsion

The maximum molecular attraction is realized in the diatomic molecular bond by exchange of two electrons [11]. This is the case of the hydrogen molecule H_2 in which the two hydrogen atoms put in common (exchange) their electrons.

Similarly, the maximum of NN attraction is given by the exchange of two pions. Each nucleon puts in common (exchanges) a pion degree of freedom with the other nucleon. This means two pion degrees of freedom are slightly de-localized. The NN potential in this case is practically two times the potential given by relation (13). The minimum value of the potential gets −44 MeV, which is comparable with the minimum value (−50 MeV) of the CD Bonn potential [2].

If one adds to this two pion exchange potential $2\ V(R)$, where $V(R)$ is given by relation (13), a hard core repulsion at $r_0 \le 0.6$ fm, a typical value for phenomenological nucleon-nucleon potentials [1] [2] [3] [4] [5], it results the NN potential shown in **Figure 3**.

The Schrodinger equation for this two pion exchange potential $2V(R)$ with hard core repulsion was solved numerically for different values of the hard core radius r_0. In **Figure 4** it is shown the total energy of the two nucleons in function of the hard core radius.

For a value of the hard core repulsion radius equal to 0.5 fm, the binding energy is equal to the deuteron binding energy. For this hard core radius

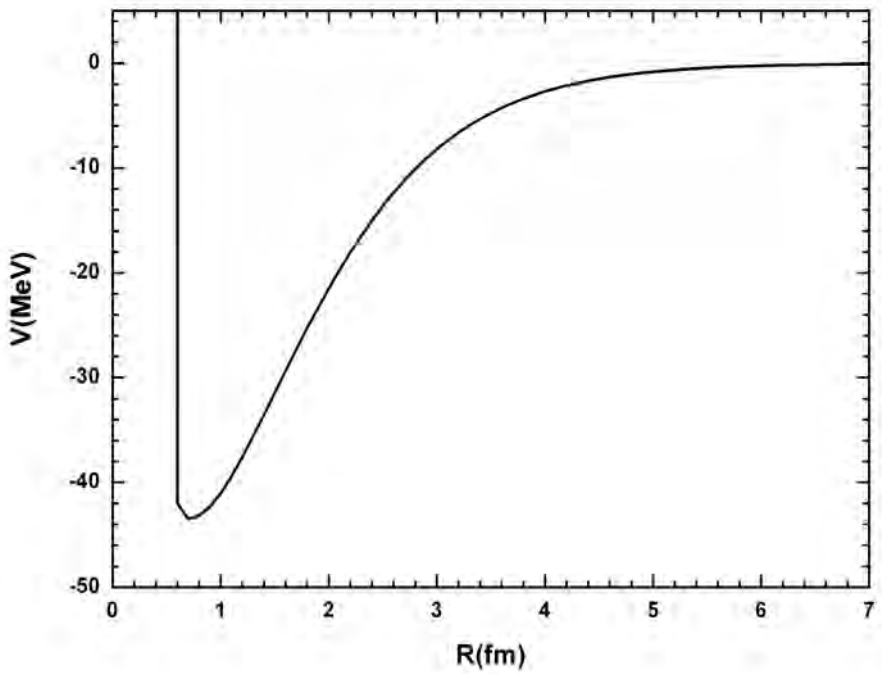

Figure 3. The NN potential in the case of two pion exchange and hard core repulsion at 0.6 fm.

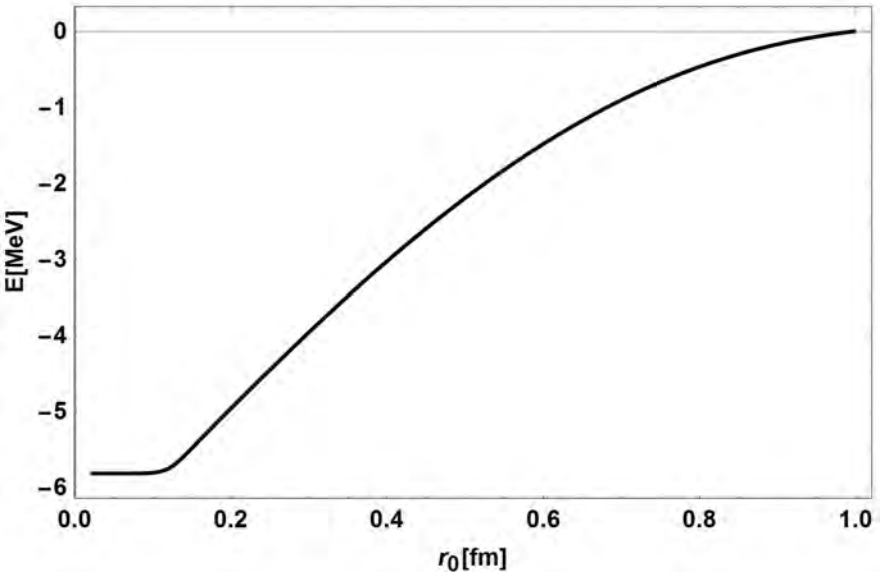

Figure 4. The total energy of the two nucleons as a function of hard core repulsion radius r_0 for the two pion exchange potential.

($r_0 = 0.5$ fm) in **Figure 5** is given the dependence of the total energy of the two nucleons bound by two pion exchange in function of the pion mass m_π.

With pion mass increase, for pion masses higher than about 60 MeV, the total energy increases, *i.e.* the binding energy decreases, and gets zero at about 190 MeV, a result comparable with that obtained in [4] for deuteron binding energy. In [17] the binding energy becomes zero at about 300 MeV.

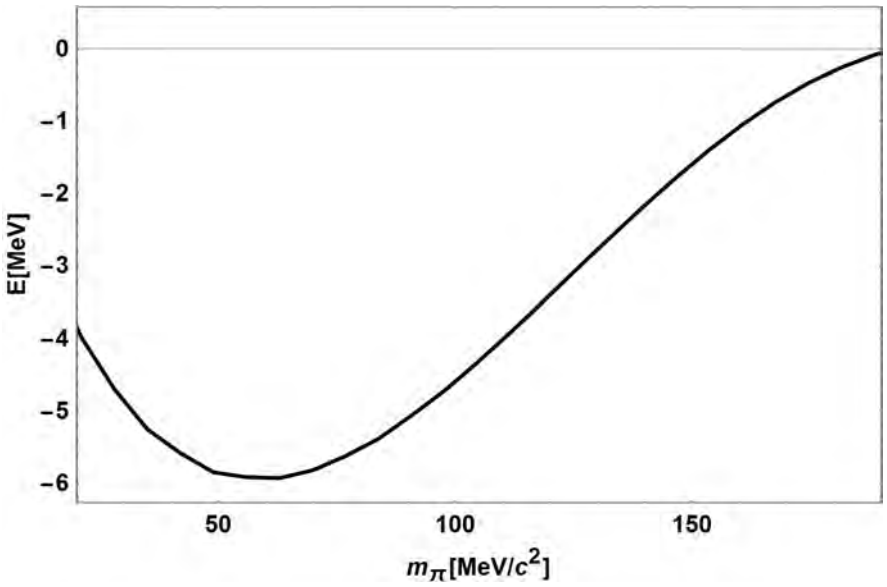

Figure 5. The total energy of the two nucleons as a function of the pion mass m_π, for the two pion exchange potential and a hard core repulsion radius $r_0 = 0.5$ fm.

5. Discussion and Conclusions

The pion exchange is at the origin of the nuclear attraction, in a similar way that the electron exchange is at the origin of attraction in the molecular covalent bond. The decrease of the kinetic energy (in fact dynamical mass decrease from a relativistic point of view) of the exchange electron in the H_2^+ ion, directly responsible for the formation of the molecular bound state, is replaced by the decrease of the dynamical mass of the pion degree of freedom in the case of the nuclear attraction by pion exchange. The slight de-localization of the pion degree of freedom, which is at the origin of this dynamical mass decrease, is drastically limited by an exponential function, which represents the probability for the pion to penetrate the potential barrier between the two nucleons. A similar exponential function exists in the case of molecular bond.

The analytical formula of the central nuclear potential (13) derived for the NN interaction by pion exchange does not contain any unknown parameter. The minimum value of the NN potential and the position of the minimum are similar with the values reported in literature for the central NN potential obtained by lattice QCD, which shares the features of the phenomenological NN potentials. A very small binding energy (0.1 MeV) was obtained by solving numerically the Schrodinger equation. The binding energy increases for pion masses lower than the real pion mass. For masses higher than the real pion mass the nucleon-nucleon system is unbound.

The fall of the potential (13) towards zero value for small R (**Figure 1**) is compatible with the beginning of the well known hard core repulsion region which is dominant at short range. On the other hand the Yukawa potential, derived in analogy with the coulomb attraction (virtual photon exchange), gets infinite attractive for $R \to 0$ due to factor $-1/R$ [1] [2].

Since the maximum value of $R\mathrm{e}^{-2R/\lambda\!\!\!^{-}_{\pi}}$ is 0.26 fm (for $R=\lambda\!\!\!^{-}_{\pi}/2$), this means substantially smaller than $\lambda\!\!\!^{-}_{\pi}=1.41\,\mathrm{fm}$, relation (13) can be written in a good approximation as:

$$V(R)\approx -m_{\pi}c^{2}\frac{R}{\lambda\!\!\!^{-}_{\pi}}\mathrm{e}^{-2R/\lambda\!\!\!^{-}_{\pi}} \tag{16}$$

The NN nuclear potential is proportional to the mass of the interaction field. It is also proportional to the ratio $R/\lambda\!\!\!^{-}_{\pi}$, which is directly related to the slight de-localization of the pion degree of freedom and its (dynamical) mass decrease. This de-localization is drastically limited by the exponential function, which is similar to an exponential potential except the factor 2. Due to this exponential function the width of potential (16) gets larger for pion masses lower than the real pion mass and this explains the increase of the binding energy with the pion mass decrease (**Figure 2**). For too small pion masses this dependence reverses because the depth of potential (16) becomes too low.

In the case of two pion exchange the minimum of the potential gets comparable with the minimum value of the CD Bonn potential. The potential in this case is in a good approximation:

$$V_{2\pi}(R)\approx -2m_{\pi}c^{2}\frac{R}{\lambda\!\!\!^{-}_{\pi}}\mathrm{e}^{-2R/\lambda\!\!\!^{-}_{\pi}} \tag{17}$$

The dependence of the type $x\mathrm{e}^{-x}$ of the nuclear potential, where $x=2R/\lambda\!\!\!^{-}_{\pi}$, is similar with the attractive part of the Rydberg potential used to describe the molecular covalent bonding [18].

A hard core repulsion was added to this two pion exchange potential and the Schrodinger equation was solved numerically for different values of the hard core repulsion radius. For a radius of 0.5 fm the binding energy is equal to the deuteron binding energy.

Let's compare the strength of the nuclear potential $V_{2\pi}(R)$ from relation (17) with the coulombian potential $V_{C}=\frac{q^{2}}{R}$. The ratio of the two potentials for $R=\lambda\!\!\!^{-}_{\pi}$ is:

$$V_{2\pi}(\lambda\!\!\!^{-}_{\pi})/V_{C}(\lambda\!\!\!^{-}_{\pi})=2\frac{\hbar c}{q^{2}}\mathrm{e}^{-2}=2\frac{1}{\alpha}\mathrm{e}^{-2} \tag{18}$$

where α is the e.m coupling constant, a typical result for the relative strength of the nuclear interaction to the e.m. interaction.

If we analyze the mechanism of NN interaction at quark level, we could say that by pion exchange between two nucleons some quark degrees of freedom are implicitly exchanged and in consequence are slightly de-localized. The confinement region of a quark slightly increases and accordingly its dynamical mass decreases. This suggests to interpret the nuclear interaction as a residual strong interaction.

Acknowledgements

We thank E. Dudas and V. V. Baran for helpful discussions and suggestions.

Nicolae Mandache thanks to Sola Florinuta for constant support.

References

[1] Ericson, T. and Weise, W. (1988) Pions and Nuclei. Clarendon Press Oxford.

[2] Machleidt, R. (1989) *Advances in Nuclear Physics*, **19**, 189.

[3] Lacroix, D. (2010) Nuclear Theory Introduction—Strong Interaction in the Nuclear Medium: New Trends. arXiv:1001.5001v1 [nucl-th]

[4] Epelbaum, E., Hammer, H.W. and Meissner, U.-G. (2008) Modern Theory of Nuclear Forces. arXiv:0811.1338v1 [nucl-th]

[5] Machleidt, R. (2013) Origin and Properties of Strong Inter-Nucleon Interactions. arXiv:1308.0103v1 [nucl-th]

[6] Muhin, K.N. *Fizica Nucleara Experimentala* (in Romanian), Editura Tehnica, (*Experimentalnaia Iadernaia Fizika* (in Russian), Atomizdat, Moscow (1974)).

[7] Thomas, A.W., Theberge, S. and Miller, G.A. (1981) *Physical Review D*, **24**, 216. https://doi.org/10.1103/PhysRevD.24.216

[8] Vanderhaeghen, M. and Walcher, T. (2010) Long Range Structure of the Nucleon. arXiv:1008.4225, [hep-ph]

[9] Mandache, N.B. (2012) *Romanian Reports in Physics*, **64**, 1307.

[10] Mandache, N. and Palade, D. (2017) The Physical Origin of the Nucleon-Nucleon Attraction by Pion Exchange. hal-01655838

[11] Feynman, R. Leighton, R. and Sands, M. (1964) Feynman Lectures on Physics, Vol. 3, Quantum Mechanics, Chapters 3, 7 and 10. Addison-Wesley.

[12] Ruedenberg, K. (1962) *Reviews of Modern Physics*, **34**, 326. https://doi.org/10.1103/RevModPhys.34.326

[13] Rioux, F. (1997) *Chemical Educator*, **2**.

[14] Bacskay, G.B. and Nordholm, S. (2013) *The Journal of Physical Chemistry A*, **117**, 33. https://doi.org/10.1021/jp403284g

[15] Ishii, N., Aoki, S. and Hatsuda, T. (2007) *Physical Review Letters*, **99**, 022001. https://doi.org/10.1103/PhysRevLett.99.022001

[16] Aoki, S., Doi, T., Hatsuda, T., Ikeda, Y., Inoue, T., Ishii, N., Murano, K., Nemura, H. and Sasaki, K. (HAL QCD Collaboration) (2012) Lattice QCD Approach to Nuclear Physics. arXiv:1206.5088v [hep-lat].

[17] Iritani, T., Aoki, S., Doi, T., Hatsuda, T., Ikeda, Y., Inoue, T., Ishii, N., Nemura, H., and Sasaki, K. (HAL QCD Collaboration) (2017) *Physical Review D*, **96**, 034521.

[18] Varshni, Y.P. (1957) *Reviews of Modern Physics*, **29**, 664.

Journal of Modern Physics, 2018, 9, 1469-1483
http://www.scirp.org/journal/jmp
ISSN Online: 2153-120X
ISSN Print: 2153-1196

Clues to the Fundamental Nature of Gravity, Dark Energy and Dark Matter

Eugene Terry Tatum[1], U. V. S. Seshavatharam[2]

[1]760 Campbell Ln. Ste. 106 #161, Bowling Green, KY 42104, USA
[2]Honorary Faculty, I-SERVE, Hyderabad, India
Email: ett@twc.com, seshavatharam.uvs@gmail.com

How to cite this paper: Tatum, E.T. and Seshavatharam, U.V.S. (2018) Clues to the Fundamental Nature of Gravity, Dark Energy and Dark Matter. *Journal of Modern Physics*, **9**, 1469-1483.
https://doi.org/10.4236/jmp.2018.98091

Received: May 29, 2018
Accepted: July 9, 2018
Published: July 12, 2018

Copyright © 2018 by authors and Scientific Research Publishing Inc.
This work is licensed under the Creative Commons Attribution International License (CC BY 4.0).
http://creativecommons.org/licenses/by/4.0/
Open Access

Abstract

This paper integrates the Flat Space Cosmology (FSC) model into the Friedmann equations containing a cosmological term. The Lambda Λ term within this model scales according to $3H_t^2/c^2$ and $3/R_t^2$. Use of the Bekenstein-Hawking definition of closed gravitational system total entropy provides for FSC cosmic parameter definitions in terms of $\sqrt{S}$. Cosmic time, radius, total matter mass-energy and vacuum energy in this model scale in exactly the same way as $\sqrt{S}$. This analysis opens the way for understanding gravity, dark energy and dark matter as being deeply connected with cosmic entropy. The recent theoretical work of Roger Penrose and Erik Verlinde is discussed in this context. The results of this FSC model analysis dovetail nicely with Verlinde's work suggesting gravity as being fundamentally an emergent property of cosmic entropy. This emergent-property-of-entropy definition of gravity, if true, would also indicate that gravitational inertia, dark matter and dark energy are simply manifestations of cosmic entropy. Thus, they would likely have no identifiable connection to quantum physics, including the standard particle model.

Keywords

Cosmology Theory, Dark Energy, Dark Matter, Cosmic Entropy, Entropic Arrow of Time, Cosmic Inflation, Black Holes, Cosmological Constant Problem, Emergent Gravity

1. Introduction and Background

Flat Space Cosmology (FSC) is a mathematical model of universal expansion which has proven to be remarkably accurate in comparison to observations [1] [2] [3] [4] [5]. FSC was initially developed as a heuristic mathematical model of

the Hawking-Penrose idea that an expanding universe arising from a singularity state can be modeled as a time-reversed giant black hole. This idea was an extension of Penrose's paper [6] on the singularities of black holes and cosmology. Hawking's doctoral thesis took the idea further by proving the validity of time-reversal in the treatment of general relativity as it concerns cosmology [7]. Finally, the FSC model completes this idea by incorporating scaling black hole equations suitable for cosmology. Thus, the proven accuracy of FSC with respect to current astronomical observations does not appear to be an accident.

FSC has recently been proven to be a general relativity model by successfully integrating the FSC assumptions into the Friedmann equations which include a cosmological term and a global curvature term k set to zero. The relevant equations are repeated in this paper for clarity. One of the results of integrating FSC into the Friedmann equations is that the following relation holds true in FSC:

$$\frac{3H^2c^2}{8\pi G} \cong \frac{\Lambda c^4}{8\pi G} \tag{1}$$

This is merely a reflection that global space-time in FSC is flat during the cosmic expansion. As stipulated by the space-time curvature rules of general relativity, a globally flat universe *must* have a net energy density of zero. Otherwise, if the positive energy density and negative energy density terms were not equal in magnitude, there would be an observable global space-time curvature representative of the greater energy density term.

The purpose of this paper is to show how the FSC Friedmann equations evolve further from Equation (1) and what they might imply with respect to the fundamental nature of gravity, dark energy and dark matter. Before doing so, however, it is useful to review the five current assumptions of FSC and its observational correlations.

1.1. The Five Assumptions of Flat Space Cosmology

1) The cosmic model is an ever-expanding sphere such that the cosmic horizon always translates at speed of light c with respect to its geometric center at all times t. The observer is defined to be at this geometric center at all times t.

2) The cosmic radius R_t and total matter mass M_t follow the Schwarzschild formula $R_t \cong 2GM_t/c^2$ at all times t.

3) The cosmic Hubble parameter is defined to be $H_t \cong c/R_t$ at all times t.

4) Incorporating our cosmological scaling adaptation of Hawking's black hole temperature formula, at any radius R_t, cosmic temperature T_t is inversely proportional to the geometric mean of cosmic total matter mass M_t and the Planck mass M_{pl}. R_{pl} is defined as twice the Planck length (*i.e.*, as the Schwarzschild radius of the Planck mass black hole). With subscript t for any time stage of cosmic evolution and subscript pl for the Planck scale epoch, and incorporating the Schwarzschild relationship between M_t and R_t,

$$\left.\begin{aligned} k_B T_t &\cong \frac{\hbar c^3}{8\pi G\sqrt{M_t M_{pl}}} \cong \frac{\hbar c}{4\pi\sqrt{R_t R_{pl}}} \\ M_t &\cong \left(\frac{\hbar c^3}{8\pi G k_B T_t}\right)^2 \frac{1}{M_{pl}} \qquad (2A) \\ R_t &\cong \frac{1}{R_{pl}}\left(\frac{\hbar c}{4\pi k_B}\right)^2 \left(\frac{1}{T_t}\right)^2 \qquad (2B) \\ R_t T_t^2 &\cong \frac{1}{R_{pl}}\left(\frac{\hbar c}{4\pi k_B}\right)^2 \qquad (2C) \\ H_t &\cong \frac{c}{R_t} \qquad (2D) \end{aligned}\right\} \tag{2}$$

5) Total entropy of the cosmic model follows the Bekenstein-Hawking black hole formula [8] [9]

$$S_t \cong \frac{\pi R_t^2}{L_p^2} \tag{3}$$

As previously reported [Tatum, *et al* (2015)], a number of past and current cosmological parameters can be calculated using the FSC model and are found to be in tight correlation with observations and the Hawking-Penrose theory. The accuracy of these correlations with observations is largely accomplished by incorporating the appropriate cosmological scaling formula for cosmic temperature [see the top equation in relation (2)]. This equation, by incorporating elementary and fundamental constants of nature, allows for FSC scaling from the Planck scale to the current scale. Thus, *FSC can be considered a quantum cosmology model*.

1.2. Cosmological Parameter Derivations of FSC

Incorporation of the FSC assumptions into the cosmological scaling temperature formula allows for the following cosmological parameter definitions. Current observational parameters are calculated in the right-hand column. *The only free parameter in any of these equations is the cosmic temperature*. The currently observed cosmic temperature value: $T_0 = 2.72548$ K.

$$R \cong \frac{\hbar^{3/2} c^{7/2}}{32\pi^2 k_B^2 T^2 G^{1/2}}, \qquad R_0 \cong \frac{\hbar^{3/2} c^{7/2}}{32\pi^2 k_B^2 T_0^2 G^{1/2}} \tag{4}$$

$$H \cong \frac{32\pi^2 k_B^2 T^2 G^{1/2}}{\hbar^{3/2} c^{5/2}}, \qquad H_0 \cong \frac{32\pi^2 k_B^2 T_0^2 G^{1/2}}{\hbar^{3/2} c^{5/2}} \tag{5}$$

$$t \cong \frac{\hbar^{3/2} c^{5/2}}{32\pi^2 k_B^2 T^2 G^{1/2}}, \qquad t_0 \cong \frac{\hbar^{3/2} c^{5/2}}{32\pi^2 k_B^2 T_0^2 G^{1/2}} \tag{6}$$

$$M \cong \frac{\hbar^{3/2} c^{11/2}}{64\pi^2 k_B^2 T^2 G^{3/2}}, \qquad M_0 \cong \frac{\hbar^{3/2} c^{11/2}}{64\pi^2 k_B^2 T_0^2 G^{3/2}} \tag{7}$$

$$Mc^2 \cong \frac{\hbar^{3/2} c^{15/2}}{64\pi^2 k_B^2 T^2 G^{3/2}}, \qquad M_0 c^2 \cong \frac{\hbar^{3/2} c^{15/2}}{64\pi^2 k_B^2 T_0^2 G^{3/2}} \tag{8}$$

$$H_0 = 2.167862848658891\times10^{-18}\ \mathrm{s}^{-1}\left(66.89325791854758\ \mathrm{km}\cdot\mathrm{s}^{-1}\cdot\mathrm{Mpc}^{-1}\right)$$

This derived current Hubble parameter value fits very closely with the low end range of the 2015 Planck Collaboration consensus observational value of 67.8 +/− 0.9 $\mathrm{km}\cdot\mathrm{s}^{-1}\cdot\mathrm{Mpc}^{-1}$

$$t_0 \cong \frac{1}{H_0} = 4.612837941379141\times10^{17}\ \mathrm{s}\left(14.61694683819266\times10^{9}\ \text{sidereal yrs}\right)$$

(multiplying by 1 sidereal yr/3.155814954 × 10^7 s)

$$R_0 \cong \frac{c}{H_0} = 1.382894024801713\times10^{26}\ \mathrm{m}\left(14.61720137583068\times10^{9}\ \text{light-yrs}\right)$$

(multiplying by 1 Julian light-yr/9.4607304725808 × 10^{15} m)

This current cosmic radius value correlates with current cosmic time by $R_o = ct_o$. For reasons given in the seminal FSC papers, a perpetually flat and finite space-time cosmology model has no need to incorporate a superluminal inflationary mechanism to solve the flatness and horizon problems.

$$Vol_0 = \frac{4\pi}{3}\left(\frac{c}{H_0}\right)^3 = 1.107784564915062\times10^{79}\ \mathrm{m}^3$$

$$M_0 = \frac{c^3}{2GH_0} = 9.311265291518025\times10^{52}\ \mathrm{kg}$$

This total matter mass number can be compared very favorably to a rough estimate made from astronomical observations. The visible matter consists of roughly 100 billion galaxies averaging roughly 100 billion stars each, of average star mass equal to roughly 1.4 × 10^{30} kg (70 percent of solar mass), totaling to roughly 1.4 × 10^{52} kg. The 2015 Planck Collaboration report indicates a universal matter ratio of approximately 5.47 parts dark matter to 1 part visible (baryonic) matter. This brings the total estimated matter in the observable universe to approximately 9.1 × 10^{52} kg. A recent study [10] of average mass density of intergalactic dust gives a value of approximately 10^{-30} $\mathrm{kg}\cdot\mathrm{m}^{-3}$. Since this is approximately 1 part intergalactic dust to 1000 parts galactic and perigalactic matter, intergalactic dust does not appreciably modify the total observational estimated mass of matter given above. Accordingly, this observational estimate is remarkably close to the above FSC theoretical calculation of total cosmic matter mass. By the FSC Friedmann equations (below), the positive total matter mass-energy must always be equal in absolute magnitude to the negative dark energy. This predicts a 50/50 cosmic energy density percentage ratio as opposed to the approximately 30/70 ratio currently claimed by standard cosmology proponents. However, without unequivocally *proving* cosmic acceleration, standard cosmology cannot yet rightfully claim this 30/70 ratio. This has been discussed in numerous recent analyses of the Supernova Cosmology Project compilation data [11] [12] [13] [14] and in a recent FSC paper [15].

$$M_0c^2 = \frac{c^5}{2GH_0} = 8.368547901344209\times10^{69}\ \mathrm{J}$$

$$\rho_0 = \frac{3H_0^2}{8\pi G} = 8.405303329200976\times 10^{-27}\ \text{kg}\cdot\text{m}^{-3}\left(\text{critical mass density}\right)$$

This closely approximates the observational critical density.

$$\rho_0 c^2 = \frac{3H_0^2 c^2}{8\pi G} = 7.554309895973191\times 10^{-10}\ \text{J}\cdot\text{m}^{-3}$$

This closely approximates the observational critical energy density and the observational vacuum energy density. They are equal in absolute magnitude in FSC.

2. Flat Space Cosmology Friedmann Equations

With respect to the Friedmann equations, those incorporating a non-zero cosmological term (*i.e.*, a dark energy term) are now the most relevant since the 1998 Type Ia supernovae discoveries. Therefore, accepting Friedmann's starting assumptions of homogeneity, isotropism and an expanding cosmic system with a stress-energy tensor of a perfect fluid, we have his cosmological equation

$$\frac{\dot{a}^2 + kc^2}{a^2} \cong \frac{8\pi G\rho + \Lambda c^2}{3} \tag{9}$$

This equation is derived from the 00 component of the Einstein field equations. Since the global curvature term k is always zero in FSC, Equation (9) reduces to

$$\left(\frac{\dot{a}}{a}\right)^2 \cong H^2 \cong \frac{8\pi G\rho}{3} + \frac{\Lambda c^2}{3} \tag{10}$$

With rearrangement, we have

$$\frac{3H^2}{8\pi G} - \frac{\Lambda c^2}{8\pi G} \cong \rho \tag{11}$$

This is the relevant Friedmann equation for cosmic mass density. Multiplying all terms by c^2 gives us the relevant Friedmann equation for cosmic energy density

$$\frac{3H^2 c^2}{8\pi G} - \frac{\Lambda c^4}{8\pi G} \cong \rho c^2 \tag{12}$$

At this point it is crucial to remember that Friedmann's energy density derivation of Einstein's field equations for the cosmic system as a whole (*i.e.*, globally) can be interpreted in the form of additive space-time curvatures represented by the individual terms. The first term can be read as the positive energy density (*i.e.*, the positive space-time curvature) term; the second term can be read as the negative energy density (*i.e.*, the negative space-time curvature) term; and the third term can be read as the summation (*i.e.*, *net*) energy density term for global cosmic space-time curvature. Since global space-time is treated as constantly and perfectly flat in FSC, the third term must always have a net value of zero energy density. This is entirely in keeping with the general theory of relativity, as applied to cosmology, as well as current cosmological observations of flatness (*i.e.*,

critical density). Hence, in FSC

$$\frac{3H^2}{8\pi G} \cong \frac{\Lambda c^2}{8\pi G} \tag{13}$$

And

$$\frac{3H^2c^2}{8\pi G} \cong \frac{\Lambda c^4}{8\pi G} \tag{14}$$

From these respective critical mass density and energy density equations, it is obvious that the FSC model defines the Lambda term Λ by

$$\Lambda \cong \frac{3H^2}{c^2} \tag{15}$$

In FSC and other realistic linear Milne-type models, Hubble parameter H is a quantity which scales with cosmic time and is defined as

$$H \cong \frac{c}{R} \tag{16}$$

where c is the speed of light and R is the cosmic radius as defined by the Schwarzschild formula

$$R \cong \frac{2GM}{c^2} \tag{17}$$

where M represents the total matter mass of the cosmic system and G is the universal gravitational constant. Therefore, FSC Equation (15) substituted by equation (16) gives

$$\Lambda \cong \frac{3}{R^2} \tag{18}$$

So the Lambda term Λ is also a scalar quantity (*i.e.*, like the Hubble parameter, not actually a constant) over the great span of cosmic time. This indicates that *FSC is a dynamic dark energy quintessence model*.

Crucially, Equation (18) allows one to compare the Lambda term Λ with total entropy for the FSC cosmic system over the span of cosmic time. Recalling the Bekenstein-Hawking derivation of black hole entropy [Bekenstein (1974); Hawking (1976)] as directly proportional to the event horizon surface area $\left(4\pi R^2\right)$, we can apply their formula for cosmic entropy

$$S_t \cong \frac{\pi R_t^2}{L_p^2} \tag{19}$$

Then substituting Equation (18) into Equation (19) and rearranging terms

$$\Lambda \cong \frac{3\pi}{SL_p^2} \tag{20}$$

Thus, the Lambda term Λ in FSC is inversely proportional to total cosmic entropy S at all times. Substituting Equation (20) into Equation (15) gives

$$S \cong \frac{\pi c^2}{H^2 L_p^2} \tag{21}$$

and

$$H \cong \frac{c}{L_p}\sqrt{\frac{\pi}{S}} \tag{22}$$

And, since the reciprocal of the Hubble parameter is the measure of cosmic time t in FSC

$$t \cong \frac{L_p}{c}\sqrt{\frac{S}{\pi}} \tag{23}$$

So cosmic time is always directly proportional to $\sqrt{S}$, with entropy S as defined by Bekenstein and Hawking. Thus, the "entropic arrow of time" is clearly defined in the FSC model.

The dark energy density cosmological term is not only expressed as $\left(\Lambda c^4/8\pi G\right)$ in FSC Friedmann Equation (14) but, by incorporating equation (20) into this term, we now have a dark energy density equation

$$\frac{\Lambda c^4}{8\pi G} \cong \frac{3c^4}{8GSL_p^2} \cong \frac{3H^2c^2}{8\pi G} \tag{24}$$

where in any of these terms can be used interchangeably to quantify the absolute magnitude of the cosmic dark energy density at all times.

Given the above relations, simple algebraic rearrangements allow for expressions of the following FSC parameters in terms of $\sqrt{S}$

$$\sqrt{S} = \frac{c\sqrt{\pi}}{L_p}t \tag{25}$$

Showing direct proportionality between cosmic entropy and cosmic time *t*.

$$\sqrt{S} = \frac{\sqrt{\pi}}{L_p}R \tag{26}$$

Showing direct proportionality between cosmic entropy and cosmic radius *R*.

$$\sqrt{S} = \frac{2G\sqrt{\pi}}{c^2L_p}M \tag{27}$$

Showing direct proportionality between cosmic entropy and total cosmic matter mass *M*.

$$\sqrt{S} = \frac{\hbar c^5}{32\pi^{\frac{3}{2}}k_B^2G}T_U^{-1} = \frac{\hbar c^5}{32\pi^{\frac{3}{2}}k_B^2G}T^{-2} \tag{28}$$

Showing indirect proportionality between cosmic entropy and cosmic temperatures T_U and T.

$$\sqrt{S} = \frac{c\sqrt{\pi}}{L_p}H^{-1} \tag{29}$$

Showing indirect proportionality between cosmic entropy and Hubble parameter *H*.

$$\sqrt{S} = \frac{\sqrt{3\pi}}{L_p} \Lambda^{-\frac{1}{2}} \tag{30}$$

Showing indirect proportionality between cosmic entropy and cosmic Lambda.

$$\sqrt{S} = \frac{2G\sqrt{\pi}}{c^4 L_p} Mc^2 \tag{31A}$$

$$\sqrt{S} = \frac{2G\sqrt{\pi}}{c^4 L_p} (V \cdot E) \tag{31B}$$

Showing direct proportionality between cosmic entropy and total cosmic matter mass-energy and negative vacuum energy.

$$\frac{M}{R} = \frac{c^2}{2G} \tag{32}$$

Showing the Schwarzschild relation between total cosmic matter mass M and radius R.

$$\frac{GM^2}{R^2} = \frac{c^4}{4G} \tag{33}$$

Showing an FSC Newtonian gravitational force relation based upon the Schwarzschild relation.

$$Mc^2 = \frac{c^4}{2G} R \tag{34A}$$

$$|V \cdot E| = \frac{c^4}{2G} R \tag{34B}$$

Showing FSC energy definitions of total cosmic matter mass-energy and vacuum energy.

$$\frac{Mc^2}{2} = \frac{GM^2}{R^2} R \tag{35A}$$

$$\frac{|V \cdot E|}{2} = \frac{GM^2}{R^2} R \tag{35B}$$

Showing FSC matter mass-energy and vacuum energy relations with FSC Newtonian gravitational work (incorporating $E = Mc^2$, of course).

$$\frac{Mc^2}{2} + \frac{V \cdot E}{2} = \left(\frac{GM^2}{R^2}\right) R - \left(\frac{GM^2}{R^2}\right) R = 0 \tag{36}$$

Showing how conservation of energy works in the expanding FSC closed energy system. Such a spatially flat cosmic system, if it *begins* with net zero energy, must *always be* at net zero energy.

3. Discussion

Incorporation of the FSC assumptions into the Friedmann equations containing a cosmological term provides unique insights into the possible nature of gravity,

dark energy and dark matter. The cosmological term is usually expressed in the form of a negative energy density in counterbalance to the positive energy density of total matter (baryonic plus dark matter). Given the recent discovery of dark energy [16] [17] [18], and in the context of general relativity, dark energy is believed to represent a *systemic* negative gravitational energy within the cosmological vacuum. It seems reasonable to assume that dark energy and the negative vacuum energy represented by Friedmann's cosmological term are one and the same. The important question concerns whether dark energy is a completely new physical entity or one which we already know by another name.

Gravitational energy within the vacuum of a closed gravitating system has long been known to be a negative energy. For an excellent discusson as to why gravitational energy, in the form of potential energy, must be a negative energy in comparison to matter energy, the interested reader is referred to pages 11 - 14 and 289 - 293 in Alan Guth's excellent book entitled, "The Inflationary Universe" [19]. Gravitational systems perform work on mass bodies when aggregating them. Thus, by $E = mc^2$, all aggregating bodies acquire additional increments of mass corresponding to their newly-acquired energy. By convention, this is regarded as a gain in the positive energy of matter. However, the generalized vacuum part of any such closed system must gain an equal amount of negative energy during all such gravitational interactions, in order to obey the Law of Conservation of Energy. No net energy can be gained or lost by a gravitating closed system, whether it is expanding, contracting or fixed in radius. Thus, increasingly negative gravitational energy of the vacuum becomes a strong candidate for dark energy.

In this context, it is easy to understand the meaning of FSC mass density and energy density Equations (13) and (14), respectively. Equality between these total matter and vacuum energy terms is *mandatory* in a closed system such as FSC. And, because these terms are of opposite signs with respect to their energy densities, *the net global energy density of a spatially flat closed gravitating system must be perpetually zero from inception*. The FSC assumptions, by virtue of the Schwarzschild formula relationship between total matter mass M_t and radius R_t, and by virtue of the Hubble parameter definition as c/R_p, create a flat universe perpetually at the Friedmann critical energy density of $\left(3H^2c^2/8\pi G\right)$. By incorporating the Schwarzschild relation [Equation (32)] into total matter and vacuum energy Equations (34A) and (34B), one can readily see how Newtonian gravitational work (now slightly modified by incorporating $E = mc^2$, of course) can be expressed in Equations (35A) and (35B). Incorporating the correct negative energy signage of vacuum energy (*i.e.*, dark energy) into Equation (36) shows how a closed net zero energy (*i.e.*, flat) gravitating universe could evolve from a net zero energy quantum fluctuation event.

In sharp contrast to FSC, standard inflationary cosmology has an entirely different explanation for cosmological flatness in universal observations going all the way back to the *very* early universe [the Cosmic Microwave Background (CMB) radiation was released *before* 3 one-hundred-thousandths (0.0000277) of

the current age of the universe]. Standard cosmology maintains that a quantum fluctuation event within a zero energy pre-Big Bang state kicked off the universal expansion. It also maintains that gravity was the first of four fundamental forces to "freeze out" following an exceedingly brief exponential inflationary phase. Standard model cosmologists believe our current universe to contain an extremely small *net* negative energy. In other words, they believe in cosmic acceleration (as opposed to constant velocity light speed expansion), despite these current observations of extreme flatness. However, *if our universe began from a zero energy state and now has a non-zero energy density, however small, this would appear to violate conservation of energy*! Furthermore, one must ask what kind of force drove the inflationary ("inflaton") field if gravity did not already exist at the inception of the universe. Cosmic inflation energy appears to be suspiciously like early cosmic dark energy, which *must* be negative gravitational energy in nature. The Big Bang theory is derived from general relativity, which is *entirely* a gravity theory. To require that a gravity theory incorporate a pre-gravity phase within its cosmology, however brief in duration, sounds very much like nonsense. Moreover, cosmic inflation is an ad hoc theory "…contrived with the goal of arranging for the density perturbations to come out right" [Guth (1997), page 238]. Cosmic inflation, in its many different ad hoc forms, appears to be a deeply flawed theory, as nicely elaborated by one of its founders [20].

The purpose of this paper, however, is not to explain why the FSC model, now integrated into the flat universe Friedmann equations with a cosmological term, rigorously follows observations of cosmic flatness within the CMB. This point has been made in previous FSC publications [Tatum (2015)]. Rather, it is the purpose of this paper to further explore the possible nature of gravity, dark energy and dark matter. While the FSC model clearly indicates that dark energy is systemic negative gravitational energy, the key question becomes "How does this finite constant velocity expanding cosmic system work at its most fundamental level? Specifically, *what is the fundamental nature of its gravity, especially in relation to dark energy and dark matter*?"

Possible clues to the fundamental nature of gravity and dark energy are provided in the new FSC Friedmann equations incorporating a cosmic entropy term. In Equation (18) Lambda term Λ is always inversely proportional to the square of the cosmic radius. Thus, Lambda scales approximately 121.26 base 10 orders of magnitude from the Planck scale. Interestingly, 10^{121} is the magnitude of the "cosmological constant problem" [21] [22]. Furthermore, Equation (18) is seen (in rearranged form) on page 277 of Roger Penrose's latest book [23], if one assumes the standard $4\pi R^2$ formula for the cosmic horizon surface area A_{cosm}. Notably, this equation occurs in Penrose's discussion of cosmic entropy, which assumes the Bekenstein-Hawking definition of cosmic entropy [see FSC Equation (19)]. So, while Lambda in general relativity is assumed to be a constant by proponents of standard cosmology, the FSC model and Penrose clearly indicate Lambda to be a declining scalar of negative energy density in an expanding

closed general relativity model. Lambda is clearly an inverse scalar of cosmic entropy, as best seen in FSC Equation (20). However, most importantly, as seen by integrating Equation (26) into (34B), *total vacuum energy scales in direct proportion to total cosmic entropy*, specifically in the form of $\sqrt{S}$. One must keep in mind that the Bekenstein-Hawking definition of cosmic entropy is a unit-less ratio, so $\sqrt{S}$ is also a measure of cosmic entropy, but on a scale identical to that of the other scaling FSC parameters. **Figure 1** and **Figure 2** below graphically show the intimate relationship between scaling FSC parameters and total cosmic entropy term $\sqrt{S}$. *It is entirely appropriate to use* $\sqrt{S}$ *as a cosmological clock because Equation* (25) *clearly demonstrates that FSC models the "entropic arrow of time."* Notice also that the recently-introduced FSC "Universal Temperature" T_u [24] inversely scales to the same degree as $\sqrt{S}$ (60.63 logs of 10 from the Planck scale). T_u has a direct one-to-one correspondence to the T Kelvin temperature scale by the Universal Temperature definition, $T_u = T^2$.

This idea that total cosmic entropy can be regarded as a cosmological clock is not entirely new, although the FSC model clearly indicates the similarly scaling entropy clock to be in the form of $\sqrt{S}$. Furthermore, the FSC Friedmann entropy equations introduced in this paper clearly point to cosmic entropy being fundamental to the nature of gravity. Penrose introduces the concept of gravitational entropy to readers on page 256 of his book. Gravitational entropy differs significantly from the entropy of an equilibrated ideal gas, wherein maximum average particle separation at a given temperature characterizes the maximum entropy state. In contrast, *in a gravitating universe*, *the ongoing clustering of stars and galaxies*, *and particularly black holes*, *is in the direction of greater gravitational entropy!* This is made abundantly clear by comparing deep space observational astronomy with observations of (approximately) co-moving galaxies. Supermassive black holes, in particular, are now thought to be huge repositories of total cosmic entropy.

A review of the possible fundamental nature of gravity with respect to cosmic entropy should begin with a landmark paper by Erik Verlinde [25]. In this paper, Verlinde makes a very persuasive argument that *cosmic entropy manifests itself as gravity*! He shows in great detail, by a heuristic approach, how *gravity could well be an emergent property of cosmic entropy. In other words*, *at the quantum level*, *our conventional conception of gravity as a fundamental force might be just as meaningless as a conception of consciousness within two connecting neurons*. Emergent properties are most evident in complex systems with high degrees of freedom. They are difficult, if not impossible, to observe at the smallest scales. This could very well nullify the assumption of string theorists that gravity should ultimately be definable *fundamentally* at the quantum scale. This does not bode well for a "quantum gravity" theory to be any different from FSC "quantum cosmology" as first presented in 2015 and now presented in its final form in the present paper.

If Verlinde's compelling emergent property argument ultimately prevails, gravitational inertia (including that of dark matter!) and dark energy would also be

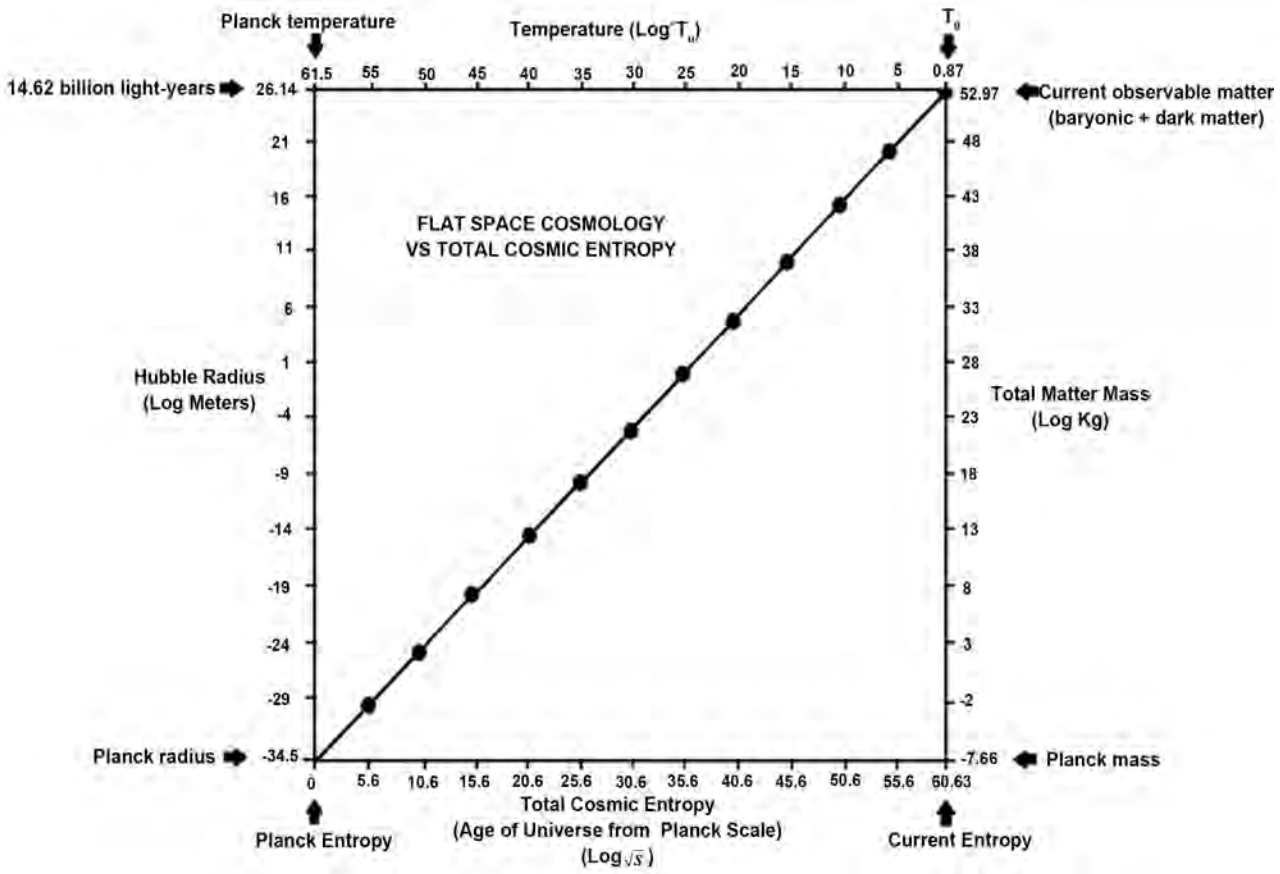

Figure 1. Universal Temperature T_u, Radius and Total Matter Mass vs. Entropy.

emergent properties of cosmic entropy. *The total matter mass attributable to gravitational entropy, by equations* (27) *and* (31A), *must include dark matter. This may well explain why dark matter does not integrate into the standard particle model. The majority of the dark matter yet to be discovered may not, in fact, be particulate, but rather the previously unaccounted for entropic gravitational inertia of visible matter.*

Verlinde's heuristic approach to a fundamental understanding of gravity as an emergent property of cosmic entropy dovetails nicely with this updated FSC cosmology model. FSC also began as a heuristic model, as did Einstein's (and Planck's) photon. Importantly, neither approach relies in any way on a *curved* (*i.e.*, non-flat) geometrical description of gravity. Although general relativity's curved space-time is a supremely accurate and beautiful *geometrical description* of gravity, it is not *fundamental* to the nature of gravity. W.S. Krogdahl, for instance, achieved a similarly accurate mathematical model of gravity and cosmology in flat space-time by starting his development with the integration of $E = mc^2$ into Newtonian gravity [26] [27] [28]. Krogdahl's approach appears to be vindicated by Equations (33) thru (36) in the present paper. These equations also give meaning to Newton's discovery that the force of gravity is inversely proportional to R^2!

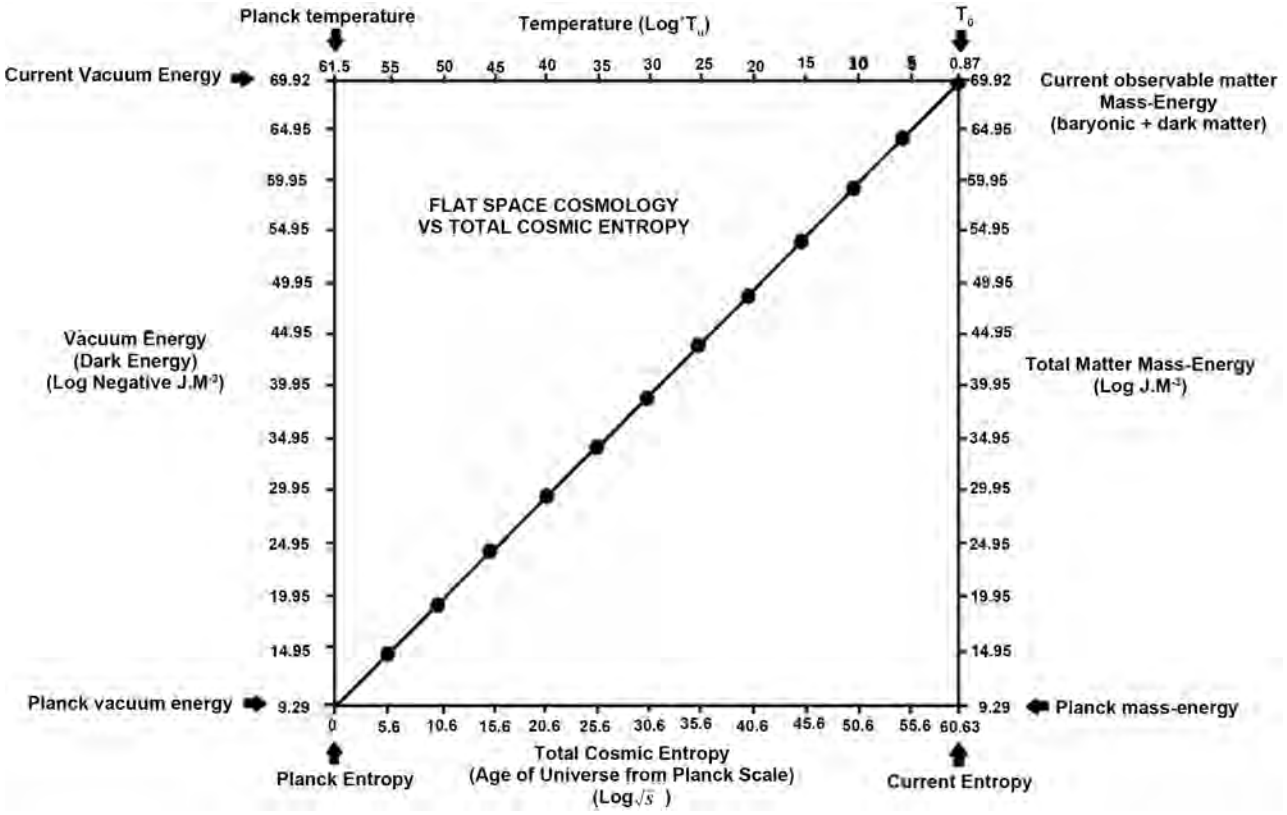

Figure 2. Universal temperature T_u, vacuum energy and total mass-energy vs. entropy.

4. Summary and Conclusions

The purpose of this paper has been to integrate the highly successful FSC model assumptions into the Friedmann equations in an effort to explore the fundamental nature of gravity, dark matter and dark energy. In doing so, there should be no doubt that the results are within the rules of general relativity, particularly in light of the fact that black hole equations already follow the rules of general relativity.

The results of this exercise are quite intriguing. The Lambda term Λ in FSC must follow Equations (15) and (18), indicating that FSC is a dynamic scalar dark energy (quintessence) model of the wCDM type (the FSC equation of state term w is perpetually −1.0). Lambda is shown to be a declining scalar of negative gravitational vacuum energy density (*i.e.*, dark energy density). However, Lambda is an inverse scalar of total cosmic entropy S by Equations (20) and (30). Total matter mass-energy, vacuum energy and cosmic time are shown to be directly proportional to total cosmic entropy in the form of $\sqrt{S}$. Thus, the "entropic arrow of time" is clearly demonstrated in FSC, and $\sqrt{S}$ can be used as the FSC time clock, due to the direct proportionality shown in Equation (25) between cosmic entropy $\sqrt{S}$ and cosmic time t (see Figure 1 and Figure 2).

A search of recent literature concerning the possible relationship between total cosmic entropy and gravitational interactions identifies Roger Penrose, Stephen Hawking, and Erik Verlinde as pioneers in this field. Penrose's book shows

how gravitational entropy clearly differs from the entropy of an ideal gas in the sense that gravitational clustering in the form of stars, galaxies and black holes, is representative of a high (gravitational) entropy state. Black holes, in particular, are huge reservoirs of entropy in its highest possible state. In fact, the FSC model, in this context of gravitational entropy, clearly indicates that *black holes may be equivalently defined as localized zones of maximum possible gravitational entropy, from the Planck scale to the scale of the current universe*.

Verlinde's paper on the origin of gravity shows very clearly how *gravity could be an emergent property of total cosmic entropy*. If so, then gravity may be no more definable at the quantum level than consciousness can be defined within two connecting neurons. Moreover, if gravity is truly an emergent property of total cosmic entropy, then it existed from the inception of universal expansion, as opposed to "freezing out" after a pre-gravity inflationary phase. This emergent property of entropy concept would also indicate that all gravitational manifestations, including gravitational inertia, dark matter and dark energy, are emergent properties, with no likely identifiable connection to quantum physics, including the standard particle model.

Dedications and Acknowledgements

Both authors dedicate this paper to Dr. Stephen Hawking and Dr. Roger Penrose for their groundbreaking work on black holes and their possible application to cosmology. Dr. Tatum thanks Dr. Rudolph Schild of the Harvard Center for Astrophysics for his past support and encouragement. Author Seshavatharam UVS is indebted to professors Brahmashri M. Nagaphani Sarma, Chairman, Shri K.V. Krishna Murthy, founding Chairman, Institute of Scientific Research in Vedas (I-SERVE), Hyderabad, India, and to Shri K.V.R.S. Murthy, former scientist IICT (CSIR), Govt. of India, Director, Research and Development, I-SERVE, for their valuable guidance and great support in developing this subject.

References

[1] Tatum, E.T., Seshavatharam, U.V.S. and Lakshminarayana, S. (2015) *International Journal of Astronomy and Astrophysics*, **5**, 116-124. https://doi.org/10.4236/ijaa.2015.52015

[2] Tatum, E.T., Seshavatharam, U.V.S. and Lakshminarayana, S. (2015) *Journal of Applied Physical Science International*, **4**, 18-26.

[3] Tatum, E.T., Seshavatharam, U.V.S. and Lakshminarayana, S. (2015) *Frontiers of Astronomy, Astrophysics and Cosmology*, **1**, 98-104. http://pubs.sciepub.com/faac/1/2/3

[4] Tatum, E.T., Seshavatharam, U.V.S. and Lakshminarayana, S. (2015) *International Journal of Astronomy and Astrophysics*, **5**, 133-140. https://doi.org/10.4236/ijaa.2015.53017

[5] Planck Collaboration XIII (2016) *Astronomy & Astrophysics*, **594**, A13. http://arxiv.org/abs/1502.01589

[6] Penrose, R. (1965) *Physical Review Letters*, **14**, 57.

https://doi.org/10.1103/PhysRevLett.14.57

[7] Hawking, S. and Penrose, R. (1970) *Proceedings of the Royal Society of London. Series A*, **314**, 529-548. https://doi.org/10.1098/rspa.1970.0021

[8] Bekenstein, J.D. (1974) *Physical Review D*, **9**, 3292-3300. https://doi.org/10.1103/PhysRevD.9.3292

[9] Hawking, S. (1976) *Physical Review D*, **13**, 191-197. https://doi.org/10.1103/PhysRevD.13.191

[10] Inoue, A.K. (2004) *Monthly Notices of the Royal Astronomical Society*, **350**, 729-744. https://doi.org/10.1111/j.1365-2966.2004.07686.x

[11] Tutusaus, I., *et al.* (2017) Is Cosmic Acceleration Proven by Local Cosmological Probes? *Astronomy & Astrophysics*, 602_A73. arXiv:1706.05036v1 [astro-ph.CO].

[12] Nielsen, J.T., *et al.* (2015) Marginal Evidence for Cosmic Acceleration from Type Ia Supernovae. arXiv:1506.01354v1.

[13] Wei, J.-J., *et al.* (2015) *Astronomical Journal*, **149**, 102-112. https://doi.org/10.1088/0004-6256/149/3/102

[14] Melia, F. (2012) *Astronomical Journal*, **144**. arXiv:1206.6289 [astro-ph.CO]. https://doi.org/10.1088/0004-6256/144/4/110

[15] Tatum, E.T. and Seshavatharam, U.V.S. (2018) *Journal of Modern Physics*, **9**, 1397-1403. https://doi.org/10.4236/jmp.2018.97084

[16] Perlmutter, S., *et al.* (1999) *Astrophysical Journal*, **517**, 565-586. https://doi.org/10.1086/307221

[17] Schmidt, B., *et al.* (1998) *Astrophysical Journal*, **507**, 46-63. https://doi.org/10.1086/306308

[18] Riess, A.G., *et al.* (1998) *Astronomical Journal*, **116**, 1009-1038. https://doi.org/10.1086/300499

[19] Guth, A.H. (1997) The Inflationary Universe. Basic Books, New York.

[20] Steinhardt, P.J. (2011) *Scientific American*, **304**, 18-25. https://doi.org/10.1038/scientificamerican0411-36

[21] Weinberg, S. (1989) *Reviews of Modern Physics*, **61**, 1-23. https://doi.org/10.1103/RevModPhys.61.1

[22] Carroll, S. (2001) *Living Reviews in Relativity*, **4**, 5-56. https://doi.org/10.12942/lrr-2001-1

[23] Penrose, R. (2016) Fashion Faith and Fantasy in the New Physics of the Universe. Princeton University Press, Princeton. https://doi.org/10.1515/9781400880287

[24] Tatum, E.T. and Seshavatharam, U.V.S. (2018) *Journal of Modern Physics*, **9**, 1404-1414. https://doi.org/10.4236/jmp.2018.97085

[25] Verlinde, E. (2010) On the Origin of Gravity and the Laws of Newton. arXiv:1001.0785v1

[26] Krogdahl, W.S. (2006) Cosmology in Flat Space-Time. arXiv:gr-qc/0402016v3

[27] Tatum, E.T. (2017) *Journal of Modern Physics*, **8**, 2087-2095. https://doi.org/10.4236/jmp.2017.813127

[28] Tatum, E.T. (2017) *Journal of Modern Physics*, **8**, 2096-2103. https://doi.org/10.4236/jmp.2017.813128

Journal of Modern Physics, 2018, 9, 1484-1490
http://www.scirp.org/journal/jmp
ISSN Online: 2153-120X
ISSN Print: 2153-1196

How the CMB Anisotropy Pattern Could Be a Map of Gravitational Entropy

Eugene Terry Tatum

760 Campbell Ln. Ste. 106 #161, Bowling Green, KY 42104, USA
Email: ett@twc.com

How to cite this paper: Tatum, E.T. (2018) How the CMB Anisotropy Pattern Could Be a Map of Gravitational Entropy. *Journal of Modern Physics*, **9**, 1484-1490.
https://doi.org/10.4236/jmp.2018.98092

Received: June 12, 2018
Accepted: July 9, 2018
Published: July 12, 2018

Copyright © 2018 by author and Scientific Research Publishing Inc.
This work is licensed under the Creative Commons Attribution International License (CC BY 4.0).
http://creativecommons.org/licenses/by/4.0/
Open Access

Abstract

The rationale for Flat Space Cosmology (FSC) calculations of gravitational entropy in the form of $\sqrt{S}$ is presented. These calculations indicate a tight correlation with the COBE DMR measurement showing CMB RMS temperature variations of 18 micro Kelvins. The COBE dT/T anisotropy ratio of 0.66 $\times 10^{-5}$ falls within the FSC gravitational entropy range calculated for the beginning and ending conditions of the recombination/decoupling epoch. Thus, the FSC model incorporating gravity as an emergent property of entropy suggests that the CMB temperature anisotropy pattern could simply be a map of gravitational entropy, as opposed to a magnified "quantum fluctuation" event at a finite beginning of time.

Keywords

Flat Space Cosmology, Cosmic Microwave Background, CMB Anisotropy, Cosmology Theory, Cosmic Entropy, Gravitational Entropy, Black Holes, Standard Cosmology

1. Introduction and Background

In the July 2018 issue of Journal of Modern Physics, the paper entitled, "Clues to the Fundamental Nature of Gravity, Dark Energy and Dark Matter," makes a persuasive case in support of gravity being an emergent property of cosmic entropy S [1]. This argument is bolstered by Verlinde's landmark paper on the subject [2] and by Roger Penrose's conception of gravitational entropy [3]. Notably, Penrose's presentation on cosmic entropy, which relies on the Bekenstein-Hawking definition of black hole entropy [4] [5], relates the magnitude of cosmic horizon surface area $\left(4\pi R^2\right)$ with the Lambda term Λ in the same way as the Flat Space Cosmology (FSC) model. FSC and Penrose (page 277) have derived Λ as always being equal to $3/R_t^2$. This, of course, implies that va-

cuum energy density $\left(\Lambda c^4/8\pi G\right)$ is not a cosmological constant over the great span of cosmic time, but rather a constantly declining cosmological parameter. This relationship applies only to a general relativity model (such as FSC) of an expanding universe with a finite scaling horizon surface area. Only in a *finite* universe model can there be a holographic principle.

The key to understanding gravitational entropy, as presented by Penrose (pages 256-258), is that *in a gravitating universe, the ongoing clustering of stars and galaxies is in the direction of greater cosmic entropy.* Black holes, in particular, are thought to be local reservoirs of maximum entropy. If so, then galactic supermassive black holes must be huge repositories of cosmic entropy. As presented in "Clues to the Fundamental Nature of Gravity, Dark Energy and Dark Matter," gravitational entropy in the form of $\sqrt{S}$ scales in direct proportion to FSC cosmic time, cosmic radius, cosmic matter mass, and cosmic vacuum energy (*i.e.*, dark energy). Cosmic entropy in the correct scale form of $\sqrt{S}$ is always inversely proportional to "Universal Temperature" T_u, as defined by $T_u = T^2$, wherein T^2 is in degrees Kelvin squared. This equal-scaling and proportionality between cosmic gravitational entropy and these FSC parameters allows one to easily calculate the gravitational entropy at any time and temperature in the cosmic past or future. Of particular interest, for the purposes of this paper, is the *relative* gravitational entropy during the cosmic microwave background (CMB) recombination/decoupling epoch in comparison to the gravitational entropies at one year after the Planck epoch and at current cosmic time in years. Plasma physics and particle physics tells us that the recombination/decoupling event began when our early universe was at about 3000 K. The great preponderance of the CMB radiation was released during the cosmic time interval extending from when the universe was at 3000 K to the abrupt "end of decoupling" approximately 115,000 years later [6].

The astute observer will note that there is some difference between the time vs temperature curves used in standard inflationary cosmology as opposed to FSC. This is the subject of the June 2018 Journal of Modern Physics paper entitled, "Temperature Scaling in Flat Space Cosmology in Comparison to Standard Cosmology" [7]. A comparison of these two models in terms of cosmic temperature vs cosmological redshift z is given below. In the FSC model [8] [9] [10], the following formula is used

$$z \cong \left(\frac{T_t^2}{T_o^2} - 1\right)^{1/2} \tag{1}$$

wherein T_t is the cosmic radiation temperature at any time t and T_o is the current observed CMB temperature of 2.72548 K. In standard inflationary cosmology, the following formula is used

$$T_{CMB} \cong 2.725(1+z) \tag{2}$$

wherein T_{CMB} represents the CMB radiation temperature. As derived in the "Temperature Scaling" FSC paper,

$$T^2 t_{ys} = 1.085781647371578 \times 10^{11}\ \mathrm{K}^2 \cdot \mathrm{yr}\ (\text{sidereal years}) \quad (3)$$

wherein T^2 is in Kelvin squared units and t_{ys} is cosmic time in sidereal years.

In this context, the current paper analyzes what the FSC model can tell us about the likely effect of gravity on the CMB anisotropy pattern. The implications are discussed in terms of the well-known Sachs-Wolfe effect (See Discussion section below). Particular emphasis is given to the gravitational entropy $\sqrt{S}$ values corresponding to the recombination/decoupling epoch beginning and ending cosmic temperatures. The ensuing discussion will focus on the implications of these gravitational entropy calculations, and what effect gravitational entropy may have had on this CMB anisotropy pattern.

2. Results

Equation (3) gives an FSC cosmic time value of about 12,064 years at the beginning of the recombination/decoupling epoch (3000 K). Thus, for reasons given in the Discussion section, the "end of decoupling" event happened in the FSC model at approximately 127,000 years (924.63 K) after the Planck epoch. The Planck epoch is the time of the Planck-scale universe and is often considered to be the approximate moment of the "Big Bang" in standard cosmology. The "Clues to the Fundamental Nature of Gravity, Dark Energy and Dark Matter" paper derives

$$\sqrt{S} = \frac{c\sqrt{\pi}}{L_p} t \quad (4)$$

Showing the direct proportionality relationship between gravitational entropy $\sqrt{S}$ and cosmic time t. Speed of light c and Planck length L_p are assumed to be constants over cosmic time. Thus, if we operationally define $\sqrt{S}$ in terms of years,

$\sqrt{S}$ = 1 at 1 year of cosmic time at temperature 3.295×10^5 K

$\sqrt{S}$ = 12,064 at 12,064 years of cosmic time at temperature 3000 K

$\sqrt{S}$ = 127,000 at 127,000 years of cosmic time at temperature 924.63 K

$\sqrt{S}$ = 14.617×10^9 at 14.617×10^9 years of cosmic time at temperature 2.72548 K

The above CMB gravitational entropies (12,064 and 127,000) can then be related to current cosmic entropy (14.617×10^9) as follows:

[$\sqrt{S}$ at the beginning of CMB emission]/[$\sqrt{S}$ at current time] = 8.25×10^{-7} (0.825×10^{-6})

[$\sqrt{S}$ at the ending of CMB emission]/[$\sqrt{S}$ at current time] = 8.69×10^{-6} (0.869×10^{-5})

3. Discussion

Sachs and Wolfe [11], using a gravitational redshift theoretical argument, suggested that CMB temperature anisotropy could be a result of inhomogeneous gravitational particle clustering *already present* at the time of recombina-

tion/decoupling. Their 1967 gravitational redshift argument for what is known as "the Sachs-Wolfe effect" is now widely believed to be correct [12]. The Sachs-Wolfe effect is widely considered to be the source of large angular scale temperature fluctuations in the CMB.

However, *in a spatially flat universe, the Sachs-Wolfe effect can also be considered to be the source of the smaller angular scale fluctuations of the CMB temperature anisotropy* [13]. The Boomerang Collaboration [14] reported CMB anisotropy observations closely fitting "the theoretical predictions for a spatially flat cosmological model with an exactly scale invariant primordial power spectrum for the adiabatic growing mode" [Bucher (2015), page 6]. The Boomerang, Wilkinson Microwave Anisotropy Probe (WMAP) [15], and Planck satellite [16] CMB anisotropy studies have all confirmed global spatial flatness of the universe at the time of the recombination/decoupling epoch. Therefore, in terms of the "gravitational potential variations" explanation first proposed by Sachs and Wolfe, little in the *theory* of CMB temperature anisotropy has changed since 1967. What *has* changed since the time of the Sachs and Wolfe paper is the *precision of measurements* of the CMB temperature anisotropy. Both the WMAP study and the more sensitive Planck study have confirmed the CMB temperature anisotropy to be on the order of *approximately one part per* 100,000 (10^{-5}).

At the time of these CMB study reports, the extreme flatness observations of the CMB temperature anisotropy were credited as a victory for cosmic inflation. However, there was no basis to determine which particular theoretical version of inflation was correct, or even *whether another flat space cosmology theory without an inflationary mechanism* (*such as FSC*) *could, in fact, be an even better explanation of global cosmic flatness observations.* The following quote from physicist Philip Gibbs sums it up best: "The problem… is that no particular model of inflation has been shown to work yet. It is possible that work has not yet been completed *or that a more recent specific model will be shown to be right"* [17] [18]. In a soon-to-be-published FSC paper, this author will clearly show why the FSC model is superior to the standard inflationary model, using a series of specific FSC model predictions dating back to 2015.

As mentioned in the Introduction and Background section, current best estimates of the cosmic time interval during which the CMB radiation was released suggest that the recombination/decoupling epoch lasted approximately 115,000 years. In standard cosmology this is believed to have occurred between approximately 372,000 and 487,000 years after a "Big Bang" at or near the Planck epoch. In the FSC model, the temperature scaling is *slightly* different [Tatum, *et al* (2018)], placing the beginning of the recombination/decoupling epoch (3000 K) at approximately 12,064 years after the Planck epoch. Adding the estimated time interval of approximately 115,000 years puts the FSC "end of decoupling" event at about 127,000 years after the Planck epoch.

Gravitational entropy $\sqrt{S}$ in the FSC model follows the same log value scale as cosmic time. Thus, there should be a uniform progression from maximum gravitational potential "smoothness," corresponding to any operationally-defined

"minimal" or "beginning" anisotropy, to ongoing and progressively greater gravitational inhomogeneity (*i.e.*, "filaments", "clusters" and "voids"). Furthermore, this is consistent with the concept that cosmic entropy smoothly increases as the expanding cosmic horizon surface area (the Bekenstein-Hawking measure of entropy) increases. Thus, it would seem reasonable to assume that, *if the CMB temperature anisotropy pattern is in keeping with the Sachs-Wolfe effect for a spatially flat universe, and if gravity is truly an emergent property of cosmic entropy as indicated by Verlinde, the FSC gravitational entropy values pertaining to the recombination/decoupling epoch should also be a measure of the CMB temperature anisotropy*.

The COBE DMR experiment measured CMB RMS temperature variations of 18 micro Kelvins (1.8×10^{-5} K) [19]. This gives a dT/T anisotropy ratio of (0.000018)/2.725, equaling 6.6×10^{-6} or 0.66×10^{-5}. Little has changed in this respect, judging from the subsequent WMAP and Planck CMB temperature anisotropy findings (also approximately 10^{-5}).

It is intriguing that the FSC gravitational entropy ratios provided and calculated at the end of the Results section are 0.825×10^{-6} at the beginning of recombination/decoupling and 0.869×10^{-5} at the "end of decoupling." It should be noted that *the "last scattering surface" is actually a* 115,000 *year thick segment of microwave radiation spectrum rather than an infinitely thin "surface" at a single redshift.* In this context, the COBE DMR dT/T anisotropy ratio of 0.66×10^{-5} can only be, in some way, an *averaging* of the actual ratio numbers pertaining to the beginning and ending conditions responsible for the "last scattering surface." Therefore, the FSC model incorporating gravity as an emergent property of entropy suggests that the CMB temperature anisotropy pattern could simply be a map of gravitational entropy, as opposed to a magnified "quantum fluctuation" event at a finite beginning of time.

4. Summary and Conclusions

The purpose of this paper has been to show how the CMB temperature anisotropy pattern could be a map of gravitational entropy as defined by Roger Penrose in his book entitled, "Fashion, Faith and Fantasy in the New Physics of the Universe." This is particularly relevant with respect to Erik Verlinde's theory that gravity is an emergent property of cosmic entropy. Verlinde's theory dovetails nicely with the July 2018 Journal of Modern Physics paper entitled, "Clues to the Fundamental Nature of Gravity, Dark Energy and Dark Matter."

In the present paper, the rationale for FSC calculations of gravitational entropy in the form of $\sqrt{S}$ is presented. These calculations indicate a tight correlation with the COBE DMR measurement showing CMB RMS temperature variations of 18 micro Kelvins. The COBE dT/T anisotropy ratio of 0.66×10^{-5} falls within the FSC gravitational entropy range calculated for the beginning and ending conditions of the recombination/decoupling epoch. Thus, the FSC model incorporating gravity as an emergent property of entropy suggests that the CMB

temperature anisotropy pattern could simply be a map of gravitational entropy, as opposed to a magnified "quantum fluctuation" event at a finite beginning of time.

Dedications and Acknowledgements

This paper is dedicated to Dr. Stephen Hawking and Dr. Roger Penrose for their groundbreaking work on black holes and their possible application to cosmology. Dr. Tatum also thanks Dr. Rudolph Schild of the Harvard Center for Astrophysics for his past support and encouragement.

References

[1] Tatum, E.T. and Seshavatharam, U.V.S. (2018) *Journal of Modern Physics*, **9**, 1469-1483. https://doi.org/10.4236/jmp.2018.98091

[2] Verlinde, E. (2010) On the Origin of Gravity and the Laws of Newton. arXiv:1001.0785v1 [hep-th].

[3] Penrose, R. (2016) Fashion Faith and Fantasy in the New Physics of the Universe. Princeton University Press, Princeton, US. https://doi.org/10.1515/9781400880287

[4] Bekenstein, J.D. (1974) *Physical Review D,* **9**, 3292-3300. https://doi.org/10.1103/PhysRevD.9.3292

[5] Hawking, S. (1976) *Physical Review D*, **13**, 191-197. https://doi.org/10.1103/PhysRevD.13.191

[6] Spergel, D.N., *et al.* (2003) *Astrophysical Journal Supplement*, **148**, 175-194. arXiv:astro-ph/0302209. https://doi.org/10.1086/377226

[7] Tatum, E.T. and Seshavatharam, U.V.S. (2018) *Journal of Modern Physics*, **9**, 1404-1414. https://doi.org/10.4236/jmp.2018.97085

[8] Tatum, E.T., Seshavatharam, U.V.S. and Lakshminarayana, S. (2015) *International Journal of Astronomy and Astrophysics*, **5**, 116-124. https://doi.org/10.4236/ijaa.2015.52015

[9] Tatum, E.T., Seshavatharam, U.V.S. and Lakshminarayana, S. (2015) *Journal of Applied Physical Science International*, **4**, 18-26.

[10] Tatum, E.T., Seshavatharam, U.V.S. and Lakshminarayana, S. (2015) *Frontiers of Astronomy, Astrophysics and Cosmology*, **1**, 98-104. http://pubs.sciepub.com/faac/1/2/3

[11] Sachs, R.K. and Wolfe, A.M. (1967) *Astrophysical Journal*, **147**, 73-90. https://doi.org/10.1086/148982

[12] Wright, E.L. (2003) Theoretical Overview of Cosmic Microwave Background Anisotropy. In: Freedman, W.L., Ed., *Measuring and Modeling the Universe*, Cambridge University Press, Cambridge, 291.

[13] Bucher, M. (2015) Physics of the Cosmic Microwave Background Anisotropy. arXiv:1501.04288v1 [astro-ph.CO]. https://doi.org/10.1142/S0218271815300049

[14] De Bernardis, P., *et al.* (2000) A Flat Universe from High-Resolution Maps of the Cosmic Microwave Background Radiation. arXiv:astro-ph/0004404v1. https://doi.org/10.1038/35010035

[15] Bennett, C.L. (2013) Nine-Year Wilkinson Microwave Anisotropy Probe (WMAP) Observations: Final Maps and Results. arXiv:1212.5225v3 [astro-ph.CO].

https://doi.org/10.1088/0067-0049/208/2/20

[16] Planck Collaboration (2014) *Astronomy & Astrophysics*, **23**, 1-48.

[17] Keating, B. (2018) Losing the Nobel Prize. W. W. Norton & Company, New York.

[18] Gibbs, P.E. (2014) *Prespacetime Journal*, **5**, 230-233. https://prespacetime.com/index.php/pst/article/download/614/612

[19] Wright, E.L., *et al.* (1996) *Astrophysical Journal*, **464**, L21-L24. https://doi.org/10.1086/310073

Journal of Modern Physics, 2018, 9, 1491-1521
http://www.scirp.org/journal/jmp
ISSN Online: 2153-120X
ISSN Print: 2153-1196

Circular Time Scale Yields a Recurrent Calculation of the Schrödinger Perturbation Energy

Stanisław Olszewski

Institute of Physical Chemistry, Polish Academy of Science, Warsaw, Poland
Email: olsz@ichf.edu.pl

How to cite this paper: Olszewski, S. (2018) Circular Time Scale Yields a Recurrent Calculation of the Schrödinger Perturbation Energy. *Journal of Modern Physics*, **9**, 1491-1521.
https://doi.org/10.4236/jmp.2018.98093

Received: April 25, 2018
Accepted: July 9, 2018
Published: July 12, 2018

Copyright © 2018 by author and Scientific Research Publishing Inc.
This work is licensed under the Creative Commons Attribution International License (CC BY 4.0).
http://creativecommons.org/licenses/by/4.0/

Open Access

Abstract

An essential simplification of approach to the Schrödinger perturbation series for energy does hold when the perturbation events are arranged along a circular scale of time. The aim of the present paper is to demonstrate how such a scale of time leads to the recurrence calculation process of the Schrödinger energy terms belonging to an arbitrary perturbation order N. This process seems to have never been represented before. Only a non-degenerate quantum state and its perturbation due to the space-dependent potential are considered in the paper.

Keywords

Time, Its Circular Scale, Schrödinger Perturbation Formalism

1. Introduction

In science an identical result obtained in two different ways does not necessarily mean an effect of a secondary importance. An example is the Schrödinger perturbation formalism. In order to get it Schrödinger elaborated a special treatment of the inhomogeneous differential equations in course of which the energies and wave functions of a stationary quantum state perturbed by a time-independent potential could be calculated with the aid of the energies and wave functions representing the unperturbed quantum states of a given system [1]. Usually the unperturbed system was less complicated than a perturbed one, and the perturbation was limited to the potentials difference entering the perturbed and original state.

An effective formalism leading to the Schrödinger results is based usually on an iterative process; see e.g. [2]. When an original Hamiltonian $\hat{H}_0$ is

perturbed by $\lambda\hat{H}'$, we have to solve the time-independent Schrödinger equation given in the form

$$\hat{H}^{\text{per}}\psi^{\text{per}} = E^{\text{per}}\psi^{\text{per}}, \tag{1}$$

the problem is approached by a substitution

$$\hat{H}^{\text{per}} = \hat{H}_0 + \lambda\hat{H}', \tag{2}$$

$$\psi^{\text{per}} = \psi_0 + \lambda\psi_1 + \lambda^2\psi_2 + \cdots \tag{3}$$

and

$$E^{\text{per}} = E_0 + \lambda E_1 + \lambda^2 E_2 + \cdots. \tag{4}$$

The $\hat{H}_0$, E_0 and ψ_0 are respectively the unperturbed Hamiltonian, energy and wave function, whereas $\lambda\hat{H}'$, $\lambda E_1, \lambda^2 E_2, \cdots$ and $\lambda\psi_1, \lambda^2\psi_2, \cdots$ represent respectively the perturbed quantities. The solution of (4) can be obtained gradually for different powers of λ. In the next step the size of the parameter λ is put equal to 1; see [2].

This rather tedious procedure does not apply time, which makes it similar to the original Schrödinger approach [1]. For $\lambda = 1$ the notation of (4) is usually changed into the expression

$$E^{\text{per}} - E_0 = \Delta E_1 + \Delta E_2 + \Delta E_3 + \cdots \tag{4a}$$

where $\Delta E_1, \Delta E_2, \Delta E_3, \cdots$ are the perturbation energies corresponding to the so-called perturbation orders N equal respectively to $N = 1$, $N = 2$, $N = 3$, etc.

The time entered the Schrödinger perturbation theory—limited to the stationary quantum states—with the development of diagrams introduced by Feynman [3] [4]. But these diagrams were based on a different kind of the time scale than applied in the present paper. In order to clarify the origin of a difference between the Feynman and present perturbation formalism, a step towards the time backround entering both methods seems to be of use.

2. Physics of a Quantum System and the Notion of Time

Both physical and philosophical features connected with the notion of time are combined systematically with scientific experience and observations of everyday life. A separate component of our view on time is provided by human imagination. In effect the idea of the time notion is extended—with a variable degree of certainty—from the atomic world to universe.

In fact time is a parameter the knowledge of which depends both on the properties of the examined object as well as the abilities possessed by an observer. If we limit our "universe" to a single hydrogen atom and the observer's ability to distinguish between the atomic nucleus and electron together with the possibility to estimate the size of a distance between these two objects, we can obtain two kinds of observations. One of them is created by assuming that a constant distant does hold between the nucleus and electron. This situation cannot serve to establish any notion of time because no change of the distance parameter can be detected and observed. However another situation is obtained when the

distance between two particles changes systematically in a planar motion of the electron particle, which has its trajectory say along an ellipse. In this case the observer's measurements are spread along the interval length which is equal to a difference between the larger and smaller semiaxis of the ellipse. If the motion is perfectly periodic, any point observed within the interval length repeats after the same period of the motion time T.

In effect all time points accessible by observations are enclosed within the interval

$$0 < t < T, \tag{5}$$

which repeats incessibly because no limit is imposed on the electron motion along the ellipse.

But a huge amount of everyday observations is evidently against the limit given in (5). In fact a finite amount of T is replaced by infinity, so

$$0 < t < \infty. \tag{6}$$

On the other hand, an analysis of the contemporary situation as an effect of an earlier situation combined with imagination implies the past events qualitatively separated from the present situation by a time interval which can be also of an infinite size. This gives the interval

$$-\infty < t < \infty \tag{7}$$

where $t = 0$ can be assumed to be close to the present time.

The interval (7) encloses practically all possible events in nature but does not explain much what happens, will happen, or has happened, within (6) or (7). A characteristics of time is often expected to be obtained from physics. In fact we look for an objective method to define this character. Perhaps the best known result is given by the second law of thermodynamics which applies the notion of entropy and states that "later" means systematically a larger entropy than the entropy at an "earlier" time. An objection which can be raised here is connected mainly with the fact of applying the thermodynamics and entropy: these notions concern macroscopic systems built up regularly from a huge number of individual components.

But difficulties with a physical approach to time concern also the quantum domain. First the time intervals of numerous quantum processes are too short to be satisfactorily controlled on both the theoretical and experimental level. However opposite cases can be also considered. If an atom is in its lowest energy state, called also a ground state, and no external forces or collisions act on it, this atomic state can be preserved infinitely with no change. Therefore—according to the present state of our knowledge—no idea or scale of time can be applied in describing such an atom. However, a different situation is obtained when—at some moment—the atom is perturbed, for example by an action of an external field which can be chosen to be independent of time. If the time moment of inclusion of the perturbation potential is denoted by

$$t = t_b, \tag{8}$$

at any time moment

$$t > t_b \tag{9}$$

the properties of the atom are changed in comparison to those possessed in (8). But we can assume that in effect of the action of the perturbation potential

$$V^{\text{per}} \tag{10}$$

till some

$$t_e \gg t_b, \tag{11}$$

the atom will approach another stationary state. In effect of that the atom properties at

$$t \gg t_e \tag{12}$$

will be not much different than those possessed near

$$t = t_e. \tag{13}$$

In other words the atom behaves at (12) as an unchanged object equal to that obtained at (13), therefore the notion of time looses again its sense. But a question arises now how the time is going on between $t = t_b$ and $t = t_e$. An attempt to answer this question became a major subject of the paper.

The answer is obtained with the aid of an analysis of the events which accompany the perturbation process. According to Leibniz [5] [6] it is the sequence of events which is legitimate to provide us with a knowledge of the character of the time scale associated with a given process. In this case the problem of the size of the time intervals between subsequent events becomes of a secondary importance, but the accent is put on the properties (regularities) of the changes of the system exhibited in course of the time flow.

One of the aims of the present paper is to compare two scales of time applied to the case of the perturbation process. The first—based on a linear scale extended from the minus to plus infinity [see (6) and (7)]—was involved in the Feynman's approach to quantum mechanics [3] [4], another scale—of an essentially circular character—has been developed by the author [7]-[14].

3. Feynman's Approach and Present Approach to the Schrödinger Perturbation Energy

An essential difference between these two approaches is that in a majority of calculations postulated according to the Feynman's scheme of diagrams—especially for a large perturbation order N—there exists no reference between the energy terms provided by the Schrödinger perturbation theory and the Feynman diagrams. A reason of that is the fact that for large N the number of the Feynman diagrams equal to

$$P_N = (N-1)! \tag{14}$$

does exceed dramatically the number of the Schrödinger terms given by the formula [15] [16]:

$$S_N = \frac{(2N-2)!}{N!(N-1)!}. \tag{15}$$

The ratio between P_N and S_N is

$$\frac{P_N}{S_N} = \frac{N!\left[(N-1)!\right]^2}{(2N-2)!}; \tag{16}$$

evidently it increases rapidly with N. For example for $N = 20$ the ratio (16) attains the number of

$$\frac{P_{20}}{S_{20}} = 0.688 \times 10^8. \tag{16a}$$

This means that in average about 0.7×10^8 results of the integration prescribed by the Feynman diagrams should be combined in order to obtain one Schrödinger energy term. The task seems to be complicated even with the use of computers.

On the other hand, an evident advantage of the circular time scale is that it can provide us with a one-to-one correspondence between the diagrams based on the scale and the Schrödinger energy terms. This facilitates enormously any development of the Schrödinger perturbation calculation and serves to control its results.

4. Basic Characteristics of the Circular Scale of Time

The first rule concerning diagrams of the present theory is that they can be classified according to the perturbation orders

$$N = 1, 2, 3, 4, \cdots \tag{17}$$

characteristic for the Schrödinger perturbation scheme. This means that the number of time points taken into account on any diagram belonging to N is equal to N. But only one diagram for each N is represented by N uncontracted time points labelled successively by

$$1, 2, 3, 4, \cdots, N. \tag{18}$$

From the number N of time points entering any diagram the points

$$1, 2, 3, 4, \cdots = M = N - 1 \tag{19}$$

should be taken into account in formation of contractions of the time points characteristic for that diagram. A reason for that limitation is due to the fact that the point N, which is considered as a beginning-end point of the scale, does not enter contractions.

The contractions can be simple, i.e. between two points of time, viz.

$$\begin{aligned} t_1 : t_2 &= 1:2, \\ t_1 : t_3 &= 1:3, \\ t_1 : t_4 &= 1:4, \cdots \end{aligned} \tag{20}$$

or

$$t_2 : t_3 = 1:3,$$

$$t_2 : t_4 = 2:4,\cdots \tag{20a}$$

or

$$t_3 : t_4 = 3:4,\cdots, \tag{20b}$$

but also double contractions like

$$t_1 : t_2 : t_3 = 1:2:3,$$

$$t_1 : t_2 : t_4 = 1:2:4,$$

$$t_1 : t_3 : t_4 = 1:3:4,\cdots, \tag{20c}$$

and still more extended contractions with more than three time points involved in them can exist.

Evidently the time points are arranged on the scale, as well as in contraction ensembles, according to their rise in time:

$$t_1 < t_2 < t_3 < t_4 < \cdots \tag{21}$$

There are also possible combined time-points contractions, for example

$$t_1 : t_2 \bigcap t_3 : t_4 = 1:2 \bigcap 3:4 \tag{22}$$

or

$$t_1 : t_4 \bigcap t_2 : t_3 = 1:4 \bigcap 2:3, \tag{23}$$

which indicate a simultaneous presence of two different contractions. The rule, however, for formation of such combined sets of contractions is that the loops created by them on a diagram cannot cross (see e.g. [7]). This means that, for example, such contractions combination like

$$t_1 : t_3 \bigcap t_2 : t_4 = 1:3 \bigcap 2:4 \tag{24}$$

cannot exist.

Physically any contraction of the time points creates one or more loops of time supplementary to the main—single for a given diagram—loop of time. These supplementary loops will be called the side loops of time. They can be regularly represented by the energy perturbation terms of the order lower than the actually examined N. The main loop of time should contain the beginning-end point characteristic for any considered N. This special time point—as it is stated above—does not participate in contractions.

5. Loops of Time and Schrödinger Perturbation Terms for Energy

In this Section the loops of time obtained for the circular-scale diagrams are referred to the Schrödinger perturbation terms for energy. A single diagram without contractions is present for any N; for the case of $N = 7$ such diagram is drawn on **Figure 1**. The energy term corresponding to this diagram is

$$\langle VPVPVPVPVPV \rangle. \tag{25}$$

The number of V is 7, but the number of P is 6.

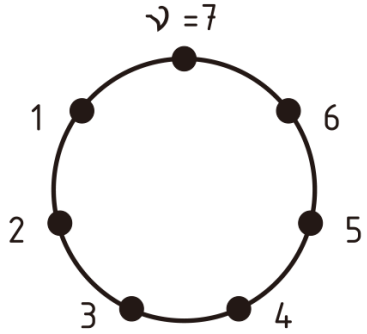

Figure 1. Diagram representing the energy term for the perturbation order $N=7$ having no contractions of the time points.

In general the symbol V represents the matrix element

$$\langle a|V^{\text{per}}|b\rangle. \tag{26}$$

The expression (25) begins with the matrix element (26) taken for $a=n$ and $b=p\neq n$ where n is the index of quantum state submitted to perturbation. The next V represent the matrix elements

$$\langle p|V^{\text{per}}|q\rangle,\ \langle q|V^{\text{per}}|r\rangle,\ \langle r|V^{\text{per}}|s\rangle,\ \langle s|V^{\text{per}}|t\rangle,\ \langle t|V^{\text{per}}|u\rangle,\cdots \tag{27}$$

and the last V in (25) is

$$\langle u|V^{\text{per}}|n\rangle. \tag{27a}$$

The successive symbols P in (25) are respectively

$$P=\frac{1}{E_n-E_p},\quad P=\frac{1}{E_n-E_q},\quad P=\frac{1}{E_n-E_r},$$
$$P=\frac{1}{E_n-E_s},\quad P=\frac{1}{E_n-E_t},\quad P=\frac{1}{E_n-E_u}, \tag{28}$$

and the whole expression (25) is a multiple sum performed over the quantum-state indices

$$p,q,r,s,t,u,\cdots\neq n. \tag{29}$$

The indices change from state 1 to infinity with the omission of state n in each sum.

A contraction of two points, say

$$p:q=1:2, \tag{30}$$

means creation of a side loop of time on the diagram of Figure 1 between the points 1 and 2; see Figure 2. In this case the perturbation term (25) changes into

$$\langle VP^2VPVPVPVPV\rangle\langle V\rangle \tag{31}$$

where

$$P^2=\frac{1}{\left(E_n-E_p\right)^2}=\frac{1}{\left(E_n-E_q\right)^2} \tag{32}$$

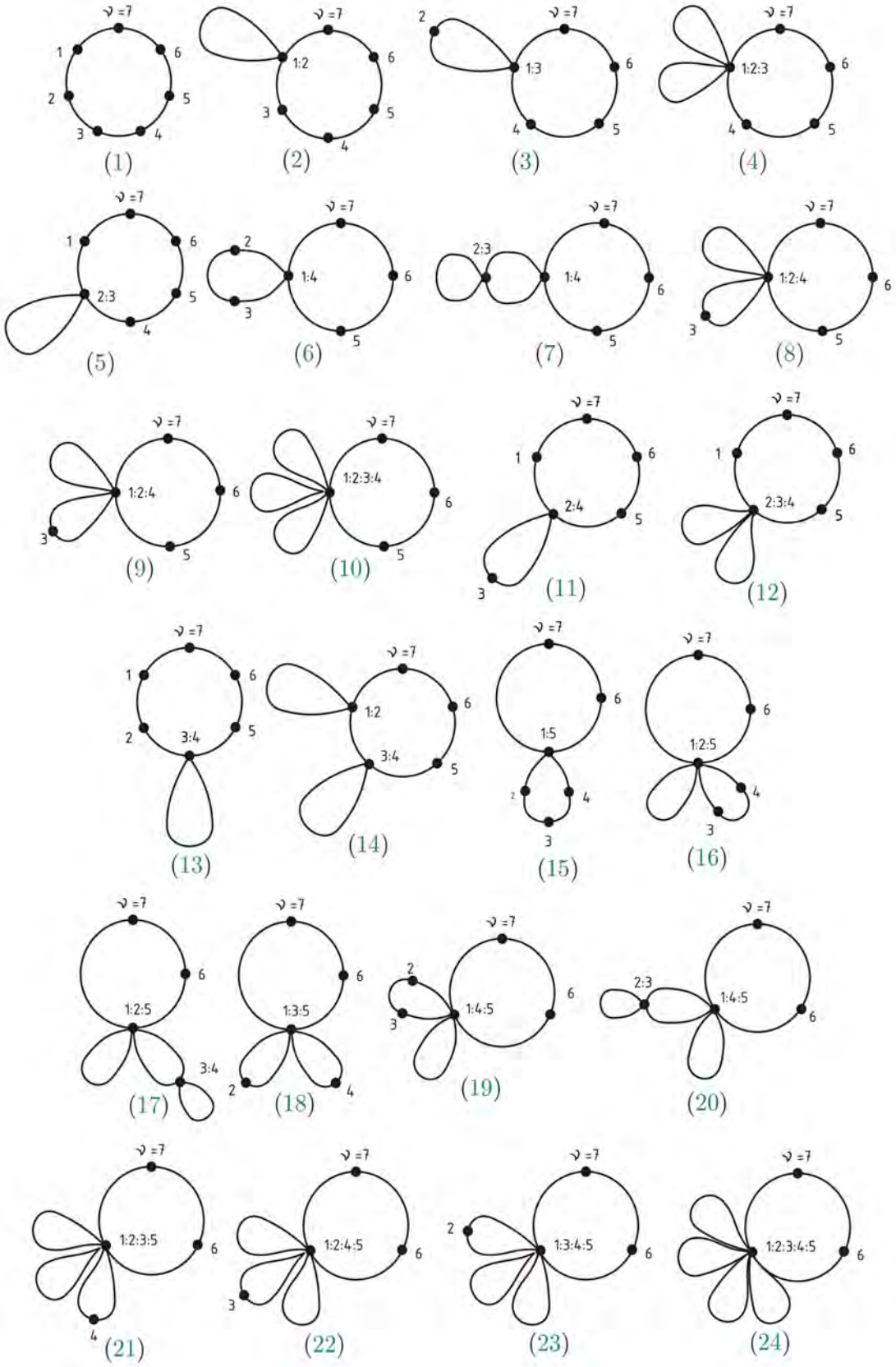
ν =7
1
2
3
4
5
6
1:2
1:3
1:2:3
2:3
1:4
1:2:4
2:4
1:2:3:4
2:3:4
1:5
1:2:5
3:4
1:3:5
1:4:5
1:2:3:5
1:2:4:5
1:3:4:5
1:2:3:4:5
(1)
(2)
(3)
(4)
(5)
(6)
(7)
(8)
(9)
(10)
(11)
(12)
(13)
(14)
(15)
(16)
(17)
(18)
(19)
(20)
(21)
(22)
(23)
(24)

(a)

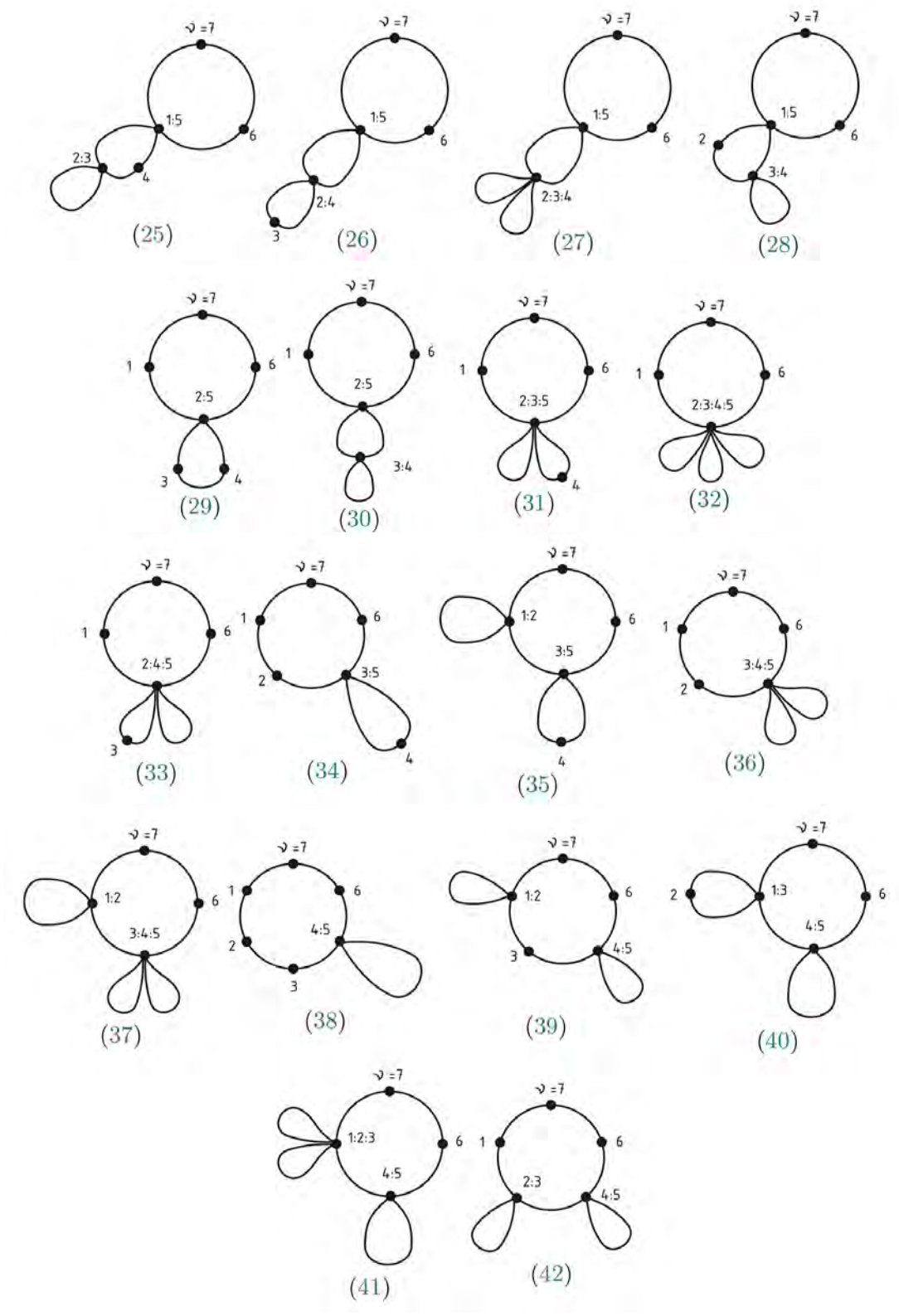

(b)

Figure 2. Diagrams representing the energy perturbation terms for $N = 7$ obtained from a small modification of diagrams valid for the perturbation order $N = 6$. The numbers below diagrams indicate the time contraction and energy term given in **Table 1**.

and

$$\langle V \rangle = \Delta E_1 \tag{32a}$$

which is the first-order perturbation energy.

Contractions $2:3$, $3:4$, $4:5$ and $5:6$ give respectively the perturbation terms:

$$\langle VPVP^2VPVPVPV \rangle \langle V \rangle \tag{33}$$

with

$$P^2 = \frac{1}{\left(E_n - E_q\right)^2} = \frac{1}{\left(E_n - E_r\right)^2}, \tag{33a}$$

the term

$$\langle VPVPVP^2VPVPV \rangle \langle V \rangle \tag{34}$$

with

$$P^2 = \frac{1}{\left(E_n - E_r\right)^2} = \frac{1}{\left(E_n - E_s\right)^2}, \tag{34a}$$

the term

$$\langle VPVPVPVP^2VPV \rangle \langle V \rangle \tag{35}$$

with

$$P^2 = \frac{1}{\left(E_n - E_s\right)^2} = \frac{1}{\left(E_n - E_t\right)^2}, \tag{35a}$$

the term

$$\langle VPVPVPVPVP^2V \rangle \langle V \rangle \tag{36}$$

with

$$P^2 = \frac{1}{\left(E_n - E_t\right)^2} = \frac{1}{\left(E_n - E_u\right)^2}. \tag{36a}$$

The summations entering (33)-(36) are extended respectively over

$$p, q = r, s, t, u \neq n, \tag{33b}$$

$$p, q, r = s, t, u \neq n, \tag{34b}$$

$$p, q, r, s = t, u \neq n, \tag{35b}$$

$$p, q, r, s, t = u \neq n. \tag{36b}$$

Similar notation applies for other contractions than presented above. For example a double contraction

$$p:q:r = 1:2:3 \tag{37}$$

gives for the energy term coming from the main loop the expression

$$\langle VP^3VPVPVPV \rangle \left(\langle V \rangle\right)^2. \tag{38}$$

The term

$$\left(\left\langle V\right\rangle\right)^2=\left(\Delta E_1\right)^2 \tag{39}$$

is due to the side loops 1:2 and 2:3 separately. The term due to the main loop is represented by

$$\left\langle VP^3VPVPVPV\right\rangle \tag{40}$$

where

$$P^3=\frac{1}{\left(E_n-E_p\right)^3}=\frac{1}{\left(E_n-E_q\right)^3}=\frac{1}{\left(E_n-E_r\right)^3}. \tag{41}$$

Three other P present in (40) are those given in (28) and summations concern the states

$$s,t,u. \tag{42}$$

In total the summations entering the brackets in (40) are extended over the states

$$p=q=r,\ \ s,t,u\neq n. \tag{43}$$

It is easy to prolongate the above notation to other contractions of the time points than considered between (30) and (43).

The sign of a perturbation term is dictated by the number of the bracket pairs which enter that term. For an odd number of the bracket pairs [see (25), (38)] the whole energy term should be taken with a positive sign, for an even number of the bracket pairs [see (31), (33)-(36)] the perturbation term should be taken with a minus sign.

6. Recurrence Procedure for Calculating the Schrödinger Perturbation Terms Belonging to Arbitrary N

It seems that the best way to represent this procedure is to apply it to an example. A particular task let be to derive the perturbation terms belonging to $N=7$ from the terms belonging to

$$N<7. \tag{44}$$

The energy perturbation terms corresponding to N entering (44) are briefly derived and given in Appendix. A question which can arise may be how similar terms should be calculated in the case of $N=7$.

The choice of $N=7$ means that a new free time point on the scale which can be submitted to contractions is

$$N-1=6. \tag{45}$$

This implies that $S_6=42$ terms belonging to $N=6$ should be modified in order to take into account the presence of a free time point 6 absent in the case of $N=6$. In practice this means that all contributions coming to energy from the main loop of time for $N=6$ can be made valid also for $N=7$ on condition—at the end of any bracket term corresponding to the mentioned main loop of time—the product

$$PV \tag{46}$$

is added; see Table 1. The diagrams corresponding to the energy terms obtained in the way outlined below (45) are presented in Figure 2. This reduces the number of unknown terms for $N=7$, namely

$$S_7 = 132, \tag{47}$$

to

$$S_7 - S_6 = 132 - 42 = 90. \tag{48}$$

But the presence of point 6 on the time scale implies that this point has also to participate in contractions. The number of these contractions is obtained when contraction

$$1:6, \tag{49}$$

together with all admissible contractions of the time points on a circular scale between 1 and 6, are taken into account. The contraction (49) and its energy terms are

$$1:6 \to -\left\langle VP^2V \right\rangle \Delta E_5. \tag{50}$$

This contraction provides us with contribution equal to 14 Schrödinger energy terms because the number of terms in ΔE_5 is $S_5 = 14$. In the next step we obtain 5 terms, viz.

$$1:2:6 \to \left\langle VP^3V \right\rangle \Delta E_1 \Delta E_4, \tag{51}$$

because of $S_1 = 1$ and $S_4 = 5$. Two perturbation terms are given by

$$1:3:6 \to \left\langle VP^3V \right\rangle \Delta E_2 \Delta E_3, \tag{52}$$

because of $S_2 = 1$ and $S_3 = 2$; the same number of terms holds for contraction

$$1:4:6 \to \left\langle VP^3V \right\rangle \Delta E_3 \Delta E_2. \tag{53}$$

Contraction

$$1:5:6 \to \left\langle VP^3V \right\rangle \Delta E_4 \Delta E_1 \tag{54}$$

gives $S_4 = 5$ terms since it is by symmetry similar to (51);

$$1:2:3:6 \to -\left\langle VP^4V \right\rangle \left(\Delta E_1\right)^2 \Delta E_3 \tag{55}$$

gives two terms because of $S_3 = 2$;

$$1:2:4:6 \to -\left\langle VP^4V \right\rangle \Delta E_1 \left(\Delta E_2\right)^2 \tag{56}$$

is a one-term contraction $\left(S_1 = S_2 = 1\right)$;

$$1:2:5:6 \to -\left\langle VP^4V \right\rangle \Delta E_1 \Delta E_3 \Delta E_1 \tag{57}$$

gives two terms because of $S_3 = 2$;

$$1:3:4:6 \to -\left\langle VP^4V \right\rangle \Delta E_2 \Delta E_1 \Delta E_2 \tag{58}$$

is a one-term contraction;

$$1:3:5:6 \to -\left\langle VP^4V \right\rangle \left(\Delta E_2\right)^2 \Delta E_1 \tag{59}$$

Table 1. Energy perturbation terms belonging to $N = 7$ obtained by adding the product PV from (46) into the main bracket terms entering the perturbation energy for $N = 6$. The terms 15, 25, 26, 27 and 28 can combine into $-\langle VP^2VPV\rangle\Delta E_4$; the terms 6 and 7, 16 and 17, 19 and 20, and 29 and 30 combine into four terms containing the factor of ΔE_3.

	contraction	energy term
1	no contraction	$\langle VPVPVPVPVPV\rangle$
2	1:2	$-\langle VP^2VPVPVPV\rangle\Delta E_1$
3	1:3	$-\langle VP^2VPVPV\rangle\Delta E_2$
4	1:2:3	$\langle VP^3VPVPV\rangle(\Delta E_1)^2$
5	2:3	$-\langle VPVP^2VPVPV\rangle\Delta E_1$
6	1:4	$-\langle VP^2VPV\rangle\Delta E_3$
7	$1:4\cap 2:3$	
8	1:2:4	$\langle VP^3VPV\rangle\Delta E_1\Delta E_2$
9	1:3:4	$\langle VP^3VPV\rangle\Delta E_2\Delta E_1$
10	1:2:3:4	$-\langle VP^4VPV\rangle(\Delta E_1)^3$
11	2:4	$-\langle VPVP^2VPV\rangle\Delta E_2$
12	2:3:4	$\langle VPVP^3VPV\rangle(\Delta E_1)^2$
13	3:4	$-\langle VPVPVP^2VPV\rangle\Delta E_1$
14	$1:2\cap 3:4$	$\langle VP^2VP^2VPV\rangle(\Delta E_1)^2$
15	1:5	$-\langle VP^2VPVVPVPV\rangle$
16	1:2:5	$\langle VP^3VPV\rangle\Delta E_1\Delta E_3$
17	$1:2:5\cap 3:4$	
18	1:3:5	$\langle VP^3VPV\rangle(\Delta E_2)^2$
19	1:4:5	$\langle VP^3VPV\rangle\Delta E_3\Delta E_1$
20	$1:4:5\cap 2:3$	
21	1:2:3:5	$-\langle VP^4VPV\rangle(\Delta E_1)^2\Delta E_2$
22	1:2:4:5	$-\langle VP^4VPV\rangle\Delta E_1\Delta E_2\Delta E_1$
23	1:3:4:5	$-\langle VP^4VPV\rangle\Delta E_2(\Delta E_1)^2$
24	1:2:3:4:5	$\langle VP^5VPV\rangle(\Delta E_1)^4$
25	$1:5\cap 2:3$	$\langle VP^2VPV\rangle\langle VP^2VPV\rangle\Delta E_1$
26	$1:5\cap 2:4$	$\langle VP^2VPV\rangle\langle VP^2V\rangle\Delta E_2$
27	$1:5\cap 2:3:4$	$\langle VP^2VPV\rangle\langle VP^3V\rangle(\Delta E_1)^2$
28	$1:5\cap 3:4$	$\langle VP^2VPV\rangle\langle VPVP^2V\rangle\Delta E_1$
29	2:5	$-\langle VPVP^2VPV\rangle\Delta E_3$
30	$2:5\cap 3:4$	
31	2:3:5	$\langle VPVP^3VPV\rangle\Delta E_1\Delta E_2$
32	2:3:4:5	$-\langle VPVP^4VPV\rangle(\Delta E_1)^3$
33	2:4:5	$\langle VPVP^3VPV\rangle\Delta E_2\Delta E_1$

Continued

34	3:5	$-\langle VPVPVP^2VPV\rangle \Delta E_2$
35	1:2∩3:5	$\langle VP^2VP^2VPV\rangle \Delta E_1 \Delta E_2$
36	3:4:5	$\langle VPVPVP^3VPV\rangle (\Delta E_1)^2$
37	1:2∩3:4:5	$-\langle VP^2VP^3VPV\rangle (\Delta E_1)^3$
38	4:5	$-\langle VPVPVPVP^2VPV\rangle \Delta E_1$
39	1:2∩4:5	$\langle VP^2VPVP^2VPV\rangle (\Delta E_1)^2$
40	1:3∩4:5	$\langle VP^2VP^2VPV\rangle \Delta E_2 \Delta E_1$
41	1:2:3∩4:5	$-\langle VP^3VP^2VPV\rangle (\Delta E_1)^3$
42	2:3∩4:5	$\langle VPVP^2VP^2VPV\rangle (\Delta E_1)^2$

gives also one term;

$$1:4:5:6 \to -\langle VP^4V\rangle \Delta E_3 (\Delta E_1)^2 \tag{60}$$

is a two-terms contraction symmetrical to (55). The remaining one-term contractions joining points 1 and 6 are

$$1:2:3:4:6 \to \langle VP^5V\rangle (\Delta E_1)^3 \Delta E_2, \tag{61}$$

$$1:2:3:5:6 \to \langle VP^5V\rangle (\Delta E_1)^2 \Delta E_2 \Delta E_1, \tag{62}$$

$$1:2:4:5:6 \to \langle VP^5V\rangle \Delta E_1 \Delta E_2 (\Delta E_1)^2, \tag{63}$$

$$1:3:4:5:6 \to \langle VP^5V\rangle \Delta E_2 (\Delta E_1)^3, \tag{64}$$

$$1:2:3:4:5:6 \to -\langle VP^6V\rangle (\Delta E_1)^5. \tag{65}$$

In total we obtain from (50)-(65) the number of terms connected with the interaction between the time points 1 and 6 equal to:

$$14+5+2+2+5+2+1+2+1+1+2+1+1+1+1+1=42. \tag{66}$$

In fact this is a number of the Schrödinger energy terms equal to

$$S_6 = 42. \tag{67}$$

The diagrams corresponding to the terms obtained in (66), or (67), are represented in **Figure 3**. The calculation of the energy terms corresponding to diagrams entering (67) reduces the unknown number of the energy terms for $N = 7$ to

$$S_7 - 2 \times S_6 = 132 - 84 = 48. \tag{68}$$

In order to present the terms (68)—see **Figure 4**—we take into account that the "interaction" of the time point 6 with point 1 can be extended by the "interaction" of point 2 with 6 in the absence of the interaction with point 1. This provides us with contraction

$$2:6 \to -\langle VPVP^2V\rangle \Delta E_4; \tag{69}$$

because of $S_4 = 5$ this formula contains five Schrödinger terms.

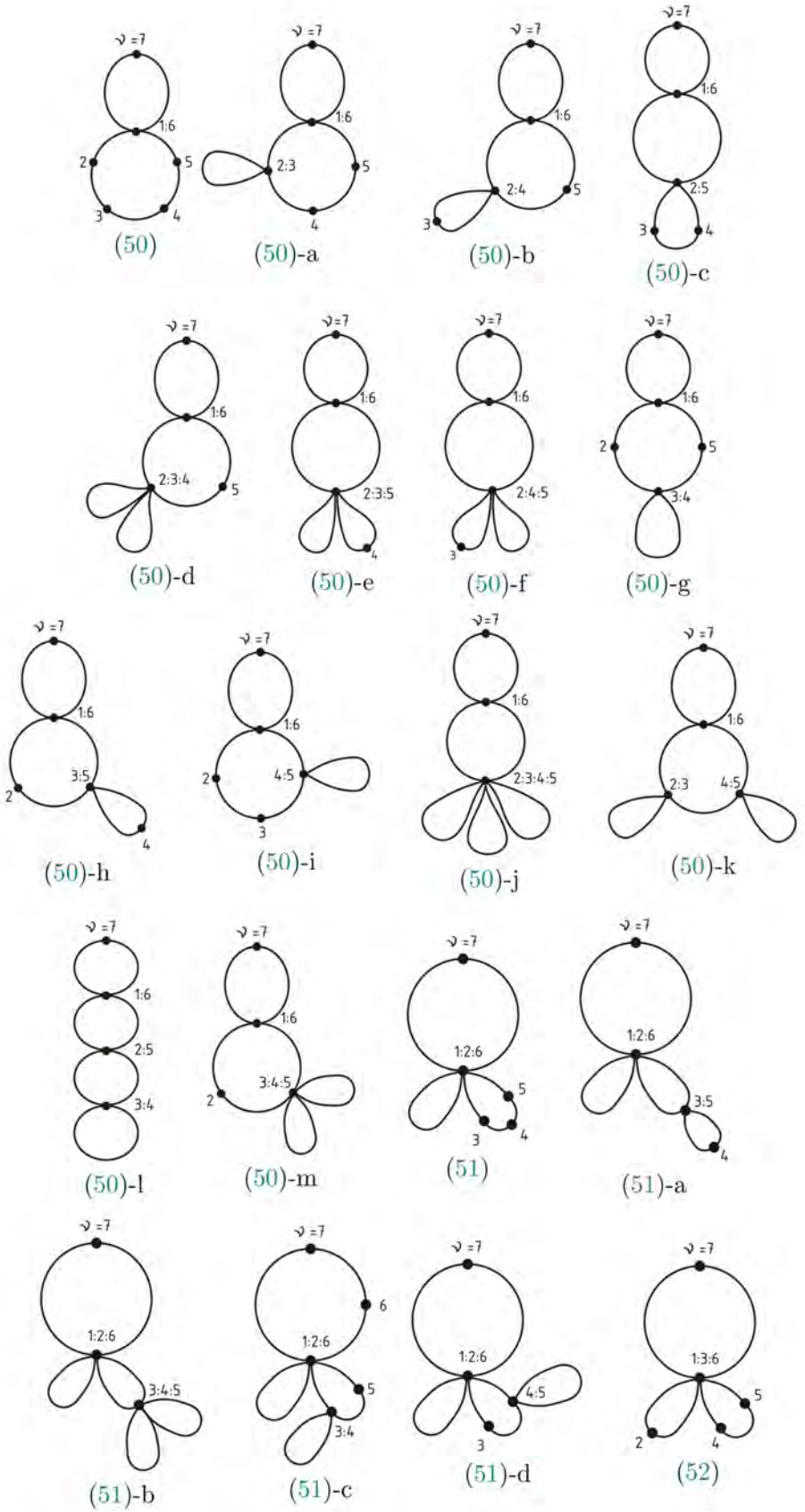
ν =7
1:6
2:5
3:4
(50)-l
ν =7
1:6
3:4:5
2
(50)-m
ν =7
1:2:6
5
3
4
(51)
ν =7
1:2:6
3:5
4
(51)-a
ν =7
1:2:6
3:4:5
(51)-b
ν =7
6
1:2:6
5
3:4
(51)-c
ν =7
1:2:6
4:5
3
(51)-d
ν =7
1:3:6
5
2
4
(52)

(a)

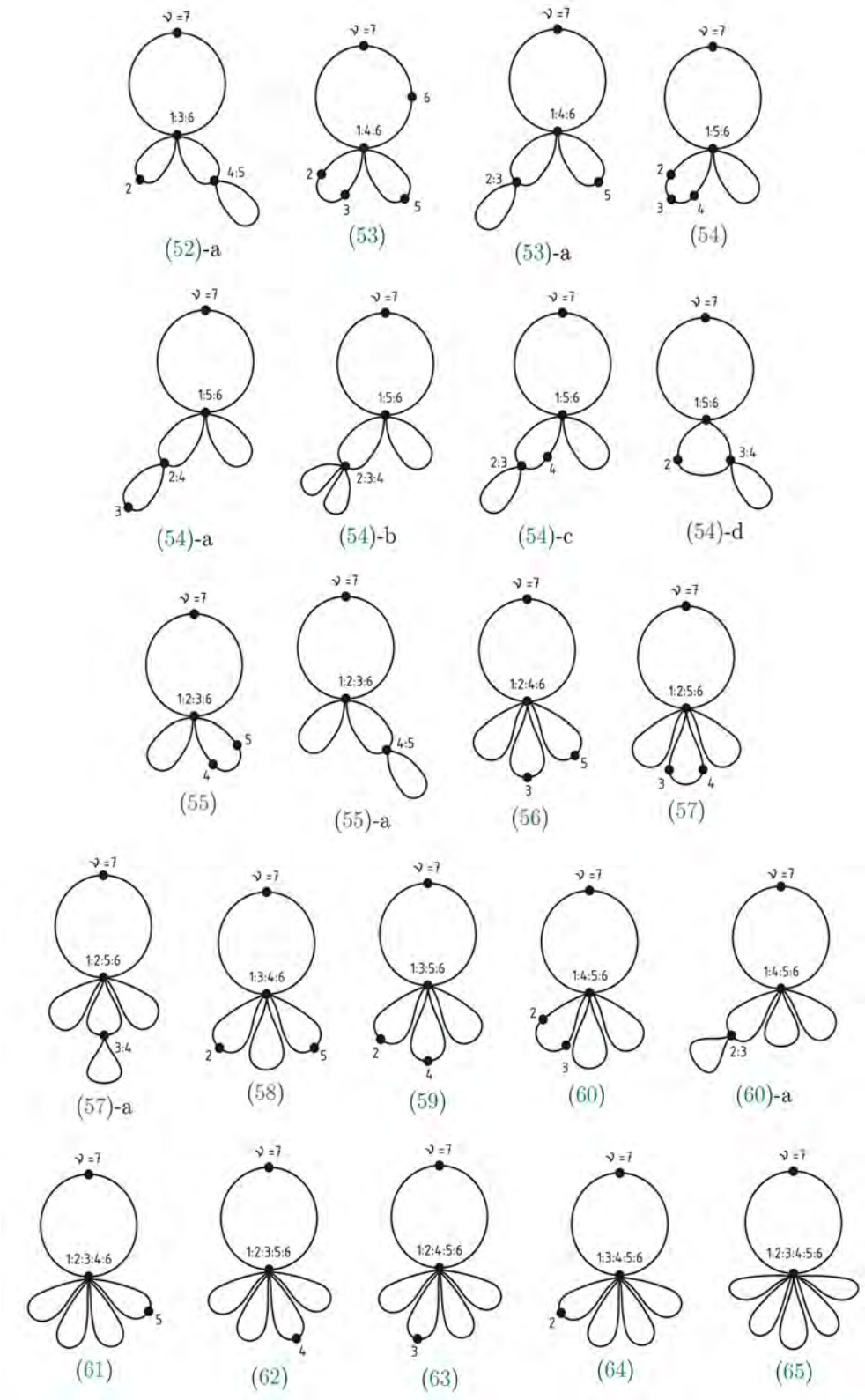

(b)

Figure 3. Diagrams representing the energy perturbation terms for $N = 7$ obtained from contractions of the time points 1 and 6, as well as contractions done together with the points between 1 and 6. The numbers below diagrams refer to the formulae in the text.

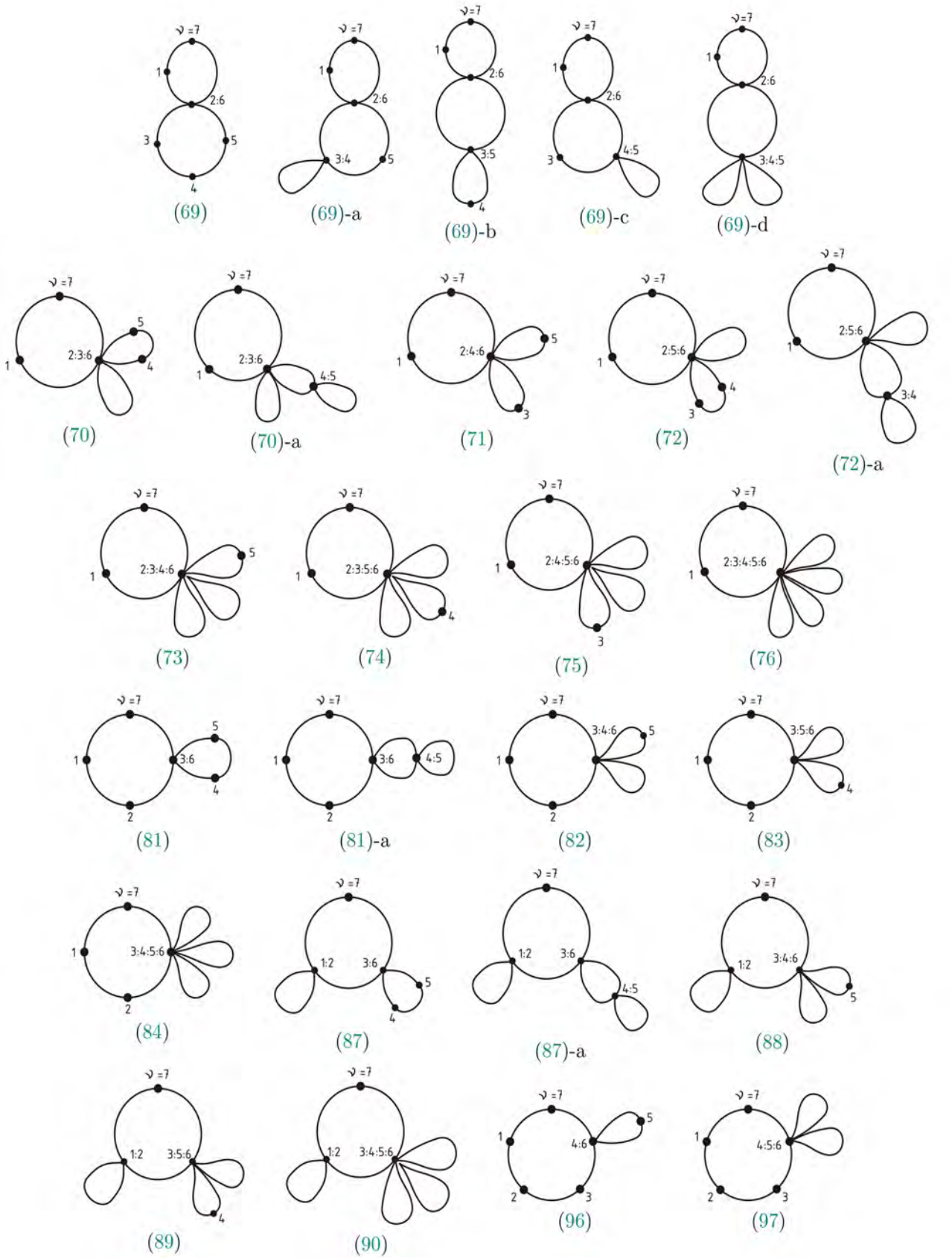
ν =7
1
2:6
3
5
4
(69)
ν =7
1
2:6
3:4
5
(69)-a
ν =7
1
2:6
3:5
4
(69)-b
ν =7
1
2:6
3
4:5
(69)-c
ν =7
1
2:6
3:4:5
(69)-d
ν =7
1
2:3:6
5
4
(70)
ν =7
1
2:3:6
4:5
(70)-a
ν =7
1
2:4:6
5
3
(71)
ν =7
1
2:5:6
4
3
(72)
ν =7
1
2:5:6
3:4
(72)-a
ν =7
1
2:3:4:6
5
(73)
ν =7
1
2:3:5:6
4
(74)
ν =7
1
2:4:5:6
3
(75)
ν =7
1
2:3:4:5:6
(76)
ν =7
1
3:6
5
4
2
(81)
ν =7
1
3:6
4:5
2
(81)-a
ν =7
1
3:4:6
5
2
(82)
ν =7
1
3:5:6
4
2
(83)
ν =7
1
3:4:5:6
2
(84)
ν =7
1:2
3:6
5
4
(87)
ν =7
1:2
3:6
4:5
(87)-a
ν =7
1:2
3:4:6
5
(88)
ν =7
1:2
3:5:6
4
(89)
ν =7
1:2
3:4:5:6
(90)
ν =7
1
4:6
5
2
3
(96)
ν =7
1
4:5:6
2
3
(97)

(a)

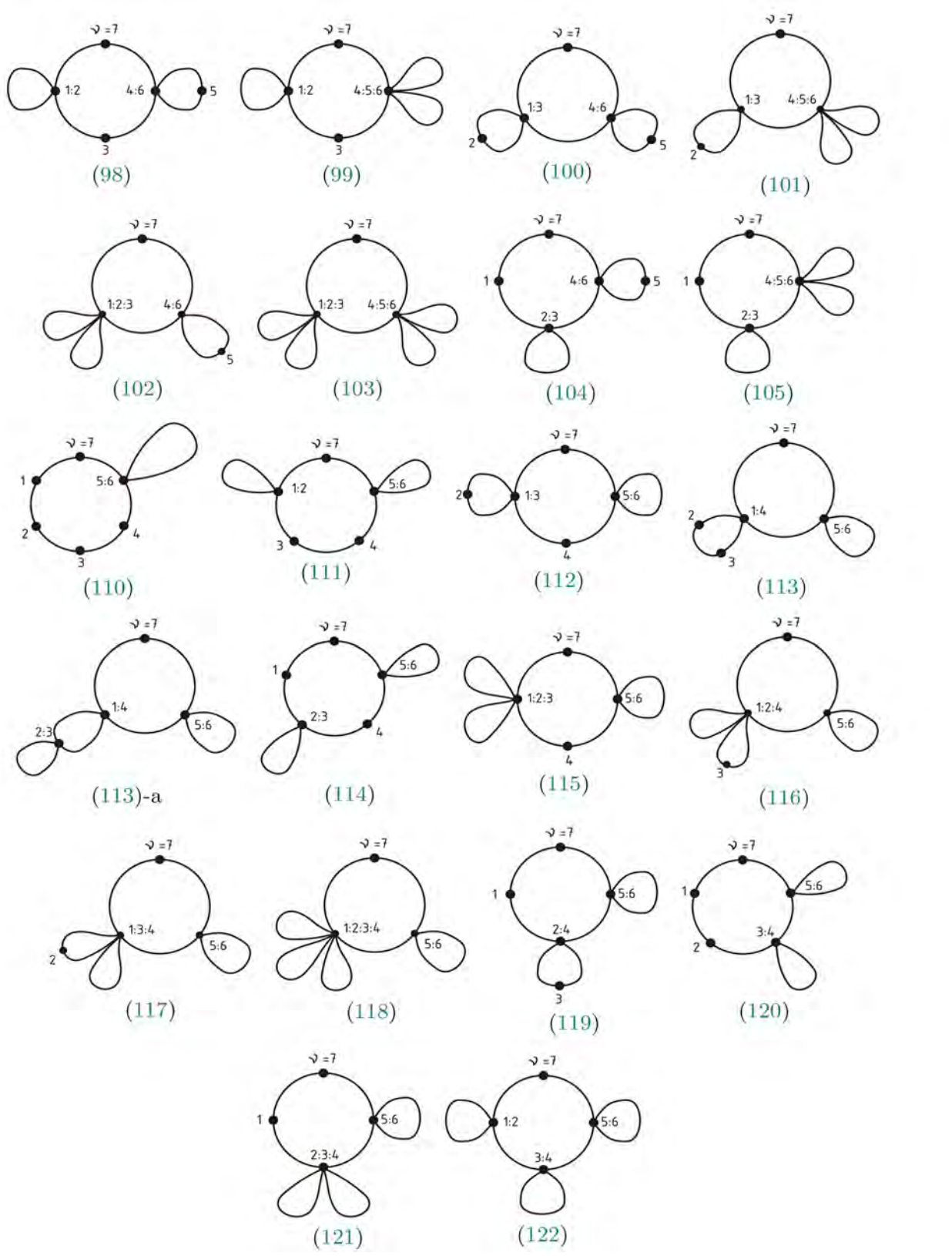

(b)

Figure 4. Diagrams representing the energy perturbation terms for $N = 7$ which did not enter **Figure 2** and **Figure 3**. Numbers below diagrams refer to the formulae presented in the text.

If beyond of (69) we take into account also all possible contractions of the time points which are between 2 and 6 (see Figure 4), we obtain

$$2:3:6 \to \left\langle VPVP^3V \right\rangle \Delta E_1 \Delta E_3 \tag{70}$$

which contributes two energy terms,

$$2:4:6 \to \left\langle VPVP^3V \right\rangle \left(\Delta E_2\right)^2 \tag{71}$$

which gives a single energy term,

$$2:5:6 \to \left\langle VPVP^3V \right\rangle \Delta E_3 \Delta E_1 \tag{72}$$

which is again a combination of two terms, and

$$2:3:4:6 \to -\left\langle VPVP^4V \right\rangle \left(\Delta E_1\right)^2 \Delta E_2, \tag{73}$$

$$2:3:5:6 \to -\left\langle VPVP^4V \right\rangle \Delta E_1 \Delta E_2 \Delta E_1, \tag{74}$$

$$2:4:5:6 \to -\left\langle VPVP^4V \right\rangle \Delta E_2 \left(\Delta E_1\right)^2, \tag{75}$$

$$2:3:4:5:6 \to \left\langle VPVP^5V \right\rangle \left(\Delta E_1\right)^4, \tag{76}$$

which are all single energy terms. Together with contraction $2:6$ in (69) all interactions containing points 2 and 6 [equations (69)-(76)] give the number of energy terms equal to

$$5+2+1+2+1+1+1+1=14=S_5. \tag{77}$$

In effect the lacking number of diagrams for $N=7$ is reduced to

$$S_7 - 2\times S_6 - S_5 = 48-14=34. \tag{78}$$

A new "interaction" which is between points 3 and 6, symbolized by

$$3:6, \tag{79}$$

but involving also contractions with the points 4 and 5 placed between 3 and 6, gives

$$S_4 = 5 \tag{80}$$

new energy diagrams corresponding to contractions

$$3:6 \to -\left\langle VPVPVP^2V \right\rangle \Delta E_3, \tag{81}$$

$$3:4:6 \to \left\langle VPVPVP^3V \right\rangle \Delta E_1 \Delta E_2, \tag{82}$$

$$3:5:6 \to \left\langle VPVPVP^3V \right\rangle \Delta E_2 \Delta E_1, \tag{83}$$

$$3:4:5:6 \to -\left\langle VPVPVP^4V \right\rangle \left(\Delta E_1\right)^3. \tag{84}$$

In fact the formulae (81)-(84) give

$$2+1+1+1=5=S_4 \tag{85}$$

energy terms.

But this situation ignores a mutual relation between points 1 and 2 being outside contraction $3:6$. This relation is represented by contraction of 1 and 2 given in (86) below. In effect we have two possibilities which have to be

considered: one is when 1 and 2 remain free, but another one is when 1 and 2 "interact" in the form of contraction

$$1:2 \tag{86}$$

independently of the presence of (79) and (80). In result the number of diagrams represented by (80) should be taken twice: once it should be combined with free time points 1 and 2 [the terms (81)-(84)], otherwise it should be combined with the "interaction" of 1 and 2 given by contraction $1:2$. In this second case the following 5 energy terms are obtained:

$$1:2\bigcap 3:6 \to \left\langle VP^2VP^2V\right\rangle \Delta E_1\Delta E_3, \tag{87}$$

$$1:2\bigcap 3:4:6 \to -\left\langle VP^2VP^3V\right\rangle \left(\Delta E_1\right)^2 \Delta E_2, \tag{88}$$

$$1:2\bigcap 3:5:6 \to -\left\langle VP^2VP^3V\right\rangle \Delta E_1\Delta E_2\Delta E_1, \tag{89}$$

$$1:2\bigcap 3:4:5:6 \to \left\langle VP^2VP^4V\right\rangle \left(\Delta E_1\right)^4, \tag{90}$$

if we note that ΔE_3 in (87) combines two terms.

The number of diagrams still necessary to calculate is

$$S_7 - 2\times S_6 - S_5 - 2\times S_4 = 34 - 10 = 24. \tag{91}$$

The last but one step is "interaction" of point 6 with point 4, namely

$$4:6. \tag{92}$$

Since point 5 should not be isolated from the "interaction" with 4 and 6, still one contraction, namely

$$4:5:6, \tag{93}$$

has to be considered together with (92). But because the points 1, 2, and 3 are remaining free beyond of 4 and 6, the two energy diagrams which correspond respectively to (92) and (93) should combine with situations due to the presence of 1, 2, and 3. These points give $S_4 = 5$ cases:

$$1,2,3 \text{ are free} \tag{94}$$

and four contractions of (94) which are

$$1:2,\quad 1:3,\quad 1:2:3 \quad \text{and} \quad 2:3. \tag{95}$$

The five situations given in (94) and (95) combined with two cases presented in (92) and (93) give in total

$$2\times S_4 = 10 \tag{96}$$

of new energy terms belonging to $N = 7$. These are:

$$4:6 \to -\left\langle VPVPVPVP^2V\right\rangle \Delta E_2, \tag{97}$$

$$4:5:6 \to \left\langle VPVPVPVP^3V\right\rangle \left(\Delta E_1\right)^2, \tag{98}$$

$$1:2\bigcap 4:6 \to \left\langle VP^2VPVP^2V\right\rangle \Delta E_1\Delta E_2, \tag{99}$$

$$1:2\bigcap 4:5:6 \to -\left\langle VP^2VPVP^3V\right\rangle \left(\Delta E_1\right)^3, \tag{100}$$

$$1:3\bigcap 4:6 \to \left\langle VP^2VP^2V\right\rangle \left(\Delta E_2\right)^2, \tag{101}$$

$$1:3\bigcap 4:5:6\to -\left\langle VP^2VP^3V\right\rangle \Delta E_2\left(\Delta E_1\right)^2, \tag{102}$$

$$2:3\bigcap 4:6\to \left\langle VPVP^2VP^2V\right\rangle \Delta E_1\Delta E_2, \tag{103}$$

$$2:3\bigcap 4:5:6\to -\left\langle VPVP^2VP^3V\right\rangle \left(\Delta E_1\right)^3, \tag{104}$$

$$1:2:3\bigcap 4:6\to -\left\langle VP^3VP^2V\right\rangle \left(\Delta E_1\right)^2\Delta E_2, \tag{105}$$

$$1:2:3\bigcap 4:5:6\to \left\langle VP^3VP^3V\right\rangle \left(\Delta E_1\right)^4. \tag{106}$$

The effect of (92)-(106) is reduction of the unknown terms to the number

$$S_7-2\times S_6-S_5-4\times S_4=24-10=14. \tag{107}$$

But the number 14 in (107) can be obtained from a single contraction which remains to be considered, namely that between 6 and 5:

$$5:6. \tag{108}$$

For in case of (108) four time points remain free on the scale: 1, 2 , 3 and 4. Their combinations are:

$$1,2,3, \text{ and } 4 \text{ remain free} \tag{109}$$

or the points give contractions:

$$\begin{gathered}1:2,\quad 1:3,\quad 1:4,\quad 2:3,\quad 2:4,\quad 3:4,\\ 1:2:3,\quad 1:2:4,\quad 1:3:4,\quad 2:3:4,\\ 1:2:3:4,\quad 1:2\bigcap 3:4,\quad 1:4\bigcap 2:3.\end{gathered} \tag{110}$$

The effect of (109) and (110) is that they give precisely $S_5=14$ configurations of the time points 1, 2, 3 and 4 necessary to construct the remainder of energy diagrams dictated by the result in (107). The energy terms due to (108)-(110) are:

$$5:6\to -\left\langle VPVPVPVPVP^2V\right\rangle \Delta E_1, \tag{111}$$

$$1:2\bigcap 5:6\to \left\langle VP^2VPVPVP^2V\right\rangle \left(\Delta E_1\right)^2, \tag{112}$$

$$1:3\bigcap 5:6\to \left\langle VP^2VPVP^2V\right\rangle \Delta E_2\Delta E_1, \tag{113}$$

$$1:4\bigcap 5:6 \text{ and } 1:4\bigcap 2:3\bigcap 5:6\to \left\langle VP^2VP^2V\right\rangle \Delta E_3\Delta E_1, \tag{114}$$

which is a combination of two energy terms,

$$2:3\bigcap 5:6\to \left\langle VPVP^2VPVP^2V\right\rangle \left(\Delta E_1\right)^2, \tag{115}$$

$$1:2:3\bigcap 5:6\to -\left\langle VP^3VPVP^2V\right\rangle \left(\Delta E_1\right)^3, \tag{116}$$

$$1:2:4\bigcap 5:6\to -\left\langle VP^3VP^2V\right\rangle \Delta E_1\Delta E_2\Delta E_1, \tag{117}$$

$$1:3:4\bigcap 5:6\to -\left\langle VP^3VP^2V\right\rangle \Delta E_2\left(\Delta E_1\right)^2, \tag{118}$$

$$1:2:3:4\bigcap 5:6\to \left\langle VP^4VP^2V\right\rangle \left(\Delta E_1\right)^4, \tag{119}$$

$$2:4\bigcap 5:6\to \left\langle VPVP^2VP^2V\right\rangle \Delta E_2\Delta E_1, \tag{120}$$

$$3:4\bigcap 5:6\to \left\langle VPVPVP^2VP^2V\right\rangle \left(\Delta E_1\right)^2, \tag{121}$$

$$2:3:4\cap 5:6\to -\left\langle VPVP^3VP^2V\right\rangle\left(\Delta E_1\right)^3, \tag{122}$$

$$1:2\cap 3:4\cap 5:6\to -\left\langle VP^2VP^2VP^2V\right\rangle\left(\Delta E_1\right)^3. \tag{123}$$

In Table 2 we collect the Schrödinger terms belonging to $N = 7$ which are due to the time contractions given below (78).

In effect the total value of the Schrödinger perturbation energy belonging to $N = 7$ is given by a sum of: (a) the terms present in Table 1, (b) the terms given in formulae (50)-(65), (c) the terms in the formulae (69)-(76), (d) the terms collected in Table 2.

In the next section we present the balance of the Huby-Tong number of the perturbation energy terms with the total number of energy diagrams obtained—for a given N—from contractions of the time points on the circular scale.

7. Balance of the Number of Perturbation Energy Terms Obtained from the Huby-Tong Formula and within the Framework of the Present Theory

Let us take the perturbation orders $N = 8$, 9 and 10 for which the number of the Schrödinger perturbation terms calculated from the Huby-Tong formula [see (15)] is respectively equal to:

$$S_8 = \frac{(2\times 8-2)!}{8!7!} = 429, \tag{124}$$

$$S_9 = \frac{(2\times 9-2)!}{9!8!} = 1430, \tag{125}$$

$$S_{10} = \frac{(2\times 10-2)!}{10!9!} = 4862. \tag{126}$$

These results will be compared with the number of time diagrams obtained on the circular scale taken for the same N as quoted above. The calculations performed with the aid of the circular scale are of a recurrent character which means that the knowledge of diagrams for $N - 1$, $N - 2$, etc., is used for calculation of the diagrams characteristic for N. The general rule is the same as presented in the preceding Section: we consider for a given N the time scale characteristic by the presence of the number of $N - 1$ time points suitable to contractions and add one time point to that ensemble.

Beginning with $N = 8$ we have 7 time points "active" on the scale because the 8th point is the beginning-end point which cannot participate in contractions. The time point 7 is new for the "active" part of the scale for $N = 7$ which had only 6 points of an active kind; see Section 6. The presence of point 7 gives

$$S_7 = 132 \tag{127}$$

new diagrams valid for $N = 8$ on condition a modification of the diagrams energy by PV present in formula (46) is taken into account.

The next set of S_7 diagrams participating in calculation of the terms belonging to $N = 8$ is obtained from contraction

Table 2. The 34 Schrödinger energy terms belonging to $N = 7$ due to the time contractions presented below the formula (78). Each of expressions having ΔE_3 combines two Schrödinger terms.

$-\langle VPVPVP^2V\rangle\Delta E_3$	[see (81)],
$\langle VPVPVP^3V\rangle\Delta E_1\Delta E_2$	[see (82)],
$\langle VPVPVP^3V\rangle\Delta E_2\Delta E_1$	[see (83)],
$-\langle VPVPVP^2V\rangle(\Delta E_1)^3$	[see (84)],
$\langle VP^2VP^2V\rangle\Delta E_1\Delta E_3$	[see (87)],
$-\langle VP^2VP^3V\rangle(\Delta E_1)^2\Delta E_2$	[see (88)],
$-\langle VP^2VP^3V\rangle\Delta E_1\Delta E_2\Delta E_1$	[see (89)],
$\langle VP^2VP^4V\rangle(\Delta E_1)^4$	[see (90)],
$-\langle VPVPVPVP^2V\rangle\Delta E_2$	[see (97)],
$\langle VPVPVPVP^3V\rangle(\Delta E_1)^2$	[see (98)],
$\langle VP^2VPVP^2V\rangle\Delta E_1\Delta E_2$	[see (99)],
$-\langle VP^2V\ PVP^3V\rangle(\Delta E_1)^3$	[see (100)],
$\langle VP^2VP^2V\rangle(\Delta E_2)^2$	[see (101)],
$-\langle VP^2VP^3V\rangle\Delta E_2(\Delta E_1)^2$	[see (102)],
$\langle VPVP^2VP^2V\rangle\Delta E_1\Delta E_2$	[see (103)],
$-\langle VPVP^2VP^3V\rangle(\Delta E_1)^3$	[see (104)],
$-\langle VP^3VP^2V\rangle(\Delta E_1)^2\Delta E_2$	[see (105)],
$\langle VP^3VP^3V\rangle(\Delta E_1)^4$	[see (106)],
$-\langle VPVPVPVPVP^2V\rangle\Delta E_1$	[see (111)],
$\langle VP^2VPVPVP^2V\rangle(\Delta E_1)^2$	[see (112)],
$\langle VP^2VPVP^2V\rangle\Delta E_2\Delta E_1$	[see (113)],
$\langle VP^2VP^2V\rangle\Delta E_3\Delta E_1$	[see (114)],
$\langle VPVP^2VPVP^2V\rangle(\Delta E_1)^2$	[see (115)],
$-\langle VP^3VPVP^2V\rangle(\Delta E_1)^3$	[see (116)],
$-\langle VP^3VP^2V\rangle\Delta E_1\Delta E_2\Delta E_1$	[see (117)],
$-\langle VP^3VP^2V\rangle\Delta E_2(\Delta E_1)^2$	[see (118)],
$\langle VP^4VP^2V\rangle(\Delta E_1)^4$	[see (119)],
$\langle VPVP^2VP^2V\rangle\Delta E_2\Delta E_1$	[see (120)],
$\langle VPVPVP^2VP^2V\rangle(\Delta E_1)^2$	[see (121)],
$-\langle VPVP^3VP^2V\rangle(\Delta E_1)^3$	[see (122)],
$-\langle VP^2VP^2VP^2V\rangle(\Delta E_1)^3$	[see (123)].

$$1:7 \tag{128}$$

done together with contractions of the time points between 1 and 7 (namely 2, 3, 4 , 5 and 6).

Other components of S_8 are given by

$$S_6 = 42 \tag{129}$$

diagrams due to contraction $2:7$ combined with points 3, 4 , 5 and 6 enclosed between 2 and 7. Only one set of terms equal to (129) is obtained in this way because the only free time point 1 on the scale does not combine with any other time point.

The situation becomes different for contraction

$$3:7 \tag{130}$$

which—together with points 4, 5, and 6—can give

$$S_5 = 14 \tag{131}$$

diagrams for any arrangement of points 1 and 2. Since two such arrangements are possible (for contracted and free pair see Sec. 6), so in fact contraction (130) gives $2S_5 = 28$ energy terms.

The contraction

$$4:7, \tag{132}$$

together with its associates, gives only $S_4 = 5$ terms but these terms apply to $S_5 = 5$ situations dictated by the arrangement of the time points 1, 2, and 3. In effect $5 \times 5 = 25$ energy terms are obtained.

The remaining situations are given by contractions

$$5:7 \tag{133}$$

and

$$6:7. \tag{134}$$

The contraction in (133) has its associate in contraction

$$5:6:7, \tag{133a}$$

so two diagrams given by (133) and (133a) should be multiplied by

$$S_5 = 14$$

arrangements of the time points 1, 2, 3, and 4 which are outside of contractions (133) and (133a). This gives 2×14 new energy terms.

Finally a single contraction (134) corresponds to

$$S_6 = 42 \tag{135}$$

arrangements of the points 1, 2, 3, 4, and 5 outside $6:7$ giving the number of energy terms equal to S_6 in (135).

The total number of terms for $N = 8$ due to contractions taken into account between the formulae (127) and (135) becomes:

$$\begin{aligned} &2 \times S_7 + S_6 + 2 \times S_5 + S_4 \times S_4 + 2 \times S_5 + S_6 \\ &= 264 + 42 + 28 + 25 + 28 + 42 = 429 \end{aligned} \tag{136}$$

which is the result equal to that given in (124). This implies a complete number of necessary contractions considered in the $N = 8$ case.

Calculations similar to those for $N = 8$ can be done for other N, too. The components entering them can be arranged in a more transparent way than in

the case of (136); see Table 3. The results fully agree with those obtained in (125), (126) and those calculated from (15).

8. Summary

The present paper considers the well-known Schrödinger perturbation series for energy of a non-degenerate quantum state; the applied perturbation potential does not depend on time.

A usual problem of the Schrödinger perturbation theory is that their formulae are derived in a tediously obtainable and complicated way. This concerns especially the case when a large order N of the perturbation energy is examined. A difficulty concerns also the Schrödinger perturbation calculation developed with the aid of the Feynman diagrams. Here large N imply a huge number of diagrams which have to be derived and considered in calculations; in effect the number of the Feynman diagrams can exceed by several orders of times the number of kinds of the perturbation terms entering the Schrödinger theory [3]. It should be noted that the scale of time applied by Feynman is a conventional scale extended from minus to plus infinity; see Section 2.

The paper demonstrates that a difficulty connected with construction of the Schrödinger perturbation terms can be overcomed with the aid of a circular scale of time. According to Leibniz, time is a successive sequence of events, or sets of events. In such a picture the time intervals between separate events, or their sets, play a secondary role. The history of a system is built up by following the development in time of the system configurations.

In case of the Schrödinger theory the time events are assumed to represent a gradual change of a quantum state upon the action of the perturbation potential. The events are successive collisions of the quantum system with that potential. The number of collisions is grouped in sets according to the size of the perturbation orders N: the N points of time are belonging to any set. These points are assumed to be arranged successively along a topological circle. In each set of N points one of the points does represent the beginning-end point of the circular scale belonging to that N.

A result which seems to be important is that all kinds of the Schrödinger perturbation terms can be obtained—almost automatically, i.e. without calculations—from the arrangements of the time points present on the circle. To this purpose a special kind of interactions between the time points—called also contractions—should be assumed. A general rule concerning contractions is that the time loops created by them do not cross. In effect, the number of diagrams obtained due to contractions for a given N agrees precisely with the number of kinds of the Schrödinger perturbation terms for that N.

The main aim of the paper became to present a recursive process to obtain all kinds of the Schrödinger perturbation terms belonging to a given N. This means we assume that the terms characteristic for $N-1, N-2, N-3, \cdots$ are known, and from them—and the points arrangement on the circular scale—all terms for N can be obtained. The main feature of the process is to take properly into

Table 3. Number of the perturbation terms for different N obtained from the Huby-Tong formula in equation (15) compared with the terms number derived on the basis of the present theory; see also [17].

$N=2$:	$S_1S_1=1=S_2$
$N=3$:	$S_1S_2+S_2S_1=1+1=2=S_3$
$N=4$:	$S_1S_3+S_2S_2+S_3S_1=2+1+2=5=S_4$
$N=5$:	$S_1S_4+S_2S_3+S_3S_2+S_4S_1=5+2+2+5=14=S_5$
$N=6$:	$S_1S_5+S_2S_4+S_3S_3+S_4S_2+S_5S_1=14+5+4+5+14=42=S_6$
$N=7$:	$S_1S_6+S_2S_5+S_3S_4+S_4S_3+S_5S_2+S_6S_1$ $=42+14+10+10+14+42=132=S_7$
$N=8$:	$S_1S_7+S_2S_6+S_3S_5+S_4S_4+S_5S_3+S_6S_2+S_1S_1$ $=2\times(132+42+28)+25=429=S_8$
$N=9$:	$S_1S_8+S_2S_7+S_3S_6+S_4S_5+S_5S_4+S_6S_3+S_7S_2+S_8S_1$ $=2\times(429+132+84+70)=2\times715=1430=S_9$
$N=10$:	$S_1S_9+S_2S_8+S_3S_7+S_4S_6+S_5S_5+S_6S_4+S_7S_3+S_8S_2+S_9S_1$ $=2\times(1430+429+264+210)+196=4862=S_{10}$

account the fact that any time point present on the scale—beyond of the beginning-end point—should "interact" with other time points on that scale in a way characteristic for the contraction properties possessed by the time points on the scale.

In result we find that a tedious process of solving the perturbed Schrödinger equation—established in an ordinary three-dimensional space—can be replaced, with the aid of a new scale of time, by a very simple calculation of the Schrödinger energy solution.

References

[1] Schrödinger, E. (1926) *Annalen der Physik*, **80**, 437. https://doi.org/10.1002/andp.19263851302

[2] Schiff, L.I. (1955) Quantum Mechanics. 2nd Edition, McGraw-Hill, New York.

[3] Mattuck, R.D. (1976) A Guide to Feynman Diagrams in a Many-Body Problem. 2nd Edition, McGraw-Hill, New York.

[4] Feynman, R.P. (1966) *Science*, **153**, 699. https://doi.org/10.1126/science.153.3737.699

[5] Leibniz, G.W. (1924) Hauptschriften zur Grundlagen der Philosophie. Vol. 1, Leipzig.

[6] Rescher, N. (2013) On Leibniz. University of Pittsburgh Press. https://doi.org/10.2307/j.ctt7zw8g2

[7] Olszewski, S. (1991) *Zeitschrift fur Naturforschung*, **46A**, 313.

[8] Olszewski, S. and Kwiatkowski, T. (1998) *Computers in Chemistry*, **22**, 445. https://doi.org/10.1016/S0097-8485(98)00023-0

[9] Olszewski, S. (2003) *Trends in Physical Chemistry*, **9**, 69.

[10] Olszewski, S. (2013) *Quantum Matter*, **2**, 481. https://doi.org/10.1166/qm.2013.1085

[11] Olszewski, S. (2014) *Journal of Modern Physics*, **5**, 1502;

Olszewski, S. (2017) *Journal of Modern Physics*, **8**, 1650.

[12] Olszewski, S. (2014) *Journal of Quantum Information Science*, **4**, 269. https://doi.org/10.4236/jqis.2014.44022

[13] Olszewski, S. (2015) *Quantum Matter*, **4**, 5523.

[14] Olszewski, S. (2004) *Studia Philosophae Christianae*, **40**, 57.

[15] Huby, R. (1961) *Proceedings of the Physical Society* (*London*), **78**, 529. https://doi.org/10.1088/0370-1328/78/4/306

[16] Tong, B.Y. (1962) *Proceedings of the Physical Society* (*London*), **80**, 1101. https://doi.org/10.1088/0370-1328/80/5/308

[17] Olszewski, S. (2011) *Journal of Quantum Information Science*, **1**, 142. https://doi.org/10.4236/jqis.2011.13020

Appendix: Perturbation Energy Calculation Due to the Present Method Outlined for Low N (from $N = 1$ to $N = 6$)

We begin with the result that for $N = 1$ the perturbation energy is

$$\Delta E_1 = \langle V \rangle = \langle n | V^{\text{per}} | n \rangle, \tag{A1}$$

and the loop of time is a topological circle with a single time point on it [7]-[14]. Consequently to the rule outlined in the present paper [see (46)] for $N = 2$ we have

$$\Delta E_2 = \langle VPV \rangle. \tag{A2}$$

The presence of a single P in (2) indicates a single infinite summation over the unperturbed quantum states with exclusion of the perturbed state n; see (28) and (29). The time scale—beyond of the beginning-end point—has only one point on it [7]-[14].

The first step for $N = 3$ is to substitute PV at the end of the expression on the right of (A2). We obtain the first (positive) term for ΔE_3 which is a double sum over the quantum states:

$$\langle VPVPV \rangle. \tag{A3}$$

But beyond of the beginning-end point on the scale we have still two free time points on it, say 1 and 2. They should contract together giving the next term of ΔE_3 equal to

$$-\langle VP^2V \rangle \langle V \rangle; \tag{A4}$$

this term is a single sum over the unperturbed states. The ΔE_3 is

$$\Delta E_3 = \langle VPVPV \rangle - \langle VP^2V \rangle \langle V \rangle. \tag{A5}$$

In order to calculate the first two terms for $N = 4$ we increase the term in (A3) again by PV at the brackets end, and the same we are doing with the larger bracket term in (A4). We obtain two terms belonging to ΔE_4:

$$\langle VPVPVPV \rangle \tag{A6}$$

and

$$-\langle VP^2VPV \rangle \langle V \rangle = -\langle VP^2VPV \rangle \Delta E_1. \tag{A7}$$

A suplementary point 3 which comes for $N = 4$ can contract with points 1 and 2 entering the scale already for $N = 3$. The interaction between 3 and 1 gives two contractions:

$$1:3, \quad 1:2:3, \tag{A8}$$

whereas the interaction between 3 and 2 alone is reduced to contraction

$$2:3. \tag{A9}$$

The energy terms representing (A8) are respectively

$$-\langle VP^2V \rangle \langle VPV \rangle = -\langle VP^2V \rangle \Delta E_2 \tag{A10}$$

and

$$\langle VP^3V \rangle \langle V \rangle \langle V \rangle = \langle VP^3V \rangle (\Delta E_1)^2 \tag{A11}$$

and the term represented by (A9) is

$$-\langle VPVP^2V\rangle\langle V\rangle = -\langle VPVP^2V\rangle\Delta E_1. \tag{A12}$$

Terms (A6), (A7) and (A10)-(A12) give together $S_4 = 5$ terms which is the number of the Schrödinger energy terms predicted by Huby and Tong [15] [16]. The sum of these terms gives:

$$\begin{aligned}\Delta E_4 = {} & \langle VPVPVPV\rangle - \langle VP^2VPV\rangle\Delta E_1 - \langle VP^2V\rangle\Delta E_2 \\ & + \langle VP^3V\rangle(\Delta E_1)^2 - \langle VPVP^2V\rangle\Delta E_1.\end{aligned} \tag{A13}$$

The first five Schrödinger terms belonging to ΔE_5 are given by modification of (A13). These are:

$$\begin{aligned}&\langle VPVPVPVPV\rangle,\ -\langle VP^2VPVPV\rangle\Delta E_1,\ -\langle VP^2VPV\rangle\Delta E_2,\\ &\langle VP^3VPV\rangle(\Delta E_1)^2 \text{ and } \langle -VPVP^2VPV\rangle\Delta E_1.\end{aligned} \tag{A14}$$

The remaining nine terms of ΔE_5 come, first, from five contractions of a supplementary point 4 with point 1 and points between 1 and 4:

$$1:4,\quad 1:2:4,\quad 1:3:4,\quad 1:2:3:4,\quad 1:4\bigcap 2:3. \tag{A15}$$

They give respectively the five terms

$$-\langle VP^2V\rangle\Delta E_3,\ \langle VP^3V\rangle\Delta E_1\Delta E_2,\ \langle VP^3V\rangle\Delta E_2\Delta E_1,\ -\langle VP^4V\rangle(\Delta E_1)^3, \tag{A15a}$$

since the first term is due to combination of 2 terms, namely these given by the first and last contraction expression in (A15).

Other Schrödinger terms are due to contraction between points 2 and 4:

$$2:4,\quad 2:3:4; \tag{A16}$$

and between points

$$3:4. \tag{A17}$$

The last contraction leaves points 1 and 2 as free to contract together, so (A17) gives in fact two kinds of the Schrödinger terms: one term for uncontracted 1 and 2, and one for the contracted case. In effect we have four terms belonging to ΔE_5 coming from (A16) and (A17):

$$\begin{aligned}&-\langle VPVP^2V\rangle\Delta E_2,\ \langle VPVP^3V\rangle(\Delta E_1)^2,\\ &-\langle VPVPVP^2V\rangle\Delta E_1,\ \langle VP^2VP^2V\rangle(\Delta E_1)^2,\end{aligned} \tag{A18}$$

where the last term is due to contraction $1:2\bigcap 3:4$.

The sum of results obtained in (A14)-(A18) gives the 5th order perturbation energy combined by 14 Schrodinger terms:

$$\begin{aligned}\Delta E_5 = {} & \langle VPVPVPVPV\rangle - \langle VP^2VPVPV\rangle\Delta E_1 - \langle VP^2VPV\rangle\Delta E_2 \\ & + \langle VP^3VPV\rangle(\Delta E_1)^2 - \langle VPVP^2VPV\rangle\Delta E_1 \\ & - \langle VP^2V\rangle\Delta E_3 + \langle VP^3V\rangle\Delta E_1\Delta E_2 + \langle VP^3V\rangle\Delta E_2\Delta E_1 \\ & - \langle VP^4V\rangle(\Delta E_1)^3 - \langle VPVP^2V\rangle\Delta E_2 + \langle VPVP^3V\rangle(\Delta E_1)^2 \\ & - \langle VPVPVP^2V\rangle\Delta E_1 + \langle VP^2VP^2V\rangle(\Delta E_1)^2.\end{aligned} \tag{A19}$$

The last perturbation order of energy considered in **Appendix** is $N = 6$. In the first step we obtain 14 components of ΔE_6 by modifying the energy components of ΔE_5. They are obtained by adding PV at the end of the main brackets term:

$$\begin{gathered}
\langle VPVPVPVPVPV\rangle, \\
-\langle VP^2VPVPVPV\rangle\langle V\rangle = -\langle VP^2VPVPVPV\rangle\Delta E_1, \\
-\langle VP^2VPVPV\rangle\langle VPV\rangle = -\langle VP^2VPVPV\rangle\Delta E_2, \\
\langle VP^3VPVPV\rangle(\langle V\rangle)^2 = \langle VP^3VPVPV\rangle(\Delta E_1)^2, \\
-\langle VPVP^2VPVPV\rangle\langle V\rangle = -\langle VPVP^2VPVPV\rangle\Delta E_1, \\
-\langle VP^2VPV\rangle\Delta E_3, \\
\langle VP^3VPV\rangle\Delta E_1\Delta E_2, \\
\langle VP^3VPV\rangle\Delta E_2\Delta E_1, \\
-\langle VP^4VPV\rangle(\Delta E_1)^3, \\
-\langle VPVP^2VPV\rangle\Delta E_2, \\
\langle VPVP^3VPV\rangle(\Delta E_1)^2, \\
-\langle VPVPVP^2VPV\rangle\Delta E_1 \\
\langle VP^2VP^2VPV\rangle(\Delta E_1)^2.
\end{gathered} \tag{A20}$$

The term having ΔE_3 as a multiplier combines two Schrödinger terms.

The next 14 terms belonging to ΔE_6 are different than (A20); they are:

$$\begin{gathered}
1:5 \to -\langle VP^2V\rangle\Delta E_4, \\
1:2:5 \to \langle VP^3V\rangle\Delta E_1\Delta E_3, \\
1:3:5 \to \langle VP^3V\rangle(\Delta E_2)^2, \\
1:4:5 \to \langle VP^3V\rangle\Delta E_3\Delta E_1, \\
1:2:3:5 \to -\langle VP^4V\rangle(\Delta E_1)^2\Delta E_2, \\
1:2:4:5 \to -\langle VP^4V\rangle\Delta E_1\Delta E_2\Delta E_1, \\
1:3:4:5 \to -\langle VP^4V\rangle\Delta E_2(\Delta E_1)^2, \\
1:2:3:4:5 \to \langle VP^5V\rangle(\Delta E_1)^4.
\end{gathered} \tag{A21}$$

The ΔE_4 combines 5 Schrödinger terms and ΔE_3 combines 2 terms. On the other hand, the last 14 terms of ΔE_6 combine with the terms of (A20):

$$\begin{gathered}
2:5 \to -\langle VPVP^2V\rangle\Delta E_3, \\
2:3:5 \to \langle VPVP^3V\rangle\Delta E_1\Delta E_2,
\end{gathered}$$

$$2:4:5\to\left\langle VPVP^3V\right\rangle\Delta E_2\Delta E_1,$$

$$2:3:4:5\to-\left\langle VPVP^4V\right\rangle\left(\Delta E_1\right)^3,$$

$$3:5\to-\left\langle VPVPVP^2V\right\rangle\Delta E_2,$$

$$3:4:5\to\left\langle VPVPVP^3V\right\rangle\left(\Delta E_1\right)^2,$$

$$1:2\bigcap 3:5\to\left\langle VP^2VP^2V\right\rangle\Delta E_1\Delta E_2,$$

$$1:2\bigcap 3:4:5\to-\left\langle VP^2VP^3V\right\rangle\left(\Delta E_1\right)^3,$$

$$4:5\to-\left\langle VPV\ PV\ PV\ P^2V\right\rangle\Delta E_1,$$

$$1:2\bigcap 4:5\to\left\langle VP^2V\ PVP^2V\right\rangle\left(\Delta E_1\right)^2,$$

$$1:3\bigcap 4:5\to-\left\langle VP^2VP^2V\right\rangle\Delta E_2\Delta E_1,$$

$$1:2:3\bigcap 4:5\to-\left\langle VP^3VP^2V\right\rangle\left(\Delta E_1\right)^3,$$

$$2:3\bigcap 4:5\to\left\langle VPV\ P^2VP^2V\right\rangle\left(\Delta E_1\right)^2. \quad \text{(A22)}$$

In total we obtain for $N=6$ from (A20)-(A22) the number of terms

$$14+14+14=42=S_6. \quad \text{(A23)}$$

The perturbation energy ΔE_6 is equal to a sum of the terms presented in (A20)-(A22).

Journal of Modern Physics, 2018, 9, 1522-1544
http://www.scirp.org/journal/jmp
ISSN Online: 2153-120X
ISSN Print: 2153-1196

Conceptual Content of the Generalized Theory of Gravitation of Jefimenko

Andrew Chubykalo, Augusto Espinoza, David Pérez Carlos

Unidad Académica de Física, Universidad Autónoma de Zacatecas, Zacatecas, México
Email: achubykalo@yahoo.com.mx

How to cite this paper: Chubykalo, A., Espinoza, A. and Carlos, D.P. (2018) Conceptual Content of the Generalized Theory of Gravitation of Jefimenko. *Journal of Modern Physics*, **9**, 1522-1544.
https://doi.org/10.4236/jmp.2018.98094

Received: May 24, 2018
Accepted: July 15, 2018
Published: July 18, 2018

Copyright © 2018 by authors and Scientific Research Publishing Inc.
This work is licensed under the Creative Commons Attribution International License (CC BY 4.0).
http://creativecommons.org/licenses/by/4.0/
Open Access

Abstract

In this work, we make a brief exposition of the Jefimenko's generalized theory of gravitation, describe its conceptual content, explain the mathematical apparatus used for the formulations of the theory and present the fundamental equations of the theory. We elucidate the main difference between Newton's original theory of gravitation and the generalized theory of gravitation.

Keywords

Cogravitation, Gravitational Waves, Gravikinetic Field

1. Introduction

It is obvious that the reader will quickly and easily perceive any new scientific theory not from a monograph, but from an article published in a readable scientific journal. Gravitational interaction of celestial bodies is a *very mysterious phenomenon*. It is traditionally attributed (without any further explanation) to the action of forces of "universal gravitation". But where are the threads, the ropes, the chains or the springs that pull celestial bodies one to the other? How does the Earth "know" that it needs to revolve around the Sun? How does it "feel" where the Sun is located? As far as we know there exists no material connection between celestial bodies. But if there is no material connection, does it not mean that gravitational interactions are not a manifestation of the action of forces, but a manifestation of the existence of some heretofore overlooked agent or mechanism? The Jefimenko's generalized theory of gravitation answers this question with perfect clarity.

Therefore, we decided to present the conceptual content of the Jefimenko's generalized theory of gravitation in a possibly short article.

The Jefimenko's generalized theory of gravitation arose from the analogy be-

tween the laws of gravitation and electromagnetism; that is, there existed a second gravitational field called cogravitational field, analogous to the magnetic field. Such analogy was proposed for the first time by Heaviside in a paper "A gravitational and electromagnetic Analogy" [1] published more than a century ago, where he supposed there must exist a second field due to moving masses and acting over moving masses only, called by Jefimenko, cogravitational field (sometimes this field is called Heaviside's field). The Heaviside paper was forgotten for a long time until Jefimenko returned his work and made improvement to the Heaviside's work in two books published and reissued since the 90's decade [2] [3]. Although there are, detractors of the Jefimenko's theory of gravitation[1] (see for example [5]).

The gravitodynamical theory [4] assumes that gravitational interactions are mediated by gravitational and cogravitational force fields.

A gravitational field is a region of space where a mass experience a gravitational force. Quantitatively, a gravitational field is defined in terms of the gravitational field vector $\boldsymbol{g}$ by the same equation by which it is defined in Newton's theory:

$$\boldsymbol{g} = -\boldsymbol{F}/m_t, \tag{1}$$

where $\boldsymbol{F}$ is the force exerted by the gravitational field on a stationary test mass m_t.

A cogravitational field is a region of space where a mass experience a cogravitational force. Quantitatively, a cogravitational field is defined in terms of the cogravitational field vector $\boldsymbol{K}$ by the equation

$$\boldsymbol{F} = m_t(\boldsymbol{v} \times \boldsymbol{K}), \tag{2}$$

where $\boldsymbol{F}$ is the force exerted by the cogravitational field on a stationary test mass m_t, moving with velocity $\boldsymbol{v}$. As noted in Chapter 1 of [3], cogravitational fields are created by moving masses only and act upon moving masses only. It should be noted that the cogravitational field $\boldsymbol{K}$ has not yet been actually observed. However, it is very likely that it can be revealed by the *Gravity Probe B* launched in 2004 by NASA in a polar orbit around the Earth. For the various theoretical considerations demanding the existence of the cogravitational field see O. Jefimenko [2] pp. 80-100.

It is assumed that both gravitational and cogravitational fields propagate in space with finite velocity. This velocity is not yet known, but is believed to be equal to the velocity of light. However, the generalized theory of gravitation is compatible with a propagation velocity of gravitation different from the velocity of light and is not affected by the actual speed with which gravitation propagates. Although we say that gravitational and cogravitational fields "propagate," it is not entirely clear what physical entity actually propagates, since by definition gravitational and cogravitational fields are "region of space". It is conceivable that what actually propagates is some particles that somehow create gravitational

[1]Called by us in a previous work *gravitodynamical theory [4]*.

and cogravitational fields. It is possible that these particles have already been described (see [6]), and it is possible that some of their effects have already been observed (see [7] pp. 137-223). Yet, there is not enough information about these particles for making any definite statement about their existence, nature, or properties.

The generalized theory of gravitation agrees with the principle of causality because, as we shall presently see, in this theory the gravitational and cogravitational fields are expressed in terms of retarded integrals whose integrands are the causative sources of the fields.

The generalized theory of gravitation agrees also with the law of conservation of momentum because according to this theory, gravitational-cogravitational fields are repositories of gravitational-cogravitational field momentum, and because mechanical momentum of a body moving in a gravitational-cogravitational field can be converted into the field momentum and the field momentum can be converted into the mechanical momentum of the body. As the result of this conversion, the sum of the mechanical and field momentum of the combined field-body system is always the same, and the total momentum of the system is thus conserved (see Chapter 8 in [3]).

According to the generalized theory of gravitation, gravitational-cogravitational fields are also repositories of field energy. Kinetic energy of a body moving in a gravitational-cogravitational field can be converted into the energy of the field, and the energy of the field can be converted into kinetic energy of the body. As a result of this conversion, the sum of the mechanical and field energy of the combined field-body system is always the same, and the total energy of the system is thus conserved (see Chapter 8 in [3] for a general proof of energy conservation in such systems).

Obviously, there are not derivations of the formulas presented in this text, because this is a review about the work made by Jefimenko. Also it is important to note that we can obtain all the results by replacing all variables and constants presented in **Table 1** in Maxwell equations. Too, it is important to note that this theory is developed from two standpoints, one of them is to postulate the retarded solutions and making use of the identities from vectorial calculus, we get the Jefimenko equations, and equivalently, we can potulate the system of Jefimenko equations and we get the retarded solutions given by (3) and (4).

2. Fundamental Equations of the Generalized Theory of Gravitation

The two principal equations of the generalized theory of gravitation are the equations for the gravitational field and $\boldsymbol{g}$ the cogravitational field $\boldsymbol{K}$:

$$\boldsymbol{g} = -G\int\left\{\frac{[\varrho]}{r^3}+\frac{1}{r^2c}\left[\frac{\partial\varrho}{\partial t}\right]\right\}\boldsymbol{r}\mathrm{d}V' + \frac{G}{c^2}\int\frac{1}{r}\left[\frac{\partial(\varrho\boldsymbol{v})}{\partial t}\right]\mathrm{d}V' \tag{3}$$

And

Table 1. Corresponding electromagnetic and gravitational-cogravitational symbols and constants.

Electric	Gravitational
q (charge)	m (mass)
ϱ (volume charge density)	ϱ (volume mass density)
σ (surface charge density)	σ (surface mass density)
λ (line charge density)	λ (line mass density)
φ (scalar potential)	φ (scalar potential)
$\boldsymbol{A}$ (vector potential)	$\boldsymbol{A}$ (vector potential)
$\boldsymbol{J}$ (convection current density)	$\boldsymbol{J}$ (mass-current density)
I (electric current)	I (mass current)
$\boldsymbol{E}$ (electric field)	$\boldsymbol{g}$ (gravitational field)
$\boldsymbol{B}$ (magnetic field)	$\boldsymbol{K}$ (cogravitational field)
ε_0 (permittivity of space)	$-1/4\pi G$
μ_0 (permeability of space)	$-4\pi G/c^2$
$-1/4\pi\varepsilon_0$ or $-\mu_0 c^2/4\pi$	G (gravitational constant)

$$\boldsymbol{K} = -\frac{G}{c^2}\int\left\{\frac{[\varrho\boldsymbol{v}]}{r^3}+\frac{1}{r^2 c}\left[\frac{\partial[\varrho\boldsymbol{v}]}{\partial t}\right]\right\}\times\boldsymbol{r}\mathrm{d}V', \tag{4}$$

where $\boldsymbol{g}$ is the gravitational field created by the mass m distributed in space with density ϱ, $r=\left[(x-x')^2+(y-y')^2+(z-z')^2\right]^{1/2}$ is the distance from the *source point* (x',y',z'), where the volume element of integration $\mathrm{d}V'$ is located, to the field point (x,y,z), where $\boldsymbol{g}$ is been observed or computed, $\boldsymbol{r}$ is the radius vector directed from $\mathrm{d}V'$ to the field point, $\boldsymbol{v}$ is the velocity with which the mass distribution ϱ moves (the product $\varrho\boldsymbol{v}$ constitutes the "mass-current density), and c is the velocity of the propagation of gravitation (usually assumed to be the same as the velocity of light). The square brackets in these equations are the retardation symbol indicating that the quantities between the brackets are to be evaluated for the "retarded" time, $t'=t-r/c$, where t is the time for which $\boldsymbol{g}$ and $\boldsymbol{K}$ are evaluated. The integration in the integrals of Equations (3) and (4) is over all space.

According to Equations (3) and (4), the gravitational field has three causative sources: the mass density, the time derivative of ϱ, and the time derivative of the mass-current density $\varrho\boldsymbol{v}$; cogravitational field has two causative sources: the mass-current density $\varrho\boldsymbol{v}$ and the time derivative of $\varrho\boldsymbol{v}$.

In addition to Equations (3) and (4) for the gravitational and cogravitational fields, the following equations constitute the mathematical foundation of the generalized theory of gravitation:

1) *The mass conservation equation* ("*continuity equation*")

$$\nabla\cdot(\varrho\boldsymbol{v}) = -\frac{\partial\varrho}{\partial t}, \tag{5}$$

or, in the integral form,

$$\oint \varrho \boldsymbol{v} \cdot \mathrm{d}\boldsymbol{S} = -\frac{\partial}{\partial t}\int \varrho \mathrm{d}V. \tag{6}$$

According to these equations, whenever a mass contained in a region of space diminishes or increases, there is an outflow or inflow of mass from or into this region.

2) *Force acting on the mass distribution of density* ϱ

$$\boldsymbol{F} = \int \varrho\left(\boldsymbol{g} + \boldsymbol{v} \times \boldsymbol{K}\right)\mathrm{d}V, \tag{7}$$

where $\boldsymbol{v}$ is the velocity of ϱ and the integral is extended over the region of space containing the mass under consideration.

3) *Density of the field energy contained in the gravitational-cogravitational field*

$$U_v = -\frac{1}{8\pi G}\left(\boldsymbol{g}^2 + c^2\boldsymbol{K}^2\right), \tag{8}$$

it is important to note that the gravitational-cogravitational field energy is negative. This means that *no energy can be extracted from the gravitational-cogravitational field by destroying the field. In the contrary, energy must be delivered to the field in order to destroy the field.*

4) *Field energy contained in a region of the gravitational-cogravitational field*

$$U = -\frac{1}{8\pi G}\int\left(\boldsymbol{g}^2 + c^2\boldsymbol{K}^2\right)\mathrm{d}V, \tag{9}$$

where the integration is extended over the region under consideration.

5) *Energy flow vector in the gravitational-cogravitational field* ("*gravitational Poynting vector*")

$$\boldsymbol{P} = \frac{c^2}{4\pi G}\boldsymbol{K} \times \boldsymbol{g}. \tag{10}$$

This vector represents the direction and rate of gravitational-cogravitational energy flow per unit area at a point of space under consideration. Equation (10) together with Equation s. (3), (4), (5) and (8) ensures the conservation of energy in gravitational-cogravitational interactions.

6) *Density of the field momentum contained in the gravitational-cogravitational field*

$$\boldsymbol{G}_{vf} = \frac{1}{4\pi G}\boldsymbol{K} \times \boldsymbol{g}. \tag{11}$$

7) *Field momentum contained in the gravitational-cogravitational field*

$$\boldsymbol{G}_f = \frac{1}{4\pi G}\int \boldsymbol{K} \times \boldsymbol{g}\mathrm{d}V, \tag{12}$$

where the integration is extended over the region under consideration.

8) *Correlations between the mechanical momentum,* $\boldsymbol{G}_m$*, and the gravitational-cogravitational field*

$$\frac{\mathrm{d}\boldsymbol{G}_M}{\mathrm{d}t} = -\frac{1}{4\pi G}\int \frac{\partial}{\partial t}\left(\boldsymbol{K}\times\boldsymbol{g}\right)\mathrm{d}V + \frac{1}{4\pi G}\left[\frac{1}{2}\oint\left(\boldsymbol{g}^2 + c^2\boldsymbol{K}^2\right)\mathrm{d}\boldsymbol{S} - \oint \boldsymbol{g}\left(\boldsymbol{g}\cdot\mathrm{d}\boldsymbol{S}\right) - c^2\oint \boldsymbol{K}\left(\boldsymbol{K}\cdot\mathrm{d}\boldsymbol{S}\right)\right], \tag{13}$$

where $\boldsymbol{g}$ and $\boldsymbol{K}$ are the gravitational and cogravitational fields in the system under consideration. In this equation, the derivative on the left represents the rate of change of the momentum of a body located in a gravitational-cogravitational field, the volume integral represents the rate of change of the field momentum in the region of the field where the bode is located, and the surface integrals represent the flux of the field momentum through the surface enclosing the region under consideration. Together with Equations (3), (4), (5), (7) and (11) this equation ensures the conservation of momentum in gravitational-cogravitational interactions.

3. Gravitational and Cogravitational Forces According to the Generalized Theory of Gravitation

One of the most important differences between Newton's original theory of gravitation and the generalized theory of gravitation is in the interpretation of the mechanism of gravitational interactions. Whereas in Newton's original theory of gravitation gravitational interaction between two bodies involves one single force of gravitational attraction, in the generalized theory of gravitation gravitational interaction between two bodies involves an intricate juxtaposition of several different forces. Mathematically, these forces result from Equations (3), (4) and (7). When Equations. (3) and (4) are written as five separate integrals, they become, using $\boldsymbol{J}$ for $\varrho\boldsymbol{v}$,

$$\boldsymbol{g} = -G\int\frac{[\varrho]}{r^3}\boldsymbol{r}\mathrm{d}V' - G\int\frac{1}{r^2c}\left[\frac{\partial\varrho}{\partial t}\right]\boldsymbol{r}\mathrm{d}V' + \frac{G}{c^2}\int\frac{1}{r}\left[\frac{\partial\boldsymbol{J}}{\partial t}\right]\mathrm{d}V' \tag{14}$$

and

$$\boldsymbol{K} = -\frac{G}{c^2}\int\frac{[\boldsymbol{J}]}{r^3}\times\boldsymbol{r}\mathrm{d}V' - \frac{G}{c^2}\int\frac{1}{r^2c}\left[\frac{\partial[\boldsymbol{J}]}{\partial t}\right]\times\boldsymbol{r}\mathrm{d}V'. \tag{15}$$

Each of these integrals represents a force field. Therefore, according to the generalized theory of gravitation, gravitational interaction between two bodies involve at least five different forces. Let us consider the physical sources of these forces.

First let us consider Equation (14). The field represented by the first integral of this equation is the ordinary Newtonian gravitational field created by the mass distribution ϱ corrected for the finite speed of the propagation of the field, as indicated by the square brackets (the retardation symbol) in the numerator. The field represented by the second integral is created by a mass whose density varies with time. Like the ordinary Newtonian gravitational field, these two fields are directed toward the masses, which create them. The field represented by the last integral in Equation (14) is created by a mass current whose magnitude and/or

direction varies with time. The direction of this field is parallel to the direction along which the mass current increases. All three fields in Equation (14) act on stationary as well as on moving masses.

Consider now Equation (15). The first integral in this equation represents the cogravitational field created by the mass current. The direction of this field is normal to the mass current vector. The second integral represents the field created by a time variable mass current. The direction of this field is normal to the direction along which the mass current increases. By Equation (7), both fields in Equation (15) act on moving masses only.

If the mass under consideration does not move and does not change with time, then there is no retardation and no mass current. In this case, both integrals in Equation (15) vanish and only the first integral remains in Equation (14). As a result, one simply obtains the integral representing the ordinary Newtonian gravitational field. Thus, the ordinary Newtonian gravitational theory is a special case of the generalized theory, as it should be.

As far as the gravitational interaction between two masses is concerned, the meaning of the five integrals discussed above can be explained with the help of **Figure 1**. The upper part of **Figure 1** shows the force, which the mass m_1 experiences under the action of the mass m_2 according to the ordinary Newtonian theory. The lower part of **Figure 1** shows five forces which the same mass m_1 experiences under the action of the mass m_2 according to the generalized theory. The time for which the positions of the two masses and the force experienced by m_1 are observed is indicated by the letter t. Let us not first of all that, according to the ordinary Newtonian theory, the mass m_1 is subjected to one single force directed to the mass m_2 at its present location, that is, to its location at the time t. However, according to the generalized theory, all forces acting on the mass m_1 are associated not with the position of the mass m_2 at the time of observation, but with the position of m_2 at an earlier time $t' < t$. Therefore, the magnitude of the mass m_2, its position and its state of motion at the present time t have no effect at all on the mass m_1.

The subscripts identifying the five forces shown in the lower part of **Figure 1** correspond to the five integrals in the Equations (14) and (15). The force $\boldsymbol{F}_1$ is associated simply with the mass m_2 and differs from the ordinary Newtonian gravitational force only insofar as it is it is directed not to the mass m_2 at its present position, but to the place where m_2 was located at the past time t'. The force $\boldsymbol{F}_2$ is associated with the variation of the density of the mass m_2 with time; the direction of thus force is the same as that of $\boldsymbol{F}_1$. The force $\boldsymbol{F}_3$ is associated with the time variation of the mass current produced by m_2; tis force is directed along the acceleration vector $\boldsymbol{a}$ (or along the velocity vector $\boldsymbol{v}_2$) which the mass m_2 had at the time t'. The three forces are produced by the gravitational field $\boldsymbol{g}$ (if m_2 is a point mass moving at constant velocity, $\boldsymbol{g}$ and the resultant of the three forces are directed toward the *present position* of m_2; see Chapter 5 in [3]).

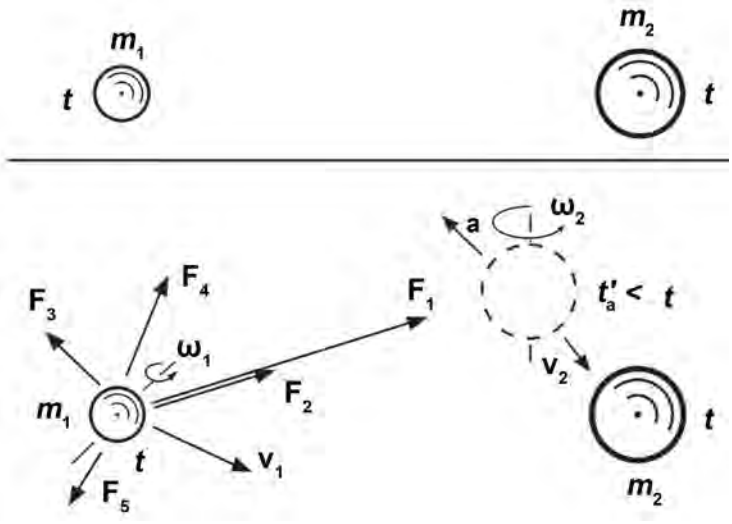

Figure 1. The upper part of this figure shows the force that the mass m_1 experiences under the action of the mass m_2 according to the ordinary Newtonian theory. Lower part shows five forces, which the same mass m_1 experiences under the action of the mass m_2 according to the generalized Newtonian theory.

The forces $\boldsymbol{F}_4$ and $\boldsymbol{F}_5$ are due to the cogravitational field $\boldsymbol{K}$. The force $\boldsymbol{F}_4$ is associated with the mass current created by the mass m_2 and with the velocity of the mass m_1. Its direction is normal to the velocity vector $\boldsymbol{v}_2$ which the mass m_2 had at the time t' and normal to the velocity vector $\boldsymbol{v}_1$ which the mass m_1 has at the present time t. The force $\boldsymbol{F}_5$ is associated with the velocity of the mass m_1 and with the variation of the mass current of the mass m_2 with time; the direction of this force is normal to the acceleration vector (or to the velocity vector) that the mass m_2 had at the time t' and normal to the velocity vector that the mass m_1 has at present time t. Although not shown in **Figure 1**, additional forces associated with the rotation of m_1 and m_2 (angular velocities ω_1 and ω_2) are generally involved in the interaction between t5he two masses (see Chapters 14 and 15 in [3]).

The forces $\boldsymbol{F}_2$, $\boldsymbol{F}_3$, $\boldsymbol{F}_4$ and $\boldsymbol{F}_5$ are usually much weaker than the force $\boldsymbol{F}_1$ because of the presence of the speed of gravitation c (usually assumed to be the same as the speed of light) in the denominators of the integrals representing the fields responsible for these four forces. This means that only when the translational or rotational velocity of m_1 or m_2 is close to c, are the forces $\boldsymbol{F}_2$, $\boldsymbol{F}_3$, $\boldsymbol{F}_4$ and $\boldsymbol{F}_5$ dominant. Of course, the cumulative effect of these forces in long-lasting gravitational systems (such as Solar system, for example) may be significant regardless of the velocities of the interacting masses.

4. The Relationship between the Generalized Theory of Gravitation and the Special Relativity Theory

Until recently it was believed that the analogy between electromagnetic and gravitational equations could not apply to fast moving systems, because the electric

charge is not affected by velocity, but the mass of a moving body was though to vary with velocity. It is now generally accepted that mass, just like the electric charge, does not depend on velocity. For a discussion of the history and use of the concept of relativistic mass, see C. Adler, "Does mass really depend on velocity, dad?" [8], also L. Okun, "The concept of mass" [9] and the letter in response to these articles by T. Sandin, "In defense of relativistic mass" [10]. This also means that transformation equations of the special relativity theory developed for electromagnetic systems (see [11] pp. 148-206) have their gravitational and cogravitational counterparts.

Thus there is no need to *derive* relativistic gravitational-cogravitational transformation equations, because we can easily obtain them by replacing symbols and constants appearing in relativistic electromagnetic equations by the corresponding gravitational-cogravitational symbols and constants with the help of the following table [3].

The basic relativistic gravitational-cogravitational transformation equations obtained in this way are listed below. It is important to note that these equations can be derived directly, without using the analogy between electromagnetic and gravitational-cogravitational systems (see O. Jefimenko, "Derivation of Relativistic Transformation for Gravitational Fields from Retarded Field Integrals" [12]). In these equations, the unprimed quantities are those measured in the stationary reference frame Σ ("laboratory"), and the primed quantities are those measured in the moving reference frame Σ'.

Transformation equations correlating quantities measured in Σ with quantities measured in Σ':

a) *Equations for space and time coordinates*

$$x = \gamma\left(x' + vt'\right), \tag{4.1}$$

$$y = y', \tag{4.2}$$

$$z = z', \tag{4.3}$$

$$t = \gamma\left(t' + vx'/c^2\right). \tag{4.4}$$

b) *Equations for the gravitational field*

$$g_x = g'_x, \tag{4.5}$$

$$g_y = \gamma\left(g'_y + vK'_z\right), \tag{4.6}$$

$$g_z = \gamma\left(g'_z + vK'_y\right), \tag{4.7}$$

c) *Equations for the cogravitational field*

$$K_x = K'_x, \tag{4.8}$$

$$K_y = \gamma\left(K'_y - vg'_z/c^2\right), \tag{4.9}$$

$$K_z = \gamma\left(K'_z - vg'_y/c^2\right), \tag{4.10}$$

d) *Equations for the mass and mass-current densities*

$$\varrho = \gamma\left[\varrho' + \left(v/c^2\right)J'_x\right], \tag{4.11}$$

$$J_x = \gamma\left(J'_x + v\varrho'\right), \tag{4.12}$$

$$J_y = J'_y, \tag{4.13}$$

$$J_z = J'_z. \tag{4.14}$$

e) *Equations for gravitational and cogravitational potentials*

$$\varphi = \gamma\left(\varphi' + vA'_x\right), \tag{4.15}$$

$$A_x = \gamma\left[A'_x + \left(v/c^2\right)\varphi'\right], \tag{4.16}$$

$$A_y = A'_y, \tag{4.17}$$

$$A_z = A'_z. \tag{4.18}$$

Transformation equations correlating quantities measured in Σ′ with quantities measured in Σ:

a) *Equations for space and time coordinates*

$$x' = \gamma\left(x - vt\right), \tag{4.19}$$

$$y' = y, \tag{4.20}$$

$$z' = z, \tag{4.21}$$

$$t' = \gamma\left(t - vx/c^2\right). \tag{4.22}$$

b) *Equations for the gravitational field*

$$g'_x = g_x, \tag{4.23}$$

$$g'_y = \gamma\left(g_y - vK_z\right), \tag{4.24}$$

$$g'_z = \gamma\left(g_z - vK_y\right). \tag{4.25}$$

c) *Equations for the cogravitational field*

$$K'_x = K_x, \tag{4.26}$$

$$K'_y = \gamma\left(K_y + vg_z/c^2\right), \tag{4.27}$$

$$K'_z = \gamma\left(K_z + vg_y/c^2\right). \tag{4.28}$$

d) *Equations for the mass and mass-current densities*

$$\varrho' = \gamma\left[\varrho - \left(v/c^2\right)J_x\right], \tag{4.29}$$

$$J'_x = \gamma\left(J_x - v\varrho\right), \tag{4.30}$$

$$J'_y = J_y, \tag{4.31}$$

$$J'_z = J_z. \tag{4.32}$$

e) *Equations for gravitational and cogravitational potentials*

$$\varphi' = \gamma\left(\varphi - vA_x\right), \tag{4.33}$$

$$A'_x = \gamma\left[A_x - \left(v/c^2\right)\varphi\right], \tag{4.34}$$

$$A'_y = A_y, \tag{4.35}$$

$$A'_z = A_z. \tag{4.36}$$

Quite clearly, transformation equations for physical quantities not involving electric and magnetic fields (such as velocity, acceleration, force, etc.) remain valid for gravitational-cogravitational systems as well. However, the constant c appearing in the conventional relativistic transformation equations represents the velocity of propagation of electromagnetic fields in a vacuum, which is the same as the velocity of light. The velocity of propagation of gravitational and cogravitational fields is not known, although it is generally believed to be equal to the velocity of light. If the velocity of propagation of gravitational fields is not the same as the velocity of light, our relativistic transformation equations for gravitation would still remain correct, but the constant c appearing in them would be different from c appearing in the corresponding electromagnetic equations. Therefore, the behavior of rapidly moving bodies involved in gravitational interactions would be different from the behavior of rapidly moving bodies involved in electromagnetic interactions. In effect there would be two different mechanics: the "gravitational-cogravitational mechanics," and the "electromagnetic mechanics" involving different effective masses, different effective momenta, and different rest energies.

A possibility exists that our gravitational relativistic transformation equations are not entirely correct. According to Einstein's mass-energy equation, any energy has a certain mass. But a mass is a source of gravitation. Therefore the gravitational field of a mass distribution may be caused not only by the mass of the distribution as such, dut also by the gravitational energy of this distribution (for a detail discussion of this effect, including the possibility of antigravitational mass distributions arising from it, see Chapter 19 in [3]). If this effect is taken into account, the equation for the divergence of the gravitational field (see Eq. (7-1.1) in [3])

$$\nabla \cdot \boldsymbol{g} = -4\pi G\varrho \tag{16}$$

becomes only approximately correct, and all equations derived with the help of Equation. (16) also become only approximately correct. It is important to note, however, that this energy effect, if it exists, is extremely small[2]. In connection with the foregoing, we recommend that the reader become familiar with the work "Binormal Motion of Curves of Constant Curvature and Torsion. Generation of Soliton Surfaces." [13].

5. Covariant Formulation of the Generalized Theory of Gravitation

Covariant formulation of physical formulas and equations is considered by some authors to be the most appropriate formulation for expressing the laws of phys-

[2]Contrary to the prevailing belief, equations relativistic electrodynamics and the entire theory of special relativity is also only approximately correct, since it is valid only for inertial systems ("inertial frames of reference"). In reality such systems do not exist, because everywhere in the Universe there is a gravitational force field, making all systems and locations in the Universe non-inertial.

ics in a frame-independent form. It is also believed by some authors to be more concise and occasionally more informative than the conventional formulation. Since any equation invariant under relativistic transformations should be expressible ib a covariant form, and since the principle of relativity is considered to be a fundamental law of nature, the laws of physics that cannot be expressed in a covariant form are considered by some authors to be incomplete or incorrect. This view is *unquestionably wrong*, since according to it, even Maxwell's equations in their vector form should be classified as "incomplete" or "incorrect." Note also that covariant formulation changes the form of equations but does not create new physical laws and thus is of very limited utility.

Newton's gravitational law is an example of a physical law that *cannot be expressed in a covariant form*. The problem of finding an invariant form of the law of gravitation was first considered be Poincaré, but without success (see his article "Sur la dynamique de L'Électron" [14]). It is interesting to note that Poincaré attempted to solve the problem on the basis of just one gravitational field (the gravitational analog of the electrostatic field). But even if the theory of gravitation is built upon two fields, a covariant theory of gravitation is not possible unless the gravitational mass, just like the electric charge, does not depend on the velocity with which the mass moves.

However, it is now generally accepted that mass does not depend on the velocity with which a body moves (see C. Adler, "Does mass really depend on velocity, dad?" [8], also L. Okun, "The concept of mass" [9] and the letter in response to these articles by T. Sandin, "In defense of relativistic mass" [10]). Therefore a covariant formulation of the theory of gravitation based on gravitational-cogravitational fields is not only possible but can be constucted straightaway from the covariant theory of electromagnetism by a mere substitution of symbols and constants in accordance with the list above.

In particular, from electromagnetic equations (see [11] pp. 284-292). We can directly obtain for the covariant "position 4-vector"

$$\boldsymbol{r} = \left(x_1, x_2, x_3, x_4\right) = \left(x, y, z, ict\right). \tag{17}$$

From the 4-vector electric current [11] we obtain by substitutions the the covariant expressions for the 4-vector mass current

$$\boldsymbol{J} = \left(J_1, J_2, J_3, J_4\right) = \left(J_x, J_y, J_z, ic\varrho\right), \tag{18}$$

where J_x, J_y and J_z are x, y and z components of mass current density. From the electromagnetic field tensor [11] we obtain the gravitational-cogravitational field tensor by replacing the x, y and z components of $\boldsymbol{E}$ by the corresponding components of $\boldsymbol{g}$ and the x, y and z components of $\boldsymbol{B}$ by the corresponding components of $\boldsymbol{K}$

$$F_{\mu\nu} = \begin{bmatrix} 0 & K_z & -K_y & -ig_x/c \\ -K_z & 0 & K_x & -ig_y/c \\ K_y & -K_x & 0 & -ig_z/c \\ ig_x/c & ig_y/c & ig_z/c & 0 \end{bmatrix}, \tag{19}$$

or

$$F^{\mu\nu}=\begin{bmatrix} 0 & K_z & -K_y & ig_x/c \\ -K_z & 0 & K_x & ig_y/c \\ K_y & -K_x & 0 & ig_z/c \\ -ig_x/c & -ig_y/c & -ig_z/c & 0 \end{bmatrix}, \tag{20}$$

where the subscript μ indicates the row (1, 2, 3, 4 top to bottom) and the subscript ν indicates the column (1, 2, 3, 4 left to right). Finally, in the same manner, we obtain covariant expressions of the present-time differential equations for gravitational-cogravitational fields:

$$\sum_{\nu=1}^{4}\frac{\partial F_{\mu\nu}}{\partial x_\nu}=-\frac{4\pi G}{c^2}J_\mu \tag{21}$$

and

$$\frac{\partial F_{\mu\nu}}{\partial x_\lambda}+\frac{\partial F_{\nu\lambda}}{\partial x_\mu}+\frac{\partial F_{\lambda\mu}}{\partial x_\nu}=0. \tag{22}$$

It should be note, however, that c in the gravitational-cogravitational equations stands for the speed of propagation of gravitational-cogravitational fields, which is generally assumed to be the same as the speed of light, but has never been actually measured. In 2002 Fomalont Kopeikin tried indirectly to measure the speed of gravitation and reported in the paper "The measurement of the light deflection from Jupiter: Experimental results" [15] that the velocity of gravitation was found to be equal to the velocity of light.

6. The Gravikinetic Field

As we have already shown, one of the main differences between the generalized theory of gravitation and Newton's gravitational theory is that in the generalized theory of gravitation there is especial force field – the cogravitational, or Heaviside's field. The cogravitational field is produced by all moving masses, and it acts ob all moving masses. In this Section we shall learn that in the generalized theory of gravitation there is yet *another* force field prodiced by moving masses. However, in contrast with the cogravitational field, thid field is produced only by masses whose velocity changes in time and, again in contrast with the cogravitational field, it acts on *all masses*, moving as well as stationary.

As we already know, the principal gravitatonal field equation of the generalized theory of gravitation is

$$\boldsymbol{g}=-G\int\left\{\frac{[\varrho]}{r^3}+\frac{1}{r^2c}\left[\frac{\partial\varrho}{\partial t}\right]\right\}\boldsymbol{r}\mathrm{d}V'+\frac{G}{c^2}\int\frac{1}{r}\left[\frac{\partial\boldsymbol{J}}{\partial t}\right]\mathrm{d}V', \tag{23}$$

where $\boldsymbol{J}=\varrho\boldsymbol{v}$ is the mass current density produced by a moving mass distribution ϱ. The first term on the right in Equation (23) represents the retarded Newtonian gravitational field. Just like the ordinary Newtonian field, this field originates at any mass distribution ϱ and is responsible for the gravitational attraction. However, the last term on the right of Equation (23) represents a gra-

vitational field very different from the Newtonian field. As can be seen from Equation (23), this new field is produced by a time-variable mass current $\partial \boldsymbol{J}/\partial t$ and it differs in two in two importabt respects from the Newtonian gravitational field: it is directed along the mass-current (more accurately, along its partial time derivative) rather than along a radius vector, and it exists only as long as the current is changing in time. Therefore the gravitational force caused by this field is also different from the ordinary Newtonian force. This force (designated as $\boldsymbol{F}_3$ in Figure 1) is directed along $\partial \boldsymbol{J}/\partial t$ and it lasts only as long as the mass current is changing. Unlike the Newtonian gravitational force, which is always an interaction between graviting masses, the force due to the time-variable $\boldsymbol{J}$ is basically a *dragging* force. If only the magnitude but not the direction $\boldsymbol{J}$ changes, this force is directed parallel or antiparallel (if $\partial \boldsymbol{J}/\partial t$ is negative) to $\boldsymbol{J}$, causing a mass subjected to this force to move parallel or antiparallel to (rather than toward) the mass distribution forming the mass current. However, like the Newtonian force, the force due to the time-variable $\boldsymbol{J}$ acts upon all masses. It is important to note that unlike that unlike the cogravitational field, the field produced by $\partial \boldsymbol{J}/\partial t$ usually is not created by masses moving with constant velocity $\boldsymbol{v}$,

Since the cogravitational field created by time-variable mass currents is very different from the Newtonian field and from the cogravitatational field, a special name should be given to it. Taking into account that the cause of this field is a motion of masses, we can call it the *gravikinetic field*, and we may call the force which this field exerts on other masses the *gravikinetic force*. We shall designate the gravikinetic field by the vector $\boldsymbol{g}_k$. From Equation (23) we tus have

$$\boldsymbol{g}_k = \frac{G}{c^2}\int \frac{1}{r}\left[\frac{\partial \boldsymbol{J}}{\partial t}\right] \mathrm{d}V'. \tag{24}$$

Because of the c^2 in the denominator in Equation (24) the gravikinetic field cannot be particularly strong except when the mass-current responsible for it changes very fast. On the othr hand, taking into account that the time scale in gravitational interractions taking place in the Univerce may be very long, ultimate effect of the gravikinetic field in such interactions may be very considerable regardless of the rate at which the mass current changes.

Let us now show the correlation between the gravikinetic field and the cogravitational field. If we compare Equation (24) with the expression for the retarded cogravitational vector potential $\boldsymbol{A}_{ret}$ produced by a mass current $\boldsymbol{J}$ (seee, Section 3-3 Equation (3-3.2) in [4]),

$$\boldsymbol{A}_{ret} = -\frac{G}{c^2}\int \frac{[\boldsymbol{J}]}{r}\mathrm{d}V', \tag{25}$$

we recognize that the gravikinetic field is equal to the time derivative of retarded $\boldsymbol{A}_{ret}$:

$$\boldsymbol{g}_k = -\frac{\partial \boldsymbol{A}_{ret}}{\partial t}. \tag{26}$$

Observe that Equation (26) points out the possibility of a new defibition and interpretation of the cogravitational vector potential. Let us integrate Equation (26). We otain

$$\boldsymbol{A}_{ret} = -\int \boldsymbol{g}_k \mathrm{d}t + \text{const.} \tag{27}$$

Let us call the time integral of $\boldsymbol{g}_k$ the *gravikinetic impulse*. We then can say that the cogravitational vector potential created by a mass current at a point in space is equal to the negative of the gravikinetic impulse produced by this current at that point during the action of the mass current. Since the gravikinetic impulse is, in principle, a measurable quantity, we thus have an operational definition and a physical interpretation of the cogravitational vector potential (for a related interpretation of the magnetic vector potential see [2] pp. 30, 31).

A more direct relation between the gravikinetic field and the cogravitational field one can obtain as follows. Let as assume that an initially stationary mass current $\boldsymbol{J}(x', y', z')$ (an initially stationary rotating spherical mass, for example) moves as a whole with a constant velocity v toward a stationary observer located at the origin of coordinates. The mass current is then a function of $(x' - v_x t)$, $(y' - v_y t)$ and $(z' - v_z t)$, or

$$\boldsymbol{J} = \boldsymbol{J}(x' - v_x t, y' - v_y t, z' - v_z t). \tag{28}$$

The time derivative of the current is

$$\frac{\partial \boldsymbol{J}}{\partial t} = -\frac{\partial \boldsymbol{J}}{\partial x'} v_x - \frac{\partial \boldsymbol{J}}{\partial y'} v_y - \frac{\partial \boldsymbol{J}}{\partial z'} v_z = -(\boldsymbol{v} \cdot \nabla')\boldsymbol{J}. \tag{29}$$

The gravikinetic field caused by the moving mass current is then, by Equations. (24) and (29),

$$\boldsymbol{g}_k = -\frac{G}{c^2}\int \frac{\left[(\boldsymbol{v} \cdot \nabla')\boldsymbol{J}\right]}{r}\mathrm{d}V'. \tag{30}$$

The spatial derivative appearing in Equation (30) can be eliminated as follows. Using vector identity (V-6) from [3], which can be written as

$$\nabla'(\boldsymbol{v} \cdot \boldsymbol{J}) = (\boldsymbol{v} \cdot \nabla')\boldsymbol{J} + \boldsymbol{v} \times (\nabla' \times \boldsymbol{J}) + (\boldsymbol{J} \cdot \nabla')\boldsymbol{v} + \boldsymbol{J} \times (\nabla' \times \boldsymbol{v}), \tag{31}$$

and taking into account that $\boldsymbol{v}$ is a constant vector, we obtain

$$\boldsymbol{g}_k = -\frac{G}{c^2}\int \frac{\left[\cdot \nabla'(\boldsymbol{v} \cdot \boldsymbol{J})\right]}{r}\mathrm{d}V' + \frac{G}{c^2}\int \frac{\left[\boldsymbol{v} \times (\nabla' \times \boldsymbol{J})\right]}{r}\mathrm{d}V'. \tag{32}$$

If we compare Equation, (32) with Equation (3-1.2) from [3] for the cogravitational field,

$$\boldsymbol{K} = -\frac{G}{c^2}\int \frac{\left[\nabla' \times \boldsymbol{J}\right]}{r}\mathrm{d}V', \tag{33}$$

we find that Equation, (32) can be written as

$$\boldsymbol{g}_k = -\frac{G}{c^2}\int \frac{\left[\nabla'(\boldsymbol{v} \cdot \boldsymbol{J})\right]}{r}\mathrm{d}V' - \boldsymbol{v} \times \boldsymbol{K}, \tag{34}$$

where $\boldsymbol{K}$ is the cogravitational field created by the moving mass current $\boldsymbol{J}$.

7. Dynamic Effects of Gravikinetic Fields; Gravitational Induction

We shall now present one example (fore more examples see the Section 2-2 in [3]) demonstrating force effects of the gravikinetic field. For simplicity we shall use gravikinetic fields calculated in the Section 12-2 of [3].

The force effects that we shall show constitute the gravitational analogue of electromagnetic induction and of electromagnetic Lenz's law. As we now know, electromagnetic induction is caused by the electrokinetic field (see [3]). The gravikinetic field is the gravitational counterpart of the electrokinetic field, and their dynamic effects are similar, except that the gravikinetic force exerted on a mass by an increasing/decreasing gravikinetic field is parallel/antiparallel to the field, whereas the electrokinetic force exerted on a positive charge by an increasing/decreasing electrokinetic field is antiparallel/parallel to the field.

An example: A thin-walled cylinder of radius R_0, length $2L$ and wall thickness t has a uniformly distributed mass of density ϱ is initially at rest. A ring of mass m_r and radius R us placed around the cylinder coaxially with it. The cylinder is then suddenly set in motion along its axis and attains a velocity v_c (mass current $\boldsymbol{J}_c$). The gravikinetic force causes the ring to move along (follow) the cilinder (**Figure 2**). Assuming that no other forces act on the ring, and assuming that the ring stays near the middle of the cylinder during the time that the velocity of the cylinder changes, find the final velocity $\boldsymbol{v}_f$ of the ring.

According to our assumptions, the gravikinetic field through which the ring moves is a function of time only. Therefore we can use Equation (12-1.5) from [3] for finding the final momentum and velocity of the ring. When the gravikinetic force acts on a mass distribtion ϱ, it changes the mechanical momentum $\boldsymbol{G}_M$ of the mass distribution (see [3]), and if $\boldsymbol{g}_k$ is a function of time only, the momentum change is

$$\Delta \boldsymbol{G}_M = m\int \boldsymbol{g}_k \mathrm{d}t = -m\Delta \boldsymbol{A}, \tag{35}$$

where m is the total mass of the distribution, and $\Delta \boldsymbol{A}$ is the change in the vector potential during the time interval under consideration. From Equation (35) and Equation (12-2.3) (in [3])

$$\boldsymbol{g}_k = \frac{\partial I}{\partial t}\frac{2G}{c^2}\ln\frac{2L}{R}\boldsymbol{k}, \tag{36}$$

where $\boldsymbol{k}$ is a unit vector in the direction of the mass current I, we have

$$\Delta \boldsymbol{G}_M = m_r \boldsymbol{v}_f = m_r I_c \frac{2G}{c^2}\ln\frac{2L}{R}\boldsymbol{k}, \tag{37}$$

so that the final velocity of the ring is

$$\boldsymbol{v}_f = \frac{2G}{c^2} I_c \ln\frac{2L}{R}\boldsymbol{k}. \tag{38}$$

Substituting $\varrho v_c 2\pi R_0 t$ for I_c, where ϱ is the density of the cylinder, R_0 is its radius, and t is its thickness, we obtain

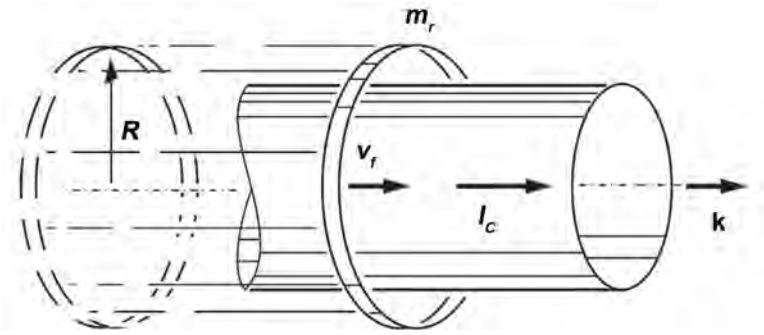

Figure 2. Accelerating cylinder drags the ring with itself.

$$\boldsymbol{v}_f = \frac{4G\varrho v_c \pi R_0 t}{c^2} \ln \frac{2L}{R} \boldsymbol{k}. \tag{39}$$

The cylinder *drags* the ring so that the ring moves in the direction of the moving cylinder. It is ineresting to not that the final velocity of the ring does not depend on its mass.

This example (along with other examples in the Section 2-2 in [3]) illustrates the phenomenon of *gravitational induction*, whereby a changing mass current induces a secondary mass current in neighboring bodies. The effect is similar to electromagnetic induction (for a detail analyses and novel interpretation of the phenomenon of electromagnetic induction see Oleg D. Jefimenko, "Presenting electromagnetic theory in accordance with the principle of causality", [16]), except that, in contrast to the latter, the direction of the induced current is the same as that of the original current if the original cerrent increases, and is opposite to the original current if the original current decreases. Thus the sign of the "gravitational Lenz's law" is opposite to that of the electromagnetic Lenz's law.

8. Instead of Conclusion: On the Truth of the Generalized Theory of Gravitation

The comparison of the generalized theory of gravitation with the general theory of relativity of Einstein (GR) involuntarily suggests.

As is known, the experimental confirmation of GR generally relies only on the fact that it allegedly explained the previously unexplained discrepancy between the theoretical (calculated) and observed displacement (precession) of the perihelion of the planet Mercury; all other predictions and conclusions of the general theory of relativity can either not be verified with sufficient accuracy, or can be explained without this theory.

Speaking about the problem of Mercury, it should be pointed out that the so-called discrepancy in the displacement of its perihelion is the difference between the observed and calculated, on the basis of the usual Newton theory, perihelion.

This difference, which is approximately 575" per century attracted the attention of Urben Leverrier, who predicted the existence of the planet Neptune and

accurately calculated its coordinates. Leverrier explained the difference in the precession of Mercury by the influence of near planets and, having calculated their effect on Mercury, found that these planets cause a precession of 532" per century. The remaining 43" he could not explain. These remaining 43" for centuries were, *as it is now believed*, explained by Einstein's general theory of relativity. But then a certain discrepancy is immediately evident. After all, the main divergence in 532" was calculated according to Newton's theory, and the remainder in 43" was calculated according to the general theory of relativity. It would be much more convincing if the entire discrepancy of 575" per century was calculated *on the basis of the same theory*. On this occasion J. Synge remarked [17]: "Such a mixture of Newtonian and Einstein's theories is psychologically unpleasant, since these theories are based on too different initial concepts." Until the *complete discrepancy* is calculated using the general theory of relativity, without invoking Newton's theory, the experimental verification of general relativity can not be considered valid.

But let us go back to the generalized theory of gravitation. We note that, as shown in [3], within the framework of the generalized theory of gravitation, one can obtain formulas according to which the perihelion precession *for all planets* is a necessary consequence of this theory. However, these formulas hardly can prove anything. The fact is that according to the generalized theory of gravitation, all celestial mechanics and its results should be revised. As it was shown above (see **Figure 1**), the action of the Sun on planets is expressed not by one force, but by five forces, and the action of each planet on each other planet is expressed not by one force, but by five forces. Therefore, as a matter of fact, all the information about our solar system, obtained on the basis of Newton's conventional theory, should be considered only approximately correct. So, from the point of view of the generalized theory, there is no point in trying to explain the 43"rd residue in the displacement of the perihelion of Mercury. After all, if we take into account all the forces that act on Mercury, including the forces associated with the movement of the Sun in relation to the Galaxy, the rotation of the Sun around its axis, the dependence of the forces acting on Mercury on the speed and acceleration of the planets, on the speed of Mercury itself, and , finally, the retardation in the action of gravitational and cogravitational forces, will we get this discrepancy at all in the displacement of the perihelion of Mercury, especially the discrepancy exactly in 43 seconds? It is clear that until all these calculations are performed, until the necessary corrections in celestial mechanics are amended, it is pointless to speak of testing the generalized theory of gravitation by analyzing the motion of Mercury.

So neither the generalized theory of gravitation of Jefimenko nor the general theory of relativity of Einstein can be verified in this way.

However, one very strong testimony to the truth of the generalized theory of gravitation can still be cited (although it is not as sensational as the explanation of the discrepancy in the displacement of Mercury's perihelion). Speech will go about one "white spot" associated with the phenomenon of gravitation. As is

known, the motion of stellar bodies and the fall of bodies under the action of the gravitational field p associated with conversion of potential energy unto kinetic energy and vice versa. In particular, when a body is falling under the action of the gravitational of the Earth, its potential energy diminishes and its kinetic energy increases. But how, exactly, does this come about? How is this energy exchange actually accomplished? In the past this phenomenon was simply interpreted as a result of the energy conservation, but the process, or mechanisms, of the energy exchange remained unknown. As we shall now see, the generalized theory of gravitation explains this heretofore hidden process with perfect clarity.

Let a body of mass m fall under the action of Earth's gravitational field $\boldsymbol{g}$ (Figure 3). Note that the magnitude of $\boldsymbol{g}$ is equal to the acceleration of gravity g. Let the velocity of the body at the moment of observation be $\boldsymbol{v}$. Like all moving masses, the falling creates around itself a cogravitational field $\boldsymbol{K}$ left-handed relative to the velocity vector of the body. Therefore, according to Equation (10) (gravotational Poynting vector equation)

$$\boldsymbol{P} = \frac{c^2}{4\pi G}\boldsymbol{K}\times\boldsymbol{g}. \tag{40}$$

there is a flow of gravitational energy U_{gr} at the surface of the falling body directed into the body. The rate at which the ghravitational energy enters the body is

$$\frac{\mathrm{d}U_{gr}}{\mathrm{d}t} = \frac{c^2}{4\pi G}\oint(\boldsymbol{K}\times\boldsymbol{g})\cdot\mathrm{d}\boldsymbol{S}_{in} = \frac{c^2}{4\pi G}\oint(\boldsymbol{g}\times\boldsymbol{K})\cdot\mathrm{d}\boldsymbol{S}, \tag{41}$$

where $\mathrm{d}\boldsymbol{S}_{in}$ is a surface element vector of the falling body directed into the body, and $\mathrm{d}\boldsymbol{S}$ is a surface element vector directed, as usually accepted in vector analysis, from the body into the surrounding space; the integration is over the entire surface of the falling body. Transposing in the integrand the cross and the dot and factoring out the constant vector $\boldsymbol{g}$ together with the dot from under the integral sign, we have

$$\frac{\mathrm{d}U_{gr}}{\mathrm{d}t} = \frac{c^2}{4\pi G}\oint\boldsymbol{g}\cdot(\boldsymbol{K}\times\mathrm{d}\boldsymbol{S}) = \frac{c^2}{4\pi G}\boldsymbol{g}\cdot\oint\boldsymbol{K}\times\mathrm{d}\boldsymbol{S}. \tag{42}$$

Converting now the last surface integtal into the volume integral, we obtain

$$\frac{\mathrm{d}U_{gr}}{\mathrm{d}t} = -\frac{c^2}{4\pi G}\boldsymbol{g}\cdot\int\nabla\times\boldsymbol{K}\mathrm{d}V. \tag{43}$$

By Equation (7-1.4) in [3]

$$\nabla\times\boldsymbol{K} = -\frac{4\pi G}{c^2}\boldsymbol{J} + \frac{1}{c^2}\frac{\partial\boldsymbol{g}}{\partial t}, \tag{44}$$

since $\boldsymbol{g}$ is not a function of time,

$$\nabla\times\boldsymbol{K} = -\frac{4\pi G}{c^2}\varrho\boldsymbol{v}. \tag{45}$$

Therefore Equation (43) reduces to

$$\frac{\mathrm{d}U_{gr}}{\mathrm{d}t} = \boldsymbol{g}\cdot\int\varrho\mathrm{v}\mathrm{d}V. \tag{46}$$

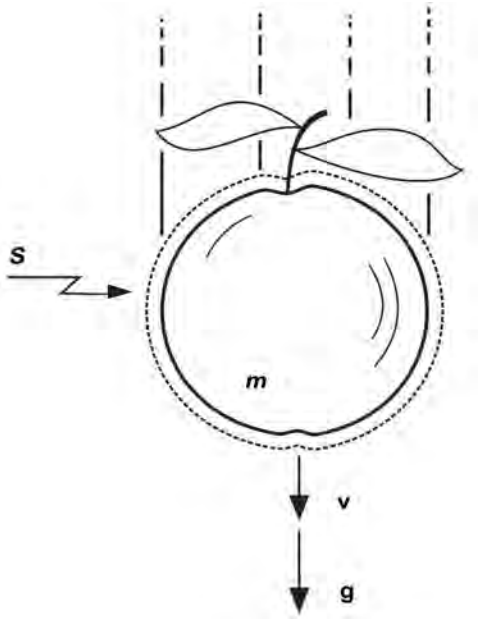

Figure 3. The generalized theory of gravitation provides a clear explanation of the mechanism of energy exchange involved in gravitational interactions: the increase of the kinetic energy of a body moving under the action of a gravitational field occurs as a consequence of the influx of gravitational field energy into the body via the gravitational Poynting vector.

Factoring out constant vector $\boldsymbol{v}$ from under the integral sign, we obtain

$$\frac{\mathrm{d}U_{gr}}{\mathrm{d}t} = \boldsymbol{g}\cdot\boldsymbol{v}\int\varrho\mathrm{d}V. \tag{47}$$

Thus, since $\boldsymbol{g}$ and $\boldsymbol{v}$ are parallel, and since the last integral in Equation (47) represents the mass of the falling body, we find that when the body is falling, there is an influx of the gravitational field energy (potential energy) into the body at the rate

$$\frac{\mathrm{d}U_{gr}}{\mathrm{d}t} = \boldsymbol{g}\cdot\boldsymbol{v}m = mvg\,. \tag{48}$$

Let us now consider the kinetic energy. The kinetic energy of a falling body increases at the rate

$$\frac{\mathrm{d}U_{gr}}{\mathrm{d}t} = \frac{\mathrm{d}}{\mathrm{d}t}\left(\frac{mv^2}{2}\right) = mv\frac{\mathrm{d}v}{\mathrm{d}t} = mvg, \tag{49}$$

where g is the acceleration of the falling body. However, as was mentioned above, g in Equation (48) is the same acceleration, and therefore the rate at which the kinetic energy of the falling body increases is equal to the rate of influx of the gravitational field energy into the body. Note that a less general case of the gravitational and kinetic energy exchange was previously considered by D. Bedford and P. Krumm in "The gravitational Poynting vector and energy transfer" [18].

Thus the generalized theory of gravitation provides a clear explanation of the

mechanism of the energy exchange involved in gravitational interactions: the increase of the kinetic energy of the body moving under the action of a gravitational field occurs as a consequence of the gravitational field energy influx into the body via the gravitational Poynting vector. Essentially the same considerations apply to the case when a body moves against the gravitational field, in which case its kinetic energy diminishes due to outflow of energy from the body into surrounding space again via the gravitational Poynting vector.

The simplicity of the above calculation tends to hide the utmost significance of the obtained results. The fact is that no gravitational theory can be considered definitive if it cannot provide a clear explanation of the mechanism of conversion of "gravitational potential energy" into the kinetic energy of falling bodies. Therefore, in spite of their simplicity, the above calculations constitute an exceptionally important proof of the validity of the generalized theory of gravitation and, at the same time, reveal the true nature of the "gravitational potential energy."

Finally, we will talk about the *existence of gravitational and cogravitational waves*. From the theoretical point of view, it is especially important that the Equations (3) and (4) can be transformed into the following differential equations in the present time:

$$\nabla \cdot \boldsymbol{g} = -4\pi G\varrho, \tag{50}$$

$$\nabla \cdot \boldsymbol{K} = 0, \tag{51}$$

$$\nabla \times \boldsymbol{g} = -\frac{\partial \boldsymbol{K}}{\partial t} \tag{52}$$

and

$$\nabla \times \boldsymbol{K} = -\frac{4\pi G}{c^2}\boldsymbol{J} + \frac{1}{c^2}\frac{\partial \boldsymbol{g}}{\partial t}. \tag{53}$$

We shall now show by direct calculation how Equations. (50)-(53) predict the existence of gravitational and cogravitational waves.

We start with Equation (52). Taking the curl of this equation, we obtain

$$\nabla \times \nabla \times \boldsymbol{g} = -\frac{\partial}{\partial t}\nabla \times \boldsymbol{K}. \tag{54}$$

Substituting Equation (53) into Equation (54), we obtain

$$\nabla \times \nabla \times \boldsymbol{g} = \frac{4\pi G}{c^2}\frac{\partial \boldsymbol{J}}{\partial t} - \frac{1}{c^2}\frac{\partial^2 \boldsymbol{g}}{\partial t^2}, \tag{55}$$

Or

$$\nabla \times \nabla \times \boldsymbol{g} + \frac{1}{c^2}\frac{\partial^2 \boldsymbol{g}}{\partial t^2} = \frac{4\pi G}{c^2}\frac{\partial \boldsymbol{J}}{\partial t}. \tag{56}$$

Similarly, taking the curl of Equation (53), we have

$$\nabla \times \nabla \times \boldsymbol{K} = -\frac{4\pi G}{c^2}\nabla \times \boldsymbol{J} + \frac{1}{c^2}\frac{\partial \nabla \times \boldsymbol{g}}{\partial t}, \tag{57}$$

and, substituting Equation (52) into Equation (57), we obtain

$$\nabla\times\nabla\times\boldsymbol{K}=-\frac{4\pi G}{c^2}\nabla\times\boldsymbol{J}-\frac{1}{c^2}\frac{\partial^2\boldsymbol{K}}{\partial t^2}, \tag{58}$$

or

$$\nabla\times\nabla\times\boldsymbol{K}+\frac{1}{c^2}\frac{\partial^2\boldsymbol{K}}{\partial t^2}=-\frac{4\pi G}{c^2}\nabla\times\boldsymbol{J}. \tag{59}$$

Equations (56) and (59) are mathematical expressions for waves propagating in space with velocity *c*. In the present case they represent waves carrying with themselves the gravitational field $\boldsymbol{g}$ and the cogravitational field $\boldsymbol{K}$, respectively.

Furthemover, by Equations. (50) and (51), in a region of space where there are no masses and no mass currents, Equations. (56) and (59) become the more familiar "wave equations"

$$\nabla^2\boldsymbol{g}-\frac{1}{c^2}\frac{\partial^2\boldsymbol{g}}{\partial t^2}=0 \tag{60}$$

and

$$\nabla^2\boldsymbol{K}-\frac{1}{c^2}\frac{\partial^2\boldsymbol{K}}{\partial t^2}=0. \tag{61}$$

Studing in [3] (pp. 303-304) energy relations in gravitational and cogravitational waves O. Jefimenko found that the energy density in these waves is *negative*.

$$U_v=-\frac{1}{8\pi G}\boldsymbol{g}^2-\frac{1}{8\pi G}c^2\boldsymbol{K}^2. \tag{63}$$

An important consequence of the negative energy density in gravitational-cogravitational waves is that in contrast to the electromagnetic waves, a gravitational-cogravitational wave striking a body pulls toward the wave, that is, exerts a negative rather than a positive pressure on the body. The calculations of the negative pressure by gravitational-cogravitational waves are similar to the corresponding calculations of the positive pressure by electromagnetic waves (see [2] pp. 132-133).

References

[1] Heaviside, O. (1893) *The Electrician*, **31**, 5125-5134.

[2] Jefimenko, O. (2000) Causality, Electromagnetic Induction and Gravitation: A Different Approach to the Theory of Electromagnetic and Gravitational Fields. Princeton University Press, Princeton, NJ.

[3] Jefimenko, O. (2006) Gravitation and Cogravitation: Developing Newton's Theory of Gravitation to Its Physical and Mathematical Conclusion. Electret Scientific, Star City.

[4] Espinoza, A., Chubykalo, A. and Carlos, D.P. (2016) *Journal of Modern Physics*, **7**, 1617-1626. https://doi.org/10.4236/jmp.2016.713146

[5] Assis, A. (2007) *Annales de la Fondation Louis de Broglie*, **32**, 117-120.

[6] Edwards, E., Ed. (2003) Pushing Gravity. Apeiron, Montreal.

[7] Eganova, I. (2005) The Nature of Space-Time. Publishing House of SB RAS, Novosibirsk.

[8] Adler, G. (1987) *American Journal of Physics*, **55**, 739-743. https://doi.org/10.1119/1.15314

[9] Okun, L. (1989) *Physics Today*, **42**, 31-36. https://doi.org/10.1063/1.881171

[10] Sandin, T. (1991) *American Journal of Physics*, **59**, 1032-1036. https://doi.org/10.1119/1.16642

[11] Jefimenko, O. (2004) Electromagnetic Retardation and Theory of Relativity. 2nd Edition, Electret Scientific, Star City.

[12] Jefimenko, O. (1995) *Galilean Electrodynamics*, **6**, 23-30.

[13] Schief, W.K. and Rogers, C. (1999) *Proceedings*: *Mathematical*, *Physical and Engineering Sciences*, **455**, 1988, 3163-3188. www.jstor.org/stable/53475

[14] Poincaré, H. (1906) *Rendiconti del Circolo Matematico di Palermo*, **21**, 129-175. https://doi.org/10.1007/BF03013466

[15] Fomalont, E. and Kopeikin, S. (2003) *The Astrophysical Journal*, **598**, 704-711. https://doi.org/10.1086/378785

[16] Jefimenko, O. (2004) *European Journal of Physics*, **25**, 287-296. https://doi.org/10.1088/0143-0807/25/2/015

[17] Synge, J. (1960) Relativity: The General Theory. North Holland, Amsterdam.

[18] Krumm, P. and Bedford, D. (1987) *American Journal of Physics*, **55**, 362-363. https://doi.org/10.1119/1.15172

Journal of Modern Physics, 2018, 9, 1545-1558
http://www.scirp.org/journal/jmp
ISSN Online: 2153-120X
ISSN Print: 2153-1196

Soldner Had Found in 1802 the Deflection of the Light by the Sun as the General Relativity Shows

Marc Mignonat

Société d'Astronomie des Pyrénées Occidentales, Pau, France
Email: mmignonat@libertysurf.fr

How to cite this paper: Mignonat, M. (2018) Soldner Had Found in 1802 the Deflection of the Light by the Sun as the General Relativity Shows. *Journal of Modern Physics*, **9**, 1545-1558.
https://doi.org/10.4236/jmp.2018.98095

Received: May 3, 2018
Accepted: July 15, 2018
Published: July 18, 2018

Copyright © 2018 by author and Scientific Research Publishing Inc.
This work is licensed under the Creative Commons Attribution International License (CC BY 4.0).
http://creativecommons.org/licenses/by/4.0/
Open Access

Abstract

Systematically, it is written in the literature that only the general relativity (GR) allows finding the just value of the deflection of the light by the sun. Yet, we noted, by reading over the original text of SOLDNER of 1801: "Ueber die Ablenkung eines Lichtstrals von seiner geradlinigen Bewegung, durch die Attraktion eines Weltkörpers, the welchem er nahe vorbei geht" (that we think it is important to put in English in full in **Appendix**) that, contrary to what we read since about 100 years, he found the right value. Soldner had started from a Newtonian gravitational calculation and, with the value of 1801, find 1.64". This calculation, with the actual values, allows finding the right value of 1.752". There are reasons to explain the wrong calculations which we usually make. However, there is no epistemological reason for questioning the general relativity. Some observations are only explained by the GR. But the Newtonian calculations are much simpler. We can continue to say that the theory of Newton is incomplete but we cannot say it is false.

Keywords

Cosmology: Theory

1. Commentary on the Article of Soldner [1]: (The Article of Soldner Is to Be Read in Appendix)

The purpose of the article of Soldner is to determine, when we observe a star, what is the correction we have to make to compensate the angle of deflection of the light which is caused by the attraction of the Earth. And if this quantity is significant and must be added to this of the refraction: "However, since also the ray-refraction is a function of height, then these two quantities must be mutually

combined...” In its article, Soldner calculates, by leaving of an inverse route Earth stars, what is the angle of deflection (“tang$\omega = AB/AD$”) and particularly what is the maximal angle of the light then horizontally arriving on the Earth. This, to correct “he aberration”, exists when we observe a star. He explains that “for convenience of the study”, “the light ray does not arrive at the place of observation, but emanates from it.” So, it was a clever way, at that time, to eliminate the problem of the speed variation of the corpuscle. The light being considered as a corpuscle, the attraction acts and so, the speed is varied. The authors, at this time (e.g. Laplace which Soldner refers), eliminated the problem with a light ray coming from the infinite, so the variation of the speed was insignificant in the zone of observation.

Other authors had made a calculation about the deflection of the light with the Newtonian method.

Michell in 1784 [2] starts from the study of the double stars and makes an analysis with the geometrical method of Newton. He suggests that corpuscles of light are attracted by gravitational forces. He specifies for which conditions the light cannot go out of the star and so, introduces the concept of the black hole.

Laplace after replacing the geometrical method of Newton by our modern mathematical analysis, in 1796 [3], from the escape velocity, calculated the exact radius (the future radius of Schwarzschild) where the light cannot go out from “un corps obscur” (a dark body).

Will in 1988 [4] wrote that: The gravitational deflection of light based on Newtonian theory and the corpuscular model of light was calculated, but never published, around 1784 by Henry Cavendish, almost 20 years earlier than the first published calculation by Johann Georg von Soldner. The two results are slightly different because, while Cavendish treated a light ray emitted from infinity, von Soldner treated a light ray emitted from the surface of the gravitating body.

Another difficulty is because of the units used in 1800 with, e.g., the velocities measured in units of length. This induce a definition of the acceleration $g = s/t^2$ and $v = 2gt$ (for us, two misprints of a factor of two since $v = gt$ and $g = s/2t^2$), but, in the calculation, these apparent mistakes cancel at the end. So, his calculation is right.

His plan (**Figure 3** in his text, **Figure 1** in this letter) is particularly clear: Soldner does his calculation on a light arriving on the celestial body and not on a ray of light which only pass and continue its course. The angle ω he calculates is the one of the light coming from an infinite distance and finishing its course “in the eye of the observer” (“ins Auge des Beobachters”) situated on Earth.

The light arriving on earth and deflected by the earth has a maximal deflection of $\omega = 0''.001$.

After he specifies if we take the light passing near the moon and arriving on earth, it would be necessary to double the value to take into account the 2 arms of the hyperbola... (der an dem Monde vorbey und auf die Erde geht, zwey Arme

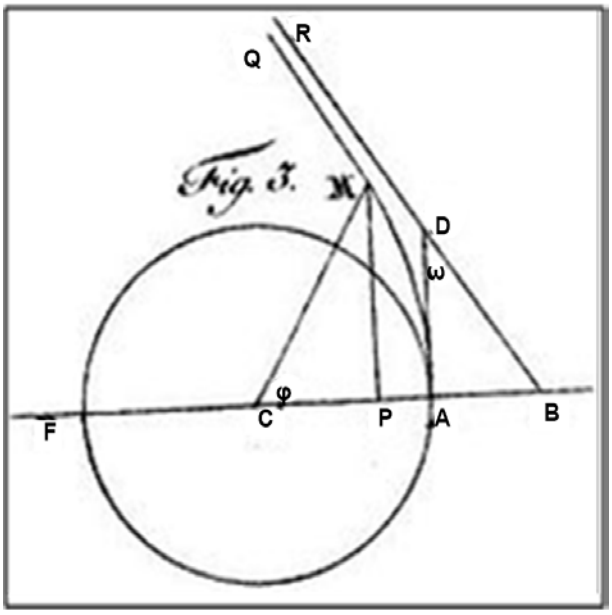

Figure 1. Original figure of Soldner where the light come from Q and finishes in A "in the eye of the observer".

der Hyperbel beschreibt). Also, we can note he calculates the conditions where the trajectory would be a parabola, an ellipse, a circle...

Then, he says that if the earth was replaced by the sun, the maximal deflection of the light arriving on the celestial body, the angle ω would be 0.84 (The light follows only an arm of the hyperbola).

It is the light arriving on sun and deflected by the sun and Soldner said (or jokes: "If it were possible to observe the fixed stars very nearly at the sun,... However, as it is well known that this doesn't happen...")

In this case, if we double the value of 0"84, (to take into account the 2 arms of the hyperbola), Soldner finds the right value of the deflection of the light passing near the sun, which is 1"64 (with the known values of the masses, of the radius and of the speeds in 1801).

2. The Wrong Answer We Often Find in the Literature

In the text of Soldner, I think it is possible to make an error for two conditions:

1) If we forget the definition of the angle ω by Soldner (angle of deflection of the light arriving on a celestial body and deflected by this celestial body)

2) And if only we read in the conclusion: "….then we find $\omega = 0$".84. If it were possible to observe the fixed stars very nearly at the sun, then we would have to take this into consideration...")

2.1. The Pseudo Error of Newton?

The reasoning, said of Newton Soldner, sometimes, is presented in the literature or on the net. A common mistake comes from the fact that the trajectory has been decomposed with three parts (**Figure 2**). It is considered the first and the

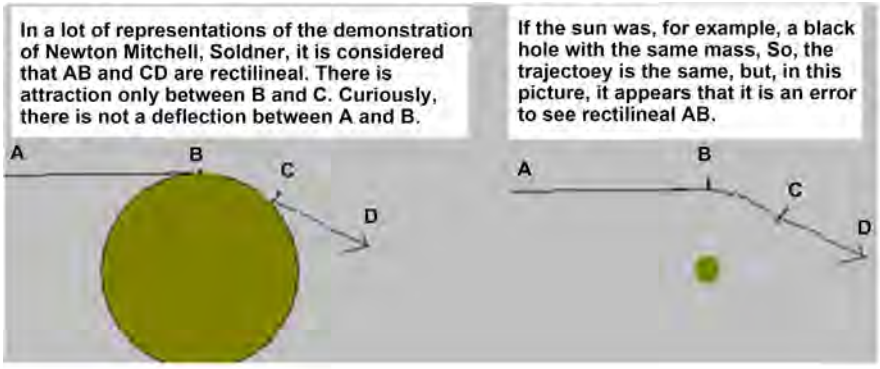

Figure 2. A common error in the representation of the trajectory of the light.

third parts are rectilineal. In the first part, the trajectory is rectilineal between infinite and the tangential point to the solar surface. So, it is considered the attraction is not exercised when the photon comes near to the Sun; the attraction is only exercised when the photon goes away! So, it is logical to find only the exact half of the correct value. Recently, in 2017, Huang [5], had also found the mistake and had made a correct calculation with a Newtonian method and clear figures. He says that there are only "minor errors" but without saying which ones, in the calculation of Soldner.

A second common error is more difficult to see (Figure 3) and, sometimes, students are provided with this figure. The deviation is also after the point of the trajectory which is tangential to the sun, but the tangential point is in A. Yet, the deviation is the same before and after a tangential point to the surface of the sun. In the figure, there is no tangential point in the zone of deviation. To have a tangential point we have to move the sun in A or turn the sun to have a radius perpendicular to the trajectory, *i.e.* we move the point A to this new point. We find again the problem of the Figure 2.

2.2. We Redid in Appendix 2 the Calculation of Soldner by a More Modern Method

The calculation was made or from the speeds or from the work of the forces with simplifications and so, perhaps the same objections identified by Soldner in his conclusion. If we take a figure with the correct path (Figure 4), the integral is made over the entire trajectory and not just half of it. The calculation allows finding the true value of the deflection of the light, so 1.75".

2.3. Hypotheses and Conclusion

It would be possible to say that the gravitational theory of Newton and the general relativity must not be so much put in contradiction. The general relativity is a more "beautiful" theory, an explanatorier theory for the curvatures, for the absence of center…

The advance of perihelion of mercury, with the pre-1920 astronomy, is only explicable with the relativity. Perhaps, the theory of Newton is incomplete but we cannot say it is false.

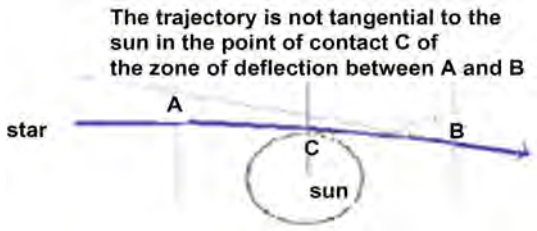

Figure 3. A second common error more difficult to see.

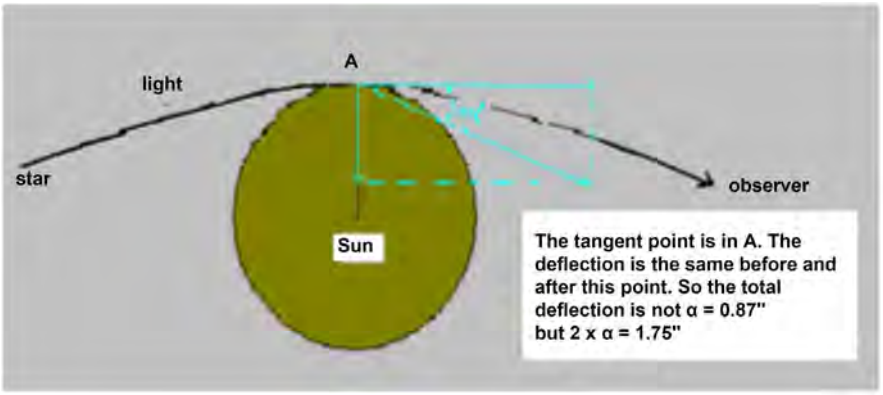

Figure 4. A representation of the path of the light with a deflection over the entire trajectory.

From a philosophic point of view, the general relativity, because coming from principles (Maupertuis, Mach) is a principle of which we can verify it is always true, and not a law in opposition with the gravitation of Newton. So, general relativity and theory of Newton perhaps are two sides or two principles of a same phenomenon.

References

[1] Soldner, J. (1804) Ueber die Ablenkung eines Lichtstrals von seiner geradlinigen Bewegung, durch die Attraktion eines Weltkörpers, an welchem er nahe vorbei geht. Berliner Astronomisches Jahrbuch, 161-172.

[2] Michell, J. (1784) *Philosophical Transactions of the Royal Society*, **74**, 35-57. https://doi.org/10.1098/rstl.1784.0008

[3] Laplace, P.S. (1796) Mécanique céleste, livre cinquième, chap. VI: Considérations sur le système du monde et sur les progrès futur de l'astronomie, 293-312.

[4] Will, C.M. (1988) *American Journal of Physics*, **56**, 413-415. https://doi.org/10.1119/1.15622

[5] Huang, F.Y. (2017) *Journal of Modern Physics*, **8**, 1894-1900. https://doi.org/10.4236/jmp.2017.811112

Appendix 1

Source:
http://en.wikisource.org/wiki/Page:Ueber_die_Ablenkung_eines_Lichtstrals_von_seiner_geradlinigen_Bewegung.djvu/1

On the deflection of a light ray from its rectilinear motion, by the attraction of a celestial body at which it nearly passes by.

By *Joh. Soldner*.

Berlin, March 1801.

At the current, so much perfected state of practical astronomy, it becomes more necessary to develop from the theory (that is from the general properties and interactions of matter) all circumstances that can have an influence on a celestial body: to take advantage from a good observation, as much as it can give.

Although it is true that we can become aware of considerable deviations from a taken rule by observation and by chance: as it was the case with the aberration of light. Yet deviations can exist which are so small, so that it is hard to decide whether they are true deviations or observational errors. Also deviations can exist, which are indeed considerable—but if they are combined with quantities whose determination is not completely finished, they can escape the notice of an experienced observer.

Of the latter kind may also be the deflection of a light ray from the straight line, when it comes near to a celestial body, and therefore considerably experiences its attraction. Since we can easily see that this deflection is greatest when (as seen at the surface of the attracted body) the light ray arrives in horizontal direction, and becomes zero in perpendicular direction, then the magnitude of deflection will be a function of height. However, since also the ray-refraction is a function of height, then these two quantities must be mutually combined: therefore it might be possible, that the deflection would amount several seconds in its maximum, although it couldn't be determined by observations so far.

These are nearly the considerations, which drove me to still think about the perturbation of light rays, which as far as I know was not studied by anyone.

Before I start the investigation, I still want to give some general remarks, by which the calculation will be simplified. Since at the beginning I only want to specify the maximum of such a deflection, I horizontally let pass the light at the location of observation (at the surface of the attracting body), or I assume that the star from which it comes, is apparently rising. For convenience of the study we assume: the light ray doesn't arrive at the place of observation, but emanates from it. We can easily see, that this is completely irrelevant for the determination of the figure of the trajectory. Furthermore if a light ray arrives at a point at the surface of the attracting body in horizontal direction, and then again continues its way (at the beginning horizontally again): then we can easily see, that with this continuation it describes the same curved line, which it has followed until here. If we draw through the place of observation and the center of the attracting body a straight line, then this line will be the major axis of the curved one for the

trajectory of light; by describing over and under this line two fully congruent sides of the curved line.

C (Figure 1) shall now be the center of the attracting body, A is the location at its surface. From A, a light ray goes into the direction AD or in the horizontal direction, by a velocity with which it traverses the way v in a second. Yet the light ray, instead of traveling at the straight line AD, will forced by the celestial body to describe a curved line AMQ, whose nature we will investigate. Upon this curved line after the time (calculated from the instant of emanation from A), the light ray is located in M, at the distance CM = r from the center of the attracting body. g be the gravitational acceleration at the surface of the body. Furthermore CP = x, MP = y and the angle MCP = h. The force, by which the light in M will be attracted by the body into the direction MC, will be $2gr^{-2}$. This force can be decomposed into two other forces,

$$2g/r^2 \cos h \quad \text{and} \quad 2g/r^2 \sin h,$$

into the directions x and y; and for that we obtain the following two equations (s. *Traité de mécanique céleste par Laplace, Tome I*, pag. 21)

$$\mathrm{d}\mathrm{d}x/\mathrm{d}t^2 = -(2g\cos h)/r^2 \tag{I}$$

$$\mathrm{d}\mathrm{d}y/\mathrm{d}t^2 = -(2g\sin h)/r^2 \tag{II}$$

If we multiply the first of these equations by $-\sin h$, the second one by $\cos h$, and sum them up, then we obtain:

$$(\mathrm{d}\mathrm{d}y\cos h - \mathrm{d}\mathrm{d}x\sin h)/\mathrm{d}t^2 = 0 \tag{III}$$

Now we multiply the first one by $\cos h$, the second one by $\sin h$ and sum them together, then we obtain:

$$(\mathrm{d}\mathrm{d}y\cos h + \mathrm{d}\mathrm{d}x\sin h)/\mathrm{d}t^2 = -2g/r^2 \tag{IV}$$

To reduce in these equations the number of variable quantities, we want to express x and y by r and h. We easily see that

$$x = r\cos h;\ y = r\sin h$$

If we differentiate, then we will obtain:

$$\mathrm{d}x = \cos h\mathrm{d}r - r\sin h\mathrm{d}h;\ \mathrm{d}y = \sin h\mathrm{d}r + r\cos h\mathrm{d}h$$

And if we differentiate again,

$$\mathrm{d}\mathrm{d}x = \cos h\mathrm{d}\mathrm{d}r - 2\sin h\mathrm{d}h\mathrm{d}r - r\sin h\mathrm{d}\mathrm{d}h - r\cos h\mathrm{d}h^2$$

and

$$\mathrm{d}\mathrm{d}y = \sin h\mathrm{d}\mathrm{d}r + 2\cos h\mathrm{d}h\mathrm{d}r + r\cos h\mathrm{d}\mathrm{d}h - r\sin h\mathrm{d}h^2$$

If we substitute these values for $\mathrm{d}\mathrm{d}x$ and $\mathrm{d}\mathrm{d}y$ in the previous equations, the we obtain from (III): $(\mathrm{d}\mathrm{d}y\cos h - \mathrm{d}\mathrm{d}x\sin h)/\mathrm{d}t^2 = (2\mathrm{d}h\mathrm{d}r + r\mathrm{d}\mathrm{d}h)/\mathrm{d}t^2$
Thus we have:

$$(2\mathrm{d}h\mathrm{d}r + r\mathrm{d}\mathrm{d}h)/\mathrm{d}t^2 = 0 \tag{V}$$

And furthermore by (IV),

$$\left(\mathrm{d}\mathrm{d}r - r\mathrm{d}h^2\right)\Big/\mathrm{d}t^2 = -2g/r^2 \qquad \text{(VI)}$$

To make Equation (V) a true differential quantity, we multiply it by $r\mathrm{d}t$, thus:

$$\left(2r\mathrm{d}h\mathrm{d}r + r^2\mathrm{d}\mathrm{d}h\right)\Big/\mathrm{d}t = 0$$

and if we again integrate, we will obtain:

$$r^2\mathrm{d}h = C\mathrm{d}t,$$

where C is an arbitrary constant magnitude. To specify C, we note that $r^2\mathrm{d}h\left(=rr\mathrm{d}h\right)$ is equal to: the double area of the small triangle which described the radius vector r in the time $\mathrm{d}t$. The double area of the triangle that is described in the first second of time, is however: = AC v; thus we have C = AC v. And if we assume the radius AC of the attracting body as unity, what we will always do in the following, then $C = v$. If we substitute this value for C into the previous equations, then: $r^2\mathrm{d}h = v\mathrm{d}t$,

Thus we have

$$\mathrm{d}h = v\mathrm{d}t/r^2 \qquad \text{(VII)}$$

If this value for $\mathrm{d}h$ is substituted into Equations (VI), we obtain:

$$\left(\mathrm{d}\mathrm{d}r/\mathrm{d}t^2\right) - v^2/r^3 = -2g/r^2$$

If we multiply this equations by $2\mathrm{d}r$, then:

$$\left(2\mathrm{d}r\mathrm{d}\mathrm{d}r\right)\Big/\mathrm{d}t^2 - 2v^2\mathrm{d}r/r^3 = 4g\mathrm{d}r/r^2$$

and if we integrate again,

$$\mathrm{d}r^2/\mathrm{d}t^2 + v^2/r^3 = 4g/r + D$$

where D is a constant magnitude, that depends on the constant magnitudes which are contained in the equation. From this equation that is found now, the time can be eliminated, hence:

$$\mathrm{d}t = \mathrm{d}r\Big/\left(D + 4g/r - v^2/r^2\right)^{1/2}$$

If we substitute this value for $\mathrm{d}t$ into Equation (VII), then we obtain:

$$\mathrm{d}h = v\mathrm{d}r/r^2\left(D + 4g/r - v^2/r^2\right)^{1/2}$$

To integrate this equations, we bring it into the form:

$$\mathrm{d}h = v\mathrm{d}r/r^2\left[D + 4g^2/v^2 - \left(v/r - 2g/v\right)^2\right]^{1/2}$$

Now we put

$$v/r - 2g/v = z$$

then we have $v\mathrm{d}r/r^2 = -\mathrm{d}z$

If this and z is substituted into the equation for $\mathrm{d}h$, the we will have:

$$\mathrm{d}h = -\mathrm{d}z\Big/\left(D + 4g^2/v^2 - z^2\right)^{1/2}$$

From that the integral is now: $h = \arccos z\Big/\left(D + 4g^2/v^2\right)^{1/2} + \alpha$

where α is a constant magnitude. By well-known properties it is furthermore:

$$\cos(h-\alpha) = z\Big/\left(D+4g^2/v^2\right)^{1/2}$$

and if we also substitute instead of z its value:

$$\cos(h-\alpha) = \left(v^2-2gr\right)\Big/r\left(v^2D+4g^2\right)^{1/2}$$

$h-\alpha$ would be the angle that r forms with the major axis of the curved line that has to be specified. Since furthermore h is the angle which r forms with the line AF (the axis of the coordinates x and y), then α must be the angle that forms the major axis with the line AF. However, since AF goes through the observation place and the center of the attracting body, then by the preceding, AF must be the major axis; also α 0, and thus:

$$\cos h = \left(v^2-2gr\right)\Big/r\left(v^2D+4g^2\right)^{1/2}$$

For $h = 0$ it must be r = AC = 1, and we obtain from this equation:

$$\left(v^2D+4g^2\right)^{1/2} = v^2-2g$$

If we substitute this in the previous equation, then the still unknown D and also the square-root sign vanish; and we obtain:

$$\cos h = \left(v^2-2gr\right)\Big/r\left(v^2-2g\right)$$

furthermore by that

$$r+\left[\left(v^2-2g\right)\Big/2g\right]r\cos h = v^2/2g \qquad \text{(VIII)}$$

From this finite equation between r and h, the curved line can be specified. To achieve this more conveniently, we again want to reduce the equation to coordinates. Let (**Figure 1**) AP = x and MP = y, then we have:

$$x = 1-r\cos h;\ y = r\sin h$$

and

$$r = \left[(1-x)^2+y^2\right]^{1/2}$$

If we substitute this into equation (VIII), then we find:

$$y^2 = \left[v^2\left(v^2-4g\right)\Big/4g^2\right](1-x)^2-\left[v^2\left(v^2-2g\right)\Big/2g^2\right](1-x)+v^2/4g^2$$

and if we properly develop everything,

$$y^2 = v^2x/g+\left[v^2\left(v^2-4g\right)\Big/4g^2\right]x^2/4g^2 \qquad \text{(IX)}$$

Since this equation is of second degree, *then the curved line is a conic section*, that can be studied more closely now.

If p is the parameter and a the semi-major axis, then (if we calculate the abscissa with its start at the vertex) the general equation for all conic sections is:

$$y^2 = px+px^2/2a$$

This equation contains the properties of the parabola, when the coefficient of x^2

is zero; that of the ellipse when it is negative; and that of the hyperbola when it is positive. The latter is evidently the case in our equation (IX). Since for all our known celestial bodies $4g$ is smaller than v^2, then the coefficient of x^2 must be positive.

If thus a light ray passes a celestial body, then it will be forced by the attraction of the body to describe a hyperbola whose concave side is directed against the attracting body, instead of progressing in a straight direction.

The conditions, under which the light ray would describe another conic section, can now easily be specified. It would describe a parabola when $4g = v^2$, an ellipse when $4g$ were greater than v^2, and a circle when $2g = v^2$. Since we don't know any celestial body whose mass is so great that it can generate such an acceleration at its surface, then the light ray always describes a hyperbola in our known world.

Now, it only remains to investigate, to what extend the light ray will be deflected from its straight line; or how great is the perturbation angle (which is the way I want to call it).

Since the figure of the trajectory is now specified, we can consider the light ray again as arriving. And because I at first want to specify only the maximum of the perturbation angle, I assume that the light ray comes from an infinitely great distance. The maximum must take place in this case, because the attracting body longer acts on the light ray when it comes from a greater than from a smaller distance. If the light ray comes from an infinite distance, then its initial direction is that of the asymptote BR (**Figure 1**) of the hyperbola, because in an infinitely great distant the asymptote falls into the tangent. Yet the light ray comes into the eye of the observer in the direction DA, thus ADB will be the perturbation angle. If we call this angle ω, then we have, since the triangle ABD at A is right-angled:

$$\text{tang}\,\varpi = \text{AB}/\text{AD}$$

However, it is known from the nature of the hyperbola, that AB is the semi-major axis, and AD the semi-lateral axis. Thus this magnitudes must also be specified. When a is the semi-major axis, and b the semi-lateral axis, then the parameter is:

$$p = 2b^2/a$$

If we substitute this value into the general equation of hyperbola

$$y^2 = px + px^2/2a$$

then it transforms into:

$$y^2 = 2b^2x/a + b^2x^2/a^2$$

If we compare this coefficients of x and x^2 with those in (IX), then we obtain the semi-major axis

$$a = 2g/\left(v^2 - 4g\right) = \text{AB}$$

the semi-lateral axis

$$b = v/\left(v^2 - 4g\right)^{1/2} = \text{AD}$$

If we substitute this values for AB and AD into the expression for tangω, then we have:

$$\text{tang}\omega = 2g \Big/ v\left(v^2 - 4g\right)^{1/2}$$

We now want to give an application of this formula on earth, and investigate, to what extend a light ray is deflected from its straight line, when it passes by at the surface of earth.

Under the presupposition, that light requires 564.8 seconds of time to come from the sun to earth, we find that it traverses 15.562085 earth radii in a second. Thus v = 15.562085. If we take under the geographical latitude its square of the sine 1/3 (that corresponds to a latitude of 35˚16'), the earth radius by 6,369,514 meters, and the acceleration of gravity by 3.66394 meters (s. *Traité de mécanique céleste par Laplace, Tome I,* pag. 118): then, expressed in earth radii, g = 0.000000575231. I use this arrangement, to take the most recent and most reliable specifications of the size of earth's radius and the acceleration of gravity, without specific reduction from the *Traité de mécanique céleste*. By that, nothing will be changed in the final result, because it is only about the relation of the velocity of light to the velocity of a falling body on earth. The earth radius and the acceleration of gravity must therefore taken under the mentioned degree of latitude, since the earth spheroid (regarding its physical content) is equal to a sphere which has earth's radius (or 6,369,514 meters) as its radius.

If we substitute these values for v and g into the equation of tang ω, then we obtain (in sexagesimal seconds) ω = 0".0009798, or in even number, ω = 0".001. Since this maximum is totally insignificant, it would be superfluous to go further; or to specify how this value decreases with the height above the horizon; and by what value it decreases, when the distance of the star from which the light ray comes, is assumed as finite and equal to a certain size. A specification that would bear no difficulty.

If we want to investigate by the given formula, to what extend a light ray is deflected by the moon when it passes the moon and travels to earth, then we must (after the relevant magnitudes are substituted and the radius of the moon is taken as unity) double the value that was found by the formula; because the light ray that passes the moon and falls upon earth, describes two arms of the hyperbola. But nevertheless the maximum must still be much smaller than that of earth; because the mass of the moon, and thus g, is much smaller. The inflexion must therefore only stem from cohesion, scattering of light, and the atmosphere of the moon; the general attraction doesn't contribute anything significant.

If we substitute into the formula for tang ω the acceleration of gravity on the surface of the sun, and assume the radius of this body as unity, then we find ω = 0".84. If it were possible to observe the fixed stars very nearly at the sun, then we would have to take this into consideration. However, as it is well known that this doesn't happen, then also the perturbation of the sun shall be neglected. For light rays that come from Venus (which was observed by *Vidal* only two minutes from the border of the sun, *s. Hr. O. L. v. Zachs monatliche Correspondenz etc. II.*

Band pag 87.) it amounts much less; because we cannot assume the distances of Venus and Earth from the sun as infinitely great.

By combination of several bodies, that might be encountered by the light ray on its way, the results would be somewhat greater; but certainly always imperceptible for our observations.

Thus it is proven: that it is not necessary, at least at the current state of practical astronomy, to consider the perturbation of light rays by attracting celestial bodies.

Now I must anticipate two objections, that possibly could raised against me.

One will notice, that I departed from the ordinary method, because I specified several general properties of curved lines before the calculation; which is what usually happens only after, and which might also could have happened at this place. Yet the calculation was very shortened by that, and why should we calculate, when that what has to be proven, can be shown much more evident by a little reasoning?

Hopefully no one finds it problematic, that I treat a light ray almost as a ponderable body. That light rays possess all absolute properties of matter, can be seen at the phenomenon of aberration, which is only possible when light rays are really material. And furthermore, we cannot think of things that exist and act on our senses, without having the properties of matter.

nihil est quod possis dicere ab omni
corpore seiunctum secretumque esse ab inani,
quod quasi tertia sit numero natura reperta.
Lucretius de nat. rer. I, 431

Furthermore I don't think that it is necessary for me to apologize, that I published this investigation; since the result leads to the imperceptibility of all perturbations. Because it also must be even nearly as important for us to know what exists according to the theory, but which has no perceptible influence in practice; as it concerns us, what has a real influence in respect to practice. Our knowledge will be equally extended by both. For example, we prove that the diurnal aberration, the disturbance of the rotation of earth and other such things in addition are imperceptibly small.

Appendix 2

Example of a calculation of the deflection of the light passing near the sun with the universal gravitation of Newton:

A photon passing near the Sun is submitted to an attractive force (**Figure A1**). First, we calculate the deviation from the ratio of the speeds in a point such that $\mathrm{tg}\alpha = \Delta vp/c$, with Δvp = perpendicular speed to the initial direction and c = speed of the light.

$$m \cdot \Delta v = F \cdot \Delta t \quad \text{(a)}$$

or

$$F = mg \quad (1),$$

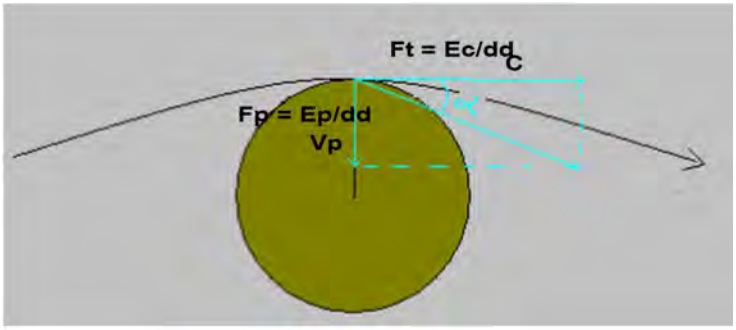

Figure A1. Bending of the light caused by the attractive force.

$$g = \left(GM/d^2\right)\cdot u \tag{2}$$

with G, the gravitational constant, M mass of the sun 1.99×10^{30} kg and d the distance between the point where is the photon and the sun, with (1) (2), (a) becomes

$$\Delta v = \left(GM/d^2\right)\cdot \Delta t \tag{a'}$$

Δt is the time of the travel of the photon, so $\Delta t = 2d/c$ since d is the distance from the point being in −infinity and the tangential point to the sun and so the distance between the tangential point to the sun and +infinity. Replacing Δt by $2d/c$, so (a') becomes

$$\Delta v = \left(2GM/dc\right)\cdot u \tag{a''}$$

The angle between Δv and Δvp is extremely weak (or between the distance d and the perpendicular motion dd), so we can use the astronomic simplification where the tangent tang a in radians is equal to $1/d$. So, we have $\Delta vp \sim \left(1/d\right)\Delta v$ and with (a''), we obtain $\Delta vp = \left(2GM/d^2c\right)\cdot u$

(with a more rigorous way, when the photon comes, we have to consider the angle a and multiply by $1/d$; when the photon goes away, so the angle is Π-a and we have to multiply by $-1/d$)

$$\text{tang}\alpha = \Delta vp/c = 2GM/d^2c^2 \tag{a'''}$$

when a point is between −infinity and the tangential point to the sun;

$\text{tang}\alpha = \Delta vp/c = -2GM/d^2c^2$ when a point is between the tangential point to the sun and +infinity)

The total angle of deviation A is calculated by integrating d between −infinity and R and between R and +infinity, R is the radius of the sun

$A \approx \text{tang}A \approx \int\left(2GM/d^2c^2\right)dd$ so between −infinity and R: $A' = 2GM/Rc^2$, thus between −infinity and + infinity, $A = 4GM/Rc^2$. It is this value of A that we find by calculating from the general relativity.

Also, the deviation can be calculated from the forces and from the work of these forces if we consider the work Wp of the perpendicular force Fp to the initial direction and the work Wt of the la tangential force Ft to the initial direction, so $Wp = Fpdd; Wt = Ftdd$. So the deviation α in a point is

$\text{tang}\alpha = Fp/Ft = Wp/Wt$. Like the tangential speed cannot exceed c, the work

Wt always equals the kinetic energy Ec corresponding to a speed c. The work Wp can be calculated from the "potential" energy E. Ep is the perpendicular component.

$E = mgd$ with m mass of the photon, g gravitational acceleration, d distance from the center of the sun to the photon $g = GM/d^2$ thus $E = mGM/d$. Like previously, we can write $Ep = E(1/d)$ so $Ep = mGM/d^2$ $Ec = 1/2(mc^2)$ with c, the speed of the photon at 3×10^8 m·s^{-1} (difficult to read for a photon without mass! But, fortunately this mass disappears during the calculation).

The angle of deviation α of the photon in a point of the trajectory is:

$$\text{tang}\alpha = Wp/Wt = Ep/Ec = (2GM/c^2)\cdot(1/d^2) \quad (3)$$

The total deviation for all the trajectory is given by the integral of the Equation (3) as above.

Numerical application:

With a solar radius R of 6958×10^5 m,

The deviation between −infinity and R is equal to 0.876", Similarly the deviation between R and + infinity is equal to 0.876"

Thus, the total deviation from −infinity to +infinity is 1.752"; this result is in perfect conformity with the observation and so precise this from the general relativity.

Journal of Modern Physics, 2018, 9, 1559-1563
http://www.scirp.org/journal/jmp
ISSN Online: 2153-120X
ISSN Print: 2153-1196

Predicted Dark Matter Quantitation in Flat Space Cosmology

Eugene Terry Tatum

760 Campbell Ln. Ste. 106 #161, Bowling Green, KY 42104, USA
Email: ett@twc.com

How to cite this paper: Tatum, E.T. (2018) Predicted Dark Matter Quantitation in Flat Space Cosmology. *Journal of Modern Physics*, **9**, 1559-1563.
https://doi.org/10.4236/jmp.2018.98096

Received: June 25, 2018
Accepted: July 15, 2018
Published: July 18, 2018

Copyright © 2018 by author and Scientific Research Publishing Inc.
This work is licensed under the Creative Commons Attribution International License (CC BY 4.0).
http://creativecommons.org/licenses/by/4.0/

Open Access

Abstract

The purpose of this paper is to show how the dark matter predictions of FSC differ with respect to the standard cosmology assertion of a universal dark matter-to-visible matter ratio of approximately 5.3-to-1. FSC predicts the correct ratio to be approximately 9-to-1, based primarily on the universal observations of global spatial flatness in the context of general relativity. The FSC Friedmann equations incorporating a Lambda Λ cosmological term clearly indicate that a spatially flat universe *must* have equality of the positive curvature (matter mass-energy) and negative curvature (dark energy) density components. Thus, FSC predicts that observations of the Milky Way and the nearly co-moving galaxies within 100 million light years will prove the 5.3-to-1 ratio to be incorrect. The most recent galactic and perigalactic observations indicate a range of dark matter-to-visible matter ratios varying from essentially zero (NGC 1052-DF2) to approximately 23-to-1 (Milky Way). The latter ratio is simply astonishing and promises an exciting next few years for astrophysicists and cosmologists. Within the next few years, the mining of huge data bases (especially the Gaia catalogue and Hubble data) will resolve whether standard cosmology will need to change its current claims for the cosmic energy density partition to be more in line with FSC, or whether FSC is falsified. A prediction is that standard cosmology must eventually realize the *necessity* of resolving the tension between their flatness observations and their assertion of dark energy dominance. The author makes the further prediction that FSC will soon become the new paradigm in cosmology.

Keywords

Flat Space Cosmology, Standard Cosmology, Cosmology Theory, Dark Matter, Cosmic Microwave Background, Planck Collaboration, Gravitational Entropy, Black Holes

1. Introduction and Background

In sharp contrast to standard cosmology, Flat Space Cosmology (FSC) makes quite a number of predictions which would invalidate the theory if proven false. Many of these predictions can be derived from the FSC Friedmann equation which must always hold true in FSC [1]:

$$\frac{3H^2c^2}{8\pi G} \cong \frac{\Lambda c^4}{8\pi G} \tag{1}$$

Wherein the left-hand term is the total matter energy density and the right-hand term is the dark energy density. The H^2 symbol is the squared Hubble parameter value in metric units (s^{-2}) and the Λ symbol is the cosmological parameter in metric units (m^{-2}). In a globally spatially flat expanding universe, *which we observe*, general relativity *stipulates* that the global positive curvature of total matter mass-energy density must equate with the global negative curvature of dark energy density. If the case were otherwise, the universe would have a global spatial curvature of sign and magnitude corresponding to the dominating energy density, *which we do not observe*. Thus, when the universe is at Friedmann's critical density, as appears to be the case by astronomical observations [2], FSC stipulates that 50% of the critical density must be attributable to total matter (visible matter plus dark matter) and 50% of the critical density must be attributable to dark energy.

One of the longstanding observational facts is that the visible matter of our universe comprises only about 5% of the critical density. Thus, FSC predicts a dark matter-to-visible matter ratio of approximately 45/5 or 9-to-1. As detailed in the Planck Collaboration consensus report, the ratio of dark matter-to-visible matter is claimed to be approximately 5.3-to-1. However, so little is currently known about precisely detecting and quantifying dark matter that *this ratio is subject to higher revision in the likely event that more dark matter is discovered in the future. For this reason, the Planck Collaboration ratio must be considered as a constraint only on the low end.*

Galactic and perigalactic distributions of dark matter can be surprisingly variable, as evidenced by the 29 March 2018 report in *Nature* [3] of an exceedingly diffuse distant galaxy (NGC 1052-DF2) apparently completely lacking in dark matter! Hence, the *global* (*i.e.*, CMB) Planck Collaboration ratio of 5.3-to-1 cannot dogmatically be considered even an approximation of all galactic and perigalactic ratios, particularly if these ratios are scalar over cosmic time.

What is now required is a best estimate of the co-moving dark matter-to-visible matter ratio within approximately 50 - 100 nearby galaxies. The only observable truly co-moving galaxy for us is the Milky Way galaxy itself. All other galaxies are observationally displaced in distance and time to some degree. However, all galaxies within 100 million light years of the Milky Way should be sufficiently close to us to be considered *approximate co-movers* for the required observations. These are the galaxies of the Virgo Supercluster. There are 160 galaxy groups within 100 million light years of the Milky Way galaxy. The number

of large galaxies is approximately 2500 and the number of dwarf galaxies is approximately 25,000 [4]. Data mining of the Gaia catalogue will not only allow researchers to determine the *range* of dark matter-to-visible matter ratios within the most accessible nearby co-moving galaxies, but to determine the *average* dark matter-to-visible matter ratio. The average ratio may be calculated by dividing the sum of the dark matter numerators by the total number of nearby co-moving galaxies reliably measured. As mentioned, *FSC predicts this average ratio to be very close to* 9-*to*-1. *A radically different average co-moving ratio would falsify FSC*. Standard cosmology, on the other hand, has no capacity to predict this ratio. Therefore, whatever this average co-mover ratio turns out to be, it will be inserted into the standard inflationary model *after its determination*.

Given the recent report of the galaxy apparently devoid of dark matter, astronomers around the world are scrambling to mine the Gaia catalogue data for further clues with respect to dark matter. The most logical place to start, of course, is with the Milky Way galaxy. Remarkably, this data has just become available! This author predicts that Posti and Helmi's May 2018 arXiv.org publication of "Mass and Shape of the Milky Way's Dark Matter Halo with Globular Clusters from Gaia and Hubble" [5] will be considered a landmark publication concerning galactic and perigalactic dark matter. *This study reveals that the virial volume comprising our Milky Way Galaxy and its dark matter halo has a dark matter-to-visible matter ratio of approximately* 23.074-*to*-1. *Thus, the matter confined within the halo radius* ("*virial radius*") *of our Milky Way galaxy appears to be approximately* 95.85% *dark matter and* 4.15% *visible matter*!

So that the reader can make the same calculations, the relevant measurements made by Posti and Helmi are repeated here: the virial mass is reported to be 1.3 +/− 0.3 × 10^{12} solar masses; the mass of the Milky Way galaxy within a generous 20 kpc. (a radius of approximately 65,200 light years) is reported to be 1.91 × 10^{11} solar masses, of which Posti and Helmi attribute 1.37 × 10^{11} solar masses to intragalactic dark matter. One can, therefore, assume the remaining 0.54 × 10^{11} solar masses to be the galactic visible matter within approximately 65,200 light years of the Milky Way center, which can be safely assumed to be greater than 99% of the Milky Way visible matter. This is because numerous reliable sources indicate the visible matter of the Milky Way to be within a radius of 50,000 light years of the galactic center. Posti and Helmi measure a virial radius of 287 kpc. This is greater than 14 times their defined radius of the galactic disc, and surely must encapsulate the vast majority of the Milky Way dark matter. Hence, one can assume that the ratio of 1.3 × 10^{12} solar masses to 0.54 × 10^{11} solar masses is an excellent approximation of the Milky Way dark matter-to-visible matter ratio. This is how the author calculated the ratio and percentage numbers in the prior paragraph.

These very recent observations ranging from 0% galactic and perigalactic dark matter (NGC 1052-DF2) to 95.85% dark matter within the virial volume of the Milky Way galaxy must be somewhat jarring to standard model proponents. The

current dogmatic acceptance of approximately 30% universal total matter mass-energy and approximately 70% dark energy appears to be on a shaky foundation [6]-[11]. Within the next few years, the mining of huge data bases (especially the Gaia catalogue and Hubble data) will resolve whether standard cosmology will need to change its current claims for the cosmic energy density partition to be more in line with FSC, or whether FSC is falsified. Regardless, standard cosmology must eventually realize the *necessity* of resolving the tension between their flatness observations and their current assertion of dark energy dominance.

2. Summary and Conclusions

The purpose of this paper has been to show how the dark matter predictions of FSC differ with respect to the standard cosmology assertion of a universal dark matter-to-visible matter ratio of approximately 5.3-to-1. FSC predicts the correct ratio to be approximately 9-to-1, based primarily on the universal observations of global spatial flatness in the context of general relativity. The FSC Friedmann equations incorporating a Lambda Λ cosmological term clearly indicate that a spatially flat universe *must* have equality of the global positive curvature (matter mass-energy) and global negative curvature (dark energy) density components. Thus, FSC predicts that observations of the Milky Way and the nearly co-moving galaxies within 100 million light years will prove the 5.3-to-1 ratio to be incorrect. The most recentgalactic and perigalactic observations indicate a range of dark matter-to-visible matter ratios varying from essentially zero (NGC 1052-DF2) to approximately 23-to-1 (Milky Way). The latter ratio is simply astonishing and promises an exciting next few years for astrophysicists and cosmologists. Within the next few years, the mining of huge data bases (especially the Gaia catalogue and Hubble data) will resolve whether standard cosmology will need to change its current claims for the cosmic energy density partition to be more in line with FSC, or whether FSC is falsified. A prediction is that standard cosmology must eventually realize the *necessity* of resolving the tension between their flatness observations and their assertion of dark energy dominance. The author makes the further prediction that FSC will soon become the new paradigm in cosmology.

Dedications and Acknowledgements

This paper is dedicated to Dr. Stephen Hawking and Dr. Roger Penrose for their groundbreaking work on black holes and their possible application to cosmology. Dr. Tatum also thanks Dr. Rudolph Schild of the Harvard Center for Astrophysics for his past support and encouragement.

References

[1] Tatum, E.T. and Seshavatharam, U.V.S. (2018) *Journal of Modern Physics*, **9**, 1404-1414. https://doi.org/10.4236/jmp.2018.97085

[2] Planck Collaboration XIII. (2016) *Astronomy & Astrophysics,* **594**, A13. http://arxiv.org/abs/1502.01589

[3] van Dokkum, P., *et al.* (2018) *Nature*, **555**, 629-632. https://doi.org/10.1038/nature25767

[4] Theuns, T. (2003) The Universe within 100 Million Light Years. Institute of Computational Cosmology. http://www.icc.dur.ac.uk/~tt/Lectures/Galaxies/LocalGroup/Back/virgo.html

[5] Posti, L. and Helmi, A. (2018) Mass and Shape of the Milky Way's Dark Matter Halo with Globular Clusters from Gaia and Hubble. arXiv:1805.01408v1 [astro-ph.GA]

[6] Tatum, E.T. and Seshavatharam, U.V.S. (2018) *Journal of Modern Physics*, **9**, 1397-1403. https://doi.org/10.4236/jmp.2018.97084

[7] Tutusaus, I., *et al.* (2017) *Astronomy & Astrophysics,* **602**, A73. arXiv:1706.05036v1 [astro-ph.CO].

[8] Dam, L.H., *et al.* (2017) Apparent Cosmic Acceleration from Type Ia Supernovae. *Monthly Notices of the Royal Astronomical Society.* arXiv:1706.07236v2 [astro-ph.CO].

[9] Nielsen, J.T., *et al.* (2015) *Scientific Reports,* **6**, Article number 35596. arXiv:1506.01354 [astro-ph.CO].

[10] Wei, J.-J., *et al.* (2015) *Astronomical Journal,* **149**, 102-113. https://doi.org/10.1088/0004-6256/149/3/102

[11] Melia, F. (2012) *Astronomical Journal,* 144. arXiv:1206.6289 [astro-ph.CO] https://doi.org/10.1088/0004-6256/144/4/110

Journal of Modern Physics, 2018, 9, 1564-1567
http://www.scirp.org/journal/jmp
ISSN Online: 2153-120X
ISSN Print: 2153-1196

A Potentially Useful Galactic Dark Matter Index

Eugene Terry Tatum

760 Campbell Ln. Ste. 106 #161, Bowling Green, KY 42104, USA
Email: ett@twc.com

How to cite this paper: Tatum, E.T. (2018) A Potentially Useful Galactic Dark Matter Index. *Journal of Modern Physics*, **9**, 1564-1567.
https://doi.org/10.4236/jmp.2018.98097

Received: June 25, 2018
Accepted: July 15, 2018
Published: July 18, 2018

Copyright © 2018 by author and Scientific Research Publishing Inc.
This work is licensed under the Creative Commons Attribution International License (CC BY 4.0).
http://creativecommons.org/licenses/by/4.0/
Open Access

Abstract

There have been a number of observational surprises with respect to galactic dark matter-to-visible matter ratios. These surprises confirm our continued lack of understanding of the fundamental nature of dark matter. Because of their apparent close ties with galactic gravitational entropy, at least four recent observations appear to provide the first evidence in support of Verlinde's theory of gravity, dark energy and dark matter as emergent properties. They also appear to correlate with Roger Penrose's gravitational entropy concept, as well as entropy defined in the Flat Space Cosmology (FSC) model. Given the observational support, two different testable versions of a "Dark Matter Index" (DMI) are introduced in this paper, and its utility is discussed in terms of potentially achieving a better understanding of the fundamental nature of dark matter.

Keywords

Dark Matter, Flat Space Cosmology, Cosmology Theory, Gravitational Entropy, Black Holes, DMI

1. Introduction and Background

Recent observations have shown a distant exceedingly diffuse galaxy (NGC 1052-DF2) with no discernable dark matter whatsoever [1]. A second report indicates the virial volume of the Milky Way galaxy to have a dark matter-to-visible matter ratio of 23.074-to-1 [2] [3].

Roger Penrose, in his new book [4], introduces the concept of gravitational entropy on pages 256-258. In sharp contrast to entropy of an ideal gas, gravitational and cosmological entropy *increases* with the ongoing clustering of stars and galaxies. Thus, as Penrose pointed out, black holes (especially supermassive black holes) become huge repositories of total cosmic entropy over the great span of cosmic time. Furthermore, as detailed in "Clues to the Fundamental Nature of Gravity, Dark Energy and Dark Matter" [5], there appears to be a deep

connection within the Flat Space Cosmology (FSC) model between gravity and cosmic entropy. Thus, FSC appears to be the cosmological model correlate to Verlinde's theory that gravity is an emergent property [6] [7]. The obvious implication, as discussed in the FSC "Clues" paper, is that if gravity is indeed an emergent property, dark energy and dark matter would also likely be emergent properties. If such were the case, dark energy could well be an emergent property of the cosmic system as a whole, and "dark matter" could well be an emergent property of the galactic visible matter. Recently, Verlinde's theory as it may pertain to dark matter, was tested by Brouwer, *et al.* [8]. Their apparent lensing excess surface density (ESD) analysis of 33,613 galaxies provided the first observational support that Verlinde's theory appears to be correct with respect to galactic dark matter.

Given this observational support for Verlinde's theory, and the apparent deep connections between cosmic entropy and gravity, dark energy and dark matter in FSC, the two additional dark matter observations mentioned in the first paragraph of this paper take on a new significance. This is because they may provide evidence that dark matter observations are closely linked with galactic gravitational entropy. *Could it be that the absence of apparent dark matter in the distant and exceedingly diffuse* (*i.e.*, *gravitationally young*) *NCG* 1052-*DF*2 *galaxy is because it has an exceedingly low gravitational entropy*? *And could it be that the relative abundance of dark matter in the relatively compact, dense and gravitationally mature Milky Way galaxy* (*including of course its supermassive black hole*), *is because it has a high gravitational entropy*? If indeed Penrose's concept of gravitational entropy is correct, the answer would seem to be an emphatic "yes!" These additional observations of dark matter in the form of dark matter-to-visible matter ratios of zero and approximately 23-to-1, respectively, would appear to provide the second and third observations in support of Verlinde's theory, and of FSC as an emergent gravity cosmological model. Furthermore, the recent report [9] that dark matter appears to be relatively scarce in the massive star-forming galaxies at high redshifts would appear to be the fourth observation in support of Verlinde's theory and the FSC model presented in the "Clues" paper.

2. Recommended Dark Matter Index with Discussion

It is not always easy to quantify the amount of dark matter within a particular galaxy and its dark matter halo. Gravitational lensing, for instance, can be a hit-or-miss proposition, depending upon the alignment of more distant galaxies. However, the above recent observational results apparently in support of Verlinde's theory suggest a possible means of indexing the dark matter of any galaxy for which the following characteristics can be measured: the galactic center intrinsic brightness I_{BGC}; and the galactic redshift S. This author suggests that these measured characteristics could be expressed in the form of a "Dark Matter Index" (DMI) ratio according to:

$$DMI = I_{BGC}/S$$

If Verlinde, Penrose and the FSC model are indeed correct, one would expect high *DMI* values to be indicative of high galactic gravitational entropy, high galactic dark matter-to-visible matter ratios, and high excess gravitational lensing powers currently attributed to dark matter. The potential usefulness of such an index could be studied by comparing galaxies in the dark matter data base for which the dark matter-to-visible matter ratio has already been measured, either by gravitational lensing or other means. Even with the more labor-intensive and alignment-dependent gravitational lensing studies of the sort reported by Brouwer, *et al*, a lensing *DMI* value (represented as DMI_L below) could ultimately prove to have better correlative power than the excess surface density value alone. The proposed relation is

$$DMI_L = ESD_{DM}/S$$

wherein ESD_{DM} is Brouwer's excess surface density proposed to be attributable to dark matter and S is the galactic redshift. If correlation studies of these *DMI* and DMI_L indices prove them to be accurate quantitative measures of galactic dark matter, this may speed up the process of truly identifying the fundamental nature of dark matter.

3. Summary and Conclusions

There have been a number of observational surprises with respect to galactic dark matter-to-visible matter ratios. These surprises confirm our continued lack of understanding of the fundamental nature of dark matter. Because of their apparent close ties with galactic gravitational entropy, at least four recent observations appear to provide the first evidence in support of Verlinde's theory of gravity, dark energy and dark matter as emergent properties. They also appear to correlate with Roger Penrose's gravitational entropy concept, as well as entropy defined in the Flat Space Cosmology (FSC) model. Given the observational support, two different testable versions of a "Dark Matter Index" (*DMI*) are introduced in this paper, and its utility is discussed in terms of potentially achieving a better understanding of the fundamental nature of dark matter.

Dedications and Acknowledgements

This paper is dedicated to Dr. Stephen Hawking and Dr. Roger Penrose for their groundbreaking work on black holes and their possible application to cosmology. Dr. Tatum also thanks Dr. Rudolph Schild of the Harvard Center for Astrophysics for his past support and encouragement.

References

[1] van Dokkum, P., *et al.* (2018) *Nature*, **555**, 629-632. https://doi.org/10.1038/nature25767

[2] Posti, L. and Helmi, A. (2018) Mass and Shape of the Milky Way's Dark Matter Halo with Globular Clusters from Gaia and Hubble. arXiv:1805.01408v1 [as-

tro-ph.GA].

[3] Tatum, E.T. (2018) *Journal of Modern Physics*, **9**, 1559-1563.

[4] Penrose, R. (2016) Fashion Faith and Fantasy in the New Physics of the Universe. Princeton University Press, Princeton. https://doi.org/10.1515/9781400880287

[5] Tatum, E.T. and Seshavatharam, U.V.S. (2018) *Journal of Modern Physics*, **9**, 1469-1483. https://doi.org/10.4236/jmp.2018.98091

[6] Verlinde, E. (2010) On the Origin of Gravity and the Laws of Newton. arXiv:1001.0785v1 [hep-th].

[7] Verlinde, E. (2016) Emergent Gravity and the Dark Universe. arXiv:1611.02269v2 [hep-th].

[8] Brouwer, M.M., *et al.* (2016) First Test of Verlinde's Theory of Emergent Gravity Using Weak Gravitational Lensing Measurements. *Monthly Notices of the Royal Astronomical Society*, 1-14. arXiv:1612.03034v2 [astro-ph.CO].

[9] Genzel, R., *et al.* (2017) *Nature*, **543**, 397-401. https://doi.org/10.1038/nature21685

Journal of Modern Physics, 2018, 9, 1568-1572
http://www.scirp.org/journal/jmp
ISSN Online: 2153-120X
ISSN Print: 2153-1196

Equivalence between a Gravity Field and an Unruh Acceleration Temperature Field as a Possible Clue to "Dark Matter"

Eugene Terry Tatum[1], U. V. S. Seshavatharam[2]

[1]760 Campbell Ln. Ste. 106 #161, Bowling Green, KY 42104, USA
[2]Honorary Faculty, I-SERVE, Hyderabad, India
Email: ett@twc.com, seshavatharam.uvs@gmail.com

How to cite this paper: Tatum, E.T. and Seshavatharam, U.V.S. (2018) Equivalence between a Gravity Field and an Unruh Acceleration Temperature Field as a Possible Clue to "Dark Matter". *Journal of Modern Physics*, **9**, 1568-1572.
https://doi.org/10.4236/jmp.2018.98098

Received: June 28, 2018
Accepted: July 15, 2018
Published: July 18, 2018

Copyright © 2018 by authors and Scientific Research Publishing Inc.
This work is licensed under the Creative Commons Attribution International License (CC BY 4.0).
http://creativecommons.org/licenses/by/4.0/

Open Access

Abstract

Einstein's equivalence principle allows one to compare the magnitudes of a gravitational acceleration field with the magnitudes of a field of Unruh acceleration temperatures. The validity of such a comparison is demonstrated by using it to derive the effective Hawking black body radiation at a Schwarzschild black hole horizon. One can then extend the black hole thought experiment to a Hawking-Unruh temperature equation expressed in terms of the Schwarzschild radius. This follows an inverse radius law rather than an inverse radius-squared law. Following a brief discussion of current theoretical failures to explain galactic rotation curves, the Unruh acceleration temperature equations are brought together to show how a rotating supermassive black hole galactic system should follow an inverse radius rule of centripetal gravitational force and centripetal acceleration. This result appears to indicate that galactic observations currently attributed to dark matter may in part be attributed to classical Newtonian dynamics superimposed on a relativistic rotating system powered by a supermassive black hole.

Keywords

Dark Matter, Unruh Effect, Unruh Temperature, Supermassive Black Holes, Galactic Rotation Curves, Equivalence Principle, Hawking Radiation

1. Introduction and Background

It is well-known that an inertial reference frame within a gravity field can be treated as equivalent to an accelerating reference frame (Einstein's equivalence principle). This is why a gravity field can be represented entirely by gamma acceleration vectors. It is also well-known that an accelerating observer or detector

in a vacuum field will observe a black body radiation spectrum appearing to originate in-line with the direction of acceleration. This is most commonly known as the Unruh effect, and the black body temperature is known as the Unruh acceleration temperature. The Unruh acceleration temperature is given by the following formula [1]:

$$T \cong \left(\frac{\hbar}{2\pi c k_B} \right) a \tag{1}$$

wherein symbol "a" represents the acceleration, and all symbols in the brackets are known constants.

Of particular interest for this discussion is that one could imagine a field of Unruh acceleration temperatures around an isolated gravitating body, with its relative magnitudes corresponding in direct proportion to the gamma field magnitudes. For instance, if one were to place two identical Schwarzschild black holes of mass M at a separation distance of their Schwarzschild radii, they would experience a net attractive force per unit mass (*i.e.*, a forward acceleration "a") of $\left(\frac{c^4}{4GM} \right)$.Thus, they would each experience an Unruh acceleration temperature of $\left(\frac{\hbar c^3}{8\pi k_B GM} \right)$ at the horizon of the opposing black hole. This particular result represented by

$$T \cong \frac{\hbar c^3}{8\pi k_B GM} \tag{2}$$

is identical to the Hawking temperature derivation now known as Hawking radiation [2]. Hawking radiation can be considered the black hole black body radiation taking place at or very near every black hole horizon. Thus, temperature T in Equation (2) is also sometimes referred to as the Hawking-Unruh temperature [3].

It is also valid to use the Schwarzschild formula and substitute $\left(\frac{Rc^2}{2G} \right)$ for M, giving the equivalent Hawking-Unruh temperature in the form of

$$T \cong \frac{\hbar c}{4\pi k_B R} \tag{3}$$

wherein R represents the Schwarzschild radius and the other symbols in the right-hand term are known constants.

By Equation (1) we can imagine a proportional equivalency between the magnitudes of an Unruh acceleration temperature field and the gamma magnitudes of a gravitational field. In Equation (3) we see indirect proportionality between the magnitude of the Unruh acceleration temperature field at a black hole's horizon and the magnitude of its Schwarzschild radius R. Of particular note is that *these relationships can only be true if the gravitational field around a black hole of any size does not follow an inverse R-squared law but rather an inverse R law*!

2. Discussion

It has only recently become evident that all, or nearly all, galaxies have a central supermassive black hole. However, for a number of decades, the rotation curves of galaxies have been quite puzzling [4] [5] [6]. Their plate-like stellar rotation was a clear indication that the classical inverse *R*-squared gravitational law of our solar system could not easily be extended to galaxies. These aberrant galactic rotations have long been known to act more as if stellar centripetal forces (and their associated accelerations) vary inversely with radius distance from the galactic center, rather than the expected radius distance squared.

Over the last few decades, two basic theoretical approaches have been attempted to address this paradox [7] [8]. By far the most popular approach has been to suggest a halo-like distribution of non-visible (*i.e.*, "dark"), non-baryonic, cold matter which only interacts with ordinary visible matter by gravitational attraction. However, numerous varied and highly creative observational studies to detect and determine the exact nature of dark matter, including how it revises the Standard Particle Model, have failed in this regard. The second theoretical approach has been to find a reasonable modification of Newton's law of gravity in order to explain the aberrant galactic rotation. This search for a theory of Modified Newtonian Dynamics (MOND) has met with limited success [9], mostly by an ad hoc search for new gravitational equations, effects of which are designed to become noticeable only at the extremely small stellar centripetal accelerations within the outer two-thirds of the galactic disc.

Now recent theoretical approaches [10] [11] [12], as well as computer-generated Gaia star map analysis [13], strongly suggest that a new type of matter outside of the Standard Particle Model, or an ad hoc modification of Newtonian dynamics, may be completely unnecessary. The report on the Gaia billion-star map study by Enbang Li concluded that *the flat galactic rotation curve of the Milky Way galaxy can be entirely explained without the need for a dark matter halo*! Erik Verlinde's "emergent gravity" theory and Flat Space Cosmology [Tatum, *et al.* (2018)] provide support for inertial effects of galactic visible matter entropy as being largely responsible for "dark matter" observations. The July 2018 *Journal of Modern Physics* paper entitled "A Potentially Useful Dark Matter Index" [14] references four very recent observational studies which appear to support this concept of a possible link between "dark matter" and inertial effects of galactic gravitational entropy.

Furthermore, it occurs to this author that we have been thinking about a rotating galaxy in the wrong way. *Rather than trying to impose classical Keplerian and Newtonian solar system model kinematics and dynamics, we should think of galaxies as a rotating supermassive black hole* (*SMBH*) *system.* If we think of galactic evolution as beginning with fast-spinning quasars and blazars, we are probably better-equipped to think of modern co-moving galaxies as being relatively quiescent former dynamos which began with extremely powerful organizing magnetic fields. For this reason, perhaps, modern galaxies appear to behave

more like a spinning flywheel than a solar system.

Furthermore, and perhaps most importantly, it should not surprise us if dynamic SMBH systems have long-since locked in their plate-like stellar rotations with an inverse radius rule along the lines of Equation (3). By combining Equations (1) and (3), which can both be applied, as shown, to black holes (specifically SMBHs in this case), we get

$$\left(\frac{\hbar}{2\pi c k_B}\right) a \cong \frac{\hbar c}{4\pi k_B R} \tag{4}$$

which simplifies to

$$a \cong \frac{c^2}{2R} \tag{5}$$

One can see that this is a centripetal acceleration formula of the type $a_c \cong \frac{v^2}{R}$, wherein rotational velocity $v \cong \frac{c}{\sqrt{2}}$ is a constant at horizon radius R.

Thus, we have what appears to be classical Newtonian dynamics superimposed on a relativistic rotating galactic system powered by a SMBH.

3. Summary and Conclusions

Einstein's equivalence principle allows one to compare the magnitudes of a gravitational acceleration field with the magnitudes of a field of Unruh acceleration temperatures. The validity of such a comparison is demonstrated by using it to derive the effective Hawking black body radiation at a Schwarzschild black hole horizon. One can then extend the black hole thought experiment to a Hawking-Unruh temperature equation expressed in terms of the Schwarzschild radius. This follows an inverse radius law rather than an inverse radius-squared law. Following a brief discussion of current theoretical failures to explain galactic rotation curves, the Unruh acceleration temperature equations are brought together to show how a rotating supermassive black hole galactic system should follow an inverse radius rule of centripetal gravitational force and centripetal acceleration. This result appears to indicate that galactic observations currently attributed to dark matter may in part be attributed to classical Newtonian dynamics superimposed on a relativistic rotating system powered by a supermassive black hole.

Dedications and Acknowledgements

This paper is dedicated to Dr. Stephen Hawking and Dr. Roger Penrose for their groundbreaking work on black holes and their possible application to cosmology. Dr. Tatum also thanks Dr. Rudolph Schild of the Harvard Center for Astrophysics for his past support and encouragement.

References

[1] Unruh, W.G. (2001) Black Holes, Dumb Holes, and Entropy. In: Callender, C., Ed.,

Physics Meets Philosophy at the Planck Scale, Cambridge University Press, 152-173, Eq. 7.6. https://doi.org/10.1017/CBO9780511612909.008

[2] Hawking, S. (1976) *Physical Review D,* **13**, 191-197. https://doi.org/10.1103/PhysRevD.13.191

[3] Alsing, P.M. and Milonni, P.W. (2004) *American Journal of Physics*, **72**, 1524. arXiv:quant-ph/0401170.

[4] Rubin, V.C., Thonnard, N. and Ford, W.K. (1978) *The Astrophysical Journal Letters*, **225**, L107-L111.

[5] Salucci, P. and De Laurentis, M. (2012) *Proceedings of Science* (DSU 2012). arXiv:1302.2268.

[6] Salucci, P., *et al.* (2007) *Monthly Notices of the Royal Astronomical Society*, **378**, 41-47. arXiv:astro-ph/0703115. https://doi.org/10.1111/j.1365-2966.2007.11696.x

[7] McGaugh, S. (2014) *Canadian Journal of Physics*, **93**, 250-259. arXiv:1404.7525

[8] Milgrom, M. (1983) *Astrophysical Journal*, **270**, 365-370.

[9] Kroupa, P., Pawlowski, M. and Milgrom, M. (2012) *International Journal of Modern Physics D*, **21**, 1230003.arXiv:1301.3907

[10] Verlinde, E. (2011) *Journal of High Energy Physics*, **4**, 29-55. arXiv:1001.0785v1 [hep-th] https://doi.org/10.1007/JHEP04(2011)029

[11] Verlinde, E. (2016) Emergent Gravity and the Dark Universe. arXiv:1611.02269v2 [hep-th]

[12] Tatum, E.T. and Seshavatharam, U.V.S. (2018) *Journal of Modern Physics*, **9**, 1469-1483. https://doi.org/10.4236/jmp.2018.98091

[13] Li, E. (2018) Modelling Mass Distribution of the Milky Way Galaxy Using Gaia's Billion-Star Map. https://arxiv.org/ftp/arxiv/papers/1612/1612.07781.pdf

[14] Tatum, E.T. (2018) *Journal of Modern Physics*, **9**, 1564-1567.

Journal of Modern Physics, 2018, 9, 1573-1590
http://www.scirp.org/journal/jmp
ISSN Online: 2153-120X
ISSN Print: 2153-1196

Bell's Theorem and Instantaneous Influences at a Distance

Karl Hess

Center for Advanced Study, University of Illinois, Urbana, USA
Email: karlfhess@gmail.com

How to cite this paper: Hess, K. (2018) Bell's Theorem and Instantaneous Influences at a Distance. *Journal of Modern Physics*, **9**, 1573-1590.
https://doi.org/10.4236/jmp.2018.98099

Received: June 25, 2018
Accepted: July 15, 2018
Published: July 18, 2018

Copyright © 2018 by author and Scientific Research Publishing Inc.
This work is licensed under the Creative Commons Attribution International License (CC BY 4.0).
http://creativecommons.org/licenses/by/4.0/
Open Access

Abstract

An explicit model-example is presented to simulate Einstein-Podolsky-Rosen (EPR) experiments without invoking instantaneous influences at a distance. The model-example, together with the interpretation of past experiments by Kwiat and coworkers, uncovers logical inconsistencies in the application of Bell's theorem to actual EPR experiments. The inconsistencies originate from topological-combinatorial assumptions that are both necessary and sufficient to derive all Bell-type inequalities including those of Wigner-d'Espagnat and Clauser-Horne-Shimony-Holt. The model-example circumvents these inconsistencies.

Keywords

Bell's Theorem, Instantaneous Influences, EPRB Experiments

1. Introduction

Einstein and Bohr debated the completeness of quantum theory and Einstein proposed a Gedanken-experiment involving two space-like separated measurement stations that demonstrated, in his opinion, that either quantum theory was incomplete or implied the involvement of instantaneous influences at a distance. This Gedanken-experiment was discussed in great detail in the literature; first by Einstein with his coworkers Podosky and Rosen (EPR) [1], later by Bohm and most importantly for the following considerations by Bell [2]. The Gedanken-experiment was subsequently performed in a variety of ways which are usually referred to as EPRB experiments. Three of these actually performed experiments are of particular importance: experiments of Aspect and coworkers [3], because they were the first to exclude the possibility of communications between the two separated stations with the speed of light in vacuo or slower, of Weihs, Zeilinger and coworkers [4], because their

experiments were performed over the greatest distances and of Kwiat and coworkers [5], because their experiments were performed with highest statistical reliability and greatest precision.

The measurement-machinery detects a signal from a source S that is assumed to be located roughly at equal distance from both measurement stations and emanates correlated pairs of quantum entities; one part to each station. In the experiments of Zeilinger and coworkers, the space-like separation of the measurements has been as far as the separation of the islands of Tenerife and La Palma and has recently involved even satellites. The actual measurements have mostly been performed using correlated photons and the measurement equipment has involved polarizers with different measurement arrangements or "settings" which are denoted usually by unit vectors such as a at one location and b at the other. The following discussion, however, is not specialized to photons but admits any correlated particle-pairs and spin measurements that may also be performed by using Stern-Gerlach magnets. The same notation is used then for the orientation of these magnets.

As mentioned, EPR [1] intended to demonstrate that quantum mechanics is either incomplete or involves instantaneous influences at a distance. However, Bell's theorem and the violation of Bell's inequality [2] by the actual experiments appeared to deny incompleteness (the existence of so called hidden variables) and bring a decision in favor of instantaneous influences. I shall show in this paper that Bell's theorem contains two distinct claims that are based on different propositions. One of the claims is proven to contain a logical inconsistency, which becomes particularly evident from the experimental results of Kwiat and coworkers (presented in Figure 2 of [5]). As a consequence, the theorem is generally invalid and cannot decide between Einstein's alternatives. These facts are demonstrated by using an explicit model-example.

2. The Theorem of Bell

"But if [a hidden variable theory] is local it will not agree with quantum mechanics, and if it agrees with quantum mechanics it will not be local. This is what the theorem says."—JOHN STEWART BELL [6]

The word "local" has received numerous interpretations in relation to Bell's work and his theorem may be proven in a variety of ways for different meanings of the word. It is the conviction of the author that the only acceptable meaning of "local" clearly excludes any influences faster than the speed of light in vacuo and thus any instantaneous influences at a distance.

A significant number of famous physicist has spoken against the possibility of instantaneous influences at a distance including Murray Gell-Mann [7] and (in a much more detailed discussion) Marlan O. Scully, Yakir Aharonov and B. G. Englert [8].

There have been numerous publications related to problems with Bell's inequality by notables including L. Accardy, J. Christian, H.A. De Raedt, A.

Khrennikov, M. Kupczinsky, K. Michielsen, T. Nieuwenhuizen, W. Philipp, L. Sica and others including myself. Some of the essence of their work is presented and referenced in a special issue of Open Physics [9]. Of course, many papers have been published to praise Bell's work and to present variations on his theme, with the work of E. Wigner being of particular importance.

It is the purpose of this paper to show that the mathematical-physical formulation and proof of the theorem of Bell consist of two distinct parts, I and II, that are based on distinctly different premises. I shall show by example that part I of the theorem may contradict part II, because Bell's premises for the second part are much more restrictive than those of the first and include logically inconsistent topological-combinatorial assumptions. As a consequence, a way around the strictures of Bell's theorem may be found. In particular, I present an explicit model for part I that works without instantaneous influences at a distance and may be executed on two distant computer stations.

2.1. Expectation Value for Pair Measurements

Bell's original paper [2] Introduces functions $A(\boldsymbol{a},\lambda)=\pm 1$ and $B(\boldsymbol{b},\lambda)=\pm 1$, with the important requirement that the possible outcomes B, symbolizing the measurements with magnet setting $\boldsymbol{b}$ in station 2, do not depend on the magnet setting $\boldsymbol{a}$ in station 1 and vice versa. Bell's λ characterizes a pair with singlet correlations emanating from the source S. Bell regards λ as an element of reality as defined by Mach and Einstein and also states that "λ stands for any number of variables and the dependences thereon of A and B are unrestricted." Furthermore, Bell requires that the average product of these functions over many measurements must equal the quantum mechanical expectation value for singlet spin correlations, which is:

$$E(\boldsymbol{a},\boldsymbol{b})=-\boldsymbol{a}\cdot\boldsymbol{b}. \tag{1}$$

Bell then states "But it will be shown that this is not possible", a statement that forms the first part of the Bell theorem.

These facts show that Bell committed, from the start, an inaccuracy by defining λ as both an element of physical reality and also as a mathematical variable, in particular a variable of probability theory. The probability theory of Kolmogorov, however, is very careful to distinguish between variables and outcomes or actualizations (such as a given λ_{act}) of these variables. The actualizations are "chosen" by Tyche, the goddess of fortune out of an "urn" (see also [10]). We distinguish in the following carefully between variables and possible or actual outcomes and shall use in all the derivations actual or possible outcomes corresponding to elements of reality.

As shown below, there exists no difficulty in deriving the quantum expectation value of Equation [1]. An additional requirement of quantum theory, however, demands that the marginal expectation values are given by $E(\boldsymbol{a})=E(\boldsymbol{b})=0$. We show that this additional requirement can also be met in a variety of local ways.

Bell stated that it was impossible to construct a model that achieves all of these requirements of quantum theory by using functions A in one wing of the experiment and B in the other, which both depend solely on variables related to the local measurement stations and the emission from a common source. We refer to this statement as proposition I.

Bell did not prove proposition I directly. He only presented illustrations of difficulties [2] that were followed by his well known inequality, which he derived by using additional assumptions (now for the expectation values of 3 EPRB experiments). We demonstrate in a later section, by an explicit model, that these additional assumptions are generally invalid and have no bearing on the outcomes of any single-pair EPRB experiment.

2.2. Three Different Measurement-Pairs and Bell's Inequality

The second part of Bell's theorem and his proof relate to three different pairs of magnet (polarizer) settings $(\boldsymbol{a};\boldsymbol{b})$, $(\boldsymbol{a};\boldsymbol{c})$ and $(\boldsymbol{b};\boldsymbol{c})$. The semicolon ";" in between the pairs indicates that the pairs are correlated. These pairs may, in principle, be linked to the same source S or to three different sources. Kolmogorov's probability framework requires, in general, three different sample spaces and correspondingly three probability spaces; one for each magnet-setting pair. Bell, however, assumes that λ is defined on one common probability space for all three experiments. This assumption together with Bell's particular choice of setting pairs has topological-combinatorial consequences that are necessary and sufficient ([11] [12]) to prove Bell's inequality:

$$\left|E(\boldsymbol{a},\boldsymbol{b})-E(\boldsymbol{a},\boldsymbol{c})\right|\le 1+E(\boldsymbol{b},\boldsymbol{c}). \tag{2}$$

We refer to this inequality together with its specific assumptions for the 3 experiments with different magnet setting pairs (explained in detail below) as Bell's proposition II.

Proposition II is in conflict with the quantum expectation values presented in proposition I and also with the results of actual EPRB experiments. Use, for example, the unit vectors $\boldsymbol{a}=[1,0],\boldsymbol{b}=\left[\frac{1}{2},\frac{\sqrt{3}}{2}\right]$ and $\boldsymbol{c}=\left[\frac{-1}{2},\frac{\sqrt{3}}{2}\right]$ in Equation [1] and the inequality is violated. Variations of Bell's proof have been presented by many researchers, with the work of Wigner and d'Espagnat being of particular importance.

"Loopholes" in Bell's argument have been discussed previously by this author and coworkers. These loopholes are based on possible dependencies of Bell's functions on space-time [11] and on other globally defined variables, such as thresholds for the particle detectors [13].

In the present paper it is shown that proposition I is incorrect; the quantum result can be simulated by local functions as Bell required. This fact is shown by an explicit example. Furthermore, it is proven that proposition II and Bell's inequality are marred by inconsistent topological-combinatorial assumptions

and cannot be used to support proposition I, which denies the possibility to obtain the quantum theoretical result.

3. Bell's Theorem and the Alice-Bob-Tutorials

This section is to prepare the reader for the following model of EPRB experiments and to safeguard against some common prejudices that obstruct a clear logical approach to understand such models.

3.1. Alice, Bob and Relativity

One of the greatest obstacles for progress related to the conundrum posed by Bell's theorem is the indiscriminate use of the so called Bell game (discussed in more detail in the last section) to justify Bell's theorem, a theorem of mathematical physics. Any such theorem must start from a given physical situation corresponding to actual experiments, which is in the present case the measurement of a correlated pair of quantum particles by two separated magnets (polarizers) with directions a and b respectively. The scientist working on the theorem, be it its proof or refutation, may then use the tools of mathematics such as functions and prove from the form of the tools, e.g. the domain and the range of the functions, certain propositions. In the present case, Bell postulated that the domain of the used functions contain only variables that depend on the local physical situation in the measurement stations as well as on "information" that is sent from a source to the stations. It is of no concern whether or not the scientists have some global knowledge while they prove or disprove a given model of mathematical physics. The "local" quality and validity of the functions must be purely based on their mathematical form and not on what the scientists "knew" when they developed the model. It would be totally preposterous to call Newtons laws for the motion of the planets non-local in space and time, with the only reason that Newton knew where Mars was to be found six month later.

The well known tutorials related to Bell's theorem involve two "players": Alice, who has only knowledge of one wing of the EPRB experiment, and by Bob, who has only knowledge of the other wing. Reasoning involving Alice and Bob requires appropriate care. Bell himself certainly did not use any Alice-Bob arguments in his original paper which enunciated the core of his theorem. Of course, it is correct that Alice and Bob will not be able to describe the quantum correlations when they know absolutely nothing of each other. If they just measure the whole run and then combine the results by taking the count of signals on each side, a single quantum fluctuation will destroy the correlation. The true form of the correlated functions must certainly depend on the fact that they both describe the same correlated pair, but Alice and Bob can never know about the correlation without information additional to their local knowledge. Bell was not concerned about this fact when presenting his proof. He just went ahead by assuming that he was dealing with correlated pairs only and the given magnet settings in the moment of measurement. However, this assumption leads

to a mathematical ambiguity in his formalism. His variable λ and its possible outcome values are not distinctly marked as to which correlated pair they belong. In the case of at least two possible magnet settings on each side, this ambiguity leads, as we will see in a later section, to the logical mistake of indiscriminately pairing Bell-type functions who's λ may actually belong to two different correlated pairs. The requirement that Alice and Bob know nothing about each other leads thus directly to the lack of the necessary mathematical distinction of variables and their possible outcomes.

In addition we need to admit the relativity of the two measurements of the EPRB correlated pairs. Consider the well known relativity-example of two elastic balls bouncing between two parallel plates each in a different inertial system; one attended by Alice, the other by Bob. Bob and Alice know nothing of each other and have the task of determining the temporal correlations between the two bouncing balls. Of course that cannot be done. If they are taking off their blindfold and are allowed to observe both balls, they may come up with a theory for the correlations that depends on the relative velocity of their moving system. Let both systems move along the x_1-axis of a coordinate system, one with velocity a and the other with velocity b. The law of the correlations that Alice and Bob observe depends then on the velocity-difference $a-b$. In order to describe the law of the correlations by local functions, Alice may put $a = 0$ and describe the movement of Bob's bouncing ball as function of any velocity b of his system. Bob may do the same with a and b exchanged.

We deduce from this example that also the relativity of spin-correlation measurements in EPRB experiments does not have anything to do with distant influences but must rather be seen as a consequence of natural law. The important point is that we may indeed describe the physical events by functions of local variables from both the view of Alice and the view of Bob. The laws of physics are the same for each of them, but the physical circumstances of their respective measurements are different. In our model below, we put the magnet setting in the left wing to $\boldsymbol{a} = [1,0]$ and express the results in the right wing as function of arbitrary local magnet setting $\boldsymbol{b}$ only. Any such model must be commensurate with the relativity of all motion. In a general situation, it may thus depend even on the relative angle between the magnets (polarizers), without indicating deviations from locality. Muchowski has advanced ideas along these lines in his considerations of Bell's work as related to EPRB experiments with photon pairs [14].

3.2. Completely "Random" Measurements

A particularly difficult situation for the discussions of Bell's work is created when both Alice and Bob supposedly switch their magnet settings absolutely randomly and, in addition, do not know what happens in the other wing. However, this imagined situation only obfuscates the problem and does not address the way how EPRB experiments are actually performed. The random

switching done by the Aspect and Zeilinger groups does not mean that the magnet settings for the actual measurements are random. Quite the contrary, only 3 or 4 pairs of settings are chosen in random sequence. In addition each of these sequential pairs must have at least one magnet setting in common with the other pairs. The only important randomness of the settings occurs in between the measurements, which is only relevant for reasoning about the locality of the actual experiments but not for any simulation with local functions.

The so called "random pairs" may thus be sorted into 3 or 4 sets, which is exactly what Wigner did in his set theoretical approach that will be discussed in a later section. It is important to realize that each of these sets concatenated by Wigner form a given sample space in the sense of Kolmogorov's set theoretic probability theory and can be, under a certain condition, regarded as a run of measurements equivalent to a completely separate EPRB experiment with a different source. The condition for the equivalence is the absence of memory effects in source and measurement equipment. Such effects are usually considered to be "far out" and have exclusively been used to argue against Bell's inequality.

3.3. Counterfactuals and Other Issues

Numerous attempts have been made to prove Bell's theorem by counterfactual reasoning (that would not be permitted in the courts of law). We have shown that counterfactual reasoning does not apply when Bell's functions depend explicitly on the measurement time, as explained in detail in [15]. Our model presented below does exhibit such time-dependence. In addition we show under which circumstance and how counterfactual arguments may and may not be applied (see discussion of the proof of d'Espagnat).

We are not able to cover all of the issues that have been discussed in the vast literature surrounding the work of Bell and like to offer only the following observation. There are many ways to violate Bell's inequality by admitting some global knowledge as, for example, the knowledge of the relativity of all motion. The moment, however, we exclude all global knowledge, we are only left with some magic instantaneous influences from a distantly occurring measurement.

4. Explicit Model for the Quantum Result

The following explicit model may be implemented on two independent computers as well as checked by hand and represents a counterexample to Bell's claims. I refer to this model as the EQRC-model. The acronym refers to the Expectation value of the Quantum Result, with the C indicating that the model may be executed on conventional computers.

In the derivation of this EQRC-model, the space-time coordinates (x_1, x_2, x_3, x_4) of special relativity may be used. We use, however, for the sake of transparency exclusively coordinates of the laboratory reference frame, with x_4 being time-like and x_1, x_2, x_3 being space-like. In addition we use a global gauge

field which we shall specify below. This gauge field may also be viewed as a global "crypto key" and the whole model may be regarded as model of a computer experiment involving two (or more) computers, which have a common crypto-key that is available as a local computer-application.

We assume as usual that a pair with singlet spin correlations emanates from a source in opposite directions along the x_1-axis. The element of reality characterizing the singlet pair is denoted by $\lambda^1_{st(n)}$, where the subscript indicates space-time coordinates $st(n)$ related to the emission from the source and n is a number indicating that we deal with a correlated pair.

The magnet (or polarizer) directions are denoted by two dimensional unit vectors $\boldsymbol{a},\boldsymbol{b}$ perpendicular to the x_1-axis and parallel to the (x_2,x_3) plane. Each Stern-Gerlach magnet transmits to two detectors that are arranged perpendicular to the x_1-axis in the direction of $\boldsymbol{a}$ in the left wing (detectors D^1_L and D^2_L) and $\boldsymbol{b}$ in the right wing (detectors D^1_R and D^2_R), respectively.

We need to decide consistently under which circumstance we regard outcomes in the two wings as equal or different (anti-correlated) in order to derive Bell-type inequalities, which can be achieved by first fixing the magnet direction (and detector alignment) of the left wing to $\boldsymbol{a}=[1,0]$ through suitable choice of the coordinate system. Then we turn the magnet direction (and detector alignment) of the right wing such that anti-correlated outcomes are maximized (ideally occur with probability 1).

Anti-correlated means that the detections in the left wing are registered by detector 1, while the detections in the right wing are registered by detector 2 or vice versa. We define the position $\boldsymbol{b}'$ that maximizes anti-correlated outcomes as the position of equal settings $\boldsymbol{b}'=\boldsymbol{a}=[1,0]$ in the right wing. (This procedure is particularly necessary when photons, polarizers and optical fibers are involved.) We then turn the direction of the detectors in the right wing to any $\boldsymbol{b}\neq\boldsymbol{a}$ again perpendicular to the x_1-axis. Outcomes are defined as different, if they are registered in detectors with a different number (1, 2) or (2, 1) in the two wings. If the outcomes are with equal detector-numbers (1, 1) or (2, 2), we define the outcomes as equal. If polarizers are involved instead of magnets we need to proceed somewhat differently, but the differences matter little for the following discussions.

All Bell-type inequalities, including that of Wigner [16] and d'Espagnat [17], are inequalities related to the number of equal outcomes as opposed to non-equal outcomes for Bell's three different setting pairs (four or more pairs in the case of other inequalities). Having in mind these details about detection, we may simplify the notation by just denoting all outcomes at detectors 1 (one in each wing) by +1 and those at detectors 2 by −1 and assign the value of +1 or −1 as the (possible) outcome for Bell's functions A and B respectively. If the product of the correlated outcomes in the two wings is positive, the outcomes are equal and if negative they are different. In this way both Bell's and Wigner's inequality (and all other forms of Bell-type inequalities) may be covered by the model that follows.

Note that there is a certain arbitrariness in the definition of equal and different outcomes, because the detection of two tilt detector pairs, one in each wing, is regarded as equal if only the detections occur for the detectors with the equal number, independent of their actual setting-directions. In case one deals with more than one detector pair in each wing (as is the case for the Aspect- and Zeilinger-types of experiment), appropriate care should be taken to guarantee consistent definition of equal and different outcomes (see below).

In addition to these conventions, we introduce a global gauge function, that is identical for all x_1, x_2, x_3 and varies only with the global time like coordinate x_4. This function may be regarded in analogy to the concept of gauge fields in physics or, as mentioned, one may regard this function as a global crypto-key for computers, if the model is implemented as a computer experiment. The global gauge or crypto-key, both functions of space-time, or just of x_4 in our example, are assumed to have either no effect at all, or alternatively, to result in a signal transfer to the alternate detector. We denote this global function by $rm(x_4) = +1$ if it has no effect and by $rm(x_4) = -1$ if it changes detectors.

We furthermore choose for our model a very simple $\lambda^1_{st(n)}$ and let it randomly assume a value that corresponds to a real number of the unit interval, which results in $0 \le \lambda^1_{st(n)} \le 1$ for each pair of measurements.

To derive the quantum result we need to consider only the outcomes for an arbitrary setting $\boldsymbol{b}$ perpendicular to the x_1-axis in the right wing. As mentioned, we choose the coordinate system of the laboratory such that $\boldsymbol{a} = [1, 0]$. The introduction of *rm* accomplishes vanishing marginal expectation values.

It is not claimed that these very simplified assumptions satisfactorily simulate all aspects of natures actual mechanisms. More complicated time dependencies [12] are certainly possible. We will see, however, that the model suffices to simulate the results of quantum theory for EPRB experiments. (To calculate the correlation with the other side quickly and explicitly from the equations given below, you may just use at first $rm = +1$.)

We assign the following possible outcomes for the functions A in the left wing:

$$A\left(\boldsymbol{a}, \lambda^1_{st(n)}, x^n_4\right) = +rm\left(x^n_4\right) \text{ for all } \lambda^1_{st(n)}, \tag{3}$$

where n numbers the n's pair of the experimental run and x^n_4 is the time like coordinate for the measurement of the n's pair.

We use the unit vector $\boldsymbol{b}$ indicating arbitrary right-wing magnet setting:

$$\boldsymbol{b} = \frac{1}{\sqrt{b_2'^2 + b_3'^2}}\left[b_2', b_3'\right] = \left[b_2, b_3\right]. \tag{4}$$

For the values of the functions B we assign:

$$B\left(\boldsymbol{b}, \lambda^1_{st(n)}, x^n_4\right) = -rm\left(x^n_4\right) \tag{5}$$

if we have:

$$\lambda^1_{st(n)} \le \frac{1}{2}\left(1 + b_2\right), \tag{6}$$

and

$$B\left(\boldsymbol{b},\lambda_{st(n)}^{1},x_{4}^{n}\right)=+rm\left(x_{4}^{n}\right) \tag{7}$$

otherwise.

The expectation value $E(\boldsymbol{a},\boldsymbol{b})$ of the product AB may be calculated with mathematical rigor (using Kolmogorov-type random variables and Lebesque integration) or in a more pedestrian way as follows. We note that $rm\left(x_{4}^{n}\right)^{2}=+1$ and thus obtain for the average of the product AB over N measurements:

$$\frac{1}{N}\sum_{n=1}^{N}AB=\frac{1}{N}\sum_{n=1}^{N}B', \tag{8}$$

with $B'=-1$ for $\lambda_{st(n)}^{1}\le\frac{1}{2}(1+b_{2})$ and $B'=+1$ otherwise. We denote the probability measure for the events of $B'=-1$ by $P_{\boldsymbol{b}}=\frac{1}{2}(1+b_{2})$ and therefore obtain for the limit of $N\to\infty$:

$$\frac{1}{N}\sum_{n=1}^{N}B'=-P_{\boldsymbol{b}}+\left(1-P_{\boldsymbol{b}}\right)=-b_{2}=-\boldsymbol{a}\cdot\boldsymbol{b}. \tag{9}$$

The additional requirement of quantum mechanics that the marginal expectation values $E(\boldsymbol{a})=0$ and $E(\boldsymbol{b})=0$ may easily be achieved by suitable choice of the function $rm\left(x_{4}^{n}\right)$. As an explicit example, one may use for *rm* the *j*'s Rademacher function $r_{j}=sign\left[\sin\left(2^{j+1}\pi t_{n}\right)\right]$, where $j=1,2,3,\cdots$ may be chosen appropriately and t_{n} is a dimensionless parameter corresponding to the time-like x_{4}^{n}.

It is important to note the following: The above formalism contains no influences from the other wing and the functions *A*, *B* corresponding to Bell's functions contain only dependencies on the respective local magnet settings. The model may be generalized by replacing $rm\left(x_{4}^{n}\right)$ by the product $rm\left(x_{4}^{n}\right)rarb\left(x_{4}^{n}\right)$, where $rarb\left(x_{4}^{n}\right)=\pm1$ is an arbitrary function of the time-like variable. Other generalizations may be used to remove asymmetries between the left and right wing. One may alternatively use, of course, a given setting in the right wing and let the left wing vary. In general, one may even choose an infinite variety of conditioning in both wings in order to obtain the quantum result. Such conditioning, however, needs to be on the angle between the two magnet settings which, as we have discussed in the previous section from the viewpoint of relativity, does not necessarily imply any inadmissible non-locality.

The law of our model for the expectation values, as given by Equation [8], is both gauge invariant and in its form invariant to rotations of the magnet settings $\boldsymbol{b}$ around the x_{1} axis. This model, which we call the the EQRC-model refutes proposition I of Bell. (Note that the quantum expectation values and corresponding quantum probability obey, of course, also a number of symmetries [18]. It is the symmetry of the quantum probability that signals one definite distinction from general Kolmogorov probabilities.)

The question arises then why Bell's inequality and his proposition II appear to

contradict the possibility of such a model and why proposition II is invalid. This is discussed next.

5. Inapplicability of Bell's Inequality to the EQRC-Model

In his proof of proposition II, Bell introduced three different setting pairs for magnets or polarizers. Three different equipment pairs require in general three different Kolmogorov-type sample spaces and, therefore, three different probability spaces [19]. Bell [2] and Wigner [16] (particularly in the formulation of d'Espagnat [17]) created by their choice of particular setting pairs and one common probability space, unknowingly, a very restrictive and logically inconsistent topological-combinatorial situation containing a cyclicity [20] as explained below.

5.1. The Cyclicity

In the notation of our EQRC-model Bell's 3 different setting pairs and possible outcomes correspond to the functions:

$$\begin{aligned} &A\left(\boldsymbol{a},\lambda_{st(n)}^{1},x_{4}^{n}\right);-A\left(\boldsymbol{b},\lambda_{st(n)}^{1},x_{4}^{n}\right)\\ &A\left(\boldsymbol{a},\lambda_{st(m)}^{2},x_{4}^{m}\right);-A\left(\boldsymbol{c},\lambda_{st(m)}^{2},x_{4}^{m}\right)\\ &A\left(\boldsymbol{b},\lambda_{st(k)}^{3},x_{4}^{k}\right);-A\left(\boldsymbol{c},\lambda_{st(k)}^{3},x_{4}^{k}\right) \end{aligned} \tag{10}$$

where we have used the fact that $B=-A$, which was also used by Bell. If N measurements are performed for each pair, we have $n=1,2,3,\cdots,N$, $m=N+1,N+2,N+3,\cdots,2N$ and $k=2N+1,2N+2,2N+3,\cdots,3N$. We have thus labeled the space and time related variables of the different experiments by a different number. Note that the space and time coordinates of the different experiments (symbolized by st and x_4) are, in general, all different.

Bell introduced now a logically and physically inconsistent assumption based on his conviction stated in his first and other papers: "λ stands for any number of variables and the dependences thereon of A and B are unrestricted." He, therefore, believed incorrectly that he needed to introduce only one symbol λ that could stand for a whole set of variables (including space and time-like variables). Using Equation [12] of his original paper [2], Bell put λ on one single probability space and thus assumed the functions A to be functions on that single probability space (see also [12]). As a consequence and because Bell assumed that λ could represent a set of variables, he used for each of the 3 pairs in the lines [10] the same actualization λ_{act} of his random variable λ and did not include any explicit time dependence. Therefore, the 3 lines [10] are reduced to:

$$\begin{aligned} &A\left(\boldsymbol{a},\lambda_{act}^{h}\right);-A\left(\boldsymbol{b},\lambda_{act}^{h}\right)\\ &A\left(\boldsymbol{a},\lambda_{act}^{h}\right);-A\left(\boldsymbol{c},\lambda_{act}^{h}\right)\\ &A\left(\boldsymbol{b},\lambda_{act}^{h}\right);-A\left(\boldsymbol{c},\lambda_{act}^{h}\right) \end{aligned} \tag{11}$$

where $h = 1, 2, 3, \cdots, N$.

This procedure concatenates each 6 possible outcomes into 3, which is equivalent to assuming the existence of a joint triple probability for the possible outcomes with settings $\boldsymbol{a}, \boldsymbol{b}, \boldsymbol{c}$. The procedure fails logically, because it creates a closed loop [12]: Two of the functions in the first two lines completely determine the functions in the third line. This is logically and physically inconsistent, because the functions of the first two lines relate to both correlated pairs in two wings and uncorrelated pairs in one wing. The third line, however, is for correlated pairs only. Bell and all of his followers have disregarded this important distinction by introducing only one common probability space. The following discussion of the experiments of Kwiat and coworkers in terms of the EQRC-model illustrates this situation clearly.

Some may still believe that Wigner's variation of Bell's inequality must hold, because it is thought to be based on set theory only. We show in the following section that it is not.

5.2. Wigner-d'Espagnat

Bell's derivations were investigated in great detail by Wigner and d'Espagnat, who presented a confirmation and extension of Bell's work. The derivations of Wigner and d'Espagnat seem to be based only on the rules of set theory and it is claimed in numerous publications that indeed they are.This claim, however, is false because Wigner and d'Espagnat used an assumption that lacks generality precisely as Bell's assumption does [21] and is also based on a mathematical mistake that I explain now using the EQRC-model.

D'Espagnat uses the 6 possible outcomes for the 3 setting pairs of Bell and transforms them into 3 triples with 9 possible outcomes. He accomplishes this transformation by adding an arbitrary third possible outcome for the magnet-setting that is not included in any of Bell's pairs. We denote these additions of possible outcomes by functions A'. In order to simplify the notation, we hide all variables except for the equipment settings $\boldsymbol{a}, \boldsymbol{b}, \boldsymbol{c}$. Thus we obtain lists (columns) for the Bell-pair possible outcomes together with the added added third listings of A'):

$$A(\boldsymbol{a})A(\boldsymbol{b})A'(\boldsymbol{c}), A(\boldsymbol{a})A(\boldsymbol{c})A'(\boldsymbol{b}), A(\boldsymbol{b})A(\boldsymbol{c})A'(\boldsymbol{a}) \tag{12}$$

D'Espagnat [17] and Wigner [16] *incorrectly* deduce from the existence of these sets of triples the existence of a common joint triple probability measure for all three triples of line [12]. The existence of a common joint triple probability measure and use of Bell's cyclical arrangement of settings lead immediately to the Wigner-d'Espagnat inequality, which corresponds roughly to Bell's inequality (The Wigner-d'Espagnat inequality is an inequality involving the frequency of equal and different pair outcomes for Bell's three setting pairs).

D'Espagnat's procedure, published in Scientific American [17], shows clearly how the existence of a common joint triple probability was incorrectly deduced.

It is actually indeed guaranteed that a joint triple probability measure may be deduced for each separate triple of [12]. The mere fact that the triples of Equation. [12] can be listed by using the possible pair-measurement outcomes with arbitrary additions A' gives us that guarantee. The mistake of d'Espagnat and Wigner was, however, that they assumed the existence of one common triple probability measure for all three triples, while in fact each of the three triples may have its own different triple probability measure.

One can prove this latter fact and demonstrate the mistake by using the possible outcomes of our EQRC-model given by Equations [5] and [7] (with $B=-A$) and the settings $\boldsymbol{a}=[1,0]$, $\boldsymbol{b}=\left[\frac{1}{2},\frac{\sqrt{3}}{2}\right]$, $\boldsymbol{c}=\left[\frac{-1}{2},\frac{\sqrt{3}}{2}\right]$. Consider only the first two triples, use for the moment $rm=+1$ and generate the possible pair outcomes by using the EQRC-model. Second add third columns $A'(\boldsymbol{c})=+1$ and $A'(\boldsymbol{b})=+1$, respectively.

This way we obtain all +1 possible-outcome-columns for both settings $\boldsymbol{a}$ and $\boldsymbol{c}$ in the first triple $A(\boldsymbol{a})A(\boldsymbol{b})A'(\boldsymbol{c})$. For the column with setting $\boldsymbol{b}=\left[\frac{1}{2},\frac{\sqrt{3}}{2}\right]$ we encounter +1 with probability $P_{\boldsymbol{b}}=\frac{1}{2}(1+b_2)=\frac{3}{4}$ (see explanation after Equation (8) and remember that $A=-B$). Denoting the joint triple probability for all positive outcomes of this first triple by $P_{abc'}(+1,+1,+1)$, we obtain $P_{abc'}(+1,+1,+1)=\frac{3}{4}$ and, after reinstallation of the function $rm(x_4)$ we have $P_{abc'}(+1,+1,+1)=\frac{3}{8}$.

For the second triple $A(\boldsymbol{a})A(\boldsymbol{b})A'(\boldsymbol{c})$ we obtain the same way all +1 for the settings $\boldsymbol{a}$ and $\boldsymbol{b}$, while for setting $\boldsymbol{c}=\left[\frac{-1}{2},\frac{\sqrt{3}}{2}\right]$ we encounter +1 with probability $P_{\boldsymbol{c}}=\frac{1}{2}(1+c_2)=\frac{1}{4}$. Denoting the joint triple probability for all positive outcomes of this second triple by $P_{ab'c}(+1,+1,+1)$ we thus obtain $P_{ab'c}(+1,+1,+1)=\frac{1}{4}$ and then after reinstallation of the function $rm(x_4)$ we obtain $P_{ab'c}(+1,+1,+1)=\frac{1}{8}$.

Therefore, d'Espagnats and Wigners assumption of one common joint triple probability for the line [12] is incorrect. Infinitely many other examples may be given.

The derivations of the Bell- as well as other inequalities in all textbooks are based on errors similar to that of d'Espagnat and Wigner (see for example [22] or Norsen's table [23]).

The same arguments as outlined above apply also to all other Bell-type inequalities, because they are based on joint probabilities that do not exist and are thus not applicable to actual EPRB experiments, nor to the EQRC-model.

6. Comparison with Experiments

6.1. Single Setting in One Wing

The EQRC-model may directly be applied to simulate the very precise experiments presented in Fig. 2 of Kwiat and coworkers [5], because they chose for these results a single given setting in one wing and performed many measurements with many different settings in the other. The precision of the EQRC-model depends only on the number N of simulations and agreement with the quantum result can be made as perfect as desired. Kwiat and coworkers did not include random changes of the polarizers before the registration of the actual measurement. However, there is little doubt that they would have obtained the same results if they had changed the polarizer setting just before turning to the measurement-setting.

We may obtain from the EQRC simulations, as well as from the actual experiments, the quantum result for the setting-pairs $(\boldsymbol{a};\boldsymbol{b})$ and $(\boldsymbol{a};\boldsymbol{c})$. The averages over the outcomes with both settings $\boldsymbol{b},\boldsymbol{c}$ in the right wing, on the other hand, do not result in the quantum expectation value, because they do not correspond to simulations involving correlated pairs. This way Bell's inequality is naturally fulfilled, by both the EQRC-model and the actual experiments, for the "triangles" of outcomes that exhibit equal sign for the setting $\boldsymbol{a}$ in the left wing and arbitrary sign for $\boldsymbol{b},\boldsymbol{c}$ in the right wing. There exists no contradiction here, because measurements with both the $\boldsymbol{b}$ and $\boldsymbol{c}$ settings in the right wing do not correspond to a correlated pair but to elements of reality originating from different pairs. Both the actual experiments (of Figure 2 in [5]) and the EQRC-model clearly distinguish the actual or possible outcomes corresponding to correlated and uncorrelated pairs.

However, Bell's mathematical model does not and cannot make that distinction. Bell's use of one single probability space enforces the use of identical functions for the settings $\boldsymbol{b}$ and $\boldsymbol{c}$ independent of the question of the origins of the given λ_{act}^{h}. Bell's identical notation for λ_{act}^{h} independent of its origins from one or two different pairs represents, as far as the experiments of Kwiat and coworkers in their Figure 2 are concerned, only a mathematical sloppiness. The application of Bell's functions to other experiments of Kwiat and coworkers [5] (not presented in Figure 2) and the experiments of the Aspect and Zeilinger groups, however, represents a serious mathematical inconsistency, because now the same mathematical abstractions λ_{act}^{h} and the same functions are used for both correlated and uncorrelated elements of reality.

6.2. Multiple Settings in Both Wings

Thus, experiments involving multiple magnet settings in both wings (see below) must not be modeled using Bell's original cyclic functions, because this procedure mixes indiscriminately correlated and uncorrelated pairs. It is, of course, possible to use additional indexing and time dependencies of the functions (as done in lines [10]) to avoid the inappropriate use of a single

probability space, but then it may become cumbersome to directly show the locality of the functions. The easiest way around the problems and the way that shows the locality of the procedure most directly, is probably the following: We use a symmetry law that applies to the actual experiments, the symmetry with respect to rotations around the x_1-axis. We, therefore consider idealized-actual experiments by rotating the actual original magnet setting such that all the left-wing magnet settings of the idealized experiments point in the $[1,0]$ direction of a chosen coordinate system. This idealized experiment must exhibit the same correlations as the original experiment because of the existing symmetry. The technical problem with the single probability space, however, has been avoided for the idealized experiment, because we have now all different sample spaces and just have Wigner sets with a consistent notation.

It is important to realize that the magnet settings of both the actual and idealized experiments may, of course, be arbitrarily switched just before the measurement and then brought into measurement position just as the correlated pair is being registered. This whole random switching is only necessary to exclude information exchange between the two wings of the actual experiment. The functions we use in the simulations do not depend on the other wing anyway.

Assume then that three actual EPRB experiments have the respective magnet setting pairs $\left([1,0];\left[\frac{1}{2},\frac{\sqrt{3}}{2}\right]\right)$, $\left([1,0];\left[\frac{-1}{2},\frac{\sqrt{3}}{2}\right]\right)$ and $\left(\left[\frac{1}{2},\frac{\sqrt{3}}{2}\right];\left[\frac{-1}{2},\frac{\sqrt{3}}{2}\right]\right)$. Each pair represents one of the well known Bell-angles. We rotate then the third pair of magnets to the position of our idealized experiment $(\boldsymbol{a};\boldsymbol{c}')=\left([1,0];\left[\frac{1}{2},\frac{\sqrt{3}}{2}\right]\right)$ and are now able to simulate the experimental outcomes with the EQRC-model and to obtain the quantum results with arbitrary accuracy for all three setting pairs.

The Aspect [3] and Zeilinger [4] experiments do not use Bell's 3 setting pairs but 4 settings pairs corresponding to 4 experiments with $(\boldsymbol{a};\boldsymbol{b})$ in experiment 1, $(\boldsymbol{a};\boldsymbol{c})$ in experiment 2, $(\boldsymbol{d};\boldsymbol{b})$ in experiment 3 and $(\boldsymbol{d};\boldsymbol{c})$ in experiment 4. These 4 pairs of magnet- (polarizer-)settings are used to investigate the Clauser-Horne-Shimony-Holt (CHSH) [24] inequality for the expectation values:

$$\left|E(\boldsymbol{a},\boldsymbol{b})+E(\boldsymbol{a},\boldsymbol{c})+E(\boldsymbol{d},\boldsymbol{b})-E(\boldsymbol{d},\boldsymbol{c})\right|\le 2. \tag{13}$$

As above, we transform the actual CHSH type of experiments and their actual magnet (polarizer) settings into our idealized experiment by magnet rotation, now obtaining the 4 setting pairs: $\left([1,0];\left[\frac{1}{\sqrt{2}},\frac{1}{\sqrt{2}}\right]\right)$, $\left([1,0];\left[\frac{1}{\sqrt{2}},\frac{-1}{\sqrt{2}}\right]\right)$, $\left([1,0];\left[\frac{1}{\sqrt{2}},\frac{-1}{\sqrt{2}}\right]\right)$ and $\left([1,0];\left[\frac{-1}{\sqrt{2}},\frac{-1}{\sqrt{2}}\right]\right)$. Again the EQRC-model may be applied to these setting pairs and gives the correlations of quantum theory, which violate the CHSH inequality.

Thus, according to Bell and CHSH, it is impossible to model actual EPRB experiments with local functions A for certain magnet setting-pair combinations, while it is indeed possible to perform such modeling for the idealized experiments which involve the same magnet (polarizer) angles and must have the same correlations for reasons of symmetry. In fact, all of the experiments of Aspect's, Zeilinger's and Kwiat's groups show only dependencies on the angles between the two polarizers of any given experiment. The use of optical fibers in some of their experiments makes any designation of an "absolute" angle or direction in either wing illusory.

It is instructive to imagine that Bell would have first found the EQRC-model and accepted the possibility of being able to use all local functions (particularly when accepting the relativity of all motion). He may then also have used multiple magnet-settings to produce the quantum result of the idealized experiments. Had he then rotated the magnets to turn $\boldsymbol{c}'$ into $\boldsymbol{c}$ and performed his proof for the inequality, he would have found the logical contradiction and would have been been forced to dismiss his inconsistent use of functions.

7. The Bell Game again and Conclusion

Many researchers have been aware of the publications that have pointed to serious problems with Bell-type inequalities. Several of them have admitted to this author that there may be formal problems with the one or other Bell-type proof. Their deepest convictions, however, arose from the fact that no one could play the so called Bell-game with Alice and Bob [19].

The Bell game and its demands highlight the crux of the epistemological questions that are going hand in hand with EPRB experiments. Some of the features of the Bell game have been described above and I add here only a few comments related to the EQRC-model.

Alice and Bob have no knowledge of each other, particularly none of the measurement settings of the other wing and they are required to develop a theory about the possible outcomes of their local measurements. That theory needs to cover the correlations of at least the 3 different experiments with Bell's 3 setting pairs. All Alice is permitted to know are the functions $A\left(\boldsymbol{a},\lambda_{st(n)}^{1},x_{4}^{n}\right)$ and her randomly chosen settings $\boldsymbol{a},\boldsymbol{b}$ as well as the actualizations $\lambda_{st(n)}^{1}$ and x_{4}^{n} etc., but she may not know of $B\left(\boldsymbol{b},\lambda_{st(n)}^{1},x_{4}^{n}\right)$ and Bob's randomly chosen settings $\boldsymbol{b}$ or $\boldsymbol{c}$. The same is true for Bob, with $\boldsymbol{a},\boldsymbol{b}$ and $\boldsymbol{b},\boldsymbol{c}$ exchanged. Nor do Alice and Bob know how the pairing is actually accomplished and how the same index n of a pair is actually obtained. In simple words, neither do Alice or Bob know the macroscopic machinery that deciphers the signals on the other side, nor do they know the global gauge (or global crypto-key on the computers). Of course that game cannot be played, that theory cannot be conceived.

Some followers of Bell, however, reason that mother nature can play the game. Just let the actual measurements happen and "put the correlated pairs together" and you will obtain the correct correlations. But how can mother nature "know"

which pairs are correlated? As mentioned, a single quantum fluctuation could falsify the pair sequence. The pairs of measurement that belong together need to be identified by some globally used space-time system and by additional measurements or assumptions that let us determine the connection between the measurement-outcomes in the space-like separated systems. How else can Alice correlate her measurements to the measurements of Bob? They both need to agree on a space-time (or space and time) coordinate system of physics that lets them determine the occurrence of the measurements and their belonging together in the different wings. This determination requires some process to identify the pairs of quantum particles and the corresponding macroscopic measurement outcomes. We have discussed this problem in a recent publication [13] and have given examples how the Bell game can indeed be played by making use of additional knowledge obtained from the particle identification method. We have conjectured that sufficient knowledge of particle and pair identification will always open a window to play the game.

The EQRC-model uses only local functions but also does imply some global knowledge, for example the relativity of all motion. It is also compared only to idealized experiments that are constructed from the actual by applying a global symmetry law. This procedure is necessary to avoid the logical mistake inherent in applications of Bell-Wigner-CHSH-type functions, sets and inequalities.

The game in its originally presented form just cannot be played and mother nature does not and cannot play it either. We have in this "shaky game" [25] the choice to admit some acceptable global information, some relative "positioning" in a global space-time system, or to be left only with instantaneous influences at a distance as an explanation for how nature works. Such explanations are, in this authors opinion, the very last resort, because they abandon scientific method as Einstein so clearly stated by using the word "spooky".

References

[1] Einstein, A., Podolsky, B. and Rosen, N. (1935) *Physical Review*, **16**, 777-780. https://doi.org/10.1103/PhysRev.47.777

[2] Bell, J.S. (1964) *Physics Physique Fizika*, **1**, 195-200. https://doi.org/10.1103/PhysicsPhysiqueFizika.1.195

[3] Aspect, A., Dalibard, J. and Roger, G. (1982) *Physical Review Letters*, **49**, 1804-1807. https://doi.org/10.1103/PhysRevLett.49.1804

[4] Weihs, G., Jennewein, T., Simon, C., Weinfurther, H. and Zeilinger, A. (1998) *Physical Review Letters*, **81**, 5039-5043. https://doi.org/10.1103/PhysRevLett.81.5039

[5] Kwiat, P.G., Waks, E., Appelbaum, I. and Eberhard, P.A. (1999) *Physical Review A*, **60**, 773-776. https://doi.org/10.1103/PhysRevA.60.R773

[6] Bell, J.S. (1976) *Epistemological Letters*, **2**, 2-7.

[7] Gell-Mann, M. (1994) The Quark and the Jaguar. W. H. Freeman and Company, New York, 170.

[8] Scully, M.O., Aharonov, Y. and Englert, B.G. (1999) On the Locality and Reality of

Einstein-Podolsky-Rosen Correlations. In: Bonifacio, R., Ed., *AIP*, *Mysteries*, *Puzzles and Paradoxes in Quantum Mechanics*, 47-67.

[9] Hess, K., De Raedt, H.A. and Khrennikov, A., Eds. (2017) *Open Physics*, **15**.

[10] Hess, K. and Philipp, W. (2004) *Proceedings of the National Academy of Sciences of the United States of America*, **101**, 1799-1805. https://doi.org/10.1073/pnas.0307479100

[11] Hess, K. and Philipp, W. (2001) *Proceedings of the National Academy of Sciences of the United States of America*, **98**, 14224-14227. https://doi.org/10.1073/pnas.251524998

[12] Hess, K. and Philipp, W. (2005) *Foundations of Physics*, **35**, 1749-1767. https://doi.org/10.1007/s10701-005-6520-y

[13] De Raedt, H.A., Michielsen, K. and Hess, K. (2017) *Open Physics*, **15**, 713-733. https://doi.org/10.1515/phys-2017-0085

[14] Muchowski, E. (2017) *Open Physics*, **15**, 891-896. https://doi.org/10.1515/phys-2017-0106

[15] Hess, K., De Raedt, H.A. and Michielsen, K. (2016) *Journal of Modern Physics*, **7**, 1651-1660. https://doi.org/10.4236/jmp.2016.713150

[16] Wigner, E.P. (1970) *American Journal of Physics*, **38**, 1005-1009. https://doi.org/10.1119/1.1976526

[17] D'Espagnat, B. (1979) *Scientific American*, **241**, 158-181. https://doi.org/10.1038/scientificamerican1179-158

[18] Huang, K. (2007) Fundamental Forces of Nature, the Story of Gauge Fields. World Scientific, London, 76. https://doi.org/10.1142/6447

[19] Hess, K. (2015) Einstein Was Right. Pan Stanford Publishing, Singapore.

[20] Hess, K., Philipp, W. and Aschwanden, M. (2006) *International Journal of Quantum Information*, **4**, 608. https://doi.org/10.1142/S0219749906002080

[21] Hess, K., De Raedt, H.A. and and Michielsen, K. (2017) *Journal of Modern Physics*, **8**, 57-67. https://doi.org/10.4236/jmp.2017.81005

[22] Scully, M.O. and Zubairy, M.S. (1997) Quantum Optics. Cambridge University Press, Cambridge, 513-515.

[23] Norsen, T. (2017) Foundations of Quantum Mechanics. Undergraduate Lecture Notes in Physics, Springer, Berlin, 218.

[24] Clauser, J.F., Horne, M.A., Shimony, A. and Holt, R.A. (1969) *Physical Review Letters*, **23**, 880-884. https://doi.org/10.1103/PhysRevLett.23.880

[25] Fine, A. (1986) The Shaky Game. The University of Chicago Press, Chicago.

Scientific Research Publishing

Journal of Modern Physics, 2018, 9, 1591-1616
http://www.scirp.org/journal/jmp
ISSN Online: 2153-120X
ISSN Print: 2153-1196

Special Relativity with a Preferred Frame and the Relativity Principle

Georgy I. Burde

Alexandre Yersin Department of Solar Energy and Environmental Physics, Swiss Institute for Dryland Environmental and Energy Research, The Jacob Blaustein Institutes for Desert Research, Ben-Gurion University of the Negev, Midreshet Ben-Gurion, Israel
Email: georg@bgu.ac.il

How to cite this paper: Burde, G.I. (2018) Special Relativity with a Preferred Frame and the Relativity Principle. *Journal of Modern Physics*, **9**, 1591-1616.
https://doi.org/10.4236/jmp.2018.98100

Received: March 26, 2018
Accepted: July 17, 2018
Published: July 23, 2018

Copyright © 2018 by author and Scientific Research Publishing Inc.
This work is licensed under the Creative Commons Attribution International License (CC BY 4.0).
http://creativecommons.org/licenses/by/4.0/

Open Access

Abstract

The purpose of the present study is to develop a counterpart of the special relativity theory that is consistent with the existence of a preferred frame but, like the standard relativity theory, is based on the relativity principle and the universality of the (*two-way*) speed of light. The synthesis of such seemingly incompatible concepts as the existence of preferred frame and the relativity principle is possible at the expense of the freedom in assigning the *one-way* speeds of light that exists in special relativity. In the framework developed, a degree of anisotropy of the one-way speed acquires meaning of a characteristic of the really existing anisotropy caused by motion of an inertial frame relative to the preferred frame. The anisotropic special relativity kinematics is developed based on the symmetry principles: 1) Space-time transformations between inertial frames leave the equation of anisotropic light propagation invariant and 2) a set of the transformations possesses a group structure. The Lie group theory apparatus is applied to define groups of transformations between inertial frames. Applying the transformations to the problem of calculating the CMB temperature distribution yields a relation in which the angular dependence coincides with that obtained on the basis of the standard relativity theory but the mean temperature is corrected by the terms second order in the observer velocity.

Keywords

Principle of Relativity, Anisotropy of the One-Way Speed of Light, Lie Groups of Transformations, CMB

1. Introduction

Special relativity underpins nearly all of present day physics. Lorentz invariance

is one of the cornerstones of general relativity and other theories of fundamental physics. It is thus very crucial to investigate its fundamentals and its potential violation. It seems evident that, if one wishes to contemplate the possibility of Lorentz symmetry violation within the context of a physical theory, then one will have to abandon the relativity principle which leads to the view that there exists a preferred universal rest frame. Also, the discovery of the cosmic microwave background (CMB) radiation has shown that (at least) cosmologically a preferred frame of reference does exist—it is the frame in which the CMB is isotropic. Acceptance of the view that there exists a preferred frame of reference seems to unambiguously abolish (besides the principle of relativity) another basic principle of the special relativity theory, namely, the principle of universality of the speed of light.

Correspondingly, the modern versions of experimental tests of special relativity and the "test theories" of special relativity (theoretical frameworks for analyzing results of experiments to verify special relativity [1] [2]) presume that a preferred inertial reference frame, identified with the CMB frame, is the only frame in which the *two-way* speed of light (the average speed from source to observer and back) is isotropic while it is anisotropic in relatively moving frames. Furthermore, it seems that accepting the existence of a preferred frame forces one to abandon the group structure for the set of space-time transformations between inertial frames. In the test theories, transformations between "moving" frames are not considered, only the transformation between a preferred "rest" frame and a particular moving frame is postulated.

The purpose of the present study is to develop a counterpart of the special relativity kinematics, that is consistent with the existence of a preferred frame but, like the standard relativity theory, is based on the relativity principle and universality of the (two-way) speed of light, and also preserves the group structure of the set of transformations between inertial frames. The analysis shows that the reconciliation and synthesis of those principles with the existence of a preferred frame is possible, and, what is more, such a possibility is naturally present in the framework of the relativity theory. Because of the freedom in assigning the *one-way* speeds of light (any one-way speeds, consistent with the two-way speed equal to c, are acceptable), a preferred frame can be defined as the frame in which the *one-way* speed of light is isotropic while, in any inertial frame moving with respect to the preferred frame, the one-way speed of light is anisotropic. It is similar to a definition accepted in a number of analyses, in which the existence of a preferred frame is assumed, but an important difference of the present analysis from others is that a degree of anisotropy of the one-way speed of light acquires meaning of a characteristic of the really existing anisotropy caused by motion of an inertial frame relative to the preferred frame. It seems to be contradictory to the common view that, because of the inescapable entanglement between remote clock synchronization and one-way speed of light (see, e.g., [3] [4] [5] [6]), the one-way speed of light is irreducibly conventional. Nevertheless, in the framework developed, the one-way speed of light in a

specific inertial farme is a physical quantity determined by a physical law in which the anisotropy parameter depends on the frame velocity with respect to a preferred frame. The entanglement between remote clock synchronization and one-way speed of light, in the case if the remote clocks are set using light signals, only implies that the synchronization procedure is implemented using the one-way speed of light determined by that law. If another method of synchronization, as for example, "external synchronization" [2], is used it changes the form of transformations for the space-time variables but the one-way speed of light is not altered by changing the synchronization method.

The analysis is based on the requirements of invariance of the equation of (anisotropic) light propagation and the group structure of a set of transformations between inertial frames which follow from the principles of special relativity. In those transformations, the anisotropy parameter k for the one-way speed of light is a variable that takes part in the transformations. Therefore the fact, that the one-way speed of light is a physical quantity determined by the frame velocity relative to a preferred frame, does not violate the relativity principle. Nothing distinguishes the frame in which $k = 0$ from others and the transformations from/to that frame are members of a group of transformations that are equivalent to others.

The space-time transformations between inertial frames derived as a result of the analysis differ from the Lorentz transformations. Since the theory is based on the special relativity principles, it means that the Lorentz invariance is violated without violation of the relativistic invariance. The theory equations contain one undefined universal constant q such that the case of $q = 0$ corresponds to the standard special relativity with isotropic one-way speed of light in all inertial frames. The measurable effects following from the theory equations can provide estimates for q and define deviations from the standard relativity that way.

Applying the theory to the problem of calculating the CMB temperature distribution eliminates the inconsistency of the usual approach when formulas of the standard special relativity, which does not allow a preferred frame, are used to define effects caused by motion with respect to the preferred frame. The CMB temperature angular dependence predicted by the present theory coincides with that obtained on the basis of the standard relativity equations while the mean temperature is corrected by the terms second order in the observer velocity.

The paper is organized, as follows. In Section 2, following the Introduction, the issue of anisotropy of the light propagation in special relativity is discussed in more details. In Section 3, the conceptual framework of the analysis is presented. In Section 4, the method is outlined and the coordinate transformations between inertial frames incorporating anisotropy of the light propagation, with the anisotropy parameter varying from frame to frame, are derived. In Section 5, the transformations are specified using the argument that the anisotropy of the light propagation is due to the observer motion with respect to the preferred frame. Consequences of the transformations are considered in Section 6. In Section 7, the results are applied to the problem of calculating the CMB effective

temperature distribution as seen by a moving observer. The approach and results are discussed in Section 8.

2. Anisotropy of the Light Propagation in Special Relativity

Anisotropy of the one-way speed of light is traditionally placed into the context of conventionality of distant simultaneity and clock synchronization [3] [4] [5] [6]. Simultaneity at distant space points of an inertial system is defined by a clock synchronization that makes use of light signals. Let a pulse of light is emitted from the master clock and reflected off the remote clock. If t_0 and t_R are respectively the times of emission and reception of the light pulse at the master clock and t is the time of reflection of the pulse at the remote clock then the conventionality of simultaneity is a statement that one is free to choose the time t to be anywhere between t_0 and t_R. This freedom may be parameterized by a parameter k_ϵ, as follows

$$t = t_0 + \frac{1+k_\epsilon}{2}\left(t_R - t_0\right); \quad \left|k_\epsilon\right| < 1 \tag{1}$$

Any choice of $k_\epsilon \neq 0$ corresponds to assigning different one-way speeds of light signals in each direction which must satisfy the condition that the average is equal to c. Speed of light in each direction is therefore

$$V_\pm = \frac{c}{1 \pm k_\epsilon} \tag{2}$$

The "standard" (Einstein) synchronization entailing equal speeds in opposite directions corresponds to $k_\epsilon = 0$. If the described procedure is used for setting up throughout the frame of a set of clocks using signals from some master clock placed at the spatial origin, a difference in the standard and nonstandard clock synchronization may be reduced to a change of coordinates [3] [4] [5] [6]

$$t = t^{(s)} + \frac{k_\epsilon x}{c}, \quad x = x^{(s)} \tag{3}$$

where $t^{(s)} = \left(t_0 + t_R\right)/2$ is the time setting according to Einstein (standard) synchronization procedure.

The analysis can be extended to the three dimensional case. If a beam of light propagates (along straight lines) from a starting point and through the reflection over suitable mirrors covers a closed part the experimental fact is that the speed of light as measured over closed part is always c (*Round-Trip Light Principle*). In accordance with that experimental fact, if the speed of light is allowed to be anisotropic it must depend on the direction of propagation as [4] [5]

$$V = \frac{c}{1 + \boldsymbol{k}_\epsilon \boldsymbol{n}} = \frac{c}{1 + k_\epsilon \cos\theta_k} \tag{4}$$

where $\boldsymbol{k}_\epsilon$ is a constant vector and θ_k is the angle between the direction of propagation $\boldsymbol{n}$ and $\boldsymbol{k}_\epsilon$. Similar to the one-dimensional case, the law (4) may be considered as a result of the transformation from "standard" coordinatization of the four-dimensional space-time manifold, with $k_\epsilon = 0$, to the "nonstandard"

one with $k_\epsilon \neq 0$:

$$t = t^{(s)} + \frac{\boldsymbol{k}_\epsilon \boldsymbol{r}}{c}, \quad \boldsymbol{r} = \boldsymbol{r}^{(s)} \tag{5}$$

The conventionality of simultaneity in the special theory of relativity, and the related issue of anisotropy of the one-way speed of light, have been much debated issues. A common view is that, due to freedom in the choice of the anisotropy parameter k_ϵ, the one-way speed of light is irreducibly conventional. The purpose of the following discussion is to show that, if there is an anisotropy in a physical system, the arguments for conventionality of the one-way speed of light are not valid and, what is more, a specific value of the one-way speed of light, *together with corresponding synchronization*, is selected in some objective way.

The arguments for conventionality of the one-way speed are based first on the possibility of introducing the transformations treated as replacing the Lorentz transformations of special relativity in the case of the anisotropic one-way speed of light (2) with $k_\epsilon \neq 0$. Such transformations have been repeatedly derived in the literature using kinematic arguments, the works [7] [8] [9] should be mentioned first. In what follows, they will be called the "ϵ-Lorentz transformations", the name is due to [8] [9]. Although the ϵ-Lorentz transformations can be obtained from the standard Lorentz transformations by a change of coordinates (3) and so they are in fact the Lorentz transformations of the standard special relativity represented using the "nonstandard" coordinatization of the four-dimensional space-time manifold, they are usually considered as describing the special relativity kinematics in an anisotropic system (for example, the most highly cited paper by Edwards [7] is entitled "Special relativity in anisotropic space"). Below, the arguments are presented showing that 1) the ϵ-Lorentz transformations, commonly considered as incorporating anisotropy, are in fact not applicable to an anisotropic system and 2) in the case of isotropic system, the particular case of the transformations corresponding to the isotropic one-way speed of light and Einstein synchronization (standard Lorentz transformations) is privileged.

The first statement is related to the issue of *invariance of the interval*. Invariance of the interval is commonly considered as an integral part of the physics of special relativity which is used as a starting point for derivation of the space-time transformations between inertial frames. Nevertheless, invariance of the interval is not a straightforward consequence of the basic principles of the theory. The two principles constituting the conceptual basis of the special relativity, the *principle of relativity* which states the equivalence of all inertial frames as regards the formulation of the laws of physics and *universality of the speed of light* in inertial frames, taken together lead to the condition of *invariance of the equation of light propagation* with respect to the coordinate transformations between inertial frames. Thus, in general, not the invariance of the interval but invariance of the equation of light propagation should be a starting point for derivation of the transformations. Therefore the use of the

interval invariance is usually preceded by a proof of its validity (see, e.g., [10] [11]) based on invariance of the equation of light propagation. However, those proofs are not valid if an anisotropy is present and the same arguments lead to the conclusion that, in the presence of anisotropy, the interval is not invariant but modified by a conformal factor [12]. The "ϵ-Lorentz transformations", like the standard Lorentz transformations, leave the interval invariant and therefore they are applicable only to the case of no anisotropy.

The second statement, that, in the case of isotropy, the particular case of the isotropic one-way speed of light and Einstein synchronization is privileged, relies on the *correspondence principle*. The correspondence principle was taken by Niels Bohr as the guiding principle to discoveries in the old quantum theory. Since then it was considered as a guideline for the selection of new theories in physical science. In the context of special relativity, the correspondence principle is traditionally mentioned as a statement that Einstein's theory of special relativity reduces to classical mechanics in the limit of small velocities in comparison to the speed of light. Being applied to the special relativity kinematics, the correspondence principle implies that *the transformations between inertial frames should turn into the Galilean transformations in the limit of small velocities*. The "ϵ-Lorentz transformations" do not satisfy the correspondence principle unless $k_\epsilon = 0$ [12] which means that the isotropic one-way speed of light and Einstein synchrony are selected if no anisotropy is present in a physical system. Similarly, in the case of an *anisotropic* system, there should also exist a privileged value of the one-way speed selected by the size of the anisotropy.

The above comments are related to the case when synchronization is implemented using light signals. Nevertheless, if another method of synchronization, as, for example, the "external synchronization" [2], is used it cannot change the value of the one-way speed of light. It can change the form of transformations for the time and space variables but, again, changing the synchronization method is equivalent to a change of coordinates (see more details in Section 8).

It is worth to mention, in connection with the issues of the correspondence principle and synchronization problem, a discussion in the literature (see, e.g., [13] [14] [15] [16]) initiated by the paper of Ohanian [13] "The role of dynamics in the synchronization problem". Ohanian argued that dynamical considerations, applied to inertial systems, necessarily entail the standard synchronization rule. He shows that the nonstandard synchronization procedure, when discussing Newtons (classical) mechanics, would result in a change in the mathematical form of the equation of motion such that the Newtons second law involves what he calls "pseudo-forces". He concludes that in an inertial reference frame any synchronization, other than the Einsteinian one, is forbidden.

Ohanian's approach has been criticized by several authors (for example, by Macdonald [14] and Martinez [15], see also a reply of Ohanian [16] to comments by Macdonald and Martinez) but their analyses are too concentrated

on such issues as a synchronization convention and the origin of the Einsteinian synchronization while more apparent inconsistencies of Ohanian's analysis are not sufficiently emphasized. Below we briefly discuss some of them. First, the Newtons second law of classical mechanics is used as a relation for choosing a synchronization rule or, in other terms, for choosing the value of anisotropy parameter for the one-way speed of light. The issues of light speed and its anisotropy are alien to Newtonian mechanics with absolute time and so such an approach is an inconsistent mixture of relativistic and classical concepts. (It would be more consistent to use in that context the correspondence principle as applied to dynamical equations of relativistic physics but, in general, using dynamical equations in the problem of clock synchronization is doubtful, see comments below.) Next, there is no reason for choosing Newtons second law, even if it were in a relativistic form, as a basic relation and considering it as more fundamental than any kinematics in the context of such purely kinematic issues as clock synchronization and light speed. Note also that (as emphasized in [14] and [15]) it is in contradiction with a consensus on considering the law of inertia as independent and prior to the force law in the definition of inertial frames. Further, a change in the mathematical form of dynamical equations resulting from different synchrony conventions do not correspond to any differences whatsoever in the actual material behavior of physical systems and so using the requirement that a dynamical equation took a specific form (even if it is the simplest one) as a basis for distinguishing a specific synchronization is not justified.

3. Conceptual Framework

The special relativity kinematics applicable to an anisotropic system should be developed based on the first principles of special relativity but without refereeing to the relations of the standard relativity theory. The principles constituting the conceptual basis of special relativity, the relativity principle, according to which physical laws should have the same forms in all inertial frames, and the universality of the speed of light in inertial frames, lead to the requirement of invariance of the equation of light propagation with respect to the coordinate transformations between inertial frames. In the present context, it should be invariance of the equation of propagation of light which incorporates the anisotropy of the one-way speed of light, with the law of variation of the speed with direction consistent with the experimentally verified round-trip light principle, as follows

$$V=\frac{c}{1+\boldsymbol{kn}}=\frac{c}{1+k\cos\theta_k} \tag{6}$$

where $\boldsymbol{k}$ is a (constant) vector characteristic of the anisotropy. The change of notation, as compared with (4), from k_ϵ to k is intended to indicate that $\boldsymbol{k}$ is a parameter value corresponding to the size of the really existing anisotropy while k_ϵ defines the anisotropy in the one-way speeds of light due to the

nonstandard synchrony equivalent to the coordinate change (5). The anisotropic equation of light propagation incorporating the law (6) has the form [12]

$$\mathrm{d}s^2 = c^2\mathrm{d}t^2 - 2kc\mathrm{d}t\mathrm{d}x - \left(1-k^2\right)\mathrm{d}x^2 - \mathrm{d}y^2 - \mathrm{d}z^2 = 0 \tag{7}$$

where (x, y, z) are coordinates and t is time. It is assumed that the x-axis is chosen to be along the anisotropy vector $\boldsymbol{k}$. Note that although the form (7) is usually attributed to the one-dimensional formulation it can be shown that, in the three-dimensional case, the equation has the same form if the anisotropy vector $\boldsymbol{k}$ is directed along the x-axis (see [12]).

Further, in the development of the anisotropic relativistic kinematics, a number of other physical requirements, associativity, reciprocity and so on are to be satisfied which all are covered by the condition that the transformations between the frames form a group. Thus, the group property should be taken as another first principle. The formulation based on the invariance and group property suggests using the *Lie group theory* apparatus for defining groups of space-time transformations between inertial frames.

At this point, it should be clarified that there can exist two different cases: 1) The size of anisotropy does not depend on the observer motion and so is the same in all inertial frames (groups of transformations for this case are studied in [12]); 2) The anisotropy is due to the observer motion with respect to a preferred frame and so the size of anisotropy varies from frame to frame (it is a subject of the present study). In the latter case, the anisotropy parameter becomes a variable which takes part in the transformations so that groups of transformations in *five* variables $\{x, y, z, t, k\}$ are studied. The preferred frame, commonly defined by that the propagation of light in that frame is isotropic, is naturally present in that framework as the frame in which $k = 0$. However, it does not violate the relativity principle since the transformations from/to that frame are not distinguished from other members of the group. Nevertheless, the fact, that the anisotropy of the one-way speed of light in an arbitrary inertial frame is due to motion of that frame relative to the preferred frame, is a part of the paradigm which is used in the analysis.

The procedure of obtaining the transformations consists of the following steps: 1) The infinitesimal invariance condition is applied to the equation of light propagation which yields determining equations for the infinitesimal group generators; 2) The determining equations are solved to define the group generators and the correspondence principle is applied to specify the solutions; 3) Having the group generators defined the finite transformations are determined as solutions of the Lie equations; 4) The group parameter is related to physical parameters using some obvious conditions; 5) Finally, the conceptual argument, that the size of anisotropy of the one-way speed of light in an arbitrary inertial frame depends on its velocity relative to the preferred frame, is used to specify the results and place them into the context of special relativity with a preferred frame. Note that implementing the steps 1)-4) for the case of no isotropy yields the standard Lorentz transformations [12].

The transformations between inertial frames derived in such a way contain a scale factor and thus do not leave the interval between two events invariant but modify it by a conformal factor (square of the scale factor). Applying the conformal invariance in physical theories originates from the papers by Bateman [17] and Cunningham [18] who discovered the form-invariance of Maxwells equations for electromagnetism with respect to conformal space-time transformations. Since then conformal symmetries have been successfully exploited for many physical systems (see, e.g., reviews [19] [20]). Transformations which conformally modify Minkowski metric have been introduced in the context of the special relativity kinematics in the presence of space anisotropy in [21] (see also references therein) and [22] (see also [23]). As a matter of fact, those works are not directly related to the subject of the present study as they consider the case of a constant anisotropy degree, not dependent on the frame motion. Nevertheless, it is worthwhile to note that in the works [21] [22] the assumption that the form of the metric changes by a conformal factor is *imposed* while, in the framework of the present analysis, conformal invariance of the metric *arises* as an intrinsic feature of special relativity based on invariance of the anisotropic equation of light propagation and the group property (see [12] for a more detailed discussion of the works [21] [22]).

4. Transformations between Inertial Frames with a Varying Anisotropy Parameter

In this section, groups of transformations between inertial frames that leave the equation for light propagation, incorporating the anisotropic law (6), form-invariant are defined. The parameter of anisotropy k is allowed to vary from frame to frame which, in particular, implies that there exists a preferred frame in which the speed of light is isotropic. The transformations are required to form a one-parameter group with the group parameter $a = a(v)$ (such that $v \ll 1$ corresponds to $a \ll 1$). Note that the group property is used not as in the traditional analysis which commonly proceeds along the lines initiated by [24] and [25] which are based on the linearity assumption and relativity arguments. The difference can be seen from the derivation of the standard Lorentz transformations using the above procedure [12].

Consider two arbitrary inertial reference frames S and S' in the standard configuration with the y- and z-axes of the two frames being parallel while the relative motion is along the common x-axis. The space and time coordinates in S and S' are denoted respectively as $\{X, Y, Z, T\}$ and $\{x, y, z, t\}$. The velocity of the S' frame along the positive x direction in S, is denoted by v. It is assumed that the frame S' moves relative to S along the direction determined by the vector $\boldsymbol{k}$ from (6). This assumption is justified by that one of the frames in a set of frames with different values of k is a preferred frame, in which $k = 0$, so that the transformations must include, as a particular case, the transformation to that preferred frame. Since the anisotropy is attributed to the fact of motion with respect to the preferred frame it is expected that the axis of anisotropy is along

the direction of motion (however, the direction of the anisotropy vector can be both coinciding and opposite to that of velocity).

The equations for light propagation in the frames S and S' are

$$c^2\mathrm{d}T^2 - 2Kc\mathrm{d}T\mathrm{d}X - \left(1-K^2\right)\mathrm{d}X^2 - \mathrm{d}Y^2 - \mathrm{d}Z^2 = 0, \tag{8}$$

$$c^2\mathrm{d}t^2 - 2kc\mathrm{d}t\mathrm{d}x - \left(1-k^2\right)\mathrm{d}x^2 - \mathrm{d}y^2 - \mathrm{d}z^2 = 0 \tag{9}$$

where the anisotropy parameters K and k in the frames S and S' are different. The relativity principle implies that the transformations of variables from $\{X,Y,Z,T,K\}$ to $\{x,y,z,t,k\}$ leave the form of the equation of light propagation invariant so that (8) is converted into (9) under the transformations. The transformations form a one-parameter group

$$\begin{aligned} &x = f\left(X,Y,Z,T,K;a\right),\ y = g\left(X,Y,Z,T,K;a\right),\\ &z = h\left(X,Y,Z,T,K;a\right),\ t = q\left(X,Y,Z,T,K;a\right);\ k = p\left(K;a\right) \end{aligned} \tag{10}$$

where a is the group parameter. Remark that k is a transformed variable taking part in the group transformations. Based on the symmetry arguments it is assumed that the transformations of the variables x and t do not involve the variables y and z and vice versa:

$$\begin{aligned} &x = f\left(X,T,K;a\right),\ t = q\left(X,T,K;a\right),\\ &y = g\left(Y,Z,K;a\right),\ z = h\left(Y,Z,K;a\right);\ k = p\left(K;a\right) \end{aligned} \tag{11}$$

The correspondence principle requires that, in the limit of small velocities $v \ll c$ (small values of the group parameter $a \ll 1$), the formula for transformation of the coordinate x turns into that of the Galilean transformation:

$$x = X - vT \tag{12}$$

Remark that the small v limit is not influenced by the presence of anisotropy of the light propagation. It is evident that there should be no traces of light anisotropy in that limit, the issues of the light speed and its anisotropy are alien to the framework of Galilean kinematics.

The group property and the invariance of the equation of light propagation suggest applying the infinitesimal Lie technique (see, e.g., [26] [27]). The infinitesimal transformations corresponding to (11) are introduced, as follows

$$\begin{aligned} &x \approx X + \xi\left(X,T,K\right)a,\ t \approx T + \tau\left(X,T,K\right)a,\\ &y \approx Y + \eta\left(Y,Z,K\right)a,\ z \approx Z + \zeta\left(Y,Z,K\right)a,\ k \approx K + a\chi\left(K\right) \end{aligned} \tag{13}$$

and Equations (8) and (9) are used to derive determining equations for the group generators $\tau\left(X,T,K\right)$, $\xi\left(X,T,K\right)$, $\eta\left(Y,Z,K\right)$, $\zeta\left(Y,Z,K\right)$ and $\chi\left(K\right)$. The infinitesimal group generators can be partially specified by applying the correspondence principle. Equation (12) is used to calculate the group generator $\xi\left(X,T\right)$, as follows

$$\xi = \left(\frac{\partial x}{\partial a}\right)_{a=0} = \left(\frac{\partial\left(X - v(a)T\right)}{\partial a}\right)_{a=0} = -bT;\ b = v'\left(0\right) \tag{14}$$

It can be set $b = 1$ without loss of generality since this constant can be eliminated by redefining the group parameter. Thus, the generator ξ is defined

by

$$\xi = -T \tag{15}$$

Then substituting the infinitesimal transformations (13), with ξ defined by (15), into Equation (9) with subsequent linearizing with respect to a and using Equation (8) to eliminate $\mathrm{d}T^2$ yields

$$\begin{aligned}&\left(-Kc^2\tau_X+\left(1-K^2\right)\left(K+c\tau_T\right)+\chi(K)cK\right)\mathrm{d}X^2\\&+c\left(c^2\tau_X+cK\tau_T+1+K^2-\chi(K)c\right)\mathrm{d}X\mathrm{d}T+\left(K+c\tau_T-c\eta_Y\right)\mathrm{d}Y^2\\&+\left(K+c\tau_T-c\zeta_Z\right)\mathrm{d}Z^2-c\left(\eta_Z+\zeta_Y\right)\mathrm{d}Y\mathrm{d}Z=0\end{aligned} \tag{16}$$

where subscripts denote differentiation with respect to the corresponding variable. In view of arbitrariness of the differentials $\mathrm{d}X$, $\mathrm{d}Y$, $\mathrm{d}Z$ and, $\mathrm{d}T$, the equality (16) can be valid only if the coefficients of all the monomials in (16) vanish which results in an overdetermined system of determining equations for the group generators.

The generators τ, η and ζ found from the determining equations yielded by (16) are

$$\begin{aligned}&\tau=-\frac{1-K^2-\chi(K)c}{c^2}X-\frac{2K}{c}T+c_2,\\&\eta=-\frac{K}{c}Y+\omega Z+c_3,\ \zeta=-\frac{K}{c}Z-\omega Y+c_4\end{aligned} \tag{17}$$

where c_2, c_3 and c_4 are arbitrary constants. The common kinematic restrictions that one event is the spacetime origin of both frames and that the x and X axes slide along another can be imposed to make the constants c_2, c_3 and c_4 vanishing (space and time shifts are eliminated). In addition, it is required that the (x,z) and (X,Z) planes coincide at all times which results in $\omega=0$ and so excludes rotations in the plane (y,z).

The finite transformations are determined by solving the Lie equations which, after rescaling the group parameter as $\hat{a}=a/c$ together with $\hat{\chi}=\chi c$ and omitting hats afterwards, take the forms

$$\frac{\mathrm{d}k(a)}{\mathrm{d}a}=\chi\left(k(a)\right);\quad k(0)=K, \tag{18}$$

$$\frac{\mathrm{d}x(a)}{\mathrm{d}a}=-ct(a),\ \frac{\mathrm{d}\left(ct(a)\right)}{\mathrm{d}a}=-\left(1-k(a)^2-\chi\left(k(a)\right)\right)x(a)-2k(a)ct(a), \tag{19}$$

$$\frac{\mathrm{d}y(a)}{\mathrm{d}a}=-k(a)y(a),\quad \frac{\mathrm{d}z(a)}{\mathrm{d}a}=-k(a)z(a); \tag{20}$$

$$x(0)=X,\ t(0)=T,\ y(0)=Y,\ z(0)=Z. \tag{21}$$

Because of the arbitrariness of $\chi\left(k(a)\right)$, the solution of the system of Equations (18), (19) and (20) contains an arbitrary function $k(a)$. Using (18) to replace $\chi\left(k(a)\right)$ in the second equation of (19) we obtain solutions of Equations (19) subject to the initial conditions (21) in the form

$$x = R\left(X\left(\cosh a + K\sinh a\right) - cT\sinh a\right), \tag{22}$$

$$ct = R\left(cT\left(\cosh a - k\left(a\right)\sinh a\right) - X\left(\left(1 - Kk\left(a\right)\right)\sinh a + \left(K - k\left(a\right)\right)\cosh a\right)\right) \tag{23}$$

where R is defined by

$$R = \mathrm{e}^{-\int_0^a k(\alpha)\mathrm{d}\alpha} \tag{24}$$

To complete the derivation of the transformations the group parameter a is to be related to the velocity v using the condition

$$x = 0 \text{ for } X = vT \tag{25}$$

which yields

$$a = \frac{1}{2}\ln\frac{1+\beta-K\beta}{1-\beta-K\beta};\ \beta = \frac{v}{c} \tag{26}$$

Substituting (26) into (22) and (23) yields

$$x = \frac{R}{\sqrt{\left(1-K\beta\right)^2 - \beta^2}}\left(X - cT\beta\right),$$

$$ct = \frac{R}{\sqrt{\left(1-K\beta\right)^2 - \beta^2}}\left(cT\left(1-K\beta-k\beta\right) - X\left(\left(1-K^2\right)\beta + K - k\right)\right) \tag{27}$$

where k is the value of $k\left(a\right)$ calculated for a given by (26).

Solving Equations (20) and using (26) in the result yields

$$y = RY,\ z = RZ \tag{28}$$

Calculating the interval

$$\mathrm{d}s^2 = c^2\mathrm{d}t^2 - 2kc\mathrm{d}t\mathrm{d}x - \left(1-k^2\right)\mathrm{d}x^2 - \mathrm{d}y^2 - \mathrm{d}z^2 \tag{29}$$

with (27) and (28) yields

$$\mathrm{d}s^2 = R^2\mathrm{d}S^2,\ \mathrm{d}S^2 = c^2\mathrm{d}T^2 - 2Kc\mathrm{d}T\mathrm{d}X - \left(1-K^2\right)\mathrm{d}X^2 - \mathrm{d}Y^2 - \mathrm{d}Z^2 \tag{30}$$

Thus, in the case when the anisotropy exists, the interval invariance is replaced by *conformal invariance* with the conformal factor dependent on the relative velocity of the frames and the anisotropy degree.

Considering inverse transformations from the frame S' to S one has to take into account that, in the presence of the light speed anisotropy, the reciprocity principle is modified [3] [8]. The reasoning behind this is that all speeds are to be affected by the anisotropy of the light speed since the speeds are timed by their coincidences at master and remote clocks, and the latter are altered. Therefore the relative velocity $v_{\_}$ of S to S' is not equal to the relative velocity v of S' to S. The modified reciprocity relation is commonly obtained using kinematic arguments [28], but, in the framework of our analysis, it straightforwardly follows from the group property of the transformations $a_{\_} = -a$, where a is given by (26) and $a_{\_}$ is also defined by Equation (26) but with β replaced by $\beta_{\_}$ and K replaced by k, as follows

$$a_{-}=\frac{1}{2}\ln\frac{1-\beta_{-}+k\beta_{-}}{1+\beta_{-}+k\beta_{-}},\quad \beta_{-}=\frac{v_{-}}{c} \tag{31}$$

Thus, the modified reciprocity relation is obtained in the form

$$\beta_{-}=\frac{\beta}{1-(k+K)\beta} \tag{32}$$

For deriving consequences of the transformations it is convenient to write the inverse transformations in terms of β (not β_{-}), as follows

$$X=\frac{R^{-1}}{\sqrt{(1-K\beta)^{2}-\beta^{2}}}\left(x(1-K\beta-k\beta)+ct\beta\right),$$

$$cT=\frac{R^{-1}}{\sqrt{(1-K\beta)^{2}-\beta^{2}}}\left(ct+x\left(\left(1-K^{2}\right)\beta+K-k\right)\right) \tag{33}$$

$$Y=R^{-1}y,\ Z=R^{-1}z \tag{34}$$

The formulas for the velocity transformation are readily obtained from (27) and (28), as follows

$$u_{x}=\frac{c(U_{X}-c\beta)}{Q},\ u_{y}=\frac{cU_{Y}\sqrt{(1-K\beta)^{2}-\beta^{2}}}{Q},\ u_{z}=\frac{cU_{Z}\sqrt{(1-K\beta)^{2}-\beta^{2}}}{Q},$$

$$Q=c(1-K\beta)+U_{X}\left(K^{2}\beta-K-\beta\right)+k(U_{X}-c\beta) \tag{35}$$

where (U_{X},U_{Y},U_{Z}) and (u_{x},u_{y},u_{z}) are the velocity components in the frames S and S' respectively.

The transformations (24)-(28) contain an indefinite function $k(a)$. The scale factor R also depends on that function. The transformations are specified in the next section.

5. Specifying the Transformations

In the derivation of the transformations in the previous section, the arguments, that there exists a preferred frame in which the light speed is isotropic and that the anisotropy of the one-way speed of light in a specific frame is due to its motion relative to the preferred frame, have not been used. In the framework of the derivation, nothing distinguishes the frame in which $k = 0$ from others and the transformations from/to that frame are members of a group of transformations that are equivalent to others. Thus, the theory developed above is a counterpart of the standard special relativity kinematics which incorporates an anisotropy of the light propagation, with the anisotropy parameter varying from frame to frame. Below the transformations between inertial frames derived in Section 2 are specified based on that anisotropy of the one-way speed of light in an inertial frame is caused by its motion with respect to the preferred frame.

First, this leads to the conclusion that the anisotropy parameter k in an arbitrary frame s moving with respect to the preferred frame with velocity $\overline{\beta}=\overline{v}/c$ should be given by some (universal) function of that velocity, as

follows

$$k = F\left(\bar{\beta}\right) \tag{36}$$

Indeed, Equations (18) and (26) imply that $k = k\left(a\left(\beta, K\right), K\right)$ which being specified for the transformation from the preferred frame to the frame s by setting $K = 0, \beta = \bar{\beta}$ yields (36). (It could be expected, in general, that a size of the anisotropy depends on the velocity relative to the preferred frame but, in the present analysis, it is not a presumption but a part of the framework.)

Next, consider three inertial reference frames $\bar{S}$, S and S'. As in the preceding analysis, the standard configuration, with the y- and z-axes of the three frames being parallel and the relative motion being along the common x-axis (and along the direction of the anisotropy vector), is assumed. The space and time coordinates and the anisotropy parameters in the frames $\bar{S}$, S and S' are denoted respectively as $\left\{\bar{x}, \bar{y}, \bar{z}, \bar{t}, \bar{k}\right\}$, $\left\{X, Y, Z, T, K\right\}$ and $\left\{x, y, z, t, k\right\}$. The frame S' moves relative to S with velocity v and velocities of the frames S and S' relative to the frame $\bar{S}$ are respectively $\bar{v}_1$ and $\bar{v}_2$. A relation between $\bar{v}_2$, v and $\bar{v}_1$ can be obtained from the equation expressing a group property of the transformations, as follows

$$a_2 = a_1 + a \tag{37}$$

where a_2, a_1 and a are the values of the group parameter corresponding to the transformations from $\bar{S}$ to S', from $\bar{S}$ to S and from S to S' respectively. Those values are expressed through the velocities and the anisotropy parameter values by a properly specified Equation (26) which, upon substituting into Equation (37), yields

$$\frac{1}{2}\ln\frac{1+\bar{\beta}_2-\bar{k}\bar{\beta}_2}{1-\bar{\beta}_2-\bar{k}\bar{\beta}_2} = \frac{1}{2}\ln\frac{1+\bar{\beta}_1-\bar{k}\bar{\beta}_1}{1-\bar{\beta}_1-\bar{k}\bar{\beta}_1} + \frac{1}{2}\ln\frac{1+\beta-K\beta}{1-\beta-K\beta} \tag{38}$$

where

$$\bar{\beta}_2 = \frac{\bar{v}_2}{c},\ \bar{\beta}_1 = \frac{\bar{v}_1}{c},\ \beta = \frac{v}{c} \tag{39}$$

Exponentiation of Equation (38) yields

$$\bar{\beta}_2 = \frac{\bar{\beta}_1 + \beta\left(1-\left(\bar{k}+K\right)\bar{\beta}_1\right)}{1+\beta\left(\bar{k}-K+\left(1-\bar{k}^2\right)\bar{\beta}_1\right)} \tag{40}$$

Let us now choose the frame $\bar{S}$ to be a preferred frame. Then, $\bar{k} = 0$ and, according to (36), for the frames S and S' we have

$$K = F\left(\bar{\beta}_1\right),\ k = F\left(\bar{\beta}_2\right) \tag{41}$$

With $\bar{\beta} = f\left(k\right)$ being a function inverse to $k = F\left(\bar{\beta}\right)$, using in (40) the equalities inverse to those of (41) together with $\bar{k} = 0$ yields

$$f\left(k\right) = \frac{f\left(K\right) + \beta\left(1-Kf\left(K\right)\right)}{1+\beta\left(-K+f\left(K\right)\right)} \tag{42}$$

If the function $f\left(k\right)$ were known, the relation (42), that implicitly defines

the anisotropy parameter k in the frame S' as a function of the anisotropy parameter K in the frame S and the relative velocity v of the frames, would provide a formula for the transformation of the anisotropy parameter k. This would allow to specify the transformations (27) and (28) by substituting that formula for k into the equation of transformation for t and calculating the scale factor R using that formula with β expressed as a function of a group parameter a from (26).

Although the function $F\left(\overline{\beta}\right)$ is not known, a further specification can be made based on the argument that an expansion of the function $F\left(\overline{\beta}\right)$ in a series with respect to $\overline{\beta}$ should not contain a quadratic term since it is expected that a direction of the anisotropy vector changes to the opposite if a direction of a motion with respect to a preferred frame is reversed: $F\left(\overline{\beta}\right)=-F\left(-\overline{\beta}\right)$. Thus, with accuracy up to the third order in $\overline{\beta}$, the dependence of the anisotropy parameter on the velocity with respect to a preferred frame can be approximated by

$$k=F\left(\overline{\beta}\right)\approx q\overline{\beta},\quad \overline{\beta}=f\left(k\right)\approx k/q \tag{43}$$

Introducing the last equation of (43) into (42) yields

$$k=\frac{q\left(K+\beta\left(q-K^2\right)\right)}{q+\beta K\left(1-q\right)} \tag{44}$$

which is the expression to be substituted for k into (27). To calculate the scale factor in (27) and (28), β is expressed as a function of a group parameter a from (26), as follows

$$\beta=\frac{\sinh a}{K\sinh a+\cosh a} \tag{45}$$

which, being substituted into (44), yields

$$k\left(a\right)=\frac{q\left(K\cosh a+q\sinh a\right)}{K\sinh a+q\cosh a} \tag{46}$$

Then using (46) in (24), with (26) substituted for a in the result, yields

$$R=\left(\frac{q^2\left(1+\beta\left(1-K\right)\right)\left(1-\beta\left(1+K\right)\right)}{\left(q+\beta K\left(1-q\right)\right)^2}\right)^{\frac{q}{2}} \tag{47}$$

Thus, after the specification, the transformations between inertial frames incorporating anisotropy of light propagation are defined by Equations (27) and (28) with k given by (44) and the scale factor given by (47). It is readily checked that the specified transformations satisfy the correspondence principle. All the equations contain only one undefined parameter, a universal constant q.

It should be clarified that, although the specification relies on the approximate relation (43), the transformations, with k and R defined by (44) and (47), are *not* approximate and they do possess the group property. The transformations (27) and (28) form a group, even with $k\left(a\right)$ (or $k\left(K,\beta\right)$) undefined, provided that

the transformation of k obeys the group property. Since the relation (42), defining that transformation, is a particular case of the relation (40) obtained from Equation (37) expressing the group property, the transformation of k satisfies the group property with any form of the function $F(\beta_s)$, and, in particular, with that defined by (43). Nevertheless, a straightforward check can be made that the specified transformation (46) obeys the group properties. Using the notation

$$\kappa(a,k)=\frac{q(k\cosh a+q\sinh a)}{k\sinh a+q\cosh a} \tag{48}$$

and introducing, in addition to S and S', the frame S_0 with the anisotropy parameter k_0, one can check that

$$\kappa(a,\kappa(a_0,k_0))=\kappa(a+a_0,k_0) \tag{49}$$

Similarly it is readily verified that $\kappa(-a,\kappa(a,k))=k$ and $\kappa(0,k)=k$. Alternatively, one can calculate the group generator $\chi(k)$ as

$$\chi(k)=\left.\frac{\partial\kappa(a,k)}{\partial a}\right|_{a=0}=q-\frac{k^2}{q} \tag{50}$$

and solve the initial value problem

$$\frac{\mathrm{d}k(a)}{\mathrm{d}a}=q-\frac{k(a)^2}{q},\quad k(0)=K \tag{51}$$

to be assured that it, as expected, yields (46). Thus, as a matter of fact, what is specified using the approximate relation (43) is the form of the group generator $\chi(k)$ in the group of transformations defined on the basis of the first principles.

The relation (42) allows defining a form of the group generator $\kappa(k)$ for arbitrary $F(\overline{\beta})$, not restricted by the approximate relation (43). Representing (42) in the form

$$f(k(K;a))=\frac{f(K)+\beta(a)(1-Kf(K))}{1+\beta(a)(-K+f(K))} \tag{52}$$

substituting (45) for $\beta(a)$ and differentiating the result with respect to a, with $\partial k(K;a)/\partial a$ separated, yields

$$\frac{\partial k(K;a)}{\partial a}=\frac{1-f(K)^2}{(\cosh a+f(K)\sinh a)^2 f'(k(a))} \tag{53}$$

Then the relation (52), with β substituted from (45), is used again to express $f(K)$ through $f(k)$ and a. Substituting that expression into (53) yields

$$\frac{\mathrm{d}k(a)}{\mathrm{d}a}=\frac{1-f^2(k(a))}{f'(k(a))} \tag{54}$$

Equation (54) is the Lie equation defining (with the initial condition $k(0)=K$)

the group transformation $k(K;a)$ which implies that the expression on the right-hand side is the group generator

$$\kappa(k)=\frac{1-f^2(k)}{f'(k)} \tag{55}$$

6. Time Dilation, Aberration Law and Doppler Effect

Time dilation. Consider a clock C' placed at rest in S' at a point on the x-axis with the coordinate $x=x_1$. When the clock records the times $t=t_1$ and $t=t_2$ the clock in S which the clock C' is passing by at those moments will record times T_1 and T_2 given by the transformations (33) where it should be evidently set $x_2=x_1$. Subtracting the two relations we obtain the time dilation relation

$$\Delta T=\frac{R^{-1}}{\sqrt{(1-K\beta)^2-\beta^2}}\Delta t \tag{56}$$

If clock were at rest in the frame S the time dilation relation would be

$$\Delta t=\frac{R(1-K\beta-k\beta)}{\sqrt{(1-K\beta)^2-\beta^2}}\Delta T=\frac{R}{\sqrt{(1-k\beta_-)^2-\beta_-^2}}\Delta T \tag{57}$$

with β_- defined by (32).

Aberration law. The light aberration law can be derived using the formulas (35) for the velocity transformation. The relation between directions of a light ray in the two inertial frames S and S' is obtained by setting $U_X=c\cos\Theta/(1+K\cos\Theta)$ and $u_x=c\cos\theta/(1+k\cos\theta)$ in the first equation of (35). Then solving for $\cos\theta$ yields

$$\cos\theta=\frac{\cos\Theta-\beta(1+K\cos\Theta)}{1-\beta(\cos\Theta+K)} \tag{58}$$

where θ and Θ are the angles between the direction of motion and that of the light propagation in the frames of a moving observer and of an immovable source respectively. (Equation (58) could be obtained in several other ways, for example, straight from the transformations (27) and (28) by rewriting them in spherical coordinates and then specifying to radial light rays.) Introducing $\tilde{\theta}=\theta-\pi$ and $\tilde{\Theta}=\Theta-\pi$ as the angles between the direction of motion and the line of sight one gets the aberration law

$$\cos\tilde{\theta}=\frac{\cos\tilde{\Theta}+\beta(1-K\cos\tilde{\Theta})}{1+\beta(\cos\tilde{\Theta}-K)} \tag{59}$$

Doppler effect. Consider a source of electromagnetic radiation (light) in a reference frame S very far from the observer in the frame S' moving with velocity v with respect to S along the X-axis with Θ being the angle between the direction of the observer motion and that of the light propagation as measured in a frame of the source. Let two pulses of the radiation are emitted from the source with the time interval $(\delta T)_e$ (period). Then the interval $(\delta T)_r$

between the times of arrival of the two pulses to the observer, as measured by a clock in the frame of the source S, is

$$\left(\delta T\right)_r = \left(\delta T\right)_e + \frac{\delta L}{V} \tag{60}$$

where δL is a difference of the distances traveled by the two pulses, measured in the frame of the source S, and V is the speed of light in the frame S given by

$$\delta L = v\left(\delta T\right)_r \cos\Theta, \quad V = \frac{c}{1+K\cos\Theta} \tag{61}$$

Substituting (61) into (60) yields

$$\left(\delta T\right)_e = \left(\delta T\right)_r \left(1-\beta\cos\Theta\left(1+K\cos\Theta\right)\right) \tag{62}$$

The interval $\left(\delta t\right)_r$ between the moments of receiving the two pulses by the observer in the frame S', as measured by a clock at rest in S', is related to $\left(\delta T\right)_r$ by the time dilation relation (56), as follows

$$\left(\delta T\right)_r = \frac{R^{-1}}{\sqrt{\left(1-K\beta\right)^2-\beta^2}}\left(\delta t\right)_r \tag{63}$$

Thus, the periods of the electromagnetic wave measured in the frames of the source and the receiver are related by

$$\left(\delta T\right)_e = \frac{R^{-1}\left(1-\beta\cos\Theta\left(1+K\cos\Theta\right)\right)}{\sqrt{\left(1-K\beta\right)^2-\beta^2}}\left(\delta t\right)_r \tag{64}$$

so that the relation for the frequencies is

$$\nu_r = \nu_e \frac{R^{-1}\left(1-\beta\cos\Theta\left(1+K\cos\Theta\right)\right)}{\sqrt{\left(1-K\beta\right)^2-\beta^2}} \tag{65}$$

where ν_e is the emitted wave frequency and ν_r is the wave frequency measured by the observer moving with respect to the source. (This formula could be derived in several other ways, for example, using the condition of invariance of the wave phase.)

To complete the derivation of the formula for the Doppler shift, the relation (65) is to be transformed such that the angle θ between the wave vector and the direction of motion measured in the frame of the observer S' figured instead of Θ which is the corresponding angle measured in the frame of the source. Using the aberration formula (58), solved for $\cos\Theta$, as follows

$$\cos\Theta = \frac{\cos\theta+\beta\left(1-K\cos\theta\right)}{1+\beta\left(\cos\theta-K\right)} \tag{66}$$

in the relation (65) yields

$$\nu_r = \nu_e \frac{R^{-1}\left(1+\beta\cos\theta\left(1-K\cos\theta\right)\right)\sqrt{\left(1-K\beta\right)^2-\beta^2}}{\left(1-K\beta+\beta\cos\theta\right)^2} \tag{67}$$

Finally, introducing the angle $\tilde{\theta} = \theta - \pi$ between the line of sight and the direction of the observer motion one obtains the relation for a shift of

frequencies due to the Doppler effect in the form

$$\nu_r = \nu_e \frac{R^{-1}\left(1-\beta\cos\tilde{\theta}\left(1+K\cos\tilde{\theta}\right)\right)\sqrt{\left(1-K\beta\right)^2-\beta^2}}{\left(1-K\beta-\beta\cos\tilde{\theta}\right)^2} \tag{68}$$

7. The CMB Effective Temperature

Let us apply the equations of the anisotropic special relativity developed above to describe effects caused by an observer motion (our galaxy's peculiar motion) with respect to the CMB frame. It is more consistent than using equations of the standard special relativity in that context—the standard relativity framework is in contradiction with existence of a preferred frame while the anisotropic special relativity naturally combines a preferred frame concept with the special relativity principles. Let choose the frame S to be a preferred frame and the frame S' to be a frame of an observer moving with respect to the preferred frame. Then the coordinate transformations from the preferred frame S to the frame S' of the moving observer are obtained by setting $K=0$ in equations (27), (28), (47) and (44) which yields

$$x = \left(X - cT\beta\right)\left(1-\beta^2\right)^{\frac{q-1}{2}},\ ct = \left(cT\left(1-q\beta^2\right)-X\beta\left(1-q\right)\right)\left(1-\beta^2\right)^{\frac{q-1}{2}}$$

$$y = Y\left(1-\beta^2\right)^{\frac{q}{2}},\quad z = Z\left(1-\beta^2\right)^{\frac{q}{2}} \tag{69}$$

where q is a universal constant. Equation of aberration of light (59) with $K=0$ converts into the common aberration law of the standard theory

$$\cos\tilde{\theta} = \frac{\cos\tilde{\Theta}+\beta}{1+\beta\cos\tilde{\Theta}} \tag{70}$$

while Equation (65), describing the Doppler frequency shift for the light emitted at the last scattering surface (LSS) and received by a moving observer, differs from its counterpart of the standard relativity by the factor R^{-1}, as follows

$$\nu_r = \nu_e \frac{R^{-1}\left(1-\beta\cos\Theta\right)}{\sqrt{1-\beta^2}} \tag{71}$$

The inverse R^{-1} of (47) for $K=0$ takes the form

$$R^{-1} = \left(1-\beta^2\right)^{-\frac{q}{2}} \tag{72}$$

Substituting (72) into (71) yields

$$\nu_r = \nu_e\left(1-\beta^2\right)^{-\frac{1}{2}\frac{q}{2}}\left(1-\beta\cos\Theta\right) \tag{73}$$

Thus, in terms of the angle Θ between the direction of the observer motion and that of the light propagation as measured in a frame of the source, the Doppler frequency shift is a pure dipole pattern as it is in the standard relativity. However, the amplitude of the shift includes an additional factor which depends on the value of the universal constant q.

Equation (68) incorporating the effect of light aberration and thus relating the frequency ν_e of the light emitted at the LSS to the frequency ν_r measured by a moving observer, with the use of (72) becomes

$$\nu_r = \nu_e \frac{\left(1-\beta^2\right)^{\frac{1}{2}\frac{q}{2}}}{1-\beta\cos\tilde{\theta}} \tag{74}$$

where $\tilde{\theta}$ is the angle between the line of sight and the direction of the observer motion as measured in the frame of the observer. In the context of the CMB anisotropy, one should switch from the frequencies to effective thermodynamic temperatures of the CMB blackbody radiation using the relation [29]

$$\frac{T\left(\tilde{\theta}\right)}{\nu_r} = \frac{T_0}{\nu_e} \tag{75}$$

where T_0 is the effective temperature measured by the observer which sees strictly isotropic blackbody radiation, and $T\left(\tilde{\theta}\right)$ is the effective temperature of the blackbody radiation for the moving observer looking in the fixed direction $\tilde{\theta}$. Substituting (74) into (75) yields

$$T\left(\tilde{\theta}\right) = \frac{M}{1-\beta\cos\tilde{\theta}}; \quad M = T_0\left(1-\beta^2\right)^{\frac{1}{2}\frac{q}{2}} \tag{76}$$

Thus, the angular distribution of the CMB effective temperature seen by an observer moving with respect to the CMB frame is not altered by the light speed anisotropy. However, the anisotropy influences the mean temperature which differs from the value yielded by applying the standard relativity by the factor $\left(1-\beta^2\right)^{\frac{q}{2}}$ (it may be also considered as a correction to the temperature T_0). Dependence of the amplitude factor M (normalized by T_0) on β for different values of the parameter q is shown in **Figure 1**. It is seen that, for negative values of q, the amplitude factor decreases with β, like as it does in the standard SR (q = 0), but the dependence becomes steeper. For positive values of q, the factor M may both decrease and increase with β and it does not depend on β for a specific value q = 1. Note, however, that q is expected to be negative both from intuitive considerations and on the basis of some arguments considering of which is beyond the scope of the current study.

Developing Equation (76) up to the second order in β yields

$$T\left(\tilde{\theta}\right) = T_0\left(1+q\frac{\beta^2}{2}+\beta\cos\tilde{\theta}+\frac{\beta^2}{2}\cos 2\tilde{\theta}\right) \tag{77}$$

which implies that, up to the order β^2, the amplitudes of the dipole and quadrupole patterns remain the same, only the constant term is modified.

It is worth reminding that, even though the specified law (43) is linear in β, it does include the second order term which is identically zero. Thus, describing the anisotropy effects, which are of the order of β^2, by Equations (76) and (77) is legitimate.

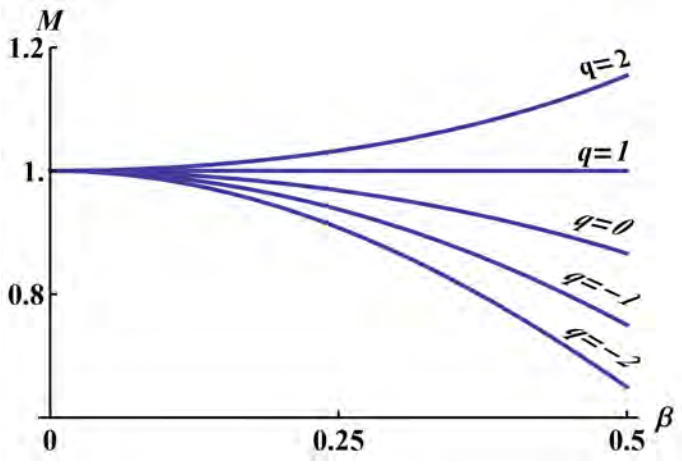

Figure 1. Dependence of the amplitude factor M (normalized by T_0) on the observer velocity β for different values of the parameter q.

8. Discussion

Analysis of the present paper, incorporating the existence of a preferred frame of reference into the special relativity framework, does not abolish the basic principles of special relativity but simply uses the freedom in applying those principles. A degree of anisotropy of the one-way velocity, which is commonly considered as irreducibly conventional, acquires meaning of a characteristic of the really existing anisotropy caused by motion of an inertial frame relative to the preferred frame. In that context, the fact, that there exists the inescapable entanglement between remote clock synchronization and one-way speed of light (if the synchronization is made using light signals), does not imply conventionality of the one-way velocity but means that, in the synchronization procedure, the one-way speed determined by the size of the anisotropy is used. The analysis yields equations differing from those of the standard relativity. The deviations depend on the value of an universal constant q where $q = 0$ corresponds to the standard relativity theory with the isotropic one-way speed of light in all the frames. The measurable effects following from the theory equations can be used to provide estimates for q and validate the theory.

Applying the theory to the problem of calculating the CMB temperature distribution is conceptually attractive since it removes the inconsistency of the usual approach when formulas of the standard special relativity, in which a preferred frame is not allowed, are applied to define effects caused by motion with respect to the preferred frame. It is worthwhile to note that even though it were found that the constant q is very small, which would mean that applying the present theory yields results practically identical to those of the standard relativity, this would not reduce the importance of the present framework which reconciles the principles of special relativity with the existence of the privileged CMB frame. As a matter of fact, it would justify the application of the standard relativity in that situation.

It is worthwhile, at the end of the discussion, to return to the much debated

issues of conventionality of simultaneity and relativity of simultaneity in special relativity and discuss the approach and results of the present paper in the light of the debates. First of all, an important difference between motivations (and, correspondingly, conceptual frameworks) of the analyses devoted to those issues and the approach of the present study should be clarified and emphasized again.

The concept of anisotropy of light propagation is always discussed in the literature in relation with the concept of remote clock synchronization. Considering different synchronization procedures, as the rule, is aimed at obtaining the transformations possessing some specific properties. For example, in the work by Tangherlini [30], a special method of synchronizing two clocks in an inertial frame is proposed in order to achieve a universal synchronization, such that spatially separated clocks remain synchronous between themselves thus establishing the common time of the moving system. In [30], it is achieved by using clocks synchronized with absolute signals, that is, signals travelling with infinite or arbitrarily large velocity. Using these signals, one arrives at the view of an absolute rest frame (or ether frame), in which the velocity of light is the same in all directions, but for observers in motion relative to this frame velocity of light is not the same in all directions. Another method of synchronization of spatially separated clocks, which leads to the same transformations that Tangherlini obtained in [30], is the so-called "external synchronization" (see, e.g., [2] [31] [32]). The external synchronization is based on the assumption that there is a preferred ("rest") inertial frame in which the one-way speed of light in vacuum is c in all directions. The clocks from the rest system, S, are synchronized using Einsteins procedure with light signals. Then, in any moving inertial frame S', the common time can be established using these already synchronized clocks of the rest inertial frame. It can be done simply by adjusting clocks of moving inertial frame to zero during those moments of time when they meet in space a clock at rest that shows zero as well. Applying any of two synchronization methods described above, together with the postulate of constancy of the two-way speed of light, yields the transformations

$$x' = \gamma\left(x - vt\right),\ t' = \frac{t}{\gamma};\ \gamma = \frac{1}{\sqrt{1-\beta^2}},\ \beta = \frac{v}{c} \tag{78}$$

where $\left(x,t\right)$ and $\left(x',t'\right)$ are space and time coordinates of a certain event in the rest frame S and in a moving frame S' respectively and v is a velocity of the frame S' relative to S. Thus, using the synchronization method, that is different from synchronization by light signals, yields the transformations (78) which exhibit absolute simultaneity. They also exhibit non-invariant one-way speed of light so that, in that approach, the anisotropy of the velocity of light in a moving inertial frame is a feature that emerges due to synchronization procedure designed to keep simultaneity unchanged between all inertial frames of reference.

The principal difference of the present analysis from those in the literature on the synchronization problem is that, in the present analysis, the one-way speed

of light in an inertial frame is a primary issue and its anisotropy is governed entirely by a physical lawc (36) (or its approximate version (43)). If a preferred frame is identified then the law (36) defines unequivocally the anisotropy size. Note that there is no ambiguity in determining the velocity $\bar{\beta}$ since it is measured in a preferred frame where the one-way speed of light is c in all directions. At the same time, the relativity principle is not violated since transformations of the parameter of anisotropy k from one inertial frame to another possess a group property and, in this respect, transformations from/to the preferred frame with $k=0$ are not distinguished from other members of the group of transformations. Specifying the function $F\left(\bar{\beta}\right)$ (or the inverse function $f\left(k\right)$) is equivalent to specifying the group generator for the variable k according to (55). In such a framework, synchronization is a concomitant issue if the remote clocks are set using light signals. In particular, since the transformations (27) are derived based on invariance of the equation of anisotropic light propagation, they correspond to the synchronization procedure using light signals with the one-way velocities defined by the relation (6) but, provided that the velocity of the frame relative to the preferred frame $\bar{\beta}$ is known, in the relation (6), *k is a definite value determined by the law* (36). That value cannot be altered by changing the synchronization method.

The same is valid if another method of synchronization, as, for example, the above discussed "external synchronization", is used. Changing the synchronization method results in a change of the form of transformations for the time and space variables which is equivalent to a change of coordinates. The Lorentz transformations

$$x'_L=\gamma\left(x-vt\right),\ t'_L=\gamma\left(t-\frac{vx}{c^2}\right) \tag{79}$$

can be obtained from the Tangherlini transformations (78) by the change of coordinates [32]

$$t'_L=t'-\frac{vx'}{c^2} \tag{80}$$

where t' and x' are defined by (78). Substituting (78) in (80), one gets the Lorentz transformations. The same can be done for the transformations (27) obtained in the present paper. In the case of the transformations from a preferred frame with the anisotropy parameter $K=0$ to an arbitrary frame with the anisotropy parameter k, the transformations (27) take the form

$$x=R\gamma\left(X-cT\beta\right),\ ct=R\gamma\left(cT\left(1-k\beta\right)-X\left(\beta-k\right)\right),\ \gamma=\frac{1}{\sqrt{1-\beta^2}} \tag{81}$$

where R is the scale factor defined by (24) (for the sake of clearness, we do not use the law (43) in these calculations). The transformations that exhibit absolute simultaneity, a counterpart of the Tangherlini transformations, are

$$x^{(T)}=R\gamma\left(X-cT\beta\right),\ ct^{(T)}=R\frac{cT}{\gamma} \tag{82}$$

and the change of variables converting (82) into (81) is

$$ct = ct^{(T)} - (\beta - k)x^{(T)} \tag{83}$$

It is readily verified that substituting (82) in (83) yields (81). Thus, any event that can be described by the transformations (81) can be described as well by the transformations with absolute simultaneity (82). Descriptions using clocks set as in (81) and clocks set as in (82) are equivalent in a sense that they are describing one and the same reality, which is independent of the coordinates chosen.

It is also worth remarking that alterations, as compared with the standard relativity, in the formulas describing physical effects caused by motion with respect to a preferred frame depend only on the scale factor R as, for example, a correction to the distribution (76) of the CMB effective temperature seen by an observer moving with respect to the CMB frame. In (76), R is given by the expression

$$R = \left(1 - \beta^2\right)^{\frac{q}{2}} \tag{84}$$

defining R as a function of the velocity of a moving frame measured in a preferred frame. The expression (84) has been obtained from (47) evaluated for $K = 0$ and so it corresponds to the approximate law (43) but it is possible to represent R defined by the general expression (24) as a function of $\bar{\beta}$ for arbitrary $F\left(\bar{\beta}\right)$. It is evident that the form $R\left(\bar{\beta}\right)$ of the scale factor does not depend on the synchronization (or on the space-time coordinates) chosen.

To conclude the discussion, the present analysis, which combines the basic principles of special relativity with the existence of a preferred frame, stands apart from the ample literature devoted to the conventionality of simultaneity, relativity of simultaneity and synchronization issues. In the present analysis, anisotropy of the one way speed of light in an inertial frame is governed by a physical law which is not influenced by changing the synchronization procedure. Synchronization emerges as a complementary issue needed for defining transformations of the space-time coordinates but physical effects are not changed by the way the clocks have been set.

Acknowledgements

The author is grateful to the referees for their helpful comments.

References

[1] Robertson, H.P. (1949) *Reviews of Modern Physics*, **21**, 378-382. https://doi.org/10.1103/RevModPhys.21.378

[2] Mansouri, R. and Sexl, S.U. (1977) *General Relativity and Gravitation*, **8**, 497-513, 515-524, 809-814. https://doi.org/10.1007/BF00762634

[3] Ungar, A.A. (1991) *Foundations of Physics*, **21**, 691-726. https://doi.org/10.1007/BF00733277

[4] Anderson, R., Vetharaniam, I. and Stedman, G.E. (1998) *Physics Reports*, **295**, 93-180. https://doi.org/10.1016/S0370-1573(97)00051-3

[5] Minguzzi, E. (2002) *Foundations of Physics Letters*, **15**, 153-169. https://doi.org/10.1023/A:1020900108093

[6] Rizzi, G., Ruggiero, M.L. and Serafini, A. (2004) *Foundations of Physics*, **34**, 1835-1887. https://doi.org/10.1007/s10701-004-1624-3

[7] Edwards, W.F. (1963) *American Journal of Physics*, **31**, 482-489. https://doi.org/10.1119/1.1969607

[8] Winnie, J.A. (1970) *Philosophy of Science*, **37**, 223-238. https://doi.org/10.1086/288296

[9] Ungar, A.A. (1986) *Philosophy of Science*, **53**, 395-402. https://doi.org/10.1086/289324

[10] Pauli, W. (1958) Theory of Relativity. Pergamon Press, London.

[11] Landau, L.D. and Lifshitz, E.M. (1971) The Classical Theory of Fields. Pergamon Press, Oxford.

[12] Burde, G.I. (2016) *Foundations of Physics*, **46**, 1573-1597. https://doi.org/10.1007/s10701-016-0029-4

[13] Ohanian, H. (2004) *American Journal of Physics*, **72**, 141-148. https://doi.org/10.1119/1.1596191

[14] Macdonald, A. (2005) *American Journal of Physics*, **73**, 454-455. https://doi.org/10.1119/1.1858448

[15] Martinez, A. (2005) *American Journal of Physics*, **73**, 452-454. https://doi.org/10.1119/1.1858446

[16] Ohanian, H. (2005) *American Journal of Physics*, **73**, 456-457. https://doi.org/10.1119/1.1858449

[17] Bateman, H. (1910) *Proceedings of the London Mathematical Society*, **8**, 223-264. https://doi.org/10.1112/plms/s2-8.1.223

[18] Cunningham, E. (1910) *Proceedings of the London Mathematical Society*, **8**, 77-98. https://doi.org/10.1112/plms/s2-8.1.77

[19] Fulton, T., Rohrlich, F. and Witten, L. (1962) *Reviews of Modern Physics*, **34**, 442-457. https://doi.org/10.1103/RevModPhys.34.442

[20] Kastrup, H.A. (2008) *Annals of Physics* (*Berlin*), **17**, 631-690. https://doi.org/10.1002/andp.200810324

[21] Bogoslovsky, G.Yu. (2006) *Physics Letters A*, **350**, 5-10. https://doi.org/10.1016/j.physleta.2005.11.007

[22] Sonego, S. and Pin, M. (2009) *Journal of Mathematical Physics*, **50**, Article ID: 042902. https://doi.org/10.1063/1.3104065

[23] Lalan, V. (1937) *Bulletin de la Société Mathématique de France*, **65**, 83-99. https://doi.org/10.24033/bsmf.1266

[24] von Ignatowski, W.A. (1910) *Physikalische Zeitschrift*, **11**, 972-976.

[25] Frank, Ph. and Rothe, H. (1911) *Annals of Physics*, **34**, 825-853. https://doi.org/10.1002/andp.19113390502

[26] Bluman, G.W. and Kumei, S. (1989) Symmetries and Differential Equations. Applied Mathematical Sciences, Vol. 81, Springer-Verlag, New York. https://doi.org/10.1007/978-1-4757-4307-4

[27] Olver, P.J. (1993) Applications of Lie Groups to Differential Equations (Graduate Texts in Mathematics: Vol. 107). Springer, New York.

[28] Winnie, J.A. (1970) *Philosophy of Science*, **37**, 81-99.

https://doi.org/10.1086/288281

[29] Peebles, P.J.E. and Wilkinson, D.T. (1968) *Physical Review*, **174**, 2168. https://doi.org/10.1103/PhysRev.174.2168

[30] Tangherlini, F.R. (1958) *The Abraham Zelmanov Journal*, **2**, 44-110.

[31] Guerra, V. and de Abreu, R. (2006) *Foundations of Physics*, **36**, 1826-1845. https://doi.org/10.1007/s10701-006-9085-5

[32] de Abreu, R. and Guerra, V. (2008) *European Journal of Physics*, **29**, 33-52. https://doi.org/10.1088/0143-0807/29/1/004

Journal of Modern Physics, 2018, 9, 1617-1632
http://www.scirp.org/journal/jmp
ISSN Online: 2153-120X
ISSN Print: 2153-1196

Rhythmic and Sporadic Changes in the Rate of Beta Decays: Possible Reasons

Alexander G. Parkhomov

Russian Academy of Natural Sciences, Moscow, Russia
Email: alexparh@mail.r

How to cite this paper: Parkhomov, A.G. (2018) Rhythmic and Sporadic Changes in the Rate of Beta Decays: Possible Reasons. *Journal of Modern Physics*, **9**, 1617-1632.
https://doi.org/10.4236/jmp.2018.98101

Received: June 19, 2018
Accepted: July 20, 2018
Published: July 23, 2018

Copyright © 2018 by author and Scientific Research Publishing Inc.
This work is licensed under the Creative Commons Attribution International License (CC BY 4.0).
http://creativecommons.org/licenses/by/4.0/

Open Access

Abstract

In a number of experiments, when detecting particles emitted in beta decays, periodic oscillations of count rate with an amplitude up to tenths of a percent and short bursts vastly exceeding the usual count rate are found. At the same time, several experiments did not detect any differences from the "normal" course of beta decays greater than 0.01%. The article shows that the inconsistency of the experimental results is due to different measurement technique. The assumption is made of the possible participation in the beta decay processes of cosmic slow neutrinos, which makes it possible to explain in a comprehensive manner not only periodic and sporadic changes in the beta decay rate, but also a number of other incomprehensible phenomena associated with beta radioactivity. On the basis of the experiments carried out, an estimate is made of the flux density of slow cosmic neutrinos.

Keywords

Beta Radioactivity, Nuclear Decay Rate, Solar Neutrinos, Relic Neutrinos, Variations of Radioactivity, Rhythmic Oscillations

1. Introduction

Until recently, the strictly exponential nature of radioactive nuclides decay rate was considered unquestionable. But recently many articles have been published with the results of measurements of radioactivity, which give rise to doubts about the inviolability of this property of radioactivity. Both periodic (first of all, with a period of 1 year) [1]-[17] and sporadic deviations [14]-[20] were detected. Attempts were made to explain these anomalies by the action of a flux of solar [6]-[12] or relic [13]-[17] neutrinos. At the same time, a number of articles show the results of measurements in which the anomalies in the rate of radioactive decay are invisible [21]-[28]. The results obtained during these careful mea-

surements, at first glance, refute reports of anomalies in the rate of radioactive decay, which calls into question the advisability of continuing research in this direction. We show that the absence of observed anomalies can be explained by an incorrect method of searching for variations.

Let us assume that the anomalies in the beta decay rate are associated with the action of neutrinos or antineutrinos in accordance with nuclear reactions

$$\nu_e + (A, Z) \to (A, Z+1) + \mathrm{e}^-$$

or

$$\tilde{\nu}_e + (A, Z) \to (A, Z-1) + \mathrm{e}^+ \quad (1)$$

This occurs against the backdrop of spontaneous decays

$$(A, Z) \to (A, Z+1) + \mathrm{e}^- + \tilde{\nu}_e$$

or

$$(A, Z) \to (A, Z-1) + \mathrm{e}^+ + \nu_e \quad (2)$$

The problem is to detect a small number of reaction acts (1) against the background of a large number of reaction acts (2). Solution of this problem is possible due to the fact that in the reactions (2) there are electrons or positrons with energies from zero to the upper boundary $E_{\max}$, characteristic for each nuclide. In the case of reaction (1), the emerging electrons or positrons have an energy exceeding $E_{\max}$ on the energy of the absorbed neutrino or antineutrinos. If neutrinos (antineutrinos) appear in nuclear reactions, for example, in the interior of the Sun, the excess reaches several MeV. If relic neutrinos with very low energy are registered, the electrons have energy close to $E_{\max}$.

If the number of induced reactions is much less than the number of spontaneous decays, in order to detect effects associated with the action of neutrinos (antineutrinos), it is necessary to have detectors that can selectively register electrons (positrons) with an energy exceeding $E_{\max}$. Geiger counters, proportional counters, ionization chambers, semiconductor and scintillation detectors allow you to directly register beta particles. Moreover, these detectors allow partially to solve the problem of high-energy particles separation by placing a layer between the source and the detector of a substance that absorbs the bulk of the particles that arise during spontaneous beta decays and which transmits most of the particles of higher energy.

It is tempting to use gamma spectrometers to register beta decays. The use of such detectors is based on the fact that in most cases, as a result of beta decays, nuclei are formed in an excited state, which remove excitation by emitting gamma quanta. But the energy of the emerging gamma rays does not depend on the energy of the emerging electrons. Therefore, by detecting gamma quanta, it is practically impossible to isolate the events of interest related to the action of neutrinos (antineutrinos).

Thus, to detect variations in the rate of beta decays, if they are associated with the action of neutrinos (antineutrinos), it is necessary to use beta spectrometers

or beta particle detectors in combination with the optimum absorbers of particles formed during spontaneous decays. The registration of gamma quanta [21] [23] [27] cannot lead to success. There can be no success in the search for variations in decays not associated with weak interactions: in isomeric transitions with gamma-ray emission (e.g., $^{121}Sn^{m}$ [21]), and also in alpha decays [12] [16], [22] [25], if they are not are members of a chain including beta active nuclides.

Some works, for example [26], refuting the presence of anomalies in the beta decay rate, are done very carefully, but they do not fulfill the conditions allowing to detect small changes associated with the desired effect on a high background of spontaneous beta decays. In this paper, just as in some others [21] [24], the ratio of the decay rates of various nuclides is investigated. But if the neutrino flux equally affects the decay rate of different nuclides, the absence of variations in the ratio of activities does not mean that there are no variations in the activities of individual radionuclides.

An attempt was made in [24] to explain the observed variations by seasonal temperature changes. There is no doubt that variability of environmental factors in one way or another affects the results of measurements. It is possible that in some studies, despite the measures taken, the influence of these factors appears. But it is important to pay attention to the fact that the instability of equipment, the impact of a changing temperature, pressure, air humidity, the background of ionizing radiations, power supplies, etc. very different in different laboratories. Nevertheless, if the effect can be detected, when measuring different radionuclides in different laboratories using different types of equipment, its period and phase are close [13] [14] [15] [16]. This indicates the existence of a non-trivial agent that equally affects the activity of various beta radionuclides. The neutrino flux coming from the Cosmos is the most suitable for the role of such an agent.

With a lot of experiments in which anomalies in the beta-decay process are discovered, one can get acquainted in [1]-[20]. This article will describe some of the results obtained by the author of this article.

2. Periodic Changes in the Beta Decay Rate

To detect anomalies in the course of radioactive decay, it was necessary to create a set of facilities that made it possible to obtain and continuously record, over the years, various information [15] [16]. The complex consists of sensors with power sources, thermostats and a device for continuous multichannel recording of information coming from sensors. Information is collected in more than 20 channels. In particular, data on the main parameters of the environment were collected. Comparison of this information with the results of measurements of radioactivity makes it possible to judge whether the detected effects are the result of effects on the equipment of changes in the environment.

The testing of various detectors has shown that the most suitable for long-term detection of beta particles are halogen Geiger counters, and for alpha particles—semiconductor detectors. To reduce the influence of temperature

changes, not only detectors with signal amplifiers were thermostated, but also power supplies.

Figure 1 shows the device of one of the installations on which the radiation of the beta source $^{90}Sr^{90}Y$ was recorded. This source consists of two equilibrium radionuclides. ^{90}Sr emits relatively soft beta particles with a maximum energy of 546 keV, and ^{90}Y emits particles with energies up to 2.3 MeV. The first Geiger counter, type SBM-12, is located in the air cavity at a distance of 2 cm from the source. The second Geiger counter of the STS-5 type is separated from the source by a layer of aluminum and polyvinylchloride. Container with a source and detectors is filled with quartz sand to exclude the influence on the measurement results of beta particles reflected by external objects. The thermostabilization system maintains a temperature of 31˚C ± 0.1˚C in the installation. The power supply of the counters is also thermostatted.

Counter located in the air cavity detects the radiation of both radionuclides, and the second, separated from the source by a layer of matter absorbing strontium radiation, registers radiation only of yttrium.

Figure 2 shows what happened as a result of 12-year measurements with averaging covering more than 10 million pulses, corrected for the exponential decay of activity (half-life 28.6 years). Such averaging is required in order for the oscillations to become clearly visible against the background of statistical fluctuations. The magnitude of these fluctuations is shown near the vertical scale. The red lines show a deviation from the average by 0.1%. In spite of the fact that the measurements were made by counters of different types and the counters were in different conditions, they registered in-phase oscillations of the counting rate with amplitude of more than 0.1% of the mean value.

Figure 3 at the top shows how the beta count rate on the average varies throughout the year. The results obtained on each calendar day of the year for 7 years are superimposed and averaged. It can be seen that the results obtained by

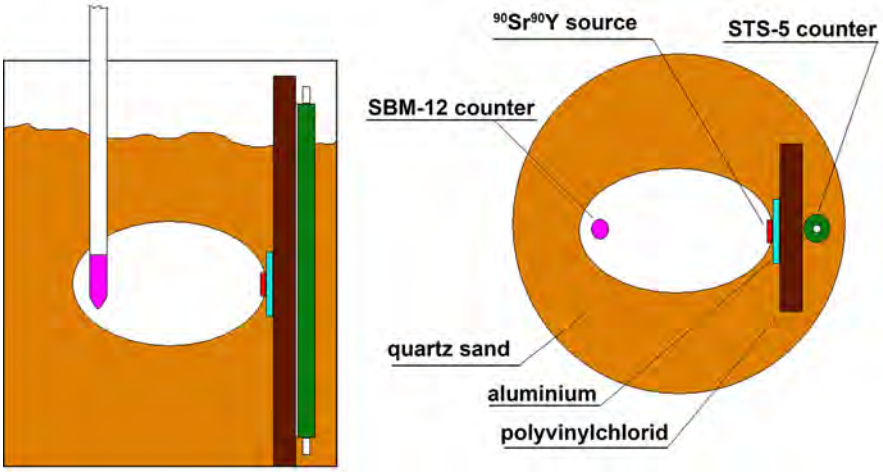

Figure 1. Scheme of installation for long-term measurement of beta source activity $^{90}Sr^{90}Y$ by two counters. The thermostating system (temperature sensor, heater, thermal insulation) is not shown in the figure.

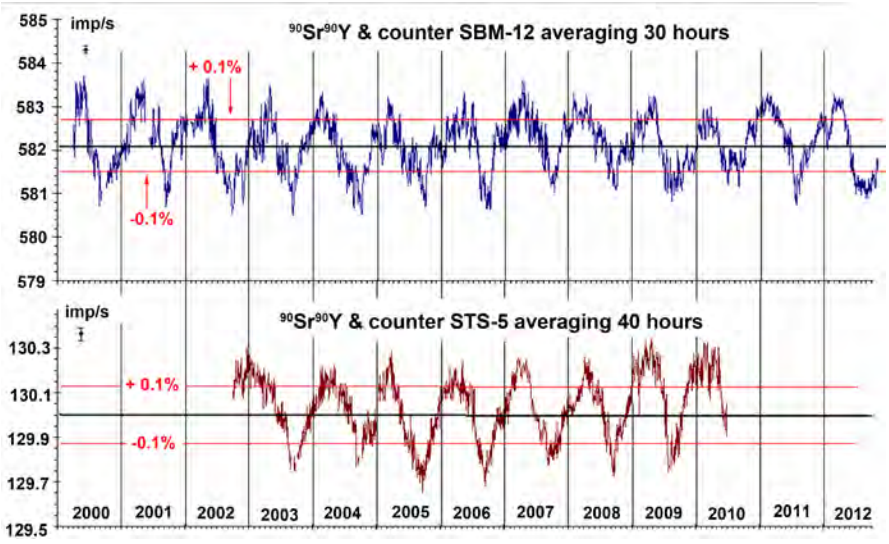

Figure 2. Results of beta source $^{90}Sr^{90}Y$ activity measurements by two Geiger counters adjusted for a decrease in activity with a half-life of 28.6 years [16].

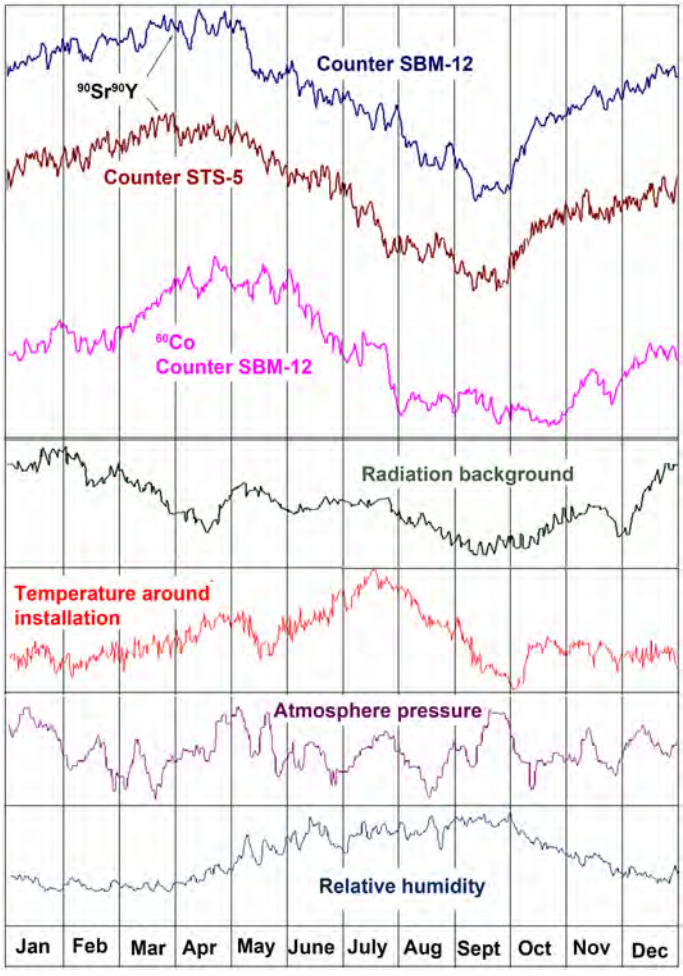

Figure 3. Beta particles count rate on the average throughout the year as well as the main environmental parameters for the annual period.

three different detectors from two different beta sources on average vary throughout the year almost identically. At the same time, the main environmental parameters that can be suspected as a source of instability of the recording equipment are radiation background, temperature, atmospheric pressure, humidity, behave differently. This indicates that there is a phenomenon associated with the beta sources, rather than the influence of variations in the parameters of the external environment.

In addition to beta radioactivity, long-term studies of the alpha decay process were carried out. To do this, the alpha source ^{239}Pu, located near to the silicon detector, was placed with the amplifier in a thermostat at a temperature of 18˚C. The results obtained for more than three years are shown in **Figure 4** [16]. The red lines show a deviation from the average by 0.1%. Green lines show a difference from the average for 3 standard Poisson deviations. It can be seen that the measurement results fluctuate chaotically. No rhythmicity at the level of hundredths of a percent is not visible.

A large amount of accumulated data makes it possible to apply frequency analysis, which allows us not only to clarify the parameters of the observed annual rhythms, but also to reveal other periodicity, imperceptible against the background of statistical fluctuations and interference acting at random times. For analysis of the results of ^{90}Sr^{90}Y beta particle count rate measurements fast Fourier transformation was applied, followed by recalculation of the frequency in the periods [13] [14] [15] [16]. On the periodogram, a peak with a period of 1 year is allocated (amplitude 0.13%) and its harmonics (half, third, quarter of the year). In the region of near-monthly periods, peaks with amplitude of about 0.01% are visible.

The question arises, which of the known rhythms can be related to the observed near-monthly periodicity? With the period of the change of the lunar phases, the period of the Moon's rotation relative to the stars, the period of the change in the distance to the Moon, and perhaps with the period of solar activity

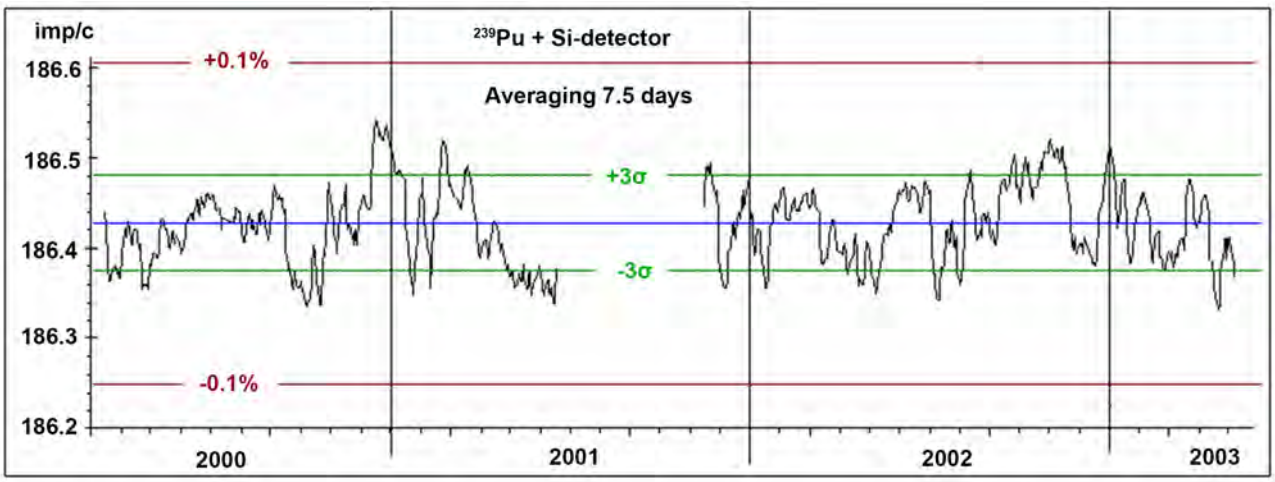

Figure 4. Long-term measurements of ^{239}Pu alpha source activity.

change associated with the rotation of the Sun-which is also close to 1 month? Analysis [15] shows that the clearest correspondence exists with the synodic lunar month having an average period of 29.5 days. This clearly demonstrates the averaging of the results of radioactivity ^{90}Sr-^{90}Y measurements for 87 cycles of the synodic month. The count rate in the new moon is, on average, 0.02% higher than in the full moon. Without special analysis, such changes, unlike annual ones, are completely invisible. Only the imposition of epochs and averaging over a large number of cycles makes it possible to determine quite reliably the rhythms of such small amplitude.

In the range of shorter periods, the peak of the solar-diurnal period is clearly visible, near which peaks corresponding to the star-day and moon-diurnal periods are visible [13] [14] [15] [16]. The amplitude of the diurnal variations does not exceed thousandths of a percent of the mean value and, unlike the variations with the annual and monthly periods, it cannot be said with certainty that they are not caused entirely or partially by temperature influences on the measuring apparatus.

Summarizing the results of this section, taking into account the results obtained with the use of other detectors and radionuclides [1]-[18], the following conclusions can be drawn. Rhythmic changes are characteristic of beta decays and are invisible in alpha decays. When using equipment that selectively records particles with energy close to the maximum energy of the beta spectrum, there are oscillations in the count rate with a period of 1 year and amplitude of up to tenths of a percent of the average, maxima from January to March, and lows from July to September. Oscillations were detected in radionuclides with half-lives from 2.6 hours to 300,000 years. Experiments, in which almost the entire spectrum of beta particles emitted is detected, do not show an anomaly greater than 0.01% of the mean velocity. This indicates that the value of periodic oscillations do not exceed 1/10,000 of the average beta decay rate.

3. Short-Term Bursts of Beta Radioactive Nuclides Activity

Strong outbursts of beta particles count rate are detected with the continuous scanning of the celestial sphere by peculiar telescopes in which the beta source is located in the focus of the parabolic mirror. One of these types telescopes, with which the most striking results are obtained, has a steel mirror with a concave parabolic surface 22 cm in diameter with a focal length of 10 cm. A small beta ^{60}Co source connected to a miniature Geiger counter is located in the focus. Like astronomical telescopes, the telescope has two axes of rotation. One is parallel to the Earth's axis. The other axis is perpendicular to the earth's axis. This design allows you to determine which area of the celestial sphere the telescope is pointing to. More detailed description of the methodology of these experiments and the results obtained can be found in [15] [16] and [20].

At the first stage of the researches, the telescope was oriented in a direction close to the east, with a fixed inclination above the horizon. Rotating with the

Earth, the telescope "viewed" a strip of the celestial sphere about 1˚ wide. The count rate was continuously recorded by the computer. The astronomical coordinates of the celestial sphere place, to which the telescope is currently directed (declination and right ascension), were determined with an error of about 1˚ on the basis of observations of the movement of the image of the Sun. Sometimes, at intervals of several months, bursts of counting counts from a few seconds to an hour were recorded, at which the count rate many times exceeded the background count (**Figure 5**). It was possible to detect these bursts only because of the long duration of almost continuous observations, since the total duration of recorded bursts did not exceed 1/1000 of the operating time of the installation.

The effectiveness of observations has increased to several bursts per day in the transition from one-dimensional scanning to two-dimensional. For this purpose, the telescope was given an oscillatory motion perpendicular to the scanning line associated with the daily rotation of the Earth. The amplitude of the oscillations is up to 40˚, the "forward stroke" is about 10 minutes, the "reverse" is about 1 minute, the time of the beginning and the end of the backward movement was recorded by a computer with an exact time reference, which made it possible to determine to what points of the celestial sphere the telescope "looks" when the bursts are discovered.

The conducted investigations give grounds for the following generalizations [15] [16] [20]. The dynamics of the bursts in time is diverse. The simplest form is single bursts lasting a few seconds. In this case, the increase in counting speed can exceed three orders of magnitude. Longer events (up to several hours) consist of short bursts of different amplitudes that are complexly distributed over time. The number of bursts per day and their connection with the orientation of the telescope are not clearly reproduced, although on the next days bursts are sometimes observed in nearby areas of the celestial sphere. The distribution of the telescope directions along the celestial sphere, at which bursts are recorded, is uneven. At different areas, the number of recorded events per square degree differs by more than 2 orders of magnitude.

Important results were obtained using detector that allows the extraction of beta particles with energy close to the maximum energy of the beta spectrum [16]. The $^{90}Sr^{90}Y$ source was placed in the focus of the parabolic mirror. The emitted beta particles were detecting by a detector consisting of stilbene scintillator and silicon photomultiplier. Such detector makes it possible not only to count particles, but also to determine their energy. The electronic circuit allows registration by two channels. In the former, pulses from particles of almost all the beta spectrum were detected. The discrimination threshold in the second channel is raised to a value at which the count rate is three orders of magnitude smaller than the counting rate in the first channel, but much larger than the background count without the source. In this channel, beta particles with energy near the upper limit of the 2.3 MeV beta spectrum were detecting.

Figure 6 shows fragment of signals recording in these two channels. In both channels, there are coincident bursts of count rate. Magnitudes of these bursts in

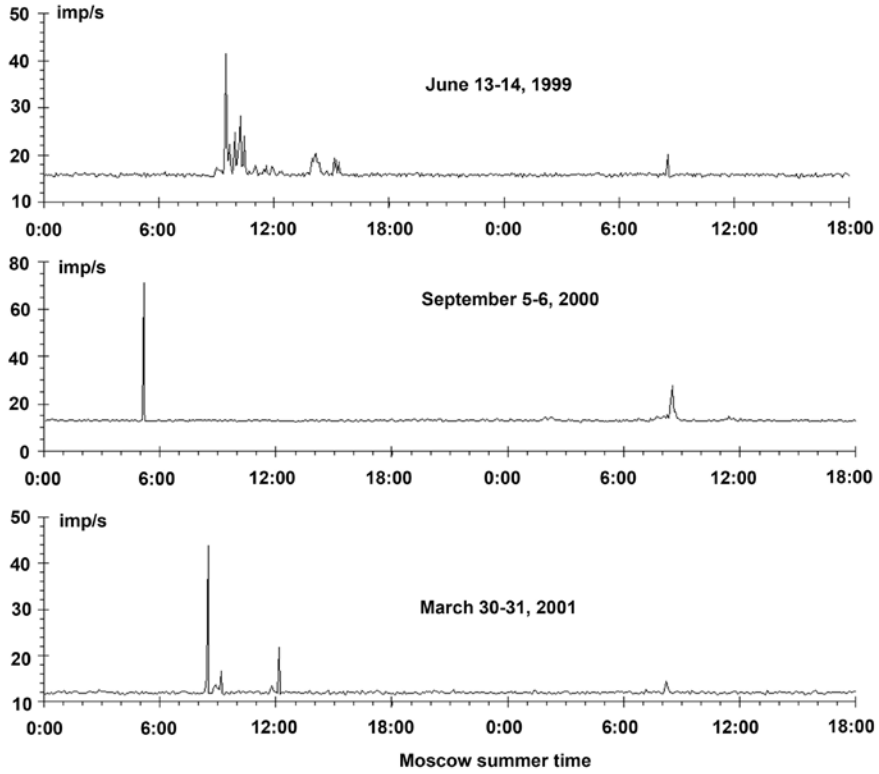

Figure 5. Examples of count rate recording of ^{60}Co, located in focus of the telescope with a parabolic mirror [15].

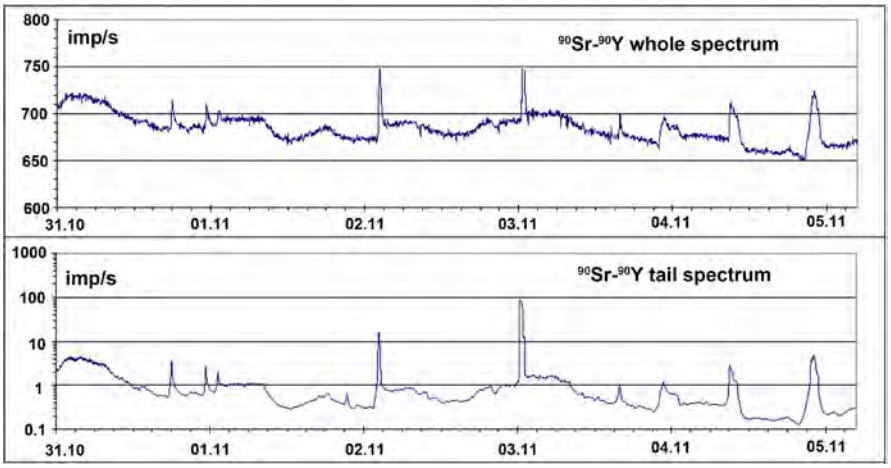

Figure 6. Comparison of count rates of bursts at different discrimination levels. On the horizontal axis the dates of 2012 [16].

the channel, where particles with an energy close to the boundary value are recorded, is approximately equal to the magnitudes of the bursts in the channel, where the particles of the whole spectrum are recorded. This indicates that the emerging particles have energy close to the boundary energy, and not the "smeared out" spectrum inherent in the usual beta decay. Thus, during the outbursts, there is no intensification of the usual "direct" beta decay, but a nuclear reaction of the "reverse" beta decay occurs, as a result of which neutrinos and

nuclei interact with the same daughter nuclei as in "direct" beta decay, But the emerging electrons are not distributed over the spectrum, but have a fixed energy.

4. Influence of Slow Neutrinos on Beta Radioactivity

The hypothesis of the connection between the variations of beta sources decay rate with neutrinos arising in nuclear processes on the Sun [6]-[12] is highly questionable in connection with the extreme weakness of interaction neutrino arising in nuclear reactions with matter. This was first pointed out by Bethe and Peierls shortly after the appearance of the neutrino hypothesis [29]. Assuming that the probabilities of direct and inverse processes are the same, they obtained the formula

$$\sigma = \lambda^3 / TV \tag{3}$$

where σ is the reaction cross section, λ is the de Broglie wavelength of the neutrino, T is the mean lifetime of radioactive nuclei, and V is the neutrino velocity.

In the case of relativistic neutrinos, which are dealt with in nuclear physics, $\lambda = hc/E$ (h is the Planck constant, c is the speed of light, E is the neutrino energy), relation (3) goes over into formula

$$\sigma = h^3 c^2 / E^3 T \tag{4}$$

Substituting in Equation (4) typical for nuclear physics values E = 1 MeV ($1.6 \cdot 10^{-13}$ J), T = 1000 s, we obtain the value of $\sigma \sim 6 \cdot 10^{-48}$ m^2, which is confirmed by experiments [30].

It follows from (4) that

$$n = N\varphi\sigma = N\varphi h^3 c^2 / E^3 T = A\varphi h^3 c^2 / E^3 \tag{5}$$

where n is the number of acts of inverse beta decays per second, $A = N/T$ is the number of direct beta decays per second (activity of the source), N is the total number of radioactive nuclei, and ϕ is the neutrino flux density.

Let us find the ratio of the rate of reverse beta decays to the rate of spontaneous beta radioactivity $K = n/A$, using the relation (5):

$$K = \varphi h^3 c^2 / E^3 \tag{6}$$

Substituting into (6) the flux density of solar neutrinos $\phi \sim 6 \cdot 10^{14}$ m^{-2}·s^{-1} [30], we obtain $K \sim 3 \cdot 10^{-30}$. Such insignificant changes in activity cannot be measured.

In the case of neutrinos of very low energies (relic neutrinos) $V \ll c$, $\lambda = h/mV$ (m is the neutrino mass), the ratio (3) goes over into formula

$$\sigma = h^3 / m^3 V^4 T \tag{7}$$

Since neutrinos, which have very small kinetic energy and mass, cannot make a significant contribution to the energy of nuclear reactions, they can react only with nuclei that do not have an energy threshold. Such nuclei have beta radioactivity

It should be noted that the term "relic neutrinos" arose in connection with the fact that initially the presence in the universe of a huge number of neutrinos with very low energies was predicted by the "big bang" theory. But it cannot be ruled out that there may be other sources of such neutrinos. For us it is important that these particles have a rest mass and the speed of motion is so low that they are kept by the gravitational fields of the Galaxy, stars and other massive objects. Therefore, it is better to call such particles "slow neutrinos". It cannot be ruled out that the anomalies in beta decays are associated not only with neutrinos, but also with other electrically neutral particles, capable of participate into weak interactions. But we are only considering neutrinos, since the initial assumption of equal probability of direct and inverse beta decays implies the identity of the decayed particles emitted from spontaneous decays and absorbed upon inverse beta decays.

It follows from (7) that in the case of neutrinos of very low energies

$$n = N\varphi\sigma = A\varphi h^3 / m^3 V^4 \tag{8}$$

Let us find the ratio of the rate of reverse beta decays to the rate of spontaneous beta radioactivity $K = n/A$ using the relation (8):

$$K = \varphi h^3 / m^3 V^4 \ . \tag{9}$$

Taking into account that $\varphi = \rho V / m$, where ρ is the mass neutrino density, we obtain

$$K = \rho h^3 / m^4 V^3 \tag{10}$$

An important feature of relations (9) and (10) is independence from the half-life of the nuclei. Any beta radioactive sources, being in the same stream of slow neutrinos, acquire the same relative increase in activity. If during its motion the Earth passes regions with different velocities or neutrinos flux density, the same relative changes in the activity of different beta sources should occur.

These calculations do not pretend to be accurate, but clearly show that neutrino fluxes can be a tangible cosmic agent. In what follows we will assume that the agent that causes additional beta decays is neutrinos moving in the gravitational field of the Galaxy. In addition to galactic neutrinos, neutrino fluxes moving in near-solar and near-Earth gravitational fields can influence beta-radioactivity [15] [17] and [32]. But an assessment of their impact on radioactivity is problematic.

Combining the results of astronomical observations with relations (9, 10), we can estimate neutrino flux density, based on the strong dependence of the magnitude of the effect on velocity. Suppose that the main reason for variations in activity with a period of 1 year is that the velocity of the neutrino flux coming to the solar system is summed with the speed of the Earth's orbital motion around the Sun.

According to [15] [32], near the solar system the fluxes of dark matter, including neutrinos, have a velocity of about $3 \cdot 10^5$ m/s and are directed predominantly perpendicular to the motion of the Sun in the Galaxy at a velocity of

about $2.5 \cdot 10^5$ m/s. The speed of the Earth's motion around the Sun is $3 \cdot 10^4$ m/s. Based on these data, we can calculate that the speed of the Earth's encounter with the flux of galactic neutrinos varies throughout the year from $V_{\min} = 3.7 \cdot 10^5$ to $V_{\max} = 4.1 \cdot 10^5$ m/s. When the velocities vary from $V_{\min}$ to $V_{\max}$, the activity increase due to the reverse beta decay changes on $\Delta K = \frac{\rho h^3}{m^4}\left(V_{\min}^{-3} - V_{\max}^{-3}\right) = 2a$, where a is the amplitude of the relative activity change, ρ is neutrino mass density, and m is neutrino mass. Therefore

$$\rho = \frac{2am^4}{h^3\left(V_{\min}^{-3} - V_{\max}^{-3}\right)}. \tag{11}$$

In [1]-[17], a change in the count rates of beta particle with an annual period up to 0.3% was found. These results prove the existence of variations, but they do not allow us to judge the value of a, since they were obtained with strong suppression of the beta particles of spontaneous decay. Precision measurements with the registering of all or most of the beta decays [21]-[28] revealed no variations with amplitude greater than 0.01%. Setting $a = 0.0001$, we can estimate the upper bound of ρ.

At present, there is no exact data on the mass of the electron neutrino (antineutrinos). A variety of experiments and astronomical observations indicate that it does not exceed 1 eV [30]. Relation (11), if we assume $a = 0.0001$ and $m = 1$ eV ($1.78 \cdot 10^{-36}$ kg), gives $\rho = 1.3 \cdot 10^{-31}$ kg/m^3 ($\phi = 3 \cdot 10^{10}$ m$^{-2}\cdot$s^{-1}).

Note that the de Broglie wavelength $\lambda = h/mV$ of slow neutrinos with a mass of 1 eV moving in the Galaxy with a velocity of about $4 \cdot 10^5$ m/s relative to the terrestrial observer has a value near 1 mm. This means that the interaction region of these particles covers an enormous number of atoms (~10^{20} in a condensed matter), in contrast to relativistic neutrinos, which interact with only one particle. This is the main reason for a radical increase in the efficiency of neutrino interaction with matter at very low energies. Another reason is that the speed of movement is small, as a result of which the duration of neutrino contact with each particle of matter becomes much greater than in the case of "nuclear" neutrinos moving at a speed close to the speed of light. The interaction of slow neutrinos with matter is similar to the interaction of light with a transparent medium: refraction, reflection, and scattering on inhomogeneities occur practically without exchange of energy. Capture is possible only when interacting with beta radioactive nuclei. In addition, interference and diffraction are possible in slow neutrino fluxes.

If surface is sufficiently smooth (unevenness is less than the wavelength), refraction and reflection occur according to the laws of geometric optics, which makes it possible to focus by means of lenses or mirrors. This circumstance makes it possible to create telescopes for slow neutrinos, using mirrors with a concave parabolic surface with a beta source located in the focus [15]. The advantage of mirrors in front of lenses is the same focus position for any focused agent. The reflection and refraction coefficients only affect the degree of ampli-

fication of the flux density at the focus.

For telescopes with a diameter D and a focal length f under the action of a monodirectional agent having wavelength λ, excess of the flux density in the focus above the unfocused flux density $\chi = 0.14kD^4/f^2\lambda^2$, where k is the coefficient that takes into account reflection losses from the mirrors or as a result of absorption in the lenses [15]. The telescope mentioned in the previous section has diameter of 22 cm and focal length of 10 cm. For such a telescope with λ = 1 mm $\chi = 3.3 \cdot 10^5 k$. The quantity k is not known. But it is clear that the telescope gives a lot of amplification even with very weak reflection from the mirror. For example, for χ = 0.01, k = 3300.

Telescopes can only be used if the active agent is narrowly directed. The presence of narrowly directed beams in slow neutrino fluxes is associated with another important feature of them: the influence of gravitational fields on their motion. Slow neutrinos trajectories, as well as other objects of dark matter, is not different from any other space objects (stars, planets, asteroids, cosmic dust, etc.) and can be calculated by conventional methods of celestial mechanics [15] [32]. When neutrino flux passing them past the celestial bodies, on the streams associated with the orbital movements, phenomena associated with the gravitational focusing are superimposed. The essence of the gravitational focusing is that the trajectories of particles flying past a massive body, such as a star, bend to the axis connecting the center of the gravitating body and the observer. The magnitude of the bend depends on the distance of the trajectory to the center of gravity. There is such a distance at which the bent trajectory falls precisely into the observer. All particles passing at such a distance from the center of gravity are "collapsed" at the observation point, as a result of which the flux density increases sharply. This effect is analogous to light gravity lensing. But due to the fact that the speed of dark matter particles (including neutrinos) is much less than the speed of light, their focusing by the gravitational fields of celestial bodies is incomparably stronger [15] [32]. Since gravitational focusing occurs with a completely determined mutual position of the focusing celestial body and target, which are in motion, this effect must be observed in the form of bursts. It is this kind of signal that was observed when working with telescopes with parabolic mirrors, in particular, with the telescope described in the previous section of this article. Strong bursts, at which the counting rate of beta particles increased by 2 - 3 orders of magnitude, were recorded quite rarely (at best, several times a day) at unpredictable instants of time. But, in addition, events were recorded that occurred at the predicted time when the telescope was being directed to a given area of the celestial sphere.

Intent of this experiment was based on the idea of gravitational focusing of slow neutrino fluxes by a certain star and secondary focusing by the Sun. This effect can be observed if the star, the center of the Sun and the observer located on the Earth are on the same straight line. Close connections of the Sun with the near-by stars are rather rare events, the time of which is easy to determine using astronomical atlases. For example, on August 19 of each year the star ν Leo

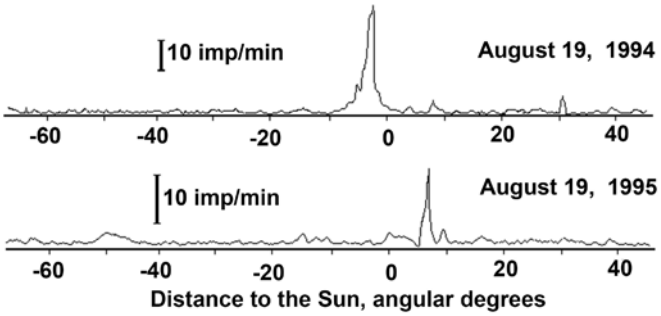

Figure 7. Count rate when scanning a near-solar region of the celestial sphere with a telescope with a focusing mirror 22 cm in diameter [15] [16].

passes at a distance of 5 angular minutes from the center of the Sun. On this day of 1994, the telescope was directed in such a way that the scanning path of the celestial sphere passed through the Sun. When the telescope was aimed at a region near the Sun, a strong burst of count rate was recorded. A similar burst was registered exactly one year later (**Figure 7**). Similar bursts were recorded on August 1 and 28, 1994, when there were close connections with the Sun of stars Cnc and 45 Leo, and also repeatedly on July 29 and 30, when the solar disk was projected onto the scattered star cluster M44 [15] [16]. On the other days of significant bursts of count rates were not found.

5. Conclusions

In a variety of experiments, periodic changes in beta particles count rate with amplitude up to tenths of percent were observed. However, such variations can be detected only with the predominant detection of particles with energies close to the maximum energy of the beta spectrum. This indicates that the observed oscillations in the count rate are associated with the action of neutrino fluxes. This is also indicated by the absence of such anomalies in alpha decays, in which the neutrino does not participate. Experiments in which most particles of beta spectrum are detected do not show periodic deviations from the usual beta decay process of more than 0.01%. This indicates that the periodic anomalies do not exceed 1/10,000 of the average beta decay rate.

Short-term irregular bursts of count rate of beta particles can be observed by placing a radioactive source in the focus of a concave parabolic mirror. These bursts can highly exceed the normal counting rate. The energy of the detected particles, as in the case of periodic anomalies, is close to the maximum energy of the spectrum of spontaneous beta decays.

In contrast to the hypothesis about the effects on beta radioactivity of solar neutrinos, the assumption of the possible involvement of space slow neutrinos in the process of beta decay allows, without departing from the scope of existing scientific knowledge, complex to explain not only the periodic and sporadic changes in the beta decay rate, but also a number of other phenomena associated with beta radioactivity, for example, inexplicable effects observed in the mea-

surement of the neutrino mass by tritium decay beta studies [15] [17] [31]. It is important to note that the hypothesis about the impact of slow neutrinos on the beta decays gives experimentally testable predictions, some of which have already been confirmed.

References

[1] Siegert, H., Shrader, H. and Schotzis, U. (1998) *Applied Radiation and Isotopes,* **49**, 1397-1401.

[2] Ellis, K.J. (1990) *Physics in Medicine and Biology,* **35**, 1079-1088. https://doi.org/10.1088/0031-9155/35/8/004

[3] Alburder, D.E., Harbottle, G. and Norton, E.F. (1986) *Earth and Planetary Science Letters*, **78**, 169.

[4] Parkhomov, A.G. (2010) Researches of Alpha and Beta Radioactivity at Long-Term Observations. arXiv:1004.1761v1 [physics.gen-ph]

[5] Sturrock, P.A., Parkhomov, A.G., Fischbach, E. and Jenkins, J.H. (2012) *Astroparticle Physics,* **35**, 755-758.

[6] Jenkins, J.H., *et al.* (2009) *Astroparticle Physics*, **3**, 42-46.

[7] Sturrock, P.A., Buncher, J.B., Fischbach, E., *et al.* (2010) Power Spectrum Analysis of Physikalisch-Technische Bundesanstalt Decay-Rate Data: Evidence for Solar Rotational Modulation. arXiv:1010.2225v1 [astro-ph.SR]

[8] Jenkins, J.H., *et al.* (2008) Evidence for Correlations between Nuclear Decay Rates and Earth-Sun Distance. arXiv:0808.3283v1 [astro-ph]

[9] Jenkins, J.H., *et al.* (2012) Additional Experimental Evidence for a Solar Influence on Nuclear Decay Rates. arXiv:1207.5783v1 [nucl-ex]

[10] Schrader, H. (2016) *Applied Radiation and Isotopes*, **114**, 202-213.

[11] Sturrock, P.A., *et al.* (2014) *Astroparticle Physics,* **59**, 47-58.

[12] Falkenberg, E.D. (2001) *Apeiron,* **8**, 32-45.

[13] Parkhomov, A.G. (2010) Periods Detected during Analysis of Radioactivity Measurements Data. arxiv:1012.4174v1 [physics.gen-ph]

[14] Parkhomov, A.G. (2011*) Journal of Modern Physics*, **2**, 1310-1317.

[15] Parkhomov, A.G. (2009) *Cosmos. Earth. New Sides of Science.* Science, Moscow. (In Russian).

[16] Parkhomov, A.G. (2013) Study of Alpha and Beta Radioactivity in Long-Term Measurements. Presentation of the Report at the INR RAS Seminar. (In Russian) http://www.inr.ru/rus/kud-sem/parkhomov-18-02-13.pdf

[17] Parkhomov, A.G. (2010) Influence of Relic Neutrinos on Beta Radioactivity. arXiv:1010.1591v1 [physics.gen-ph]

[18] Jenkins, J.H. and Fischbach, E. (2009) *Astroparticle Physics*, **31**, 407-411. https://doi.org/10.1016/j.astropartphys.2009.04.005

[19] Parkhomov, A.G. (2010) Effect of Radioactivity Decrease. Is There a Link with Solar Flares? arXiv: 1006.2295v1 [physics.gen-ph]

[20] Parkhomov, A.G. (2005) *International Journal of Pure and Applied Physics*, **1**, 119-128.

[21] Norman, E.B., Browne, E., Shugart, H.A., Joshi, T.H. and Firestone, R.B. (2009) *Astroparticle Physics*, **31**, 135-137. https://doi.org/10.1016/j.astropartphys.2008.12.004

[22] Cooper, P.S. (2008) *Astroparticle Physics*, **31**, 267-269. arXiv:0809.4248v1 [astro-ph]

[23] Bellotti, E., Broggini, C., Di Carlo, G., *et al.* (2013) *Physics Letters B*, **720**, 116-119. https://doi.org/10.1016/j.physletb.2013.02.002

[24] Semkow, T.M., *et al.* (2009) *Physics Letters B*, **675**, 415-419. https://doi.org/10.1016/j.physletb.2009.04.051

[25] Pommé, S., Stroh, H., Paepen, J., *et al.* (2016) *Physics Letters B*, **761**, 281-286. https://doi.org/10.1016/j.physletb.2016.08.038

[26] Bergeson, S.D., Peatross, J. and Ware, M.J. (2017) *Physics Letters B*, **767**, 171-176. https://doi.org/10.1016/j.physletb.2017.01.030

[27] Bellotti, E., *et al.* (2015) *Physics Letters B*, **743**, 526-530. https://doi.org/10.1016/j.physletb.2015.03.021

[28] Bellotti, E., Broggini, C., Di Carlo, G., Laubenstein, M. and Menegazzo, R. (2018) Search for Time Modulations in the Decay Constant of 40K and 226Ra at the Underground Gran Sasso Laboratory. arXiv:1802.09373v1 [nucl-ex]

[29] Bethe, H. and Peierls, R. (1934) *Nature*, **133**, 689-690. https://doi.org/10.1038/133689b0

[30] Giunti, C. and Kim, C.W. (2007) Fundamentals of Neutrino Physics and Astrophysics. Oxford University Press, Oxford. https://doi.org/10.1093/acprof:oso/9780198508717.001.0001

[31] Lobashev, V.M., Aseev, V.N. and Belesev, A.I. (1999) *Physics Letters B*, **460**, 227-232. https://doi.org/10.1016/S0370-2693(99)00781-9

[32] Parkhomov, A.G. (2004) Distribution and Motion of Dark Matter, MNTTs VENT, Moscow. (In Russian) http://www.chronos.msu.ru/old/RREPORTS/parkhomov_raspredelenie.pdf

Journal of Modern Physics, 2018, 9, 1633-1644
http://www.scirp.org/journal/jmp
ISSN Online: 2153-120X
ISSN Print: 2153-1196

Periodic System of Atoms in Biquaternionic Representation

Lyudmila Alexeyeva

Institute of Mathematics and Mathematical Modeling, Almaty, Kazakhstan
Email: alexeeva@math.kz

How to cite this paper: Alexeyeva, L. (2018) Periodic System of Atoms in Biquaternionic Representation. *Journal of Modern Physics*, **9**, 1633-1644.
https://doi.org/10.4236/jmp.2018.98102

Received: June 6, 2018
Accepted: July 21, 2018
Published: July 24, 2018

Copyright © 2018 by author and Scientific Research Publishing Inc.
This work is licensed under the Creative Commons Attribution International License (CC BY 4.0).
http://creativecommons.org/licenses/by/4.0/
Open Access

Abstract

Private monochromatic solutions of the free-field equation of electro-gravimagnetic charges and currents are constructed in the differential algebra of biquaternions, which describe elementary particles as standing electro-gravimagnetic waves. The two classes of solutions of this biquaternionic wave equation have been investigated, generated by scalar potentials (pulsars) and vectorial potentials (spinors). Their asymptotic properties are considered, on the base of which they are classified into heavy (boson) and light (lepton) elementary particles. The biquaternion representation of the hydrogen atom is given. The periodic system of elements is produced, which is built on the principle of the musical structure of a simple gamma.

Keywords

Biquaternion, Elementary Particle, Frequency, Standing EGM-Wave, Pulsar, Spinor, Boson, Lepton, Atom, Hydrogen, Periodic System, Musical Scale

1. Introduction

In [1] [2] [3], the author developed a biquaternion model of the electro-gravimagnetic field (*EGM-field*) and electro-gravimagnetic interactions. Its basis is made up of biquaternion representations of the generalized Maxwell and Dirac equations. The biquaternion representation of the Maxwell equations expresses the biquaternion of the mass-charge density and the EGM-current through the bigradient of the EGM-field tension. The biquaternionic representation of Dirac equations determines the transformation of the density of mass charges and currents under the influence of external EGM-fields. In particular, in the absence of external fields, it is the biquaternionic wave (biwave) equation for the free field of mass-charges and currents, which is a field analogue of first Newton's law (*inertia law*).

Here we construct particular monochromatic solutions of this equation that describe elementary particles as standing EGM-waves. They can be divided into two class, generated by scalar potentials (*pulsars*) and vector ones (*spinors*). Their asymptotic properties are investigated, on the basis of which they are classified into heavy (*bosons*) and light (*leptons*) elementary particles. It is shown that bosons are spherical harmonic pulsars whose mass-charge density is determined by their frequency of oscillations. This allows us to build periodic systems of elementary particles based on the classical harmonic musical scale.

In particular, the biquaternion representation of the hydrogen atom is given and the periodic system is produced, which is built on the principle of the musical structure of a simple harmonic scale.

2. Inertia Law for Monochromatic Fields of Charges-Currents

The equation for the free field of charge-currents has the form of a homogeneous biwave equation [1] [2]:

$$\nabla^{-}\Theta(\tau,x)\triangleq(\partial_{\tau}-i\nabla)\circ(i\rho(\tau,x)+J(\tau,x))=0 \tag{1}$$

Here, $\Theta(\tau,x)$ is the biquaternion of the charge-current, the secular part of which $\rho(\tau,x)$ describes the density of the electric and gravimagnetic charge (EGM-charge or *mass-charge*), and the vector $J(\tau,x)$ is the density of the electric and gravimagnetic current (EGM-current), more exactly:

$$\rho=\frac{1}{\sqrt{\varepsilon}}\rho^{E}-\frac{i}{\sqrt{\mu}}\rho^{H},$$

$$J=\sqrt{\mu}\,j^{E}-i\sqrt{\varepsilon}\,j^{H},$$

where $\rho^{E}(x,t), j^{E}(x,t)$ are the electric charge and electric current densities, $\rho^{H}(x,t), j^{H}(x,t)$ are the gravimagnetic charge density and current density; ε,μ are the constants of electric conductivity and magnetic permeability of vacuum, $c=1/\sqrt{\varepsilon\mu}$ is speed of light, i is imaginary unit.

The action of the biquaternion differential operators ∇^{-} and ∇^{+} (*mutual bigradients*) is determined, according to the quaternion multiplication rule (see **Appendix**), by the formula

$$\begin{aligned}\nabla^{\pm}\mathrm{F}(\tau,x)&=(\partial_{\tau}\pm i\nabla)\circ(f(\tau,x)+F(\tau,x))\\&=(\partial_{\tau}f\mp i\,\mathrm{div}F)+\{\pm i\,\mathrm{grad}\,f+\partial_{\tau}F\pm i\,\mathrm{rot}\,F\}\end{aligned}$$

The biquaternion of the energy-momentum of the F-field is given by

$$\Sigma(\tau,x)=W(\tau,x)+iP(\tau,x)\triangleq 0.5\mathrm{F}\circ\mathrm{F}^{*},$$

where F^{*} is the conjugate biquaternion

$$\mathrm{F}^{*}\triangleq\overline{f}(\tau,x)-\overline{F}(\tau,x).$$

Here the bar over the symbol means complex conjugation.

The scalar part W is the energy density of the F-field, and P is the analog of the generalized Poynting vector of the F-field, just as a generalized Poynting

vector is constructed in the biquaternionic representation of the electromagnetic field (in detail about the differential algebra of biquaternions with an application in electrodynamics, see [4]).

The scalar part of the Equation (1) is the *law of conservation* of the EGM-charge:

$$\partial_\tau \rho + \operatorname{div} J = 0,$$

and the vectorial part describes the relationship between charges and currents in the absence of external EGM-fields:

$$\partial_\tau J - i\operatorname{rot} J + \operatorname{grad}\rho = 0.$$

For monochromatic fields of frequency ω, the biquaternion of the charge-current can be represented in the form

$$\Theta(\tau, x) \triangleq \Theta(x, \omega)\exp(i\omega\tau), \quad \omega > 0. \tag{2}$$

In this case, from the Equation (2) we obtain the equation for biquaternions of complex amplitudes (*biamplitudes*) $\Theta(x, \omega)$:

$$(\omega - \nabla)\circ(i\rho(x) + J(x)) = 0.$$

As

$$(\omega + \nabla)\circ(\omega - \nabla) = (\omega - \nabla)\circ(\omega + \nabla) = \omega^2 + \Delta,$$

it follows that the biamplitudes satisfy the Helmholtz equation

$$\Delta\Theta + \omega^2\Theta = 0$$

and monochromatic solutions have the form:

$$\Theta(\tau, x) = \exp(i\omega\tau)(\omega + \nabla)\circ\left(\psi^0(x, \omega) + \sum_{j=1}^{3}\psi^j(x, \omega)e_j\right), \tag{3}$$

where the potentials ψ^j are arbitrary solutions of the homogeneous Helmholtz equation

$$\Delta\psi + \omega^2\psi = 0,$$

which have the form of a surface integral

$$\psi^j(x, \omega) = \int_{\|\xi\|=\omega}\varphi^j(\xi, \omega)\mathrm{e}^{-i(\xi, x)}\mathrm{d}S(\xi) \tag{4}$$

for any function ϕ^j that is integrable on a sphere of radius ω.

3. Biquaternions of Harmonic Elementary Particles

We consider particular solutions of the Helmholtz equation [5] [6]

$$\psi_{nm}(x, \omega) = j_n(\omega r)Y_n^m(\vartheta, \phi) \tag{5}$$

where $j_n(\omega r)$ are spherical Bessel functions of order $n = 0, 1, 2, \cdots$; $Y_n^m(\vartheta, \phi)$ - spherical harmonics of order $(n, m), m = 0, 1, 2, \cdots$

$$Y_n^m(\vartheta, \phi) = P_n^m(\cos\vartheta)\exp(im\phi)$$

$P_n^m(...)$ are the associated Legendre polynomials, (r, ϑ, ϕ) are spherical

coordinates.

It is natural to take these solutions for the construction of elementary particles, which can be called *harmonic*. Among them we select the ones generated by the scalar potential, which we call *pulsars*:

$$\begin{aligned}\Theta^0_{nm}(x,\omega) &= (\omega+\nabla)\circ\psi_{nm}(x,\omega)\\ &= \omega\psi_{nm}(x,\omega)+\operatorname{grad}\psi_{nm}(x,\omega)\end{aligned} \tag{6}$$

and particles, generated by a vector potential, we call *spinors*:

$$\begin{aligned}&\Theta^j_{nm}(x,\omega) = (\omega+\nabla)\circ\psi_{nm}(x,\omega)e_j\\ &= -\operatorname{div}\left(\psi_{nm}(x,\omega)e_j\right)+\left\{\omega\psi_{nm}(x,\omega)e_j+\operatorname{rot}\left(\psi_{nm}(x,\omega)e_j\right)\right\}\end{aligned} \tag{7}$$

The latter are polarized in the direction of the coordinate axes, respectively, to the index $j=1,2,3$.

4. Biquaternions of Monochromatic Structures. Crystals

Using *structural biquaternions* of arbitrary form $\mathrm{K}(x)$, on their basis, by the operation of biquaternion convolution

$$\begin{aligned}&\Theta(x,\omega)*\mathrm{K}(x) = (i\rho+J)*(k+K)\\ &= \left\{i\rho*k-\sum\nolimits_{j=1}^{3}\left(J_j*K_j\right)\right\}+\left\{i\rho*K+J*k+\sum\nolimits_{j,l,m=1}^{3}\varepsilon_{jlm}\left(J_j*K_l\right)e_m\right\}\end{aligned} \tag{8}$$

where ε_{jlm} is the Levi-Civita pseudo-tensor, it is possible to construct a variety of monochromatic fields of charge-currents:

$$\Theta(x,\omega)=\sum_{j=0}^{3}\Theta^j_{nm}(x,\omega)*\mathrm{K}_j(x) \tag{9}$$

In (8) there are functional convolutions, which for integrable functions have the integral form:

$$\rho(x)*k(x)=\int_{R^3}\rho(y)k(x-y)\mathrm{d}y_1\mathrm{d}y_2\mathrm{d}y_3$$

Component convolutions for vectors are written similarly. By virtue of the differentiation property of convolution, the convolutions (9) are also solutions of the equations (1).

Formulas (9) allow us to construct various crystal lattices from harmonic elementary particles, if we take lattices as the structural biquaternion the different shifts of the δ-function, and other generalized functions.

We give here a simple example of an inhomogeneous rectangular lattice with variable step (h_l,h_m,h_n) and weight a^{lmn}:

$$\mathrm{K}(x)=\sum_{l=0}^{L}\sum_{m=0}^{M}\sum_{n=0}^{N}a^{lmn}\delta(x_1-h_l)\delta(x_2-h_m)\delta(x_3-h_n)$$

It corresponds, for example, to such a crystalline ω-pulsar

$$\Theta(x,\omega)=\sum_{l=0}^{L}\sum_{m=0}^{M}\sum_{n=0}^{N}a^{lmn}\theta^0(x_1-lh_l,x_2-mh_m,x_3-nh_n,\omega)$$

The formulas (7)-(9) make it possible to construct a wide variety of monochromatic structures, such as crystals, bodies, tissues and filaments (for

more details, see [2]). And their frequency superpositions are generally immeasurable.

5. Elementary Spherical Harmonic Pulsars and Their Properties

Among the solutions of the Helmholtz Equations (7), only one is spherically symmetric [5]. It is

$$\psi_{00}(x,\omega)=j_0(\omega r)=\frac{\sin\omega r}{\omega r} \tag{10}$$

Here $r=\|x\|=\sqrt{x_1^2+x_2^2+x_3^2}$, $j_0(\omega r)$ are spherical Bessel functions.

The biamplitude of the corresponding pulsar is

$$\begin{aligned}&\Theta^0(x,\omega)=(\omega+\nabla)\circ\psi_{00}(x,\omega)\\&=\omega\frac{\sin\omega r}{\omega r}+\operatorname{grad}\frac{\sin\omega r}{\omega r}=\cdots=\frac{\sin\omega r}{r}+\left(\frac{\cos\omega r}{r}-\frac{\sin\omega r}{\omega r^2}\right)e_x,\ e_x=x/r\end{aligned} \tag{11}$$

Whence follows

$$i\rho_1^0+J_1^0=r^{-1}\left\{\sin\omega r+\left(\cos\omega r-\frac{\sin\omega r}{\omega r}\right)e_x\right\}\mathrm{e}^{i\omega\tau}$$

$$\rho^0=-\frac{i\sin\omega r}{r}\mathrm{e}^{i\omega\tau},\quad J^0=\left(\frac{\cos\omega r}{r}-\frac{\sin\omega r}{\omega r^2}\right)\mathrm{e}^{-i\omega\tau}e_x$$

$$\Rightarrow\left|\rho^0\right|=\frac{\left|\sin\omega r\right|}{r},\quad \left\|J^0\right\|=\left|\frac{\cos\omega r}{r}-\frac{\sin\omega r}{\omega r^2}\right|$$

We denote by

$$j(z)=\cos z-\frac{\sin z}{z}=-z\,j_1(z).$$

Calculating the biquaternion of its energy-momentum

$$\begin{aligned}\Xi^0(x,\omega)&=W^0+iP^0=0.5\Theta^0\mathrm{e}^{i\omega\tau}\circ\left(\Theta^0\right)^*\mathrm{e}^{-i\omega\tau}\\&\triangleq 0.5r^{-2}\left(\sin\omega r+j(\omega r)e_x\right)\circ\left(\sin\omega r-j(\omega r)e_x\right)\\&=0.5r^{-2}\left\{\left(\sin^2\omega r+j^2(\omega r)\right)+\sin\omega r\,j(\omega r)e_x\right.\\&\quad\left.-\sin\omega r\,j(\omega r)e_x-j^2(\omega r)\left[e_x,e_x\right]\right\},\end{aligned}$$

we get

$$W^0=0.5r^{-2}\left(\sin^2\omega r+j^2(\omega r)\right),\quad P\equiv 0. \tag{12}$$

It follows from (11)-(12) that the density of the mass-charge decreases as r^{-1} by increasing r, and the oscillation energy decays even more rapidly, as r^{-2}.

It is interesting to investigate the asymptotic of these quantities as $r\to 0,\omega=const$. Since

$$\begin{aligned}j(\omega r)&=(\omega r)^2\,j_1(\omega r)=\cos\omega r-\frac{\sin\omega r}{\omega r}\\&=1-\frac{(\omega r)^2}{2}-1+\frac{(\omega r)^3}{6\omega r}+\cdots\sim-\frac{(\omega r)^2}{3}\qquad r\to 0,\end{aligned} \tag{13}$$

from (11) and (13) we obtain: by $r \to 0$

$$\left|\rho^0\right| = \omega + o(\omega r) \sim \omega,$$

$$\left\|J^0\right\| \approx \frac{\omega r + 0.5\omega^2 r^2}{r} - \frac{\omega r - \omega^3 r^3/6}{\omega r^2} \approx 0.5\omega^2 r + \omega^2 r/6 \sim \frac{2}{3}\omega^2,$$

$$W \sim 0.5\left(\omega^2 + \omega^4 r^2/9\right) \sim 0.5\omega^2.$$

Let us now list these properties.

The properties of spherical pulsars. In spherical harmonic pulsars at the center at $x = 0$, the mass-charge density is equal to its oscillation frequency ω; the density of the EGM-current is zero; the energy density is equal to $0.5\omega^2$; and the Poynting vector equal to zero everywhere.

Proceeding from these properties of mass-charge density, spherical harmonic pulsars are heavy elementary particles—*bosons*.

Non-spherical harmonic pulsars (6) for $n > 0$ have zero density at $x = 0$, because [5]

$$j_n(z) = \frac{z^n}{(2n+1)!!}\left(1 + o(z)\right) \quad z \to 0.$$

They are light elementary particles—*leptons*.

6. Elementary Spherical Harmonic Spinors and Their Properties

Consider a spinor polarized in direction X_1:

$$\Theta_1^0(x,t) = i\rho_1^0 + J_1^0 = \Theta_1^0(x,\omega)\mathrm{e}^{i\omega\tau},$$

whose biamplitude is

$$\begin{aligned}
&\Theta_1^0(x,\omega) = (\omega + \nabla) \circ j_0(\omega r) e_1 \\
&= -\mathrm{div}\left(j_0(\omega r) e_1\right) + \omega j_0(\omega r) e_1 + \mathrm{rot}\left(j_0(\omega r) e_1\right) \\
&= -r_{,1}\left(\frac{\cos\omega r}{r} - \frac{\sin\omega r}{\omega r^2}\right) \\
&+ \left\{\frac{\sin\omega r}{r} e_1 + \left(\frac{\cos\omega r}{r} - \frac{\sin\omega r}{\omega r^2}\right)\left(r_{,3} e_2 - r_{,2} e_3\right)\right\}, \quad r_{,j} = \frac{x_j}{\|x\|}
\end{aligned} \tag{14}$$

Whence follows

$$\rho_1^0 = -\frac{ix_1}{r^2} j(\omega r),$$

$$J_1^0 = r^{-1}\left(e_1 \sin\omega r + j(\omega r)\left(r_{,3} e_2 - r_{,2} e_3\right)\right);$$

$$\left|\rho_1^0\right| = \left|\frac{r_{,1}}{r} j(\omega r)\right|, \quad \|J\| = \sqrt{\frac{\sin^2\omega r}{r^2} + j^2(\omega r)\frac{\left(x_2^2 + x_3^2\right)}{r^4}}$$

We calculate the biquaternion of the energy-momentum and its asymptotic:

$$\Xi_1^0(x,\omega) = W_1^0 + iP_1^0, \tag{15}$$

$$2W_1^0 = \frac{\sin^2 \omega r}{r^2} + \left(\frac{r_{,1}}{r}\right)^2 j^2(\omega r) + j^2(\omega r)\frac{\left(x_2^2 + x_3^2\right)}{r^4}$$
$$= \frac{\sin^2 \omega r}{r^2} + j^2(\omega r)\frac{\left(x_1^2 + x_2^2 + x_3^2\right)}{r^4}$$
$$= r^{-2}\left(\sin^2 \omega r + j^2(\omega r)\right).$$

$$P_1^0 \equiv 0.$$

We construct their asymptotic for $r \to 0$ with allowance (13):

$$\left|\rho_1^0\right| \sim \left|\frac{x_1}{r^2}\left(1 - \frac{\omega^2 r^2}{2} - 1 + \frac{\omega^3 r^3}{6\omega r}\right)\right| = \frac{1}{3}|x_1|\omega^2 \to 0,$$

$$\|J\| \sim \sqrt{\frac{(\omega r)^2}{r^2} + \frac{(\omega r)^4}{9}\frac{\left(x_2^2 + x_3^2\right)}{r^4}} \sim \omega \to \omega,$$

$$W \sim \frac{1}{2r^2}\left(1 - \frac{2\omega r}{\omega r} + \frac{8(\omega r)^3}{6\omega r} + \frac{\left(\omega r - (\omega r)^3/6\right)^2}{\omega^2 r^2}\right)$$
$$= \frac{1}{2r^2}\left(1 - 2 + \frac{4}{3}(\omega r)^2 + 1 - \frac{1}{3}(\omega r)^2 + \frac{1}{36}(\omega r)^4\right) \sim 0.5\omega^2.$$

Following (14), we easily obtain a biquaternion representation of the spherical spinor polarized along the vector $e, \|e\| = 1$:

$$\Theta_e^0(x,\omega) = (\omega + \nabla) \circ j_0(\omega r)e$$
$$= -\mathrm{div}\left(j_0(\omega r)e\right) + \omega j_0(\omega r)e + \mathrm{rot}\left(j_0(\omega r)e\right)$$
$$= i\rho_e^0 + J_e^0$$

where

$$\rho_e^0 = -\frac{e_x}{r}j(\omega r), \quad J_e^0 = r^{-1}\left(e\sin \omega r + j(\omega r)\varepsilon_{jkl}x_j x_k e_l\right)$$

with the same asymptotic properties.

So we have the following properties of the constructed spinors.

Properties of harmonic spherical spinors. For spherical harmonic spinors at the center (for $x = 0$), the mass-charge density is zero, the norm of the density of the EGM-current vector is ω, the energy density is $\omega^2/2$, the Poynting vector is equal to zero.

Thus, spherical harmonic spinors in terms of the density of the EGM-charge belong to light elementary particles—*leptons*.

7. Biquaternion Model of the Hydrogen Atom

Thus, we have shown that among the monochromatic solutions of the charge-current free field Equations (1), only harmonic spherical pulsars have a nonzero density at their center, which is not the case for harmonic spinors. This suggests that spherical harmonic pulsars can be used to construct a biquaternion model of atoms.

The simplest atom is hydrogen (H). The simplest harmonic elementary particle is the above described spherical pulsar. I think they can be identified, namely:

The hydrogen atom is a spherical harmonic pulsar with fixed oscillation frequency ω_{H_0}. *It has the following biquaternionic representation*

$$\mathrm{H}_0(\tau,x)=r^{-1}\left\{\sin\omega_{H_0}r+\left(\cos\omega_{H_0}r-\frac{\sin\omega_{H_0}r}{\omega_{H_0}r}\right)e_x\right\}\mathrm{e}^{i\omega_{H_0}\tau}. \tag{16}$$

The asymptotic properties of its density at the center of an atom are related to the frequency of the oscillations:

$$\left|\rho_{H_0}(x,\tau)\right|\sim\omega_{H_0},\quad \left\|J_{H_0}(x,\tau)\right\|\sim\frac{2}{3}\omega^2 r,\quad W_{H_0}(x)\sim 0.5\omega^2,\quad r\to 0. \tag{17}$$

The nodes of this standing wave with respect to the mass density $\left|\rho_{H_0}\right|$ are spheres whose radius is determined by a simple trigonometric equation

$$\sin\omega_{H_0}r_k=0\quad\Rightarrow\quad r_k=\frac{\pi k}{\omega_{H_0}},\ k=1,2,\cdots$$

To determine the nodes of this standing wave from the energy density W_{H_0}, it is necessary to find the zeros of the more complicated equation:

$$\omega_{H_0}^2r_k^2+\omega_{H_0}r_k\sin 2\omega_{H_0}r_k-\sin^2\omega_{H_0}r_k=0 \tag{18}$$

where $r_k=\dfrac{z_k}{\omega_{H_0}}$, z_k are the roots of the transcendental equation:

$$f(z)=z^2+z\sin 2z-\sin^2 z=0$$

However, this equation has no real roots.

Using the representation of complex charges and currents through electric and gravimagnetic charges and currents (1), we obtain for the hydrogen atom the following expressions for its electric and gravimagnetic charges, electric and gravimagnetic currents:

$$\rho_{H_0}^E(t,x)=-\frac{\sqrt{\varepsilon}}{r}\cos w_{H_0}t\sin\frac{w_{H_0}\|x\|}{c},$$

$$\rho_{H_0}^H(t,x)=\frac{\sqrt{\mu}}{r}\sin w_{H_0}t\sin\frac{w_{H_0}\|x\|}{c}$$

$$J_{H_0}^E(t,x)=\frac{1}{\sqrt{\mu}r}\cos w_{H_0}t\left(\cos\frac{w_{H_0}\|x\|}{c}-\frac{c}{w_{H_0}r}\sin\frac{w_{H_0}\|x\|}{c}\right)e_x$$

$$J_{H_0}^H(t,x)=-\frac{1}{\sqrt{\varepsilon}r}\sin w_{H_0}t\left(\cos\frac{w_{H_0}\|x\|}{c}-\frac{c}{w_{H_0}r}\sin\frac{w_{H_0}\|x\|}{c}\right)e_x$$

Accordingly, in the initial space-time, the biquaternion of hydrogen has the form:

$$\mathrm{H}_0(t,x)=\frac{\mathrm{e}^{iw_{H_0}t}}{r}\left\{-\sin\left(w_{H_0}r/c\right)+\left(\cos\left(w_{H_0}r/c\right)-\frac{c\sin\left(w_{H_0}r/c\right)}{w_{H_0}r}\right)e_x\right\}.$$

Here $e_x = x/\|x\|$, vibration frequency of a hydrogen atom $w_{H_0} = c\omega_{H_0}$. Accordingly (17), by $r \to 0$

$$\left|\rho_{H_0}(x,\tau)\right| \sim cw_{H_0}, \quad \left\|J_{H_0}(x,\tau)\right\| \sim \frac{2}{3}\left(cw_{H_0}\right)^2 r, \quad W_{H_0}(x) \sim \frac{\left(cw_{H_0}\right)^2}{2}.$$

Note that the energy density contains the square of the speed of light. Since the mass-charge density is determined by the oscillation frequency, the last formula correlates with the known Einstein's formula for the total energy of a body with a fixed mass.

8. Biquaternion Representation of Atoms. Simple Gamma

So, in the biquaternionic representation, the hydrogen atom is a spherical harmonic standing wave with a fixed frequency in the field of EGM charge-currents.

Since the main characteristic of the hydrogen atom is the oscillation frequency, which determines its mass, on its basis it is possible to construct a periodic system for atoms of substances according to the principle of the musical scale. As the frequency of vibrations increases, the mass of the atom increases.

The musical scale is a system of octaves with frequency doubling for each subsequent *octave*:

$$\omega_{H_0}, 2\omega_{H_0}, 4\omega_{H_0}, 8\omega_{H_0}, 16\omega_{H_0}, \cdots$$

The ratio of vibration frequencies for atoms inside the n-octave:

$$2^{n-1}\omega_{H_0}, \cdots, 2^n\omega_{H_0}$$

like the ratio of tone frequencies within the musical scale. Number of tones in the musical scale depends on the type of musical system.

There are many musical structures, which are largely related to the national peculiarities of the musical perception of the peoples who created them. Here in Table 1 two musical systems are given (*simple gamma*, [7]), which can be taken as a basis, in which the ratio frequency of tones is a rational number. For such tones (*notes*), there is the total period of oscillations, which is determined by the least common multiple for the period their harmonies, which makes it possible to harmoniously sound the accords from different notes. For each of them, in nature, there are substances that possess the described above properties. Which of them corresponds to Mendeleyev's periodic table? It should be the subject of a special study for specialists in area of physical chemistry, spectral properties of substances.

Perhaps among these three structures in Table 1 there is no such. But a similar musical scale should be, which contains the frequencies of these scales. The number of tones within an octave can be changed with growth octave numbers, but all the similar tones of the previous octave in it should be present, which explains the repeatability of chemical properties of substances in columns of periodic Mendeleyev's system, just as the musical sounds are harmonious for perception for octaves and chords composed of them.

Table 1. Simple gamma.

Clean structure							
Prima (ut)	Major secunda (re)	Major tertius (mi)	Quartus (fa)	Quintus (sol)	Major sextus (la)	Major septim (si)	Octabas ut
ω	$9\omega/8$	$5\omega/4$	$4\omega/3$	$3\omega/2$	$5\omega/3$	$15\omega/8$	2ω
Pentatonic structure							
Prima	Secunda	Tertius	-	Quintus	Sectus	-	Octabas
ω	$9\omega/8$	$5\omega/4$	-	$3\omega/2$	$5\ \omega/3$		2ω

Proceeding from this, the atoms can be called *musical elementary particles* with the appropriate names. The hydrogen atom is the note *ut* of the first natural octave. Correspondingly, the biquaternion of the k-th atom in the n-th octave has the form

$$\mathrm{Atom}^{n,k}(t,x)=\frac{1}{r}\mathrm{e}^{iw_{nk}t}\left\{-\sin\left(\frac{w_{nk}}{c}r\right)+\left(\cos\left(\frac{w_{nk}}{c}r\right)-\frac{c\sin\left(w_{nk}r/c\right)}{w_{nk}r}\right)e_x\right\}.$$

Here the frequency of oscillations of the atom

$$w_{nk}=2^n\gamma_k w_{H_0},$$

where γ_k is the k-th coefficient in the table of the corresponding musical scale. For it, all the above formulas for a spherical harmonic pulsar are correct by the frequency of oscillations corresponding to it.

9. Conclusions

How many such natural octaves exist? Obviously, no less than the number of rows in the periodic system of Mendeleyev.

Let us note that the twelve-tempered musical scale, now accepted in classical music, with twelve notes inside the octave, can not be taken, since the ratio of frequencies of consecutive tones in it is a number irrational $\sqrt[12]{2}$ and the general period of oscillation for any set of tones in the octave does not exist. Complete harmonious sound in this system can not be achieved. This is well known to the orchestral musicians of strings and wind instruments, the sound of which is determined by the above described musical arrangements. As is known, with disproportionate oscillation frequencies, beats occur.

Such periodic systems can be constructed for elementary harmonic leptons (spinors and asymmetric pulsars), whose addition to atoms with the same vibration frequency apparently creates isotopes of these atoms. Moreover, the addition of the spinors is connected with the magnetization of matter. It is possible to construct many different isotopes with the same asymptotic density of the EGM charge. Which of them exist in nature is also a matter of special experimental research.

We also note that this description of atoms is based on the construction of solutions to the equations of the free field of charge-currents. Under the influence

of external fields, charges and currents are transformed. Their transformation is described by the generalized Dirac equation (see [3]). In particular, under the influence of stationary EGM-fields, the oscillation spectrum shifts, which should be taken into account in the experimental substantiation of the model, are considered here.

At present, the most widespread and canonized representations of light and heavy elementary particles and atoms are constructed on the basis of solutions of the equations of quantum field theory. The bibliography in this direction is half a century old and very extensive. Here we use the names for heavy and light particles adopted in this theory. However, the represented biquaternion model is completely different, deterministic, based on the determination of the real physical characteristics of elementary particles and atoms, rather than probabilistic ones.

References

[1] Alexeyeva, L.A. (2009) *Journal of Physical Mathematics*, **1**, Article ID: S090604.

[2] Alexeyeva, L.A. (2016) *Journal of Modern Physics*, **7**, 435-444. https://doi.org/10.4236/jmp.2016.75045

[3] Alexeyeva, L.A. (2016) *Journal of Modern Physics*, **7**, 1351-1358. https://doi.org/10.4236/jmp.2016.711121

[4] Alexeyeva, L.A. (2012) *Clifford Analysis*, *Clifford Algebras and their Applications*, **7**, 19-39.

[5] Abramowitz, M. and Stegun, I., Eds. (1964) Handbook on Mathematical Functions. National Buro of Standards, Applied Mathematical Series, 55.

[6] Vladimirov, V.S. (1978) Generalized Functions in Mathematical Physics. Nauka, Moscow.

[7] Shilov, G.E. (1970) Simple Gamma. Moscow state University Publisher, Brochure 24 p.

Appendix

To use biquaternions algebra we give here some definitions.

We consider on Minkowski space $\mathbb{M}=\{(\tau,x)\}$ the functional space of biquaternions in *hamiltonian form*:

$$\mathbb{B}(\mathbb{M})=\{F=f(\tau,x)+F(\tau,x)\}$$

f is a complex function, $F=\sum_{j=1}^{3}F_j e_j$ —a three-dimensional complex vector-function; $x=\sum_{j=1}^{3}x_j e_j$, $e_0=1$, e_1,e_2,e_3 are *basic elements*.

We assume $f(\tau,x),F_j(\tau,x)$ are locally integrable and differentiable on $\mathbb{M}$ or, in general case, they are generalized functions.

Summation and *quaternionic multiplication* are defined as

$$\alpha\mathbf{F}+\beta\mathbf{B}=\alpha(f+F)+\beta(b+B)\triangleq(\alpha f+b\beta)+(\alpha F+\beta B),$$

$$\mathbf{F}\circ\mathbf{B}=(f+F)\circ(b+B)\triangleq fb-(F,B)+fB+bF+[F,B],$$

where $(F,B)=F_jB_j,[F,B]=\epsilon_{jkl}e_jF_kB_l$ are usual scalar and vector productions in R^3 (here over repeated indexes there are summation from 1 to 3, ϵ_{jkl} is Levi-Civita symbol).

The *norm* and *pseudonorm* of Bq. are denoted

$$\|\mathrm{F}\|=\sqrt{|f|^2+\|F\|^2},\quad \langle\langle\mathrm{F}\rangle\rangle=\sqrt{|f|^2-\|F\|^2},\quad |f|^2=f\bar{f},\quad \|F\|^2=(F,\bar{F}).$$

We'll use *convolution of biquaternions*:

$$\mathbf{F}*\mathbf{B}=f*b-(F_j*B_j)+f*B_je_j+b*F_je_j+\epsilon_{jkl}e_jF_k*B_l.$$

For regular components a convolution has the form:

$$f*b=\int_{\mathbb{M}}f(\tau-t,x-y)b(t,y)\mathrm{d}t\mathrm{d}y_1\mathrm{d}y_2\mathrm{d}y_3,$$

to take a convolution for singular generalized function and conditions of convolution existence see [6].

Mutual bigradients ∇^+,∇^- are the differential operators

$$\nabla^{\pm}\mathbf{B}=(\partial_\tau\pm i\nabla)\circ(b+B)\triangleq\partial_\tau b\mp i(\nabla,B)\pm i\nabla b\pm\partial_\tau B\pm i[\nabla,B]$$
$$\triangleq\partial_\tau b\mp i\mathrm{div}B\pm i\mathrm{grad}b\pm\partial_\tau B\pm i\mathrm{rot}B$$

which are taken corresponding to the sign.

Journal of Modern Physics, 2018, 9, 1645-1659
http://www.scirp.org/journal/jmp
ISSN Online: 2153-120X
ISSN Print: 2153-1196

Theoretical Perspectives of Spin Dynamics in Solid-State Nuclear Magnetic Resonance and Physics

Eugene Stephane Mananga[1,2,3]

[1]The Graduate Center, The City University of New York, New York, USA
[2]Department of Applied Physics, New York University, New York, USA
[3]Department of Engineering, Physics, and Technology, BCC, The City University of New York, New York, USA
Email: esm041@mail.harvard.edu, emananga@gradcenter.cuny.edu

How to cite this paper: Mananga, E.S. (2018) Theoretical Perspectives of Spin Dynamics in Solid-State Nuclear Magnetic Resonance and Physics. *Journal of Modern Physics*, **9**, 1645-1659.
https://doi.org/10.4236/jmp.2018.98103

Received: May 23, 2018
Accepted: July 23, 2018
Published: July 26, 2018

Copyright © 2018 by author and Scientific Research Publishing Inc.
This work is licensed under the Creative Commons Attribution International License (CC BY 4.0).
http://creativecommons.org/licenses/by/4.0/

Open Access

Abstract

Since the first demonstrations of nuclear magnetic resonance (NMR) in condensed matter in 1946, the field of NMR has yielded a continuous flow of conceptual advances and methodological innovations that continues today. Much progress has been made in the utilization of solid-state NMR to illuminate molecular structure and dynamics in systems not controllable by any other way. NMR deals with time-dependent perturbations of nuclear spin systems and solving the time-dependent Schrodinger equation is a central problem in quantum physics in general and solid-state NMR in particular. This theoretical perspective outlines the methods used to treat theoretical problems in solid-state NMR as well as the recent theoretical development of spin dynamics in NMR and physics. The purpose of this review is to unravel the versatility of theories in solid-state NMR and to present the recent theoretical developments of spin dynamics.

Keywords

Solid-state NMR, Hamiltonian Theory, Floquet Theory, Floquet-Magnus Expansion, Fer Expansion

1. Introduction

As front-line theories to control spin dynamics in solid-state nuclear magnetic resonance, the average Hamiltonian theory (AHT) and Floquet theory (FLT) have assumed great prominence and influence since the development of multiple pulse sequences and the inception of magic-angle spinning (MAS) methods in

the 1960s [1] [2] [3] [4] [5]. The first endeavor in NMR to tackle with time-dependent Hamiltonians was built on the Magnus expansion that generated in AHT [6]-[12]. The AHT formalism describes how periodic pulse sequences can be used to control or transform the symmetry of selected interactions in coupled, many-spin systems, enabling the creation of effective Hamiltonians with fascinating and useful properties. From its natural formulation, this is the most widely used approach which has been applied to almost every kind of situation, sometimes abusively [13] [14] [15] [16] [17].

Floquet theory dissimilar to AHT, is not restricted to stroboscopic observation, yield a more universal approach for the description of the full time dependence of the response of a periodically time-dependent system [18] [19] [20] [21] [22] [23]. Methods developed over the past decade have enabled us to make a significant progress in the area of solid-state NMR by introducing an alternative expansion scheme called Floquet-Magnus expansion (FME) used to solve the time-dependent Schrodinger equation which is a central problem in quantum physics in general and solid-state NMR in particular [9] [11] [24]. The FME establish the connection between the ME and the Floquet theory, and provides a new version of the ME well suited for the Floquet theory for linear ordinary differential equations with periodic coefficients [9] [11] [24] [25] [26] [27]. We have proved that the ME is a particular case of the FME which yields new aspects not present in ME and Floquet theory such as recursive expansion scheme in Hilbert space that can facilitate the implementation of new or improvement of existing pulse sequences [24] [28]. In the same vein, Madhu and Kurur have recently introduced the Fer expansion (FE) in Solid-State NMR [29] [30]. The Fer expansion was formulated by Fer and later revised by Fer [29], Klarsfeld and Oteo [31], Casas *et al.* [32], and Blanes *et al.* [33]. This expansion employs the form of a product of sub-propagators, which appears to be suitable for examination of time-dependence of the density matrix for each average Hamiltonian at different orders. Some papers which outline the comparison of both theories (FME and FE) in NMR and physics were recently published in the solid-state NMR, chemical physics, and physics [34] [35].

2. In the Beginning

Historical overview of the first observations of NMR: Normally, credit for NMR first observation should go to Rabi and co-workers in 1939 who used a beam of silver atoms [36]. The noticeable change in the fluxes of beams representing the different energy states of the nuclear magnetic moments was the detection of transitions. However, the term NMR has come to be used as a convention for experiments, which differ from those of Rabi. The experiments set by the convention in respect of NMR are those through the detection of the transitions with the energy absorbed from the RF field rather than through changes in the particle flux reaching a detector as in the beam experiments. Next, the term NMR is commonly reserved for phenomena occurring in bulk matter rather

than in a beam of essentially non-interacting atoms. As a result of these two important conventions, the first observations of NMR are attributed to two independent groups: Purcell, Torrey and Pound, working on the east coast of America and Bloch, Hansen and Packard working on the west coast. They published their discoveries almost simultaneously in the same volume of Physical Review in 1946 [37] [38] [39]. The following is the list of Nobel Price laureates awarded in NMR:

- Otto Stern, USA: Nobel Prize in Physics 1943, "*for his contribution to the development of molecular ray method and his discovery of the magnetic moment of the proton*".
- Isidor I. Rabi, USA: Nobel Prize in Physics 1944, "*for his resonance method for recording the magnetic properties of atomic nuclei*".
- Felix Bloch, USA and Edward M. Purcell, USA: Nobel Prize in Physics 1952, "*for their discovery of new methods for nuclear magnetic precision measurements and discoveries in connection therewith*".
- Richard R. Ernst, Switzerland: Nobel Prize in Chemistry 1991, "*for his contributions to the development of the methodology of high resolution nuclear magnetic resonance (NMR) spectroscopy*".
- Kurt Wüthrich, Switzerland: Nobel Prize in Chemistry 2002, "*for his development of nuclear magnetic resonance spectroscopy for determining the three-dimensional structure of biological macromolecules in solution*".
- Paul C. Lauterbur, USA and Peter Mansfield, United Kingdom: Nobel Prize in Physiology or Medicine 2003, "*for their discoveries concerning magnetic resonance imaging*".

An important landmark to describe the effect of time-dependent interactions and the accompanying improvements was the introduction of average Hamiltonian theory in solid-state NMR. Since its formal inception in 1968 by John Waugh, the average Hamiltonian theory has become the main tool to study the dynamics of spin systems subject to an RF perturbation and the most popular theoretical method in NMR. Its popularity stems from its excellently simple conceptual structure and computational elegance. AHT is a mathematical formalism that allows us to analyze how pulse sequences affect internal spin interactions. The rise of AHT in solid-state NMR began with the time-reversal experiments in dipolar-coupled spin systems [40]. Rhim and co-workers applieda suitable sequence of strong rf fields to a system of dipolar-coupled nuclear spins which was made to behave as though the sign of the dipolar Hamiltonian had been reversed. The system then appears to develop backward in time, and states of non-equilibrium magnetization can be recovered in systems which would superficially appear to have decayed to equilibrium. This behavior is consistent with dynamical and the rmodynamical principles, but shows that the spin-temperature hypothesis must be employed with caution [41] [42] [43]. The AHT is the most commonly used method to treat theoretical problems in solid-state NMR and have been used sometimes casually [17] [44]. As shown in **Figure 1**, the AHT method explains the average motion of the spin system, the effects of

multiple-pulse sequences, and the effects of a time-dependent perturbation applied to the system.

The basic understanding of AHT involves considering a time dependent Hamiltonian $H(t)$ governing the spin system evolution, and describing the effective evolution by an average Hamiltonian $\bar{H}$ within a periodic time (T). This is satisfied only if $H(t)$ is periodic (T) and the observation is stroboscopic and synchronized with period (T). Two major expansions (Baker-Cambell-Hausdorff and Magnus) and an exact computation including the diagonalization of the time evolution operator defined the average Hamiltonian. This technique has been widely used in the NMR literature in the development of multiple pulse sequences and in the context of both decoupling and recoupling experiments. AHT is especially convenient in the derivation and analysis of pulse sequences that incorporate a block of rf irradiation that is repeated many times. The AHT set the stage for stroboscopic manipulations of spins and spin interactions by radio-frequency pulses and also explains how periodic pulses can be used to transform the symmetry of selected interactions in coupled, many-spin systems considering the average or effective Hamiltonian of the RF pulse train [21]. Today, AHT finds itself under increasing pressure of complicated experiments and to adapt to ever more challenging problems. If we are not mindful, under these pressures may submerge the introduction of Floquet theory [18] [20], Floquet-Magnus expansion [24], and Fer expansion in solid-state NMR [30].

3. The Birth of Floquet Theory and Its Introduction to Solid-State NMR

In 1883, M. Gaston Floquet proved a remarkable theorem that asserts the existence of a periodic unitary transformation that maps a system of normal differential equations with periodic coefficients into a system of differential equations with constant coefficients [2]. A well-known example of such a procedure is the passage to a rotating reference frame (RRF) in the study of a system with dipole-dipole interactions in a constant magnetic field and in a circularly polarized magnetic field. The Floquet theorem allows writing the solution of the Liouville evolution equation. Unfortunately, besides for the example with a RRF, the

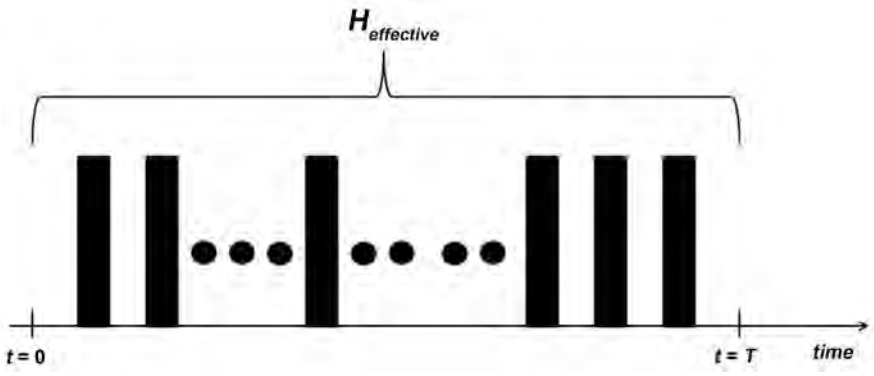

Figure 1. Basic Picture of average Hamiltonian theory.

Floquet Hamiltonian for multi-spin systems cannot be calculated exactly, and approximate methods such as AHT should therefore be used [12]. The Floquet formalism approach for solving the Schrödinger equation with a Hamiltonian representing periodically time-dependent interactions was introduced to spectroscopy by Shirley in 1965 [3]. Shirley replaced the Hilbert space finite-dimensional time-dependent Hamiltonian by an infinite-dimensional time-independent Floquet Hamiltonian HF and showed how it can be used to obtain an exact solution to the LvN equation [19] [21] [22] [23] [24] [25]. Such an approach is often convenient, in particular, for describing solid-state NMR experiments, where the Hamiltonian becomes time dependent due to external manipulations such as MAS and/or periodic RF pulse trains. Shirley's Floquet formalism is also used in atomic and molecular spectroscopy methods [25]. The effective Hamiltonian derived using Floquet theory can be obtained in various ways. The most accurate way is to exactly diagonalise the Floquet Hamiltonian and transfer its diagonal form to the Hilbert space, taking into account the diagonalisation matrix. However, full diagonalisation can become very cumbersome and is rarely required. In most cases perturbation theory on HF can be applied, as done by Vega [20] [21]. Block diagonalisation methods, such as the van Vleck transformation, are extremely powerful in this case [17]. The resulting operator form of the effective Hamiltonian can then be used to design and evaluate the performance of NMR experiments. Solid-state NMR experiments are subjected to various time dependent perturbations of different frequencies, such as RF pulse schemes and MAS. We classify Hamiltonians into single mode, bimodal, and multimode depending on the number of distinct frequencies of perturbations to which the spin system is subjected [21]. Shirley's solution to the Schrödinger equation is also valid when the Hamiltonian is modulated by more than one periodic process [3]. Thus, Floquet theory provides a general description of many NMR experiments without placing any assumptions on the time scales of the perturbations.

4. The Birth of Floquet-Magnus Expansion and Its Introduction to Solid-State NMR

The Floquet-Magnus expansion was developed nearly a decade and half ago by Casas, Oteo, and Ros [11]. This approach is a new version of Magnus expansion well suited for Floquet theory of linear ordinary differential equations with periodic coefficients. Recently, the FME has been employed frequently for the treatment of quantum Floquet systems which open new possibilities to control quantum systems under periodic driving such as in quantum transport and quantum topological phases. The FME is a useful tool to treat a periodically driven system when the period T of the driving is very small. This approach is practically useful for the high-frequency driving, in which the higher-order contribution is not relevant to dynamics at short time scale. However, in the case of finite frequencies, the problem is more complicated since, in general, the FME is not convergent series expansion in the thermodynamic limit. More discussions on

the physical meaning of the FME can be found in the literature. The connection between the Magnus expansion and the Floquet theory was established in the FME [24]. The FME approach is an alternative approach recently developed by Casas and co-workers to solve time-dependent linear differential equation which is a central problem in quantum physics in general and solid-state nuclear magnetic resonance (SSNMR) in particular [24]. The authors Casas, Oteo, and Ros build up a recursive scheme to obtain the terms in the new expansion and give an explicit sufficient condition for its convergence. The method and formulae were applied to an illustrative example from nuclear magnetic resonance, quantum mechanics, and physics [11]. When making the connection between the time-ordered products and the Magnus expansion, Oteo and Ros mentioned that the initial value problem originated from the linear homogeneous ordinary differential equation (LHODE) of first order [45]. The LHODE plays a pervasive role in many branches of mathematics, physics, and engineering with a wide range of different mathematical and physical meanings for the variable involved. Theoretical problems in solid-state NMR are widely treated with the average Hamiltonian theory and the Floquet theory. A variety of magnetic resonance phenomena has been described using both theories (AHT and FLT). These theories have been successful for designing sophisticated pulse sequences and understanding of different experiments. For instance, recently, the AHT has been used to develop a set of selection rules based on the symmetry of the internal interactions and Euler angles in order to simplify the design of NMR multiple-pulse sequences in the presence of sample rotation. This allows the development of recoupling and decoupling sequences as well as many other experiments. The selection rules reveal which types of interactions can be recoupled by a sequence with a given symmetry. Similarly, the FLT has been used to describe multiphoton effects in NMR, electron paramagnetic resonance, and nuclear quadrupole resonance. The fusion of AHT and FLT is generalized by the Floquet-Magnus expansion [1] [9] [24] [46] [47] [48] [49] [50]. The FME has been recently applied to various problems in solid-state NMR and Physics [51] [52] [53] [54] [55].

5. The Birth of Fer Expansion and Its Introduction to Solid-State NMR

The intuitive origins of Fer expansion date in the seminal 1958 Fer paper [29]. The FE approach is based on a factorization of the evolution operator as an infinite product of exponentials of Lie operators and thus exactly preserves the Poincaré integral invariants. This approach is an alternative expansion method to solving time-dependent linear differential equations. As already mentioned above, the FE was formulated by Fer and later revisited by Fer, Klarsfeld and Oteo, Casas *et al.*, and Blanes *et al.* [29] [30] [31] [32] [33]. These authors illustrated some of the salient features of Fer expansion, and applied the method to simple cases such as a driven Harmonic oscillator, two-level system, and a gene-

ralized simple harmonic oscillator. The FE approach was introduced recently to the NMR community by Madhu and Kurur via the effect of Bloch-Siegert shift and heteronuclear dipolar decoupling [30]. Unlike in Magnus expansion where an evaluation of nested commutators and their integrals are required to obtain the correction terms of a Hamiltonian, in Fer expansion only an evaluation of nested commutators is required [30]. As discussed in the next section, the convergence of Fer expansion is much faster than that of Magnus expansion, which lead to the calculation of the infinite number of commutators to be simple in most expereiments [30]. Indeed, from the point of view of physical applications, the Magnus expansion has been extensively used in a variety of issues, while the Fer expansion has been either ignored or misquoted until recently [35]. Both approaches are by no means equivalent, since, in general, the exponential operators do not commute with each other [25] [35]. The FE approach is still in its infancy in solid-state NMR and can be considered to be complimentary to the Magnus expansion (AHT) [34]. While the efficiency of Fer expansion seems obvious, more work is still required to allow the scheme to overcome difficulties such as cases involving non-periodic and non-cyclic cases [30].

6. Convergence

Setting an infinite sequence $\cdots(u_1, u_2, u_3, \cdots)$, the n^{th} partial sum σ_n is the sum of the first n terms of the sequence,

$$\sigma_n = \sum_{l=1}^{n} u_l \tag{1}$$

A series is convergent if the sequence of its partial sums $\{\sigma_1, \sigma_2, \sigma_3, \cdots\}$ become closer and closer to a given number when the number of their terms increases. Mathematically speaking, a series converges, if there exists a number p such that for any arbitrarily small positive number ξ there is a large integer Nsuch that for all $n \geq N$

$$|\sigma_n - p| \leq \xi \tag{2}$$

If the series is convergent, the unique number p is called the sum of the series. The Magnus and some of its equivalent such as Fer expansions have been applied to a wide range of problems in time-dependent quantum mechanics. Exponential time-dependent perturbation theories such as the Magnus expansion or Fer expansion, have proven useful in the treatment of a variety of problems in non-relativistic quantum dynamics. Until in the 1980's, very little was known about the convergence of exponential perturbation theory. In the original version, Magnus stated its convergence criterion in terms of the eigenvalues of the exponent itself. However, several groups have reported that application of the Magnus expansion in the Schrodinger representation to some problems of spectroscopy interest gave results which were less adequate [56]-[70]. Convergence of the Magnus expansion has also come into question in different applications. In general, the Magnus series does not converge unless the Hamiltonian is

small in a suitable sense. Magnus expansion permits significantly simplifying the analysis of the behavior of spin systems in periodic external fields. However, divergence of the Magnus expansion guides to inconsistencies in the spin dynamics of solid-state NMR [8] [56]-[61]. Indeed, the convergence of the Magnus expansion is generally discussed in terms of a radius of convergence r_c. Several results on the radius of convergence r_c in terms of the Hamiltonian have been obtained in the literature. Pechukas and Light and Karasev and Mosolova obtained a radius $r_c = \log 2 = 0.693\cdots$ [62] [63], whereas Chacon and Fomenko [64] got a radius $r_c = 0.577$. Blanes *et al.* obtained the improved bound radius of $r_c = 1.086$ [65]. Recently, a new method was developed to enlarge the largest domain of convergence of the Magnus expansion ($r_c = 1.086\cdots$) previously obtained [66]. An analytic estimate of the new domain of convergence found was almost twice the preceding one ($r_c = 2$) and this new analytic bound was in agreement with the numerical estimate of the convergence radius such as no accuracy was lost in the bound [67]. Therefore, there are more than three different convergence estimated in the literature of Magnus expansion. These convergence estimates are given with their respective proofs in the references therein. The latest improved bound $r_c = \pi$ was derived by Moan but in the context of the conventional Magnus expansion for real matrices [68]. This important results was then generalized to matrices in the Hilbert space (thus for complex matrices) by Casas [69]. A new version of Magnus expansion was reported recently by Butcher *et al.* [70]. The new scheme grows on *trees and forests* to reorder the terms of Magnus expansion for more efficient computation. While this scheme did not provide any substantial new result to the convergence of the ME, it provides a new mean to compute Magnus expansion to the desired order. This ME-type formalism has been developed in a more abstract setting of dendriform algebras. This form shows that the reordering of the terms in Magnus' expansion may be represented graphically using trees and forests, which may be collected into groups according to the order in time for which the solution is valid.

Recoupling schemes have all been extensively treated with Floquet theory in-conjunction with the Van Vleck Transformation [17] [21] [23] [71]. The Floquet theory approach has also been used successfully to the study of decoupling of dipolar interactions. The discussion of the convergence of the Floquet theory was presented by Maricq [18]. Maricq first shows the convergence of the effective Hamiltonian in the mathematical sense. Next he elucidated by example, the conditions which must be satisfied in order to truncate the series for P(t) and H_F after the first few terms. The appropriateness of the FME and FE are well related to the problem of convergence. This problem has played a pivotal role in the field of solid-state NMR and spin dynamics [8] [12] [25] [35]. FME and FE are divergent approaches and the physical nature of their divergences is discussed in the following paragraphs. The authors Casas, Oteo, and Ros investigated a sufficient condition for the absolute convergence of the FME in ref. [11], Blanes and co-workers studied succinctly the convergence of the Fer expansion by looking for conditions on the time dependent Hamiltonian [33]. The authors derived a

convergent radius of the Fer expansion to be 0.8604065 and point out that, additional properties of the time dependent Hamiltonian allow an improvement of the result to extend the range of the radius originally given by Fer who used a slightly different argument [29]. In a similar vein, Zanna showed that a similar result holds for the symmetric Fer expansion by proving that the symmetric Fer expansion converges uniformly in the periodic interval [72].

This calculated radius, $\xi = 0.60275$, of the convergence of the symmetric Fer expansion by Zanna is smaller than the calculated radius for the classical Fer expansion [72], $\xi = 0.8604065$, by Blanes [33]. However, the bounds initiated by Zanna are not optimal and could be improved [72]. An important point of the FME approach is that the rate of convergence of the FME is faster than the Fer expansion in the sense that, for a prescribed precision, one needs more $F_k's$ (for Fer expansion) than $\Lambda_k's$ (for Floquet-Magnus expansion) even if from the computational point of view, the Fer expansion could require more work than the FME. The convergence of these approaches is extensively discussed in the literature [8] [11] [18] [24] [25] [35] [58] [59] [60] [65] [72].

7. Applications of FME and FE in Physics

Using the FME and FE approaches, many problems can be attacked in other fields of physics beyond the scope of NMR. It is important to remember that these considered methods have recently found new major areas of applications such as topological materials [73]. However, researchers dealing with these new applications are not usually acquainted with the achievements of the magnetic resonance theory, where those methods were developed more than thirty years ago [74] [75]. Researchers repeat the same mistakes that were made when the methods of spin dynamics and thermodynamics were developed in the past. Even though the FME is a divergent approach in general, its finite truncation can give useful information such as on the transient dynamics in periodically driven many-body quantum systems [73] [74]. Currently, the use of FME to obtain the effective Hamiltonians for periodically driven systems is a hot topic in the investigation of dynamics of classical and quantum systems. Recently, Kuwahara and co-workers showed that the finite truncation of the FME can give useful information on the transient dynamics [85]. The authors gave a rigorous relationship between the FME and general properties of transient quantum dynamics. New avenues of exploring FME and FE can also be extended to other areas of physics such as particles and high energy physics [25] [35]. These two approaches (FME and FE) can be used to solve problems in quantum field theory (QFT) and high energy physics, in particular problems similar to the one solved or fail to be solved by ME. For instance,

1) the ME has been used as an alternative to conventional perturbation theory for quantum fields to graph rules for functions of the time-evolution operator where normal products and Wick theorem were used. This was useful in the treatment of infrared divergences for some quantum electrodynamics process

such as the scattering of an electron on an external potential or the bremsstrahlung of one hard photon [76] [77]. I believe that effective method of approaching this problem demands more inspection where FME and FE can play a major role;

2) an extension of the ME has been applied to the context of Connes-Kreimer's Hopf algebra approach to perturbative renormalization of quantum field theory showing that the generalized MEallows to solve the Bogoliubov-Atkinson recursion [78] [79] [80]. The FME and FE can also be applied in this context;

3) in the field of high energy physics, ME has also found applications such as to heavy ion collisions. ME is applied in collision problems when the use of unitary approximation scheme is necessary such as the unitary of the time evolution operator imposing some bound on the experimentally observable cross sections [80] [81]. FME and FE can also be used in this context as an intuitive method for simplifying calculations;

4) the problem in neutron oscillations which is closely related to solar neutrino problem. As neutrinos with different masses propagate with different velocities, the mixing allows for flavor conversion corresponding to neutrinos oscillations [82] [83] [84]. Fer's factorization as a symplectic integrator can, in principle, enter in the solution of the evolution operator in one basis.

The introduction of FME and FE as theoretical approaches to control the spin dynamics in the field of nuclear magnetic resonance are new exploratory and developmental researches which is a significant addition to the existing theoretical framework of AHT and FT. QFT is the basic mathematical language used to describe and analyze the physics of elementary particles. The theory by itself is an abstract representation for constructing quantum mechanics models of subatomic particles in particle physics and quasiparticles in condensed matter physics. The application of the FME and FE approaches as intuitive approaches in simplifying calculations to solve some specifics problems in the field of high energy physics and QFT such as those outlined in the above paragraph is of major interest. It is worth noting that, the FME has the advantage of having the unitary character of the evolution operator which is preserved at all orders of approximation while the FE has an advantage over the ME that only an evaluation of nested commutators is required in the calculation of the Hamiltonian [25] [35].

8. Conclusion

To summarize, our descriptions for all four theories suggest that the Fer expansion is advantageous over the other three theories (AHT, FLT, and FME) in calculation of higher-order corrections. As explained above, while the AHT and FLT are common in solid-state NMR, both the FME and Fer expansion are relatively newcomer although the mathematical formalism has been known for several decades [85]. One of the most salient features of the Fer expansion is that

the first fifth-order average Hamitonians are sufficient to control an NMR experiment, and they are included in the first correction of the Fer expansion [86].

Acknowledgements

The author thank the CUNY Office Assistant Oana Teodorescu for reading and for editing the manuscript. He acknowledges the support from the CUNY GRANT CCRG# 1517 and the CUNY RESEARCH SCHOLAR PROGRAM-2017-2018. He also acknowledges the mentee's student Francesca Serrano for helping in editing the manuscript. The contents of this paper are solely the responsibility of the author and do not represent the official views of the NIH.

Conflict of Interest

The author declares that there is no conflict of interest regarding the publication of this paper.

References

[1] Haeberlen, U. and Waugh, J.S. (1968) *Physical Review*, **175**, 453-467. https://doi.org/10.1103/PhysRev.175.453

[2] Floquet, M.G. (1883) *Annales Scientifiques de l'Ecole Normale Superieure*, **12**, 47-88. https://doi.org/10.24033/asens.220

[3] Shirley, J.H. (1965) *Physical Review B*, **138**, 979-987. https://doi.org/10.1103/PhysRev.138.B979

[4] Andrew, E.R., Bradbury, A. and Eades, R.G. (1958) *Nature*, **182**, 1659. https://doi.org/10.1038/1821659a0

[5] Lowe, I.J. (1959) *Physical Review Letters*, **2**, 285-287. https://doi.org/10.1103/PhysRevLett.2.285

[6] Evans, W. (1968) *Annals of Physics*, **48**, 72-93. https://doi.org/10.1016/0003-4916(68)90270-4

[7] Haeberlen, U. (1976) High Resolution NMR in Solids. Advances in Magnetic Resonance, Supplement 1, Academic Press, New York.

[8] Feldman, E.B. (1984) *Physical Letters A*, **104**, 479-481. https://doi.org/10.1016/0375-9601(84)90027-6

[9] Blanes, S., Casas, F., Oteo, J.A. and Ros, J. (2009) *Physics Reports*, **470**, 151-238. https://doi.org/10.1016/j.physrep.2008.11.001

[10] Magnus, W. (1954) *Communications Pure Applied Mathematics*, **VII**, 649-673. https://doi.org/10.1002/cpa.3160070404

[11] Casas, F., Oteo, J.A. and Ros, J. (2001) *Journal of Physics A*: *Mathematical and General*, **34**, 3379-3388. https://doi.org/10.1088/0305-4470/34/16/305

[12] Kuznetsova, E.I., Feldman, E.B. and Feldman, D.E. (2016) *Physics Uspekhi*, **59**, 577-582. https://doi.org/10.3367/UFNe.2016.02.037753

[13] Vandersypen, L.M.K. and Chuang, I.L. (2004) *Review of Modern Physics*, **76**, 1037-1069. https://doi.org/10.1103/RevModPhys.76.1037

[14] Mananga, E.S., Rumala, Y.S. and Boutis, G.S. (2006) *Journal of Magnetic Resonance*, **181**, 296-303. https://doi.org/10.1016/j.jmr.2006.05.015

[15] Mananga, E.S., Roopchand, R., Rumala, Y.S. and Boutis, G.S. (2007) *Journal of*

Magnetic Resonance, **185**, 28-37. https://doi.org/10.1016/j.jmr.2006.10.016

[16] Mananga, E.S., Hsu, C.D., Ishmael Islam, S.T. and Boutis, G.S. (2008) *Journal of Magnetic Resonance*, **193**, 10-22. https://doi.org/10.1016/j.jmr.2008.03.014

[17] Goldman, M., Grandinetti, P.J., Llor, A., Olejniczak, Z., Sachleben, J.R. and Zwanziger, J.W. (1992) *Journal of Chemical Physics*, **97**, 8947-8960. https://doi.org/10.1063/1.463321

[18] Maricq, M.M. (1982) *Physical Review B*, **25**, 6622. https://doi.org/10.1103/PhysRevB.25.6622

[19] Levante, T.O., Baldus, M., Meier, B.H. and Ernst, R.R. (1995) *Molecular Physics*, **86**, 1195-1212. https://doi.org/10.1080/00268979500102671

[20] Vega, S., Olejniczak, E.T. and Griffin, R.G. (1984) *Journal of Chemical Physics*, **80**, 4832-4840. https://doi.org/10.1063/1.446504

[21] Leskes, M., Madhu, P.K. and Vega, S. (2010) *Progress in Nuclear Magnetic Resonance Spectroscopy*, **57**, 345-380. https://doi.org/10.1016/j.pnmrs.2010.06.002

[22] Scholz, I., Meier, B.H. and Ernst, M. (2007) *Journal of Chemical Physics*, **127**, Article ID: 204504. https://doi.org/10.1063/1.2800319

[23] Scholz, I., Van Beek, J.D. and Ernst, M. (2010) *Solid State Nuclear Magnetic Resonance*, **37**, 39-59. https://doi.org/10.1016/j.ssnmr.2010.04.003

[24] Mananga, E.S. and Charpentier, T. (2011) *Journal of Chemical Physics*, **135**, Article ID: 044109. https://doi.org/10.1063/1.3610943

[25] Mananga, E.S. and Charpentier, T. (2016) *Physics Reports*, **609**, 1-49. https://doi.org/10.1016/j.physrep.2015.10.005

[26] Provotorov, B.N. and Fel'dman, E.B. (1980) *Journal of Experimental and Theoretical Physics*, **52**, 1116-1122.

[27] Fel'dman, E.B., Hitrin, A.K. and Provotorov, B.N. (1983) *Physics Letters A*, **99**, 114-116. https://doi.org/10.1016/0375-9601(83)90938-6

[28] Mananga, E.S., Reid, A.E. and Charpentier, T. (2012) *Solid State Nuclear Magnetic Resonance*, **41**, 32-47. https://doi.org/10.1016/j.ssnmr.2011.11.004

[29] Fer, F. (1958) *Bulletin de la Classe des Sciences*, **44**, 818-829.

[30] Madhu, P.K. and Kurur, N.D. (2006) *Chemical Physics Letters*, **418**, 235-238. https://doi.org/10.1016/j.cplett.2005.10.134

[31] Klarsfeld, S. and Oteo, J.A. (1989) *Journal of Physics A*: *Mathematical and General*, **22**, 2687-2694. https://doi.org/10.1088/0305-4470/22/14/019

[32] Casa, F., Oteo, J.A. and Ros, J. (1991) *Journal of Physics A*: *Mathematical and General*, **24**, 4037-4046. https://doi.org/10.1088/0305-4470/24/17/020

[33] Blanes, S., Casas, F., Oteo, J.A. and Ros, J. (1998) *Journal of Physics A*: *Mathematical and General*, **31**, 259-268. https://doi.org/10.1088/0305-4470/31/1/023

[34] Mananga, E.S. (2013) *Solid State Nuclear Magnetic Resonance*, **55-56**, 54-62. https://doi.org/10.1016/j.ssnmr.2013.08.002

[35] Mananga, E.S. (2016) *Physics Reports*, **608**, 1-41. https://doi.org/10.1016/j.physrep.2015.10.006

[36] Rabi, I.I., Millman, S., Kusch, P. and Zacharias, J.R. (1939) *Physical Review*, **55**, 526-535. https://doi.org/10.1103/PhysRev.55.526

[37] Mananga, E.S. (2005) High-Pressure Nuclear Magnetic Resonance Studies of Fuel Cell Membranes. Ph.D. Thesis, The City University of New York, New York.

[38] Purcell, E.M., Torrey, H.C. and Pound, R.V. (1946) *Physical Review*, **69**, 37-38. https://doi.org/10.1103/PhysRev.69.37

[39] Bloch, F., Hansen, W.W. and Packard, M. (1946) *Physical Review*, **70**, 474-485. https://doi.org/10.1103/PhysRev.70.474

[40] Rhim, W.K., Pines, A. and Waugh, J.S. (1971) *Physical Review B*, **3**, 684-695. https://doi.org/10.1103/PhysRevB.3.684

[41] Abragam, A. and Goldman, M. (1982) Nuclear Magnetism: Order and Disorder. Clarendon, Oxford.

[42] Ivanov, Y.N., Provotorov, B.N. and Fel'dman, E.B. (1978) *Journal of Experimental and Theoretical Physics Letters*, **27**, 153-156.

[43] Ivanov, Y.N., Provotorov, B.N. and Fel'dman, E.B. (1978) *Journal of Experimental and Theoretical Physics*, **48**, 930-936.

[44] Mananga, E.S. and Hu, B. (2016) *Journal of Physical Chemistry A*, **120**, 8657-8679. https://doi.org/10.1021/acs.jpca.6b06595

[45] Oteo, J.A. and Ros, J. (2000) *Journal of Mathematics Physics*, **41**, 3268-3277. https://doi.org/10.1063/1.533304

[46] Tycko, R. (2008) *Journal of Chemical Physics*, **128**, Article ID: 052101. https://doi.org/10.1063/1.2833958

[47] Ernst, R.R., Bodenhausen, G. and Wokaun, A. (1987) Principles of Nuclear Magnetic Resonance in One and Two Dimension. Clarendon, Oxford.

[48] Vega, S. and Pines, A. (1977) *Journal of Chemical Physics*, **66**, 5624-5644. https://doi.org/10.1063/1.433884

[49] Zax, D.B., Goelmn, G., Abramovich, D. and Vega, S. (1990) *Advances in Magnetic and Optical Resonance*, **14**, 219-240. https://doi.org/10.1016/B978-0-12-025514-6.50016-2

[50] Abragam, A. (1961) The Principles of Nuclear Magnetism. Clarendon, Oxford.

[51] Mananga, E.S. (2013) *Solid State Nuclear Magnetic Resonance*, **54**, 1-7. https://doi.org/10.1016/j.ssnmr.2013.04.001

[52] Mananga, E.S. (2014) *Journal of Modern Physics*, **5**, 145-148. https://doi.org/10.4236/jmp.2014.54024

[53] Mananga, E.S. and Reid, A.E. (2013) *Molecular Physics*, **111**, 243-257. https://doi.org/10.1080/00268976.2012.718379

[54] Mananga, E.S., Moghaddasi, J., Sana, A., Akinmoladun, A. and Sadoqi, M. (2015) *Journal of Nature and Science*, **1**, e109.

[55] Mananga, E.S. and Charpentier, T. (2015) *Chemical Physics*, **450**-**451**, 83-90. https://doi.org/10.1016/j.chemphys.2015.02.006

[56] Buishvili, L.L., Kobakhidze, G.V. and Menabde, M.G. (1982) *Journal of Experimental and Theoretical Physics*, **56**, 347-349.

[57] Fel'dman, E.B. (1984) *Journal of Experimental and Theoretical Physics Letters*, **39**, 657-659.

[58] Salzman, W.R. (1987) *Physical Review A*, **36**, 5074-5076. https://doi.org/10.1103/PhysRevA.36.5074

[59] Salzman, W.R. (1985) *Journal of Chemical Physics*, **82**, 822-826. https://doi.org/10.1063/1.448508

[60] Salzman, W.R. (1986) *Chemical Physics Letters*, **124**, 531-533. https://doi.org/10.1016/0009-2614(86)85070-9

[61] Llor, A. (1992) *Chemical Physics Letters*, **199**, 383-390. https://doi.org/10.1016/0009-2614(92)80136-Y

[62] Pechukas, P. and Light, J.C. (1966) *Journal of Chemical Physics*, **44**, 3897-3912. https://doi.org/10.1063/1.1726550

[63] Karasev, M.V. and Mosolova, M.V. (1977) *Theoretical Mathematics and Physics*, **28**, 721-730. https://doi.org/10.1007/BF01029029

[64] Chacon, R.V. and Fomenko, A.T. (1991) *Advances in Mathematics*, **88**, 200-257. https://doi.org/10.1016/0001-8708(91)90008-U

[65] Mananga, E.S. (2018) *Physica B: Condensed Matter Physics*, **528**, 47-59. https://doi.org/10.1016/j.physb.2017.10.087

[66] Moan, P.C. and Oteo, J.A. (2001) *Journal of Mathematics Physics*, **42**, 501-508. https://doi.org/10.1063/1.1330198

[67] Blanes, S., Casas, F., Oteo, J.A. and Ros, J. (1998) *Journal of Physics A*: *Mathematical and General*, **31**, 259-268. https://doi.org/10.1088/0305-4470/31/1/023

[68] Moan, P.C. and Niesen, J. (2008) *Foundation of Computations Mathematics*, **8**, 291-301. https://doi.org/10.1007/s10208-007-9010-0

[69] Casas, F. (2007) *Journal of Physics A*: *Mathematical and Theoretical*, **40**, 15001-15017. https://doi.org/10.1088/1751-8113/40/50/006

[70] Butcher, E.A., Sari, M., Bueler, E. and Carlson, T. (2009) *Communications in Nonlinear Science and Numerical Simulation*, **14**, 4226-4245. https://doi.org/10.1016/j.cnsns.2009.02.030

[71] Van Vleck, J.H. (1929) *Physical Review*, **33**, 467-506. https://doi.org/10.1103/PhysRev.33.467

[72] Mananga, E.S. (2014) *Journal of Modern Physics,* **5***,* 458-463. https://doi.org/10.4236/jmp.2014.56055

[73] Mikama, T., Kitamura, S., Yasuda, K., Tsuji, N., Oka, T., *et al.* (2016) *Physical Review B*, **93**, Article ID: 144307.

[74] Eckardt, A. and Anisimovas, E. (2015) *New Journal of Physics*, **17**, Article ID: 093039. https://doi.org/10.1088/1367-2630/17/9/093039

[75] Kuwahara, T., Mori, T. and Saito, K. (2016) *Annals of Physics*, **367**, 96-124. https://doi.org/10.1016/j.aop.2016.01.012

[76] Dahmen, H.D., Mannel, T. and Manakos, P. (1988) *Physical Review D, Part Fields*, **38**, 1176-1182. https://doi.org/10.1103/PhysRevD.38.1176

[77] Dahmen, H.D., Manakos, P., Mannel, T. and Ohl, T. (1991) *Zeitschrift fur Physik C Particles and Fields*, **50**, 75-84.

[78] Connes, A. and Kreimer, D. (2000) *Communication in Mathematical Physics*, **210**, 249-273. https://doi.org/10.1007/s002200050779

[79] Connes, A. and Kreimer, D. (2001) *Communication in Mathematical Physics*, **216**, 215-241. https://doi.org/10.1007/PL00005547

[80] Ebrahimi-Fard, K., Manchon, D. and Patras, F. (2008) *Journal of Algebra*, **320**, 708-727. https://doi.org/10.1016/j.jalgebra.2007.12.013

[81] Ionescu, D.C. (1994) *Physical Review A*, **49**, 3188-3195. https://doi.org/10.1103/PhysRevA.49.3188

[82] DOlivo, J.C. (1992) *Physical Review D*, **45**, 924-930. https://doi.org/10.1103/PhysRevD.45.924

[83] DOlivo, J.C. and Oteo, J.A. (1996) *Physical Review D*, **54**, 1187-1193. https://doi.org/10.1103/PhysRevD.54.1187

[84] Supanitsky, A.D., DOlivo, J.C. and Medina Tanco, G. (2008) *Physical Review D*, **78**, Article ID: 045024. https://doi.org/10.1103/PhysRevD.78.045024

[85] Kuwahara, T., Mori, T. and Saito, K. (2016) *Annals of Physics*, **367**, 96-124. https://doi.org/10.1016/j.aop.2016.01.012

[86] Takegoshi, K., Miyazawa, N., Sharma, K. and Madhu, P.K. (2015) *Journal of Chemical Physics*, **142**, Article ID: 134201. https://doi.org/10.1063/1.4916324

Journal of Modern Physics, 2018, 9, 1660-1689
http://www.scirp.org/journal/jmp
ISSN Online: 2153-120X
ISSN Print: 2153-1196

Entropy Generation through the Interaction of Laminar Boundary-Layer Flows: Sensitivity to Initial Conditions

LaVar King Isaacson

Department of Mechanical Engineering, University of Utah, Salt Lake City, UT, USA
Email: lkisaacson1@mac.com

How to cite this paper: Isaacson, L.K. (2018) Entropy Generation through the Interaction of Laminar Boundary-Layer Flows: Sensitivity to Initial Conditions. *Journal of Modern Physics*, **9**, 1660-1689.
https://doi.org/10.4236/jmp.2018.98104

Received: June 17, 2018
Accepted: July 27, 2018
Published: July 30, 2018

Copyright © 2018 by author and Scientific Research Publishing Inc.
This work is licensed under the Creative Commons Attribution International License (CC BY 4.0).
http://creativecommons.org/licenses/by/4.0/
Open Access

Abstract

A modified form of the Townsend equations for the fluctuating velocity wave vectors is applied to the interaction of a longitudinal vortex with a laminar boundary-layer flow. These three-dimensional equations are cast into a Lorenz-format system of equations for the spectral velocity component solutions. Tsallis-form empirical entropic indices are obtained from the solutions of the modified Lorenz equations. These solutions are sensitive to the initial conditions applied to the time-dependent coupled, non-linear differential equations for the spectral velocity components. Eighteen sets of initial conditions for these solutions are examined. The empirical entropic indices yield corresponding intermittency exponents which then yield the entropy generation rates for each set of initial conditions. The flow environment consists of the flow of hydrogen gas with impurities at a given temperature and pressure in the interaction of a longitudinal vortex with a laminar boundary layer flow. Results are presented that indicate a strong correlation of predicted entropy generation rates and the corresponding applied initial conditions. These initial conditions may be ascribed to the turbulence levels in the boundary layer, thus indicating a source for the subsequent entropy generation rates by the interactive instabilities.

Keywords

Interacting Laminar Boundary Layers, Intermittency Exponents, Entropy Generation Rates

1. Introduction

Results are reported for an innovative computational procedure applied to a study of the sensitivity to initial conditions in the computation of entropy gen-

eration rates generated by the non-linear interaction of a longitudinal vortex with a laminar boundary layer flow. The equations for the fluctuating velocity components in a three-dimensional shear flow have been presented by Townsend [1]. These equations are written in a Lorenz form (Sparrow [2]) and solved for the flow configuration shown in **Figure 1**. The mathematical bases and the corresponding computer program listings employed for these calculations have been discussed previously in Isaacson [3] [4] [5].

The nonlinear, time-series solutions for the spectral velocity wave components are obtained from a modified Lorenz-type set of equations that is sensitive to the initial conditions applied to the integration of the equations. The control parameters for these equations are the steady state boundary layer velocity gradients that are determined by the particular value of the kinematic viscosity for the system. Experimental measurements of the unsteady fluctuation levels in laminar boundary layers when subjected to free stream turbulence have been presented by Walsh and Hernon [6]. These results indicate that the free stream turbulence level has a significant effect on the resulting entropy generation rates in laminar boundary layers. The initial conditions for the integration of the Lorenz-type equations are heuristically assumed to be attenuated levels of the turbulence imposed on the system from the free stream.

However, the initial conditions for the integration of the modified Lorenz equations are the actual turbulent intensity levels applied to the flow system at the specific location within the boundary layer where the computational results are obtained. We have selected eighteen sets of initial conditions for the initial values for the computation of the time development of the spectral stream wise, normal and span wise velocity components.

The boundary-layer environment used in the study reported here is the flow of helium with slight impurities at a temperature of $T = 320.0$ K and a pressure of $p = 1.01325 \times 10^5$ N/m^2 at a normalized boundary-layer vertical location of $\eta = 3.00$. The kinematic viscosity for the helium mixture at these conditions is $\nu = 1.384696 \times 10^{-4}$ m^2/s.

The Falkner-Skan transformation, in the form

$$\eta = \left(\frac{u_e}{\nu x}\right)^{1/2} y \tag{1}$$

provides the definition of the normalized distance, η from the surface of the boundary layer flow. In this expression, u_e is the boundary layer edge velocity, x is the stream wise distance and the edge value for the normalized vertical distance is $\eta_\infty = 8.0$.

This article includes the following sections:

In Section 2, the laminar boundary-layer flow configuration considered in this study is described. In Section 3, eighteen sets of initial conditions for the integration of the time-dependent modified Lorenz equations are presented. Section 4 presents a brief review of the results of the study of the sensitivity of the solutions of the modified Lorenz equations for the entropy generation rates to the

initial conditions. In Section 5, the fluctuation equations of Townsend [1], Isaacson [3] [4] [5], and Hellberg and Orszag [7] are transformed into the spectral plane and written as modified Lorenz equations. Computational results for the time-dependent spectral velocity components are discussed. Section 6 describes the power spectral densities, the introduction of empirical entropies, empirical entropic indices, and intermittency exponents extracted from the numerical results of the computations. Section 7 covers the computation of the entropy generation rates for each of the sets of initial conditions, including a discussion of the strong correlation of these entropy generation rates with the corresponding initial conditions, through the intermittency exponents.

The article closes with a discussion of the results and final conclusions.

2. Boundary-Layer Interaction Environment

The solution of the modified Lorenz equations requires the input of various equation control parameters. The steady state boundary-layer velocity gradients and the time-dependent spectral wave component solutions serve as control parameters for the solution of the time-dependent fluctuating spectral velocity equations. The mathematical and computational methods used for the computation of the x-y plane and the z-y plane steady-state laminar boundary-layer velocity gradients are summarized in this section. The boundary layer steady velocity gradients vary with the stream wise distance x, indicating the initiation of instabilities within the boundary layer for several stream wise stations, similar to the development of a young turbulent spot.

Singer [8] has reported the results of the direct numerical simulation of the effect of strong free stream turbulence on the development of a young turbulent spot in laminar boundary layer flow. These studies indicate the development of a counter-clockwise stream wise vortex that produces a laminar boundary layer in the z-y plane of the flow environment as shown in **Figure 1**. Ersoy and Walker [9] discus the development of this z-y plane boundary layer produced by the interaction of the vortex tangential velocity with the flow surface. Belotserkovskii and Khlopkov [10] have computed the normalized span wise velocity at the outer edge of the vortex structure as $w_e = 0.08$. This is the value we use for the span wise velocity. Schmid and Henningson (pp. 429-436 [11]) discuss the development of streaky structures, longitudinal vortex structures and the eventual development of turbulent spots relative to the intensity levels of the free stream turbulence. These various observations provide a strong motivation to gain a better understanding of the transition of laminar flows to turbulent flows through the study of the effects of the values for the initial conditions applied to the solution of the modified Lorenz equations in the boundary layer flow.

The computer source code listings that we have used to compute the steady laminar boundary layer velocity profiles for both the x-y plane and the z-y plane were developed by Cebeci and Bradshaw [12] and Cebeci and Cousteix [13]. These orthogonal profiles are similar in nature (Hansen [14]) and thus form the

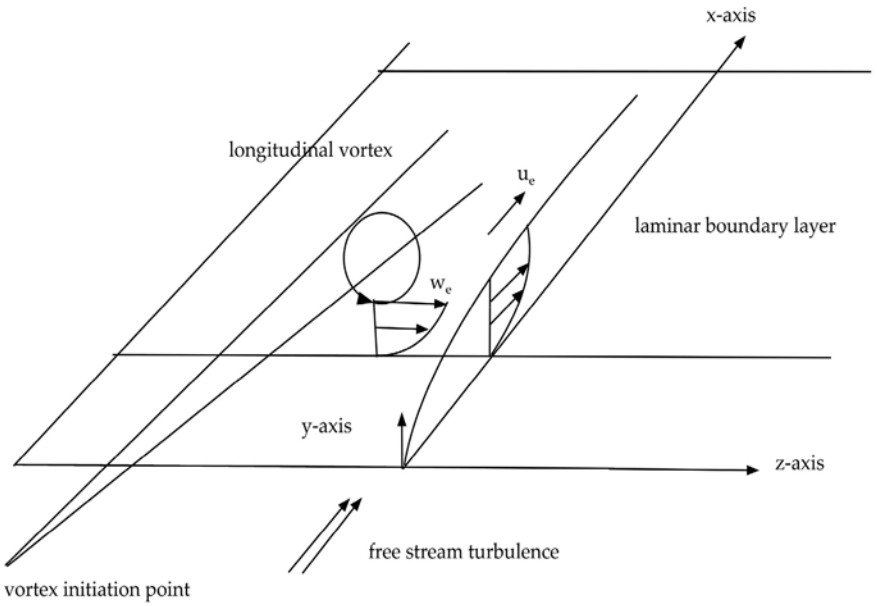

Figure 1. A schematic diagram is shown of the configuration of a longitudinal vortex tangential velocity boundary layer profile in the z-y plane normal to the stream wise boundary layer profile in the x-y plane with free stream turbulence.

steady boundary layer velocity gradient control parameters for the solution of the modified Lorenz equations. The working gas for these studies is a mixture of helium with several impurities, as described in [3], at a temperature of 320.0 K and a pressure of 0.101325 MPa.

The boundary layer profiles are determined at six stream-wise stations, with the first station designated as the transmitter station. The following five stations are designated as receiver stations, with the first receiver station designated as station 1. The results obtained for the entropy generation rates at the receiver station 3, at x = 0.120, as a function of the initial conditions, are presented in depth in this article. A computational flow chart is presented in **Figure 2** for the overall path of the computational procedure. The primary result of this study is the strong correlation of the resultant entropy generation rates with the corresponding applied initial conditions for those rates. This is discussed in the next section.

3. Selection of Initial Conditions

An essential aspect of the computational procedure discussed in this article is the inclusion of the time-dependent, coupled, nonlinear modified Lorenz equations for the prediction of the development of ordered regions within the nonlinear time series solutions. For the studies reported in [3] [4] [5], a single set of initial conditions was used to obtain the reported entropy generation rates. However, solutions of the nonlinear modified Lorenz equations are very sensitive to the initial conditions applied in the calculation of the solutions ({Sparrow [2]). We have computed the entropy generation rates for the flow configuration shown in

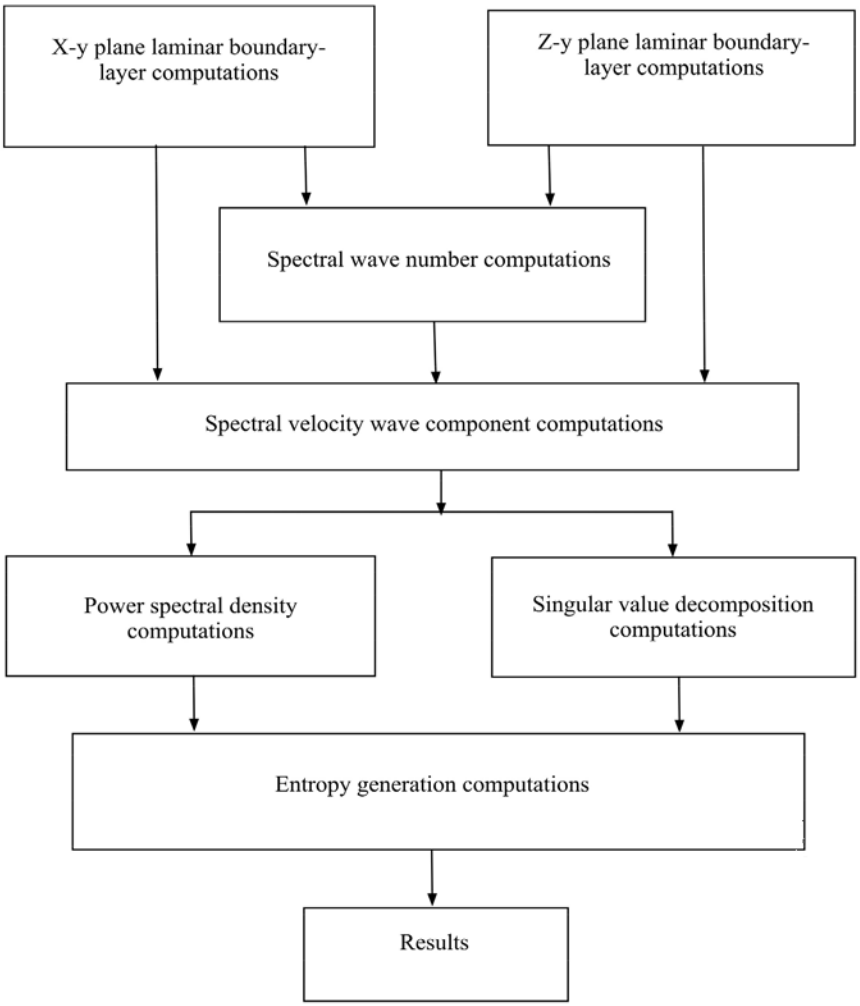

Figure 2. Computational flow chart for the calculation of the entropy generation rates [3].

Figure 1 for a range of initial values for the stream wise spectral velocity wave component from 0.0050 to 0.2000, with the corresponding normal and span wise spectral velocity components at 40 percent of the stream wise initial value. Table 1 shows the values for eighteen sets of initial conditions over this range. Also included in Table 1 are corresponding values of an equivalent turbulence level as defined by Sengupta (pp. 103-105 [15]). Each of these set numbers are shown in Figure 3, for the corresponding entropy generation rates.

4. Entropy Generation Rates: Sensitivity to Initial Conditions

Application of the computational procedure outlined in Figure 2 to the fluctuating velocity components in the three-dimensional flow shown in Figure 1 yields the entropy generation rates that occur through the dissipation of the ordered regions predicted in the nonlinear solutions of the modified Lorenz equations. The solutions of the time-dependent modified Lorenz equations require initial values for each of the three spectral velocity components. The entropy

Table 1. This table provides the initial conditions for the computation of the three spectral velocity components and the corresponding values of the equivalent turbulence level in percent.

Initial conditions, set number	Initial spectral velocity component, a_x [1]	Initial spectral velocity component, a_y [1]	Initial spectral velocity component, a_z [1]	Equivalent turbulence level, percent
1	0.00500	0.000200	0.000200	0.332
2	0.00560	0.002240	0.002240	0.371
3	0.01000	0.004000	0.004000	0.663
4	0.01500	0.006000	0.006000	0.995
5	0.02000	0.008000	0.008000	1.327
6	0.03000	0.012000	0.012000	1.990
7	0.04000	0.016000	0.016000	2.653
8	0.05000	0.020000	0.020000	3.317
9	0.06000	0.024000	0.024000	3.980
10	0.07000	0.028000	0.028000	4.643
11	0.08000	0.032000	0.032000	5.307
12	0.09000	0.036000	0.036000	5.970
13	0.10000	0.040000	0.040000	6.633
14	0.12000	0.048000	0.048000	7.960
15	0.14000	0.056000	0.056000	9.287
16	0.16000	0.064000	0.064000	10.613
17	0.18000	0.072000	0.072000	11.940
18	0.20000	0.080000	0.080000	13.266

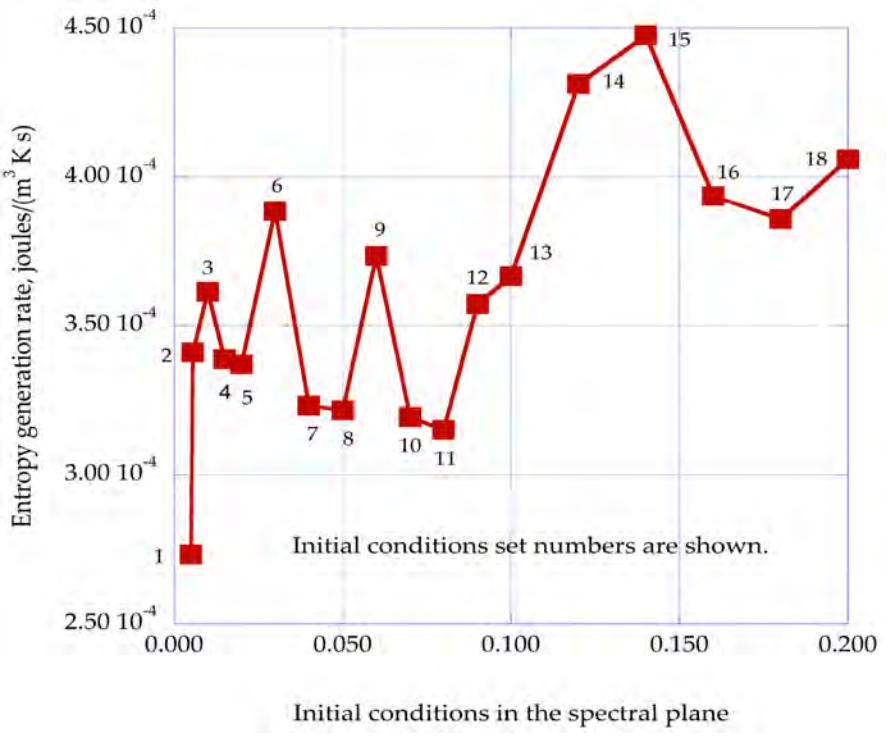

Figure 3. The entropy generation rate as a function of the initial conditions applied to the solution of the modified Lorenz equations, at the stream wise location of $x = 0.120$, the normalized vertical location of $\eta = 3.00$ and the span wise velocity of $w_e = 0.080$.

generation rate for each set of initial conditions shown in Table 1 has been computed for a three-dimensional boundary-layer flow of a helium mixture at a temperature of $T = 320.0$ K and a pressure of $p = 0.101325$ MPa. This temperature and pressure for this mixture provide a kinematic viscosity of $\nu = 1.384696 \times 10^{-4}$ m^2/s. Figure 3 shows the entropy generation rate at the stream wise station $x = 0.120$, for a normalized boundary layer distance of $\eta = 3.00$ [1] for each of the sets of initial conditions listed in Table 1.

These results indicate a strong correlation of the predicted entropy generation rates with the corresponding initial conditions applied to the equations for the time dependent solutions. If the assumption is made that these initial conditions are provided by the attenuated free stream turbulence, these computational methods may then provide a path to understanding *bypass transition*. A detailed explanation of the procedures used in the calculation of these results and a discussion of the possible sources for the indicated entropy generation rates are presented in the next sections.

5. Modified Lorenz Equations in the Time Dependent Spectral Plane

5.1. Transformation of the Townsend Equations to the Modified Lorenz Format

For the flow of a wall shear layer with velocity fluctuations, the computational procedure may be separated into the evaluation of the steady state velocity profiles and a set of equations for the fluctuating velocity field (Townsend [1]). The non-equilibrium spectral equations of Townsend [1] and Hellberg, *et al.* [7] are arranged into a Lorenz format (Sparrow [2]) for the computation of the nonlinear time series solutions for the fluctuating spectral velocity field. The time-dependent spectral equations of Townsend [1] and Hellberg, *et al.* [7] are then solved with the steady state boundary layer velocity profiles as control parameters.

The solutions of the modified Lorenz equations yield the spectral velocity components within the nonlinear time series solutions. Statistical analysis of these spectral time-series solutions yields the power spectral densities and the empirical entropies over a range of sixteen empirical modes. The correspondence of the peaks of the spectral power spectrum and the empirical modes of the singular value decomposition analysis is achieved by invoking the Weiner-Khintchine theorem (Attard (pp. 354-355 [16]). This theorem relates the power density spectrum and the autocorrelation function since both properties are computed from the same nonlinear time series data.

The equations for the velocity fluctuations within a wall shear layer may be written as (Townsend (pp. 46-49 [1])):

$$\frac{\partial u_i}{\partial t} + U_j \frac{\partial u_i}{\partial x_j} + u_j \frac{\partial U_i}{\partial x_j} + u_j \frac{\partial u_i}{\partial x_j} = -\frac{1}{\varrho}\frac{\partial p}{\partial x_i} + \nu \frac{\partial^2 u_i}{\partial x_j \partial x_j}. \tag{2}$$

Fourier transform of these equations yields the equations for the three

time-dependent spectral velocity wave components, $a_i(k)$, as (pp. 47-49 [1]):

$$\frac{\partial a_i(k)}{\partial t} = -\nu k^2 a_i(k) - \frac{\partial U_i}{\partial x_i} a_i(k) + 2\frac{k_i k_l}{k^2}\frac{\partial U_l}{\partial x_m} a_i(k) + i\sum_{k'+k''=k}\left(k_l \frac{k_i k_m}{k^2} - \delta_{im} k_l\right) a_l(k') a_m(k'') \tag{3}$$

The nonlinear coupling terms in the spectral velocity components in Equations (3) are represented in our series of equations by characterizing the transfer matrix

$$k_l\left(\delta_{im} - \frac{k_i k_m}{k^2}\right) \tag{4}$$

as basic to the formation of patterns in nonlinear time series solutions (Manneville (pp. 302-312 [17])). A model equation for this expression in the form

$$\left(1 - K * \cos\left(k(t)\right)\right) \tag{5}$$

is introduced to provide the proper weighting of the transfer matrix (Equation (4) in our computational procedure. K is an empirical amplitude factor [18] and $k(t)$ is given by:

$$k(t) = \sqrt{\left(k_x^2\right)} \tag{6}$$

Substitution of Equation (5) and with $F = K\cos\left(k(t)\right)$, the equations for the spectral velocity components, Equations (3), may be rearranged into Lorenz format as [2] [3]:

$$\frac{\mathrm{d}a_{xn}}{\mathrm{d}t} = \sigma_{yn} a_{yn} - \sigma_{xn} a_{xn}, \tag{7}$$

$$\frac{\mathrm{d}a_{yn}}{\mathrm{d}t} = -(1-F) a_{xn} a_{zn} + r_n a_{xn} - s_n a_{yn}, \tag{8}$$

$$\frac{\mathrm{d}a_{zn}}{\mathrm{d}t} = (1-F) a_{xn} a_{yn} - b_n a_{zn}. \tag{9}$$

The expressions for the coefficients σ_{yn}, σ_{xn}, r_n, s_n, and b_n are given in detail in [3]. These coefficients are functions of the wave number components, k_p, and the steady state values of the velocity gradients in the boundary layer flow, as indicated in Equation (3). These equations are designated as *the modified Lorenz equations*. These equations are solved at the initial station of x_0 = 0.06, considered as the *transmitter station*.

The solutions of these equations at the transmitter station require additional assumptions for the modified Lorenz equations. Manneville (pp. 305-312 [17]) has discussed both the format and justification for the heuristic choice of Expression (5) as the approximate replacement for the basic pattern matrix of Equation (3). This form appears in the fundamental basis for pattern formation in the study of dissipative structures in turbulent flows. Therefore, since we are looking for the formation of ordered regions in solutions of the modified Lorenz equations, the model equation of Expression (5) appears to be a logical choice.

We have found that a value of $K = 0.05$ yields instabilities in the nonlinear time series solutions of the modified Lorenz equations for a normalized boundary layer location of $\eta = 3.00$. Sengupta (pp. 158-165 [15]) reported the excitation of instabilities in wall shear layers with the application of normal wall velocities with a time dependent magnitude of sinusoidal form with a coefficient of approximately 0.05. These experimental results provide a measure of validation for our computationally determined value for the amplitude factor K.

Incorporating Expression (5) in Equation (3), with the definition of the term F, the modified Lorenz equations take the form of Equations (7-9). These equations are solved at the transmitter station for each set of initial conditions listed in **Table 1**. This station provides the initial generation of instabilities in the nonlinear time series solutions of the modified Lorenz equations at the stream wise location of $x_0 = 0.060$.

The following stations at $x_1 = 0.080$, $x_2 = 0.100$, $x_3 = 0.120$, $x_4 = 0.140$, and $x_5 = 0.160$ are designated as receiver stations. From thermodynamic considerations (Attard (pp. 329-331 [16])), for the solutions at the receiver stations, we must take into account that the solutions of the first and subsequent receiver stations will be influenced by the fluctuations produced in the transmitter station and prior receiver stations. The concept of synchronization and the application of the modified Lorenz equations at each of these receiver stations is discussed in the next section.

5.2. Synchronization Properties of the Modified Lorenz Equations

We apply the transformation of the pattern matrix (Equation (5)) to the transmitter station at x = 0.060. The time-series solutions for this station indicate the generation of nonlinear instabilities in each of the spectral velocity components. These instabilities are then transferred to the next station, or first receiver station. The modified Lorenz equations have been shown to have the property of synchronization or extraction of ordered signals from a chaotic signal. We will apply this property to each of the receiver stations in the system.

The synchronization properties of systems of Lorenz-type equations have been shown by Pecora and Carroll [19], Pérez and Cerdeira [20], and Cuomo and Oppenheim [21] to have the capability to extract messages masked by chaotic signals. The modified Lorenz equations are adapted here to exploit these synchronization properties to extract ordered signals from the nonlinear time series solutions generated for each of the spectral components at each of the stream wise receiver stations.

We apply the synchronization properties at each of the receiver stations downstream from the initial transmitter station. The various boundary layer control parameters at each of these stations are computed in the same manner as in the transmitter station. Following the results in [18], the time-dependent output for the x-direction spectral velocity component from the transmitter station is used as input to the nonlinear coupled terms in the modified Lorenz equ-

ations at the next station, which we denote as the first receiver station in the x-direction. Then, the input to the nonlinear-coupled terms at the next downstream receiver station is made up of the sum of the stream wise velocity wave component output from the transmitter station plus the x-direction spectral velocity wave component output from the first receiver station. This process is repeated for each of the five receiver stations. With this method, the memory of the initial velocity fluctuations from the transmitter station and the influence of subsequent fluctuations from the receiver stations are retained in the overall computational procedure.

For each receiver station, n, the system of nonlinear dynamic equations is written as:

$$\frac{\mathrm{d}a_{xn}}{\mathrm{d}t} = \sigma_{yn}a_{yn} - \sigma_{xn}a_{xn}, \tag{10}$$

$$\frac{\mathrm{d}a_{yn}}{\mathrm{d}t} = -a_{rn}a_{zn} + r_n a_{xn} - s_n a_{yn}, \tag{11}$$

$$\frac{\mathrm{d}a_{zn}}{\mathrm{d}t} = a_{rn}a_{yn} - b_n a_{zn}. \tag{12}$$

Note that for the initial station, characterized as the transmitter station, $a_{x0,}$ is the time-dependent spectral velocity wave component output from the transmitter station. The input driving term for the next station, the first receiver station at $x = 0.08$, is then given by a_{x0}, where a_{x0} is the output from the initial or transmitter station at $x = 0.06$.

In Equations (10-12), the input driving signal, $a_{rn,}$ carrying information from the transmitter and the previous receiver stations to the n-th station is given by the sum of the outputs from the transmitter station and the previous n-1 receiver stations:

$$a_{rn} = \sum_{i=0}^{i=n-1} a_{xi}, \quad n = 1,2,3,4,5 \tag{13}$$

The initial conditions for the fluctuating spectral velocity wave vector components for the transmitter station and for each successive receiver station are set equal to the values listed in Table 1. This process determines the result that the outputs from each of the receiver stations will be masked by the original transmitter output signal, and that the synchronization process will yield an indication of the ordered regions within the transmitter signal and the output signal from each of the receiver stations.

5.3. Sensitivity to Initial Conditions

The free stream velocity for the stream wise boundary layer flow is taken as unity, $u_e = 1.00$, while the vortex tangential velocity is $w_e = 0.08$ (pp. 101-102 [10]). The solutions of the steady boundary layer velocity gradient profiles in the x-y plane and the z-y plane at each stream wise station provide the control parameters for the solutions of the modified Lorenz equations at these stations. The solutions of the modified Lorenz equations at the transmitter station yield the

fluctuating spectral velocity wave components for the stream wise location x = 0.060 and the span wise location of z = 0.003. The boundary layer instabilities are observed within the boundary layer at a normalized distance from the horizontal surface of approximately η = 3.0. With the outer edge of the boundary layer at the normalized distanceη_∞ = 8.00, the instabilities occur at 37.5 percent of the boundary layer thickness. The time step for the time-dependent integration process is taken as h = 0.0001 s. Initial values for the spectral wave number equations are taken as k_x [1] = 0.04, k_y [1] = 0.02 and k_z [1] = 0.02. The initial conditions for the wave component solutions are kept at these values for each set of initial conditions for the spectral velocity components indicated in **Table 1**.

The solutions of nonlinear, coupled differential equations, such as the modified Lorenz equations (Equations (7-10) and Equations (10-12)), are sensitive to the particular values of the initial conditions applied in the solutions. **Table 1** presents a range of initial conditions for the solutions of these couple equations from an equivalent free stream turbulence level of 0.332 percent to a level of 13.3 percent. Eighteen different sets of initial values for a_x [1], a_y [1] and a_z [1] are included in the table. Each set of initial conditions is applied to the solution of the modified, Lorenz equations for six stream wise stations. The initial station, at x = 0.06, denoted as the transmitter station, with n = 0 has the stream wise spectral velocity component, denoted as a_{x0}. The following station is denoted as the first receiver station, n = 1, at x = 0.08, with the stream wise spectral velocity component as a_{x1}. The results presented here are the sensitivity to the initial conditions for the entropy generation rates at the receiver station of n = 3, at the stream wise location of x = 0.120. The three spectral velocity components are denoted as a_{x3}, a_{y3} and a_{z3}.

The initial conditions applied to the spectral velocity wave equations must arise from the attenuation of the external free stream turbulence level through the boundary layer flow. Schmid and Henningson (pp. 401-413 11]) and Sengupta (pp. 171-200 [15]) discuss the effect of outside disturbances on laminar boundary layer flows and the subsequent development of various instabilities that may occur in the flow environment. The incorporation of the time dependent spectral wave equations of the Lorenz format in the computational process thus opens the possibility of connecting the concept of boundary layer bypass transition to the subsequent development of ordered regions in the interaction of laminar boundary-layer environments.

5.4. Deterministic Results for the Modified Lorenz Equations

The solutions of the modified Lorenz equations have been obtained for each set of intial conditions listed in **Table 1** for the designated stream wise stations. We have chosen to present graphical results in **Figure 4** for initial conditions Set 8, **Figure 5** for Set 9 and **Figure 6** for Set 10. These results are obtained for a flow temperature of T = 320.0 K and a pressure of p = 0.101325 MPa. **Figure 4** shows the phase diagram for $a_{y3} - a_{x3}$, where a_{y3} is the normal spectral velocity wave

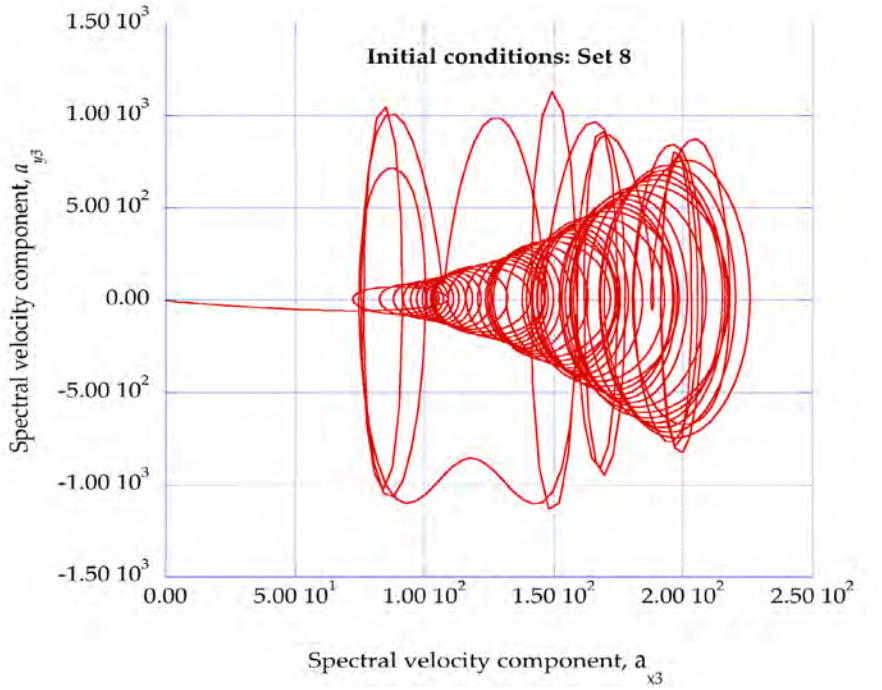

Figure 4. Shown is the normal spectral velocity component, a_{y3}, versus the stream wise spectral velocity component, a_{x3}, for the initial conditions of Set 8 at the stream wise location of $x = 0.120$, the normalized vertical location of $\eta = 3.0$ and the span wise velocity component of $w_e = 0.080$.

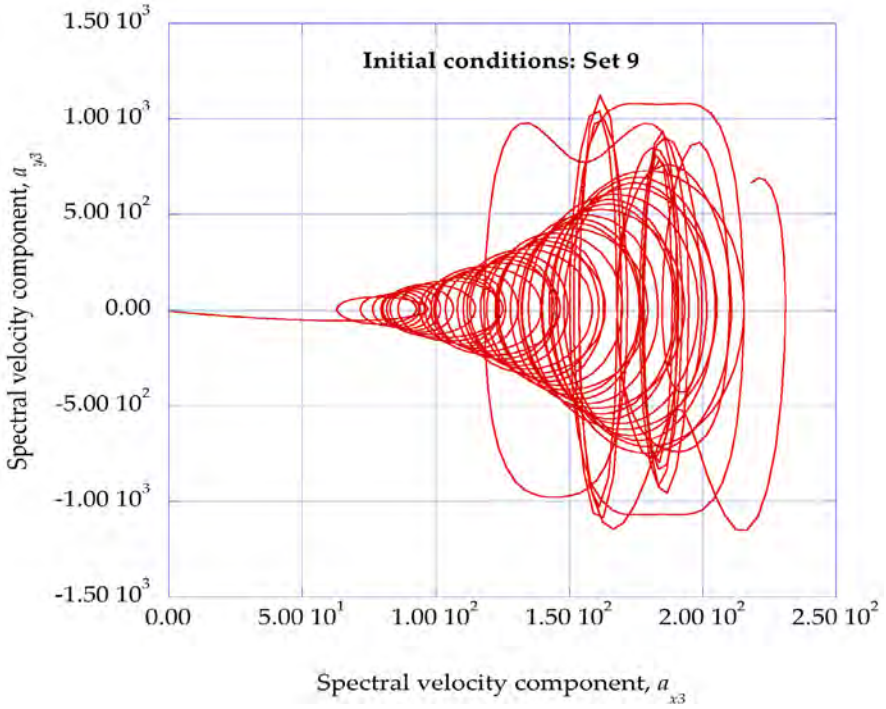

Figure 5. Shown is the normal spectral velocity component, a_{y3}, versus the stream wise spectral velocity component, a_{x3}, for the initial conditions of Set 9 at the stream wise location of $x = 0.120$, the normalized vertical location of $\eta = 3.0$ and the span wise velocity component of $w_e = 0.080$.

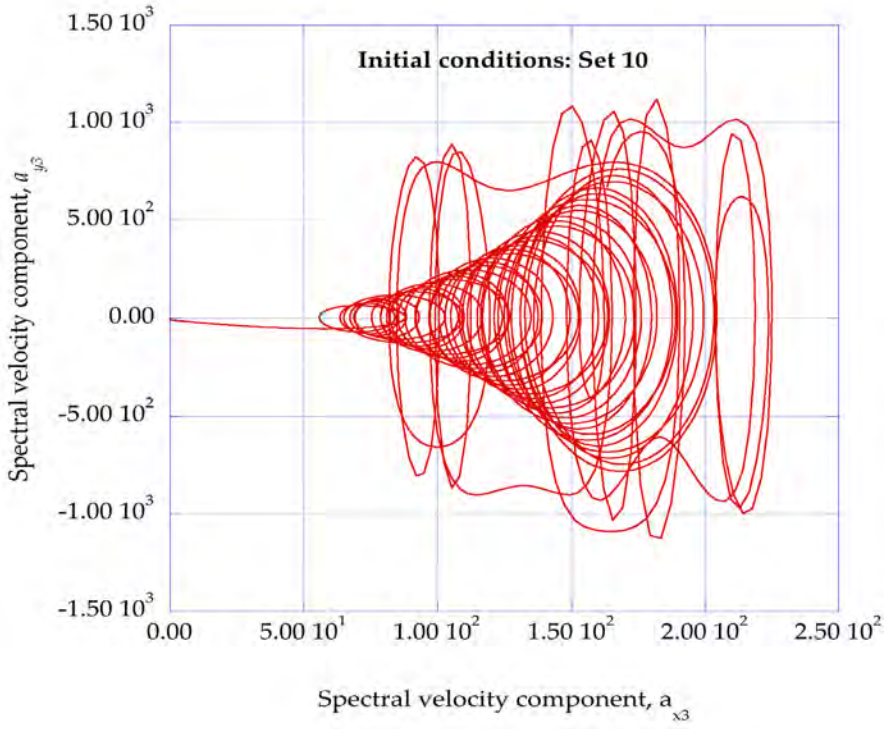

Figure 6. Shown is the normal spectral velocity component, a_{y3}, versus the stream wise spectral velocity component, a_{x3}, for the initial conditions of Set 10 at the stream wise location of $x = 0.120$, the normalized vertical location of $\eta = 3.0$ and the span wise velocity component of $w_e = 0.080$.

component and a_{z3} is the span wise spectral velocity wave component, again at the station $x = 0.120$.

Figure 6 shows the phase diagram for $a_{y3} - a_{z3}$, where a_{z3} is the span wise spectral velocity wave component and a_{y3} is the normal spectral velocity wave component, again at the station $x = 0.120$. These results indicate the formation of an initially strong spiral cone in the stream wise direction, transforming into a strongly oscillating motion in the stream wise, normal and span wise spectral planes of the flow environment.

In **Figure 3**, the entropy generation rates for initial conditions sets, Set 8, Set 9 and Set 10, are shown. The results for Sets 8 and 10 show relatively low values for the generation rates, while Set 9 indicates a spike in the generation rate. **Figure 4** and **Figure 6** indicate that for the relatively low generation rates, the stream wise spectral velocity components decrease in value relative to the component values at the end of the spiral generation sequence.

However, for the spike in entropy generation rate for Set 9, the stream wise spectral velocity component maintains a strong value, with significant structure. This pattern is repeated for initial condition Sets 6, 9, 12, 15 and 18, creating the strong patterns indicated in **Figure 3**. It is an interesting result that the solutions of the nonlinear modified Lorenz equations should exhibit such strong patterns in response to the values of the applied initial conditions.

6. Power Spectral Densities, Empirical Entropies, Empirical Entropic Indices and Intermittency Exponents

6.1. Power Spectral Density Empirical Modes

Burg's method (Chen [22]) is used to compute the power spectral densities within the nonlinear time series solutions for the modified Lorenz equations. The computer program listing for Burg's method given by Press *et al.* (pp. 572-574 [23]) are incorporated into the computational procedure, providing the spectral peaks within the time series solutions. The mathematical basis for Burg's method is found in information theory, with a thorough discussion presented by Cover and Thomas (pp. 409-425 [24]). Burg's method provides excellent spectral resolution and yields sharp spectral peaks within the power spectral density computations. We have found that Burg's method is an effective tool for extracting the underlying structural characteristics of the ordered velocity regions within the nonlinear time series solutions.

The first five sets of initial conditions in **Table 1** indicate relatively low levels of entropy generation. The nonlinear time series solutions of the modified Lorenz equations for these five sets indicate that instabilities are generated primarily in the stream wise spectral velocity component, with relatively low levels of excitation in the normal and span wise spectral velocity components. However, for the initial conditions in Set 6 of **Table 1**, strong instabilities are observed in both the normal and the span wise components of the spectral velocity components. **Figure 7** presents the power spectral density for the normal spectral velocity wave component, a_{y3} at the third receiver station at $x = 0.120$, for initial conditions, Set 6. For the power spectral density spectrum, we have assigned empirical mode numbers to the peaks, starting with mode $j = 1$ representing the highest peak in the distribution, continuing to mode $j = 16$, representing the corresponding lowest peak among the sixteen peaks.

The power spectral density for the normal spectral velocity component shown in **Figure 7** indicates that the kinetic energy available for dissipation is distributed in well-defined spectral peaks or empirical modes. The kinetic energy within each empirical mode, ξj, of the power spectral density distribution is computed using Simpson's integration rule. The sum of the individual contributions across the modes then yields the total kinetic energy contained within the ordered regions. This value is then used to get the fraction of kinetic energy in each mode that is available for dissipation into internal energy.

6.2. Singular Value Decomposition and Empirical Entropies

Additional fundamental characteristics within the nonlinear time series solutions of the modified Lorenz equations may also be found using the singular value decomposition procedure (Holmes, *et al.* (pp. 130-152 [25])). The computer program listings presented by Press *et al.* (pp. 59-65 [23]) for the singular value decomposition procedure have been incorporated into our overall computational program. The computer program for the singular value decomposition

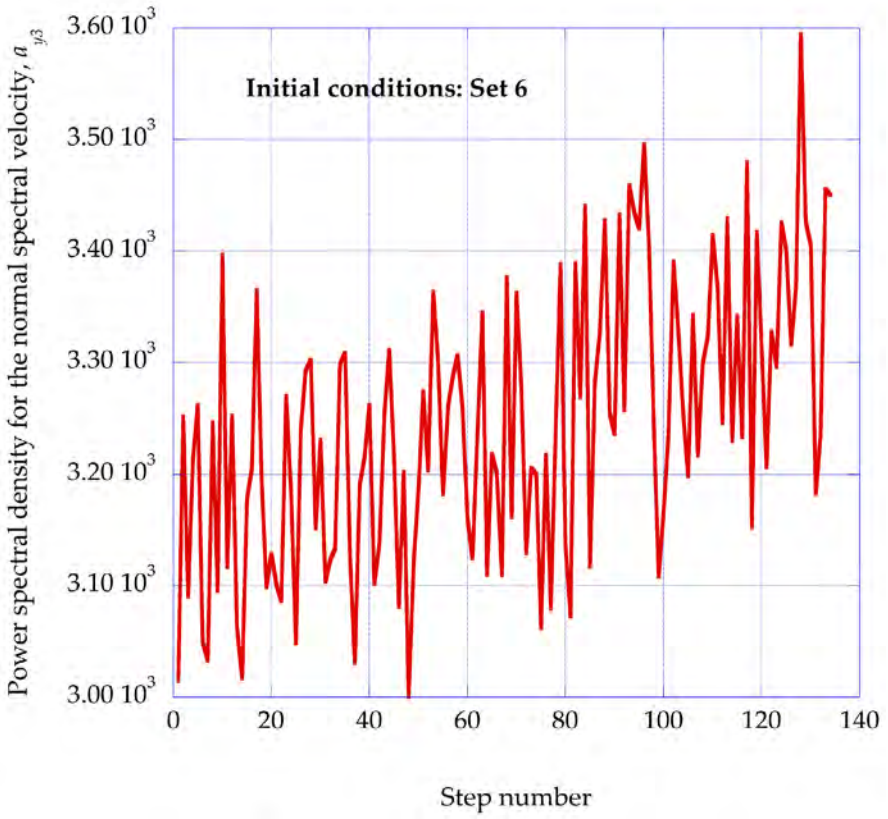

Figure 7. The power spectral density for the normal spectral velocity component for the initial conditions Set 6 at the stream wise location of $x = 0.120$, the normalized vertical location of $\eta = 3.00$ and the span wise velocity of $w_e = 0.080$.

[23] is made up of two parts, the computation of the autocorrelation matrix and the singular value decomposition of that matrix. This computer program then yields the empirical eigenvalues for each of the empirical eigenfunctions for the given nonlinear time series data segment.

The singular value decomposition of the nonlinear time series solutions of the modified Lorenz equations yields the distribution of the spectral velocity component eigenvalues λ_j across the empirical modes, j, for each set of initial conditions listed in **Table 1**. Using Parseval's theorem, (Thomas (pp. 97-100 [26])), the eigenvalues in the spectral plane, λ_j, are equivalent to the eigenvalues in the physical plane. These eigenvalues therefore represent the distribution of the kinetic energy of the fluctuating velocity components across the empirical modes, j. The fractional eigenvalues have an approximate exponential distribution over the empirical modes, j, as shown in **Figure 8** (Isaacson [27]).

Therefore, the analysis of Rissanen (pp. 58-60 [28]) is applicable and the empirical entropy, $Semp_j$, may be obtained from these eigenvalues by the expression:

$$Semp_j = -\ln\left(\lambda_j\right). \tag{14}$$

In this expression, λ_j is the empirical eigenvalue computed from the singular value decomposition procedure applied to the nonlinear time-series solution.

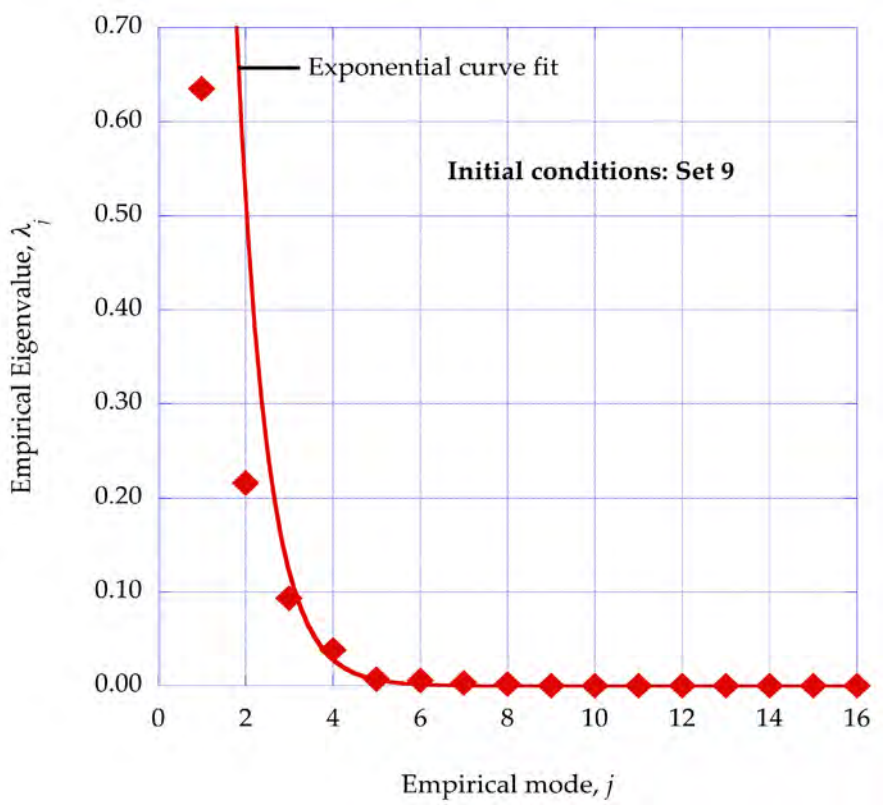

Figure 8. The fractional eigenvalues from the singular value decomposition of the normal spectral velocity component at $x = 0.120$ are shown as a function of the empirical mode, j, for the initial conditions, Set 9. Also shown is an exponential curve fit to the data.

The peaks of the spectral power density analysis and the empirical modes of the singular value decomposition analysis are computed from the same set of nonlinear time series data. Therefore, the Weiner-Khintchine theorem allows us to relate each power spectral density peak with a corresponding empirical eigenvalue. The Weiner-Khintchine theorem relates the power density spectrum to the autocorrelation function as they are operating on the same nonlinear time series data (Attard (pp. 354-355 [16]).

The results for the empirical entropy value for each of the empirical modes allows us to compute a corresponding entropic index for these modes. This process is described in the next section.

6.3. Empirical Entropic Indices

The power spectral density spectrum shown in **Figure 7** indicates regions of strongly peaked kinetic energy densities. The application of the singular value decomposition of the given time series data also provides us with a corresponding value of the empirical entropy for each peak. These two properties allow us to construct a computational method to follow these regions from ordered structures into equilibrium thermodynamic states. To accomplish this, we use the approach of the Tsallis entropic indices (Tsallis [29]).

The empirical entropy, $Semp_j$ describes the entropy of an ordered region identified by the empirical eigenvalue, λ_j, for the empirical mode, j. We have found that an expression from which we may extract an empirical entropic index, q_j, from the empirical entropy, $Semp_j$, may be written in a Tsallis entropic format as [18]:

$$Semp_j = -\ln\left(\lambda_j\right) = \frac{\left(\lambda_j\right)^{q_j} - 1}{\left(1 - q_j\right)}. \tag{15}$$

The empirical entropy index, q_j, provides a connection between the empirical entropy obtained from the singular value decomposition to the intermittency exponent of the ordered structures within the time series solutions. The intermittency exponent describes the fraction of the available kinetic energy within each empirical mode, j, that is dissipated into thermodynamic internal energy, thus increasing the entropy of the system. The intermittency exponent for each of the empirical modes is discussed in the next section.

6.4. Empirical Intermittency Exponents

The final phase of the dissipation of fluctuating kinetic energy into thermodynamic internal energy occurs through the process of intermittency exponents and a relaxation process into the final thermodynamic entropy state.

The intermittency exponents for the each of the empirical modes, ζ_j, are obtained from the empirical entropic indices of the Tsallis form extracted from the empirical entropies in Equation (15). Arimitsu and Arimitsu [30] derived, using multifractral methods, a relationship from which the intermittency exponent, ζ_j, may be extracted from the entropic index of Tsallis. The intermittency exponent provides the fraction of fluctuating kinetic energy within the non-equilibrium empirical mode, j, that is dissipated into thermodynamic internal energy [30].

The absolute value of the empirical entropic index calculated from Equation (15) is used to extract the intermittency exponent from the equation derived by Arimitsu and Arimitsu [30]. This expression for the empirical mode, j, is written as:

$$\left|q_j\right| = 1 - \frac{1 + \zeta_j - \log_2\left(1 + \sqrt{1 - 2^{-\zeta_j}}\right) * \log_2\left(1 - \sqrt{1 - 2^{-\zeta_j}}\right)}{\log_2\left(1 + \sqrt{1 - 2^{-\zeta_j}}\right) - \log_2\left(1 - \sqrt{1 - 2^{-\zeta_j}}\right)}. \tag{16}$$

The intermittency exponent, ζ_j, found from this expression, represents the fraction of kinetic energy in the empirical mode, j, that is dissipated into background thermal energy. The kinetic energy contained within the spectral mode, j, of the power spectral density is denoted as ξ_j. Thus, the product of the kinetic energy of the mode, j, and the intermittency exponent for that mode, ζ_j, summed over all of the empirical modes, represents the amount of kinetic energy in the given spectral velocity component that is dissipated into increasing the entropy of the reservoir.

The computation of the intermittency exponents yields two significant results. First, the computed value for each empirical mode allows the computation of the entropy generated through the dissipation of that mode. Second, the particular value for each empirical mode provides us with additional insight into the physical processes involved in the generation of entropy through the dissipation of the empirical modes embedded in the nonlinear solutions of the modified Lorenz equations.

Consider the entropy generation rates for initial conditions Sets 8, 9 and 10 in Figure 3. The entropy generation rate for Set 9 indicates a spike in the value of the generation rate compared to the rates generated for Sets 8 and 10. We wish to compare the intermittency exponents for each of these sets of initial conditions to better understand the physical processes related to the generation of the spike for Set 9.

Figures 9-11 show the intermittency exponents for the stream wise, normal, and span wise spectral velocity wave components a_{x3}, a_{y3} and a_{z3} as functions of the empirical mode, j for the initial conditions Sets 8, 9 and 10, respectively. Note that the stream wise intermittency is relatively low for all three sets of initial conditions. The increase in value for the stream wise intermittency exponents at the high empirical modes do not make a signifiacant contribution

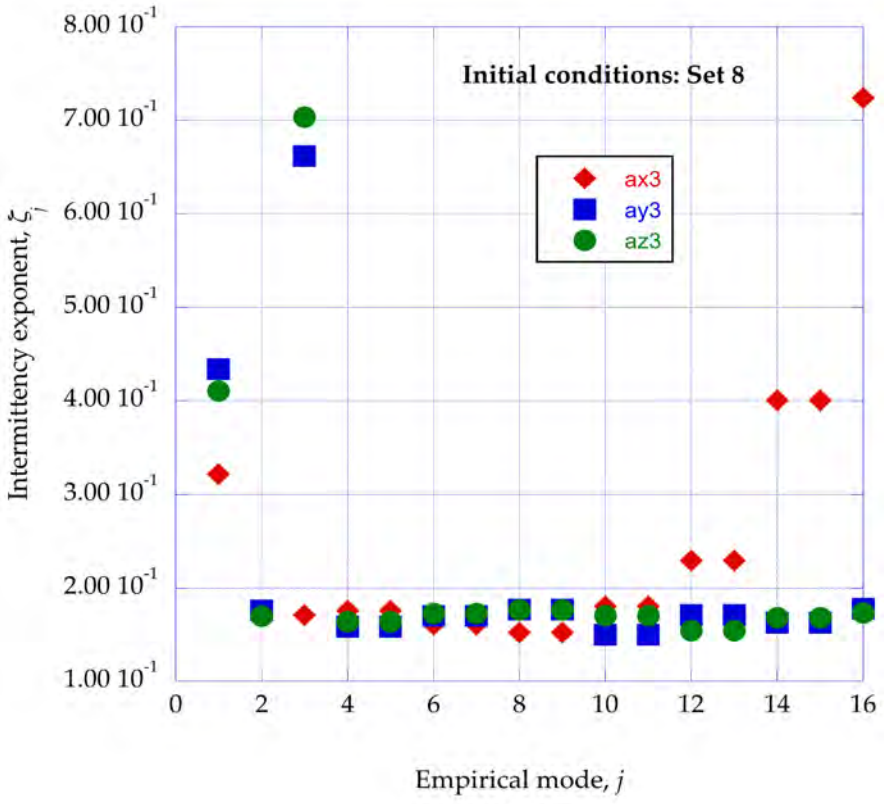

Figure 9. The intermittency exponents are shown for the spectral velocity components, a_{x3}, a_{y3}, and a_{z3}, for the initial conditions of Set 8 at the stream wise location of $x = 0.120$, the normalized vertical location of $\eta = 3.00$ and the span wise velocity of $w_c = 0.080$.

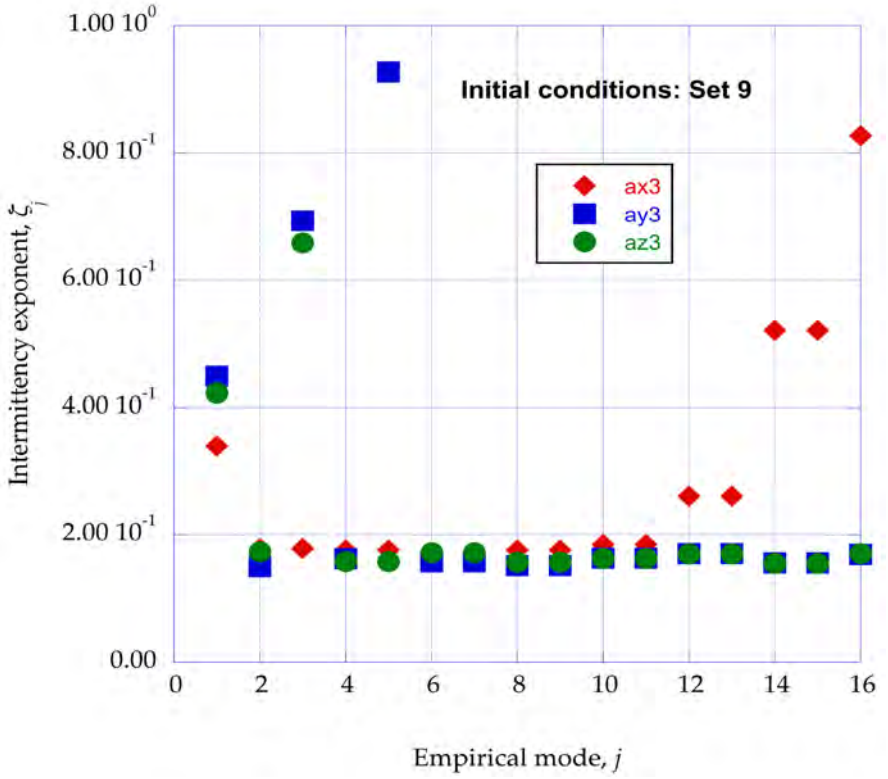

Figure 10. The intermittency exponents are shown for the spectral velocity components, a_{x3}, a_{y3}, and a_{z3}, for the initial conditions of Set 9 at the stream wise location of $x = 0.120$, the normalized vertical location of $\eta = 3.00$ and the span wise velocity of $w_e = 0.080$.

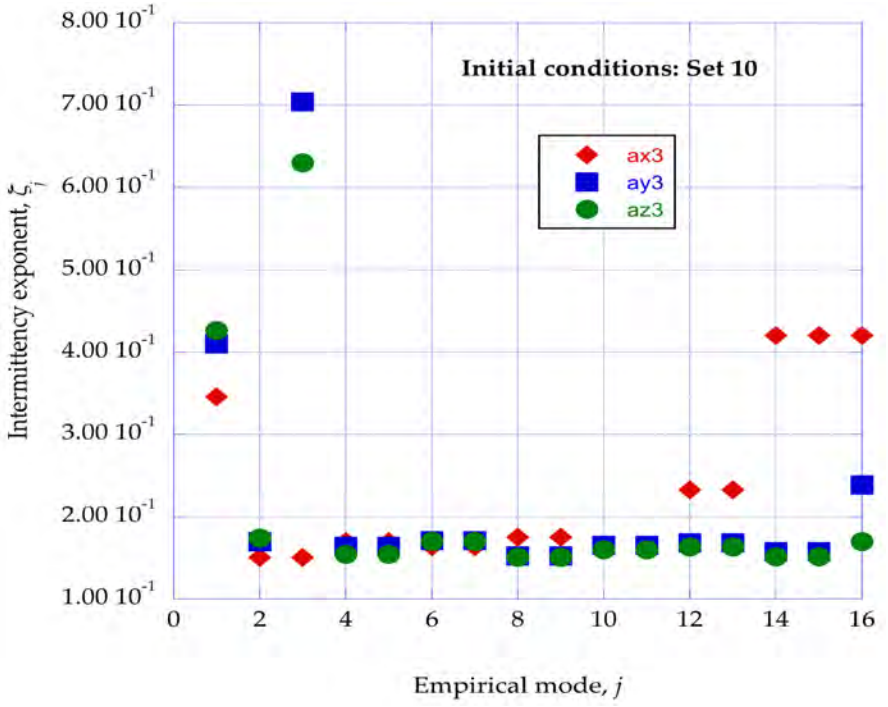

Figure 11. The intermittency exponents are shown for the spectral velocity components, a_{x3}, a_{y3}, and a_{z3}, for the initial conditions of Set 10 at the stream wise location of $x = 0.120$, the normalized vertical location of $\eta = 3.00$ and the span wise velocity of $w_e = 0.080$.

to the entropy generation rates because these modes contain very low fractions of the available stream wise kinetic energy.

However, for the normal and span wise spectral velocity components for initial conditions Sets 8 and 10, the first and third empirical modes make signifant contributions to the values of the intermittency exponents, with the third mode dominating the contributions. For the initial conditions Set 9, the fifth empirical mode comes into play with a significant increase in value. This indicates that as the initial conditions are increased in magnitude, the nonlinear time dependent solution of the modified Lorenz equations for the normal spectral velocity component predicts the spread of ordered kinetic energy over an additional empirical mode for this component. This results in the predition of a higher rate of entropy generation for this particular set of initial conditions. The repeated pattern shown in **Figure 3** for the generation rates over the first twelve sets of initial conditions is rather surprising, given that we are using coupled, nonlinear first-order differential equations in our modified Lorenz equations.

Figure 12 shows the intermittency exponents for the three spectral velocity components for initial conditions Set 15, which is the maximum entropy generation rate shown in **Figure 3**. The stream wise intermittency exponent shows an increase for empirical modes 1 and 3, with the span wise component increasing for modes 1, 3, and 5. The normal component indicates an almost linear increase in intermittency exponent value over empirical modes 1, 3, 5, and 7. This is also an interesting pattern within the nonlinear solutions of the modified Lorenze equations with the increase in intial conditions.

The foundation for the Tsallis entropic index [29] and the Arimitsu and Arimitsu intermittency exponent [30] lies in the concept of the fractal nature of the dissipation of turbulent kinetic energy (Mandelbrot [31]). Mandelbrot [31] also introduced the concept of fractals to describe the geometry of turbulent intermittency. Frisch and Parisi [32] noted that there are actually many fractal scales involved in the dissipation of turbulent energy and in the process of intermittency and introduced the concept of the multifractal model of turbulence. We have taken advantage of the considerable progress that has been made in extending these models to actual physical processes and wish to compare our results with recent theoretical and experimental results concerning the intermittency of the turbulent dissipation of kinetic energy.

To compare our computational results with results presented in the literature, we need to obtain average values for the intermittency exponents computed for a selected set of initial conditions from **Table 1**. For example, we will start with the results obtained for the initial conditions in Set 5 of **Table 1**. This set of initial conditions did not indicate the generation of significant flow instabilities and has a relatively low entropy generation rate, as indicated in **Figure 3**. The average intermittency exponent for the set of initial conditions is found by first averaging the intermittency exponents found for each empirical mode of the singular value decomposition procedure applied to each of the three spectral velocity components. Then, these three average values are averaged across the three

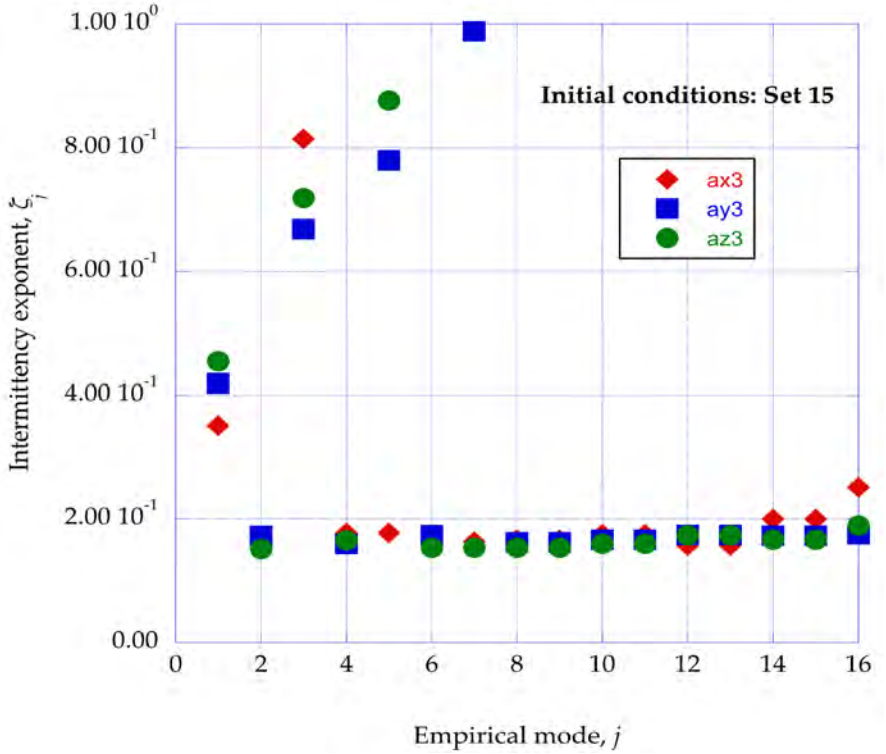

Figure 12. The intermittency exponents are shown for the spectral velocity components, a_{x3}, a_{y3}, and a_{z3}, for the initial conditions of Set 15 at the stream wise location of $x = 0.120$, the normalized vertical location of $\eta = 3.00$ and the span wise velocity of $w_e = 0.080$.

spectral velocity components to yield the average intermittency exponent for the entire Set 5 initial conditions. The resulting intermittency exponent will be designated as ζ_{5ave}. The value of the average intermittency exponent for initial conditions Set 5 is found to be $\zeta_{5ave} = 0.349$.

Arimitsu and Arimitsu [33] found, in the analysis of quantum turbulent intermittency, a value of $\zeta_{5ave} = 0.326$, while Arimitsu, *et al.* [34] found by DNS analysis of this same quantum system a value of $\zeta_{5ave} = 0.345$. We may be able to gain a better understanding of the fundamental characteristics of systems with high values of intermittency exponents through a comparison of these two different systems.

The low-temperature quantum superfluid system studied in [33] [34] appears to have negligible mutual friction between the superfluid and the normal fluid components. Therefore, the level of irreversibilities produced in the system would be very low. In the three-dimensional boundary-layer with initial conditions given in Set 5 of Table 1, very low levels of instabilities are found in the nonlinear time-series solutions of the modified Lorenz equations. Subsequently, low values are predicted for the entropy generation rates for the initial conditions of Set 5. Thus, the similarity between these two systems is that they each have very low levels of irreversibilities.

However, when we move to the initial conditions Set 6, the first significant instability is found in the nonlinear time series solutions of the modified Lorenz

equations. These instabilities give rise to a higher rate of dissipation of turbulent kinetic energy, thus increasing the irreversibilities in the process. This increase is reflected in the local peak in the entropy generation rate for Set 6, as indicated in Figure 3.

The computation of entropy generation rates reported here are for a three-dimensional laminar boundary layer located at a stream wise distance of 0.120 on a 1 m scale, with a stream wise velocity of unity, and at a normalized vertical distance in the boundary layer, η = 3.0, with the edge of the boundary layer at η_∞ = 8.00, or 37.5 percent of the boundary-layer thickness. This location is approximately the position of the hot-wire measurements reported by Meneneau and Sreenivan [35].

Table 2 shows the average intermittency exponents for a selected range of initial conditions, corresponding to the patterns apparent in Figure 3. Also shown are values of intermittency exponent used in a number of studies of the fractal nature of the dissipation of turbulent kinetic energy. The referenced values of the intermittency exponents are the values assumed in the indicated reference as either a given value for the analysis or an experimental value for comparison.

An overall average intermittency value was determined by averaging over Sets 6 - 10 and 14 - 16 with the results that ζ_{5ave} = 0.241, which agrees with the universally accepted value of approximately 0.24 [33] [36]. It should also be noted that, in an analysis of the number of steps in the cascade process of the dissipation of turbulent kinetic energy [36], the number of steps was found to be 16.4, which is close to the number of empirical modes, 16, that we have found from the power spectral density results.

6.5. Kinetic Energy Available for Dissipation

The source of the kinetic energy to be dissipated through the empirical modes is considered as the local steady-flow kinetic energy, $u^2/2$, at the normalized vertical distance, η = 3.0 in the x-y plane boundary layer. This kinetic energy is assumed to be distributed over the three fluctuating velocity components. The fraction of kinetic energy in the x-direction velocity component is denoted as κ_x, the fraction of kinetic energy in the y-direction velocity component is denoted as κ_y and the fraction in the z-direction velocity component is denoted as κ_z. The fraction of dissipation kinetic energy within each empirical mode of the power spectral energy distribution is denoted as ξ_j. Then the total rate of dissipation of the available fluctuating kinetic energy for the stream wise, normal and span wise velocity components is the summation, over the empirical modes, *j*, of the product of the kinetic energy fraction of each mode, ξ_j, times the intermittency exponent for that mode, ξ_φ [3].

The empirical intermittency exponent for each of the empirical modes has been obtained from the expression (Equation (16)) given by Arimitsu and Arimitsu [31]. Thus, values are available for the input energy source for the non-equilibrium ordered regions, the fraction of the fluctuation kinetic energy

Table 2. This table shows the average value for the intermittency exponents for a selected range of sets of initial conditions. Also shown are comparable values from selected references.

Initial conditions: Set number	Intermittency exponent: Average value	Reference intermittency value	Reference number
5	0.3487	0.345	[34]
6	0.2377	0.238	[33]
7	0.2313	0.235	[35]
8	0.2267		
9	0.2502	0.259	[36]
10	0.2187		
14	0.2636		
15	0.2647	0.260	[34]
16	0.2380	0.240	[33]

available in each of the empirical modes within the non-equilibrium ordered regions, and the fraction of the energy in each of the empirical modes that dissipates into background thermal energy, thus increasing the thermodynamic entropy. Concepts from non-equilibrium thermodynamics are used to calculate the dissipation process for the ordered regions as a general relaxation process. This is considered in the next section.

7. Entropy Generation Rates through the Dissipation of Ordered Regions

de Groot and Mazur (pp. 221-230 [37]), from the concepts of non-equilibrium thermodynamics, write the equation for the entropy generation rate in an internal relaxation process as:

$$\frac{\partial s}{\partial t} = -J(x)\frac{\partial \mu(x)}{\partial x}. \tag{17}$$

Here, s is the entropy per unit mass, μ is the mechanical potential for the transport of the ordered regions in an external context and $J(x)$ is the flux of kinetic energy through the ordered regions available for dissipation into thermal internal energy. The dissipation of the ordered regions into background thermal energy may be considered as a two-stage process from the transition of the ordered regions into equilibrium thermodynamic states and a turn-over process of the downstream velocity in the initial state to the final equilibrium state of the velocity over the internal distance x. The local boundary layer steady state velocity is written as $u = u_e f'$, where f' is the derivative of the Falkner-Skan stream function f with respect to the normalized distance η. The expression for the entropy generation rate (in Joules/(m^3·K·s)) through the non-equilibrium ordered regions is then written as [3]:

$$\left(\frac{\mathrm{d}S}{\mathrm{d}t}\right)_{gen} = \rho\left[\left(\frac{1u_e^2}{2T}\right)(f')^2\left\{\kappa_x\left(\sum_{j=1}^{16}\xi_j\zeta_j\right)_x + \kappa_y\left(\sum_{j=1}^{16}\xi_j\zeta_j\right)_y + \kappa_z\left(\sum_{j=1}^{16}\xi_j\zeta_j\right)_z\right\}\left(\frac{u_e}{x}\right)\right]. \quad (18)$$

In this expression, ρ is the density of the working substance, T is the temperature and u_e is the free stream velocity. The dissipation rate for each of the three fluctuating spectral velocity components is included in Equation (18).

The kinetic energy in each spectral mode available for final dissipation into equilibrium internal energy is computed for each of the spectral peaks shown in Figure 7. The empirical entropy for each of the regions indicated by the spectral peaks is found from the singular value decomposition process applied to the given time series data segment. The connecting parameter, the empirical entropic index, is then extracted from the resulting value of the empirical entropy. The empirical entropic indices then allow the extraction of the corresponding intermittency exponents.

8. Discussion

There are two significant issues with the computational procedure and the results reported in this article. First, there have been no comparable computational results which would validate the procedures adopted here. Second, experimental validation is sparse and applies only to selected aspects of the computational approach and the results. However, the computational procedure is innovative in that it provides a method for the incorporation of a deterministic set of equations for the development of instabilities within the steady state environment of a three-dimensional laminar boundary layer flow. The results indicate that the entropy generation rates resulting from nonlinear interactions in a three-dimensional laminar boundary-layer flow are significantly affected by the particular initial conditions that are applied to the longitudinal vortex structure and the adjacent laminar boundary layer flow.

The counter clockwise rotating longitudinal vortex structure creates a viscous boundary layer along the z-y plane of the flow configuration. This viscous boundary layer is orthogonal to the laminar boundary layer in the x-y plane in the stream wise direction. It is shown that this nonlinear interaction creates instabilities within the three-dimensional flow configuration.

The computational results reported here for the entropy generation rates for a helium mixture boundary layer flow are obtained at the stream wise location of $x = 0.120$, in the range of stream wise locations from $x = 0.06$ to $x = 0.18$, for the normalized vertical station of $\eta = 3.00$. The weighting factor K in Equation (5) has been found to yield the prediction of instabilities for a value of $K = 0.05$. In an experimental investigation of laminar boundary layer receptivity to surface mass injection, Sengupta (pp. 158-170 [15]) found that the coefficient of 0.05 for a time-dependent sinusoidal surface mass injection rate also initiated instabilities within a laminar boundary-layer flow. We thus have the implication that

Equation (5) is a proper choice for the transformation of the Townsend equations for the fluctuating velocity components into a modified Lorenz format.

Free stream turbulence levels provide the turbulent kinetic energy that enters the wall shear layer. However, this level is attenuated within the layer and only a portion is available to serve as the initial conditions for the solution of the modified Lorenz equations describing the development of instabilities within the layer. Schmid and Henningson (pp. 430-436 [11]) discuss the resulting formation of stream wise vortices, streaky structures, and the subsequence formation of turbulent spots through the interaction of this turbulence level within the wall boundary layer flow.

In the study reported here, we have modeled the interaction of a longitudinal vortex structure with a stream wise developing boundary layer through the time dependent modified Lorenz equations and have applied a range of initial conditions to the solutions of these equations.

Fluctuating spectral velocity components are found within the time-series solutions for the modified Lorenz equations. Statistical processing of the solutions indicates the presence of ordered regions embedded within the nonlinear time-series solutions. The dissipation of these ordered regions into equilibrium thermodynamic states yields the entropy generation rates for the three-dimensional interaction flow environment. Significant entropy generation rates are predicted for the specified sets of initial conditions applied to the solutions. The results for these entropy generation rates indicate a strong correlation of the entropy results with the levels of the applied initial conditions and that a pattern emerges as a function of the increasing levels of the initial condition equivalent turbulence intensities.

The sensitivity to initial conditions of the Lorenz format spectral velocity equations may provide a means of connecting the incorporation of these time dependent spectral equations in the computational procedure with the concept of bypass transition of the boundary layer flow due to outside disturbances.

9. Conclusions

The flow configuration of a longitudinal vortex structure and an adjacent laminar boundary layer for a helium mixture flow provides a three-dimensional nonlinear interaction of laminar boundary layers. In the study reported in this article, the velocity fluctuations produced by the instabilities that occur in such an interaction have been modeled through the transformation of the Townsend equations for the velocity fluctuations into a set of nonlinear deterministic Lorenz equations for the spectral velocity components of the fluctuations in the time frame.

The steady boundary-layer velocity profiles in the longitudinal-normal plane and the span wise-normal plane are computed using well-established numerical methods and serve as control parameters for the solutions of the modified Lorenz equations for the time-dependent spectral velocity components. It is shown

that the solutions of the nonlinear deterministic modified Lorenz equations are strongly dependent on the values for the initial conditions applied to the solutions. Eighteen sets of initial conditions are examined for the resulting effects on the final values for the computed entropy generation rates.

Power spectral density analysis of the nonlinear time series indicates the presence of sixteen ordered spectral velocity modes within the time series data. Integration over each of these modes provides the ordered energy available within that mode for dissipation into background thermal energy, or increase of entropy. From the singular value decomposition of the time series data, the fraction of kinetic energy in each of the sixteen modes yields a corresponding value of empirical entropy for that mode. The value of empirical entropy yields the value for the Tsallis empirical entropic index, from which the corresponding intermittency exponent for each mode is obtained. Combining these results yields the expression of the total entropy generation rate for all of the ordered modes.

The entropy generation rates through the dissipation of these ordered regions are computed for eighteen sets of initial conditions for the given helium boundary layer flow environment. Strong correlation is found between the predicted entropy generation rates and the initial conditions applied for the solutions of the modified Lorenz equations, both in amplitudes of the generation rates and the emergent of significant patterns of the entropy generation rates as a function of the intensity levels of the applied initial conditions.

These results offer a deterministic path to the understanding of *bypass transition* and a foundation for the development of an understanding of the dynamics of turbulent spots in the transition from laminar to turbulent flows.

Conflicts of Interest

The author declares no conflict of interest.

References

[1] Townsend, A.A. (1976) The Structure of Turbulent Shear Flow. 2nd Edition, Cambridge University Press, Cambridge.

[2] Sparrow, C. (1982) The Lorenz Equations: Bifurcations, Chaos, and Strange Attractors. Springer-Verlag, New York. https://doi.org/10.1007/978-1-4612-5767-7

[3] Isaacson, L.K. (2017) *Entropy*, **19**, 278. https://doi.org/10.3390/e19060278

[4] Isaacson, L.K. (2016) *Entropy*, **18**, 47. https://doi.org/10.3390/e18020047

[5] Isaacson, L.K. (2016) *Entropy*, **18**, 279. https://doi.org/10.3390/e18080279

[6] Walsh, E.J. and Hernon, E. (2006) *Entropy*, **8**, 25-30. https://doi.org/10.3390/e8010025

[7] Hellberg, C.S. and Orszag, S.A. (1988) *Physics of Fluids*, **31**, 6-8. https://doi.org/10.1063/1.867010

[8] Singer, B.A. (1996) *Physics of Fluids*, **8**, 509-521. https://doi.org/10.1063/1.868804

[9] Ersoy, S. and Walker, J.D.A. (1985) *Physics of Fluids*, **28**, 2687-2698. https://doi.org/10.1063/1.865226

[10] Belotserkovskii, O.M. and Khlopkov, Y.I. (2010) Monte Carlo Methods in Mechanics of Fluid and Gas. World Scientific Publishing, Singapore, 101-102.

[11] Schmid, P.J. and Henningson, D.S. (2001) Stability and Transition in Shear Flows. Springer-Verlag, New York, 401-465. https://doi.org/10.1007/978-1-4613-0185-1_9

[12] Cebeci, T. and Bradshaw, P. (1977) Momentum Transfer in Boundary Layers. Hemisphere, Washington DC, 319-321.

[13] Cebeci, T. and Cousteix, J. (2005) Modeling and Computation of Boundary-Layer Flows. Horizons Publishing, Long Beach.

[14] Hansen, A.G. (1964) Similarity Analyses of Boundary Value Problems in Engineering. Prentice-Hall, Englewood Cliffs, 86-92.

[15] Sengupta, T.K. (2012) Instabilities of Flows and Transition to Turbulence. CRC Press, Boca Raton, 171-200.

[16] Attard, P. (2012) Non-Equilibrium Thermodynamics and Statistical Mechanics: Foundation and Applications. Oxford University Press, Oxford. https://doi.org/10.1093/acprof:oso/9780199662760.001.0001

[17] Manneville, P. (1990) Dissipative Structures and Weak Turbulence. Academic Press, San Diego.

[18] Isaacson, L.K. (2012) *Entropy*, **14**, 131-160. https://doi.org/10.3390/e14020131

[19] Pecora, L.M. and Carroll, T.L. (1996) Synchronization in Chaotic Systems. In: Kapitaniak, T., Ed., *Controlling Chaos: Theoretical and Practical Methods in Nonlinear Dynamics*, Academic Press Inc., San Diego, 142-145. https://doi.org/10.1016/B978-012396840-1/50040-0

[20] Pérez, G. and Cerdeira, H.A. (1996) Extracting Messages Masked by Chaos. In: Kapitaniak, T., Ed., *Controlling Chaos: Theoretical and Practical Methods in Nonlinear Dynamics*, Academic Press Inc., San Diego, 157-160. https://doi.org/10.1016/B978-012396840-1/50043-6

[21] Cuomo, K.M. and Oppenheim, A.V. (1996) Circuit Implementation of Synchronized Chaos with Applications to Communications. In: Kapitaniak, T., Ed., *Controlling Chaos: Theoretical and Practical Methods in Nonlinear Dynamics*, Academic Press Inc., San Diego, 153-156. https://doi.org/10.1016/B978-012396840-1/50042-4

[22] Chen, C.H. (1982) Digital Waveform Processing and Recognition. CRC Press, Boca Raton, 131-158.

[23] Press, W.H., Teukolsky, S.A., Vetterling, W.T. and Flannery, B.P. (1992) Numerical Recipes in C: The Art of Scientific Computing. 2nd Edition, Cambridge University Press, Cambridge.

[24] Cover, T.M. and Thomas, J.A. (2006) Elements of Information Theory. 2nd Edition, John Wiley & Sons, Hoboken.

[25] Holmes, P., Lumley, J.L., Berkooz, G. and Rowley, C.W. (2012) Turbulence, Coherent Structures, Dynamical Systems and Symmetry. 2nd Edition, Cambridge University Press, Cambridge. https://doi.org/10.1017/CBO9780511919701

[26] Thomas, J.W. (1995) Numerical Partial Differential Equations: Finite Difference Methods. Springer-Verlag, New York. https://doi.org/10.1007/978-1-4899-7278-1

[27] Isaacson, L.K. (2013) *Entropy*, **15**, 4134-4158. https://doi.org/10.3390/e15104134

[28] Rissanen, J. (2007) Information and Complexity in Statistical Modeling. Springer, New York.

[29] Tsallis, C. (2009) Introduction to Nonextensive Statistical Mechanics. Springer, New

York, 37-43. https://doi.org/10.1007/978-0-387-85359-8_3

[30] Arimitsu, T. and Arimitsu, N. (2000) *Physical Review E*, **61**, 3237-3240. https://doi.org/10.1103/PhysRevE.61.3237

[31] Mandelbrot, B.B. (1983) The Fractal Geometry of Nature. W.H. Freeman and Company, New York, 97-105.

[32] Frisch, U. and Parisi, G. (1985) Fully Developed Turbulence and Intermittency. In: Ghil, M., Benzi, R. and Parisi, G., Eds., *Turbulence and Predictability in Geophysical Fluid Dynamics and Climate Dynamics*, North-Holland, New York, 84-88.

[33] Arimitsu, T. and Arimitsu, N. (2005) *Journal of Physics*: *Conference Series*, **7**, 101-120. https://doi.org/10.1088/1742-6596/7/1/009

[34] Arimitsu, T., Arimitsu, N. and Mouri, H. (2012) *Physics of Fluid Dynamics*, **4**, 1-17.

[35] Meneveau, C. and Sreenivasan, K.R. (1987) *Nuclear Physics B*, **2**, 49-76. https://doi.org/10.1016/0920-5632(87)90008-9

[36] Arimitsu, T. and Arimitsu, N. (2003) *Condensed Matter Physics*, **6**, 85-92. https://doi.org/10.5488/CMP.6.1.85

[37] De Groot, S.R. and Mazur, P. (1962) Non-Equilibrium Thermodynamics. North-Holland, Amsterdam.

Nomenclature

a_i: Fluctuating *i-th* component of velocity wave vector
b_n: Coefficient in modified Lorenz equations defined by Equation (9)
F: Time-dependent feedback factor
h: Integration time step (s)
j: Mode number empirical eigenvalue
J: Net source of kinetic energy dissipation rate, Equation (17)
k: Time-dependent wave number magnitude
k_i: Fluctuating *i-th* wave number of Fourier expansion
K: Adjustable weighting factor
n: Stream wise station number
P: Local static pressure ($N \cdot m^{-2}$)
q_j: Empirical entropic index for the empirical entropy of mode, j
r_n: Coefficient in modified Lorenz equations defined by Equation (8)
s: Entropy per unit mass ($J \cdot kg^{-1} \cdot K^{-1}$))
s_n: Coefficient in modified Lorenz equations defined by Equation (8)
$Semp_j$: Empirical entropy for empirical mode, j
$\dot{S}_{gen}$: Entropy generation rate through kinetic energy dissipation ($J \cdot m^{-3} \cdot K^{-1} \cdot s^{-1}$)
t: Time (s)
u: Mean stream wise velocity in the x-direction in Equation (4)
u': Fluctuating stream wise velocity in Equation (4)
u_e: Stream wise velocity at the outer edge of the x-y plane boundary layer
u_i: The *i-th* component of the fluctuating velocity
U_i: Mean velocity in the *i-th* direction in the modified Lorenz equations
w_e: Span wise velocity at the outer edge of the z-y plane boundary layer
x: Stream wise distance
x_i: *i-th* direction
x_j: *j-th* direction
y: Normal distance
z: Span wise distance

Greek Letters

δ: Boundary layer thickness (m)
δ_{lm}: Kronecker delta
ζ_j: Intermittency exponent for the j-th mode in Equation (18)
η: Transformed normal distance parameter
η_∞: Transformed outer edge of the boundary layer
κ_x: Fraction of kinetic energy in the stream wise component
κ_y: Fraction of kinetic energy in the normal component
κ_z: Fraction of kinetic energy in the span wise component
λ_j: Eigenvalue for the empirical mode, j
μ: Mechanical potential in Equation (17)
v: Kinematic viscosity of the gas mixture ($m^2 \cdot s^{-1}$)
ξ_j: Kinetic energy in the j-th empirical mode

ρ: Density ($kg \cdot m^{-3}$)

σ_y: Coefficient in modified Lorenz equations defined by Equation (7)

σ_x: Coefficient in modified Lorenz equations defined by Equation (7)

τ_w: Wall shear stress ($N \cdot m^{-2}$)

Subscripts

e: Outer edge of the laminar boundary layer

i, j, l, m: Tensor indices

x: Component in the x-direction

y: Component in the y-direction

z: Component in the z-direction

Journal of Modern Physics, 2018, 9, 1690-1696
http://www.scirp.org/journal/jmp
ISSN Online: 2153-120X
ISSN Print: 2153-1196

Fractional Euler Lagrange Equations for Irregular Lagrangian with Holonomic Constraints

Ola A. Jarab'ah

Applied Physics Department, Faculty of Science, Tafila Technical University, Tafila, Jordan
Email: oasj85@yahoo.com

How to cite this paper: Jarab'ah, O.A. (2018) Fractional Euler Lagrange Equations for Irregular Lagrangian with Holonomic Constraints. *Journal of Modern Physics*, **9**, 1690-1696.
https://doi.org/10.4236/jmp.2018.98105

Received: July 10, 2018
Accepted: July 28, 2018
Published: July 31, 2018

Copyright © 2018 by author and Scientific Research Publishing Inc.
This work is licensed under the Creative Commons Attribution International License (CC BY 4.0).
http://creativecommons.org/licenses/by/4.0/

Open Access

Abstract

In this paper the fractional Euler Lagrange equations for irregular Lagrangian with holonomic constraints have been presented. The equations of motion are obtained using fractional Euler Lagrange equations in a similar manner to the usual mechanics. The results of fractional calculus reduce to those obtained from classical calculus (the standard Euler Lagrange equations) when $\gamma \to 0$ and α, β are equal unity only. Two problems are considered to demonstrate the application of the formalism.

Keywords

Fractional Derivatives, Euler-Lagrange Equations, Irregular Lagrangian, Holonomic Constraints

1. Introduction

The Euler Lagrange equations and Hamilton's principle form the basis of Lagrangian or Hamiltonian mechanics. The power of Lagrangian mechanics is that the given equations are characterized with only one scalar function the Lagrangian L, or the Hamiltonian H. In general, these functions only describe conservative systems. There have been some approaches at describing nonconservative systems in such formalism. The method presented by Rayleigh introduces a function R (called Rayleigh's dissipation function).

The study of holonomic constrained systems is discussed in most references of classical mechanics [1] [2]; these systems describe dynamic systems with constraints depend only on the generalized coordinates $q_i(t)$. The canonical formalism of holonomic systems was treated by Rabei [3]. In this formalism the

author has treated the regular Lagrangian with holonomic constraints as singular systems and the Lagrange multipliers as generalized coordinates. The equations of motion are written as total differential equations then, the holonomic systems are quantized using the WKB approximation [4].

Fractional calculus is a generalization of differentiation and integration to a noninteger order. The interest in fractional calculus has been growing continually during the last few years because of its numerous applications in science and engineering [5] [6] [7]. The traditional calculus of variation cannot be used to obtain the equations of motion for the nonconservative systems.

Riewe has used the fractional calculus to develop a formalism which can be used for both conservative and nonconservative systems [8] [9]. The Hamiltonian and Lagrangian involving fractional derivative is also used to derive the equation of damped harmonic oscillator [10]. Therefore the dynamical systems with fractional order can be dissipative. For this reason, the theory and methods of fractional calculus are extensively used for describing critical phenomena in nonconservative systems of physics and mechanics [11] [12].

Recently, the classical calculus of variations was extended by Agrawal [13] for systems containing Riemann-Liouville fractional derivatives. The resulting equations are found to be similar to those for variational problems containing integral order derivatives. In other words, the results of fractional calculus of variations reduce to those obtained from traditional fractional calculus of variations when the derivative of fractional order replaced by integral order. More recently, Euler Lagrange equations for holonomic constrained systems with regular Lagrangian have been presented by Hasan [14] using the fractional variationl problems.

In the present paper as a continuation of Jarab'ah work [15] the fractional Euler Lagrange equations are used to obtain the equations of motion for irregular Lagrangian with holonomic constraints, it seems that there are several choices of fractional Lagrangian giving the same classical limit, in other words the same classical Lagrangian.

This paper is organized as follows: In Section 2, Euler Lagrange equations formulation for Irregular Lagrangian with holonomic constraints is reviewed briefly. In Section 3, basic definitions of fractional derivatives are briefly discussed. In Section 4, the fractional Euler Lagrange equations for irregular Lagrangian with holonomic constraints are explained. In Section 5, two illustrative examples are examined. The work closes with some concluding remarks (In Section 6).

2. Euler Lagrange Equations Formulation for Regular Lagrangian with Holonomic Constraints

The Lagrangian formulation for regular Lagrangian is given by

$$L_\circ = L_\circ\left(q_i, \dot{q}_i, t\right) \tag{1}$$

Here $L_\circ\left(q_i, \dot{q}_i, t\right)$ stands for the Lagrangian of the corresponding conserva-

tive systems. The standard method for incorporating the constraint functions to the equations of motion is the use of the so called Lagrange multipliers. The motion of a holonomic system could in principle be determined by making use of the n Euler Lagrange equations and m constraints.

$$\frac{\mathrm{d}}{\mathrm{d}t}\left(\frac{\partial L_{\circ}}{\partial \dot{q}_i}\right)-\frac{\partial L_{\circ}}{\partial q_i}=\lambda_{\mu}\frac{\partial f_{\mu}}{\partial q_i},\ i=1,2,\cdots,n \tag{2}$$

The constraint equation with m constraints can be written as $f_{\mu}\left(q_i,t\right)=0$, $\mu=n+1,n+2,\cdots,n+m$.

λ_{μ}: are the Lagrange multipliers.

3. Basic Definitions of Fractional Derivatives

Now, we will give the basic definition of a fractional derivatives include the left and the right Riemann Liouville fractional derivatives [16] [17] and their properties. The left Riemann Liouville fractional derivative is defined as

$${}_aD_x^{\alpha}f\left(x\right)=\frac{1}{\Gamma\left(n-\alpha\right)}\left(\frac{\mathrm{d}}{\mathrm{d}x}\right)^n\int_a^x\left(x-\tau\right)^{n-\alpha-1}f\left(\tau\right)\mathrm{d}\tau \tag{3}$$

which is denoted as the LRLFD,
and the right Riemann Liouville fractional derivative is defined as

$${}_xD_b^{\alpha}f\left(x\right)=\frac{1}{\Gamma\left(n-\alpha\right)}\left(-\frac{\mathrm{d}}{\mathrm{d}x}\right)^n\int_x^b\left(\tau-x\right)^{n-\alpha-1}f\left(\tau\right)\mathrm{d}\tau \tag{4}$$

which is denoted as the RRLFD,

Here Γ represents the Euler's gamma function, and α is the order of the derivative such that $n-1\le\alpha<n$ and is not equal to zero. If α is an integer, these derivatives are defined as follows:

$${}_aD_x^{\alpha}f\left(x\right)=\left(\frac{\mathrm{d}}{\mathrm{d}x}\right)^{\alpha}f\left(x\right) \tag{5}$$

$${}_xD_b^{\alpha}f\left(x\right)=\left(-\frac{\mathrm{d}}{\mathrm{d}x}\right)^{\alpha}f\left(x\right) \tag{6}$$

$$\alpha=1,2,\cdots$$

The fractional operator ${}_aD_x^{\alpha}f\left(x\right)$ can be written as [18].

$${}_aD_x^{\alpha}=\frac{\mathrm{d}^n}{\mathrm{d}x^n}\,{}_aD_x^{\alpha-n} \tag{7}$$

and has the following properties:

1) ${}_aD_x^{\alpha}=\dfrac{\mathrm{d}^{\alpha}}{\mathrm{d}x^{\alpha}},\quad \mathrm{Re}\left(\alpha\right)>0$

2) ${}_aD_x^{\alpha}=1,\quad \mathrm{Re}\left(\alpha\right)=0$

3) ${}_aD_x^{\alpha}=\int_a^x\left(\mathrm{d}\tau\right)^{-\alpha},\quad \mathrm{Re}\left(\alpha\right)<0$

Theorem: Let f and g be two continuous functions on $\left[a,b\right]$. Then, for all

$x \in [a,b]$, the following properties hold:

1) For $m>0$, ${}_aD_x^m\left[f(x)+g(x)\right]={}_aD_x^m f(x)+{}_aD_x^m g(x)$

2) For $m \geq n \geq 0$, ${}_aD_x^m\left({}_aD_x^{-n} f(x)\right)={}_aD_x^{m-n} f(x)$

3) For $m>0$, ${}_aD_x^m\left({}_aD_x^{-m} f(x)\right)=f(x)$

4) For $m>0$, $\int_a^b \left({}_aD_x^m f(x)\right) g(x)\mathrm{d}x=\int_a^b f(x)\left({}_xD_b^m g(x)\right)\mathrm{d}x$

4. Fractional Euler Lagrange Equations for Irregular Lagrangian with Holonomic Constraints

The Lagrangian formulation for irregular Lagrangian without fractional derivatives is given by [19]

$$L=L_\circ\left(q_i,\dot{q}_i\right)\mathrm{e}^{\gamma t} \tag{8}$$

where L is irregular Lagrangian which is a function of n generalized coordinates $q_i(t)$ and n generalized velocities $\dot{q}_i(t)$ and γ is defined as damping factor.

The Euler-Lagrange equation for the fractional calculus of variations problems is obtained as

$$\frac{\partial L}{\partial q}+{}_tD_b^\alpha\frac{\partial L}{\partial\,{}_aD_t^\alpha q}+{}_aD_t^\beta\frac{\partial L}{\partial\,{}_tD_b^\beta q}+\lambda_\mu\frac{\partial f}{\partial q}=0 \tag{9}$$

Here L is a function of the form $L=L_\circ\left(q,{}_aD_t^\alpha q,{}_tD_b^\beta q\right)\mathrm{e}^{\gamma t}$.

It is worth to mention that for $\alpha=\beta=1$, we have ${}_aD_t^\alpha=\frac{\mathrm{d}}{\mathrm{d}t}$ and ${}_tD_b^\alpha=-\frac{\mathrm{d}}{\mathrm{d}t}$ and Equation (9) reduces to the standard Euler Lagrange equation for holonomic constraints.

5. Examples

1) As a first model let us consider the following Lagrangian that describes the motion of a bead of mass m is constrained to move on a circular wire of radius R.

The Lagrangian of our problem is given by

$$L=\frac{1}{2}m\left(\dot{r}^2+r^2\dot{\theta}^2\right)-mgr\cos\theta$$

In the presence of damping factor the Lagrangian becomes

$$L=\left[\frac{1}{2}m\left(\dot{r}^2+r^2\dot{\theta}^2\right)-mgr\cos\theta\right]\mathrm{e}^{\gamma t} \tag{10}$$

Is subject to the holonomic constraint

$$f(r)=r-R=0 \tag{11}$$

The Lagrangian in fractional form can be written as

$$L=\left[\frac{1}{2}m\left({}_0D_t^\alpha r\right)^2+\frac{1}{2}mr^2\left({}_tD_1^\beta\theta\right)^2-mgr\cos\theta\right]\mathrm{e}^{\gamma t} \tag{12}$$

Using Equation (9), the corresponding Euler Lagrange equations are

$$\mathrm{e}^{\gamma t} mr\left({}_{t}D_{1}^{\beta}\theta\right)^{2} - \mathrm{e}^{\gamma t} mg\cos\theta + {}_{t}D_{1}^{\alpha}\left[m\left({}_{0}D_{t}^{\alpha} r\right)\mathrm{e}^{\gamma t}\right] + \lambda = 0 \tag{13}$$

and

$$\mathrm{e}^{\gamma t} mgr\sin\theta + {}_{0}D_{t}^{\beta}\left[mr^{2}\left({}_{t}D_{1}^{\beta}\theta\right)\mathrm{e}^{\gamma t}\right] = 0 \tag{14}$$

From Equations (13) and (14), we obtain the classical results if $\gamma \to 0$ and $\alpha, \beta = 1$. One can get the angular acceleration

$$\ddot{\theta} = \frac{g\sin\theta}{R} \tag{15}$$

and the Lagrange multiplier is given by

$$\lambda = mg\left(3\cos\theta - 2\right) \tag{16}$$

2) As a second model let us consider the following Lagrangian that describes the motion of a disk of mass m and radius R that is rolling down an inclined plane without slipping.

The Lagrangian of our problem is given by

$$L = \frac{1}{2}m\dot{y}^{2} + \frac{1}{4}mR^{2}\dot{\theta}^{2} + mgy\sin\varphi$$

In the presence of damping factor the Lagrangian becomes

$$L = \left[\frac{1}{2}m\dot{y}^{2} + \frac{1}{4}mR^{2}\dot{\theta}^{2} + mgy\sin\varphi\right]\mathrm{e}^{\gamma t} \tag{17}$$

where φ is the angle of the inline plane.

The holonomic constraint equation is

$$f\left(y,\theta\right) = y - R\theta = 0 \tag{18}$$

The Lagrangian in fractional form can be written as

$$L = \left[\frac{1}{2}m\left({}_{0}D_{t}^{\alpha} y\right)^{2} + \frac{1}{4}mR^{2}\left({}_{t}D_{1}^{\beta}\theta\right)^{2} + mgy\sin\varphi\right]\mathrm{e}^{\gamma t} \tag{19}$$

Using Equations (9), the corresponding Euler Lagrange equations are

$$\mathrm{e}^{\gamma t} mg\sin\varphi + {}_{t}D_{1}^{\alpha}\left[m\left({}_{0}D_{t}^{\alpha} y\right)\mathrm{e}^{\gamma t}\right] + \lambda = 0 \tag{20}$$

and

$$\frac{1}{2}mR^{2}\,{}_{0}D_{t}^{\beta}\left[\left({}_{t}D_{1}^{\beta}\theta\right)\mathrm{e}^{\gamma t}\right] - R\lambda = 0 \tag{21}$$

again, making use of Equations (20) and (21), if $\gamma \to 0$ and $\alpha, \beta = 1$. The angular accelerations take the following form

$$\ddot{\theta} = \frac{2}{3}\frac{g}{R}\sin\varphi \tag{22}$$

$$\ddot{y} = \frac{2}{3}g\sin\varphi \tag{23}$$

and the Lagrange multiplier

$$\lambda = \frac{-1}{3} mg \sin\varphi \tag{24}$$

which are in exact agreement with that obtained by classical method.

6. Conclusion

In this work, Euler Lagrange equations have been presented for irregular Lagrangian with holonomic constraints using fractional approach, the fractional Euler Lagrange equations for holonomic constrained systems were derived, and through this approach we have shown that, the fractional results are very similar to those for the classical results. In special cases, when $\gamma \to 0$ and α, β are equal unity only; the results of fractional calculus reduce to those obtained from classical calculus. Given the fact that many systems can be modeled more accurately using fractional derivative models, it is hoped that future research will continue in this area.

Conflicts of Interest

The authors declare no conflicts of interest regarding the publication of this paper.

References

[1] Atam, A.P. (1990) Introduction to Classical Mechanics. Allyn and Bacon, Needham Heights.

[2] Goldstein, H. (1980) Classical Mechanics. 2nd Edition, Addison-Wesley, Reading.

[3] Rabei, E.M. (1999) *Turkish Journal of Physics*, **23**, 1083. http://adsabs.harvard.edu/abs/2000NCimB.115.1159R

[4] Serhan, M., Abusini, M. and Rabei, E.M. (2009) *Journal of Theoretical Physics*, **48**, 2731. https://doi.org/10.1007/s10773-009-0063-5

[5] Miller, K.S. and Ross, B. (1993) An Introduction to the Fractional Integrals and Derivatives-Theory and Applications. John Willey and Sons, New York.

[6] Samko, S.G., Kilbas, A.A. and Marichev, O.I. (1993) Fractional Integrals and Derivatives: Theory and Applications. Gordon and Breach Science Publishers, Amsterdam.

[7] Gorenflo, R. and Mainardi, F. (1997) Fractional Calculus: Integral and Differential Equations of Fractional Orders, Fractals and Fractional Calculus in Continuums Mechanics. Springer Verlag, Wien and New York.

[8] Riewe, F. (1996) *Physical Review E*, **53**, 1890. https://doi.org/10.1103/PhysRevE.53.1890

[9] Riewe, F. (1997) *Physical Review E*, **55**, 3581. https://doi.org/10.1103/PhysRevE.55.3581

[10] Tarawneh, K.M., Rabei, E.M. and Ghassib, H.B. (2010) *Journal of Dynamics Systems and Theories*, **8**, 59-70. https://doi.org/10.1080/1726037X.2010.10698578

[11] Hilfer, R. (2000) Applications of Fractional Calculus in Physics. World Scientific Publishing Company, Singapore, New Jersey, London and Hong Kong. https://doi.org/10.1142/3779

[12] Malkawi, E., Rousan, A., Rabei, E. and Widyan, H. (2002) *Fractional Calculus and*

Applied Analysis, **5**, 155.

[13] Agrawal, O.P. (1999) An Analytical Scheme for Stochastic Dynamics Systems Containing Fractional Derivatives. *ASME Design Engineering Technical Conferences*, (7), 243-250.

[14] Hasan, E.H. (2016) *Applied Physics Research*, **8**, 60. https://doi.org/10.5539/apr.v8n3p60

[15] Jarab'ah, O. (2016) *Science International Lahore*, **28**, 3365. http://www.sci-int.com/Search?catid=71

[16] Agrawal, O.P. (2001) *Journal of Applied Mechanics*, **68**, 339. https://doi.org/10.1115/1.1352017

[17] Agrawal, O.P. (2002) *Journal of Mathematical Analysis and Applications*, **272**, 368. https://doi.org/10.1016/S0022-247X(02)00180-4

[18] Igor, M., Sokolove, J.K. and Blumen, A. (2002) *Physics Today*, American Institute of Physics S-0031-9228-0211-030-1.

[19] Jarab'ah, O., Nawafleh, K. and Ghassib, H.B. (2013) *European Scientific Journal,* **9**, 70. http://www.eujournal.org/index.php/esj/article/download/1946/1888

Journal of Modern Physics, 2018, 9, 1697-1711
http://www.scirp.org/journal/jmp
ISSN Online: 2153-120X
ISSN Print: 2153-1196

Unravelling the Quantum Maze

María Esther Burgos

Department of Physics, University of Los Andes, Mérida, Venezuela
Email: mburgos25@gmail.com

How to cite this paper: Burgos, M.E. (2018) Unravelling the Quantum Maze. *Journal of Modern Physics*, **9**, 1697-1711.
https://doi.org/10.4236/jmp.2018.98106

Received: June 15, 2018
Accepted: July 28, 2018
Published: July 31, 2018

Copyright © 2018 by author and Scientific Research Publishing Inc.
This work is licensed under the Creative Commons Attribution International License (CC BY 4.0).
http://creativecommons.org/licenses/by/4.0/
Open Access

Abstract

The restoration of philosophical realism as the basis of quantum mechanics is the main aim of the present study. A spontaneous projection approach to quantum theory previously formulated achieved this goal in cases where the Hamiltonian does not depend explicitly on time. After discussing the most relevant flaws of orthodox quantum mechanics, a formulation of the spontaneous projections approach in the general case is introduced. This approach yields experimental predictions which in general coincide with those of the orthodox version and overcomes its main flaws.

Keywords

Quantum Weirdness, Quantum Measurements, Spontaneous Quantum Jumps

1. Introduction

The foundations of quantum mechanics were laid in the period 1900-1926. Some of its achievements were introduced and discussed at the Fifth Solvay Congress (1927). Even though the theory seemed bizarre, it was accepted by the majority of participants at this meeting ([1], pp. 109-121). In 1930 Paul Dirac published the first formulation of quantum mechanics [2]. Two years later John von Neumann published *Mathematische Grundlagen der Quantenmechanik* [3]. Quantum mechanics was born.

These first versions of the theory share two characteristics: 1) The state vector $|\psi\rangle$ (wave function ψ) describes the state of an *individual system*. 2) They involve two laws of change of the system's state: Spontaneous (natural) processes, governed by the Schrödinger equation; and measurement processes, ruled by the projection postulate. This postulate gives an account for projections (collapses, reductions or quantum jumps) caused by measurements. Many other versions of quantum theory followed. Those where $|\psi\rangle$ describes the state of an individual

system *and* the projection postulate is included among its axioms are generally called standard, ordinary or orthodox quantum mechanics (OQM), sometimes referred to as the *Copenhagen Interpretation*.

From its inception OQM, and in particular its projection postulate, was the target of merciless criticism. Many scientists denounced what they considered its flaws. Among them, 1) it is incompatible with determinism; 2) it implies a kind of action-at-a-distance; and 3) it renounces philosophical realism. In addition, OQM presents a conflict with conservation laws which has been largely ignored [4] [5] [6] [7] [8] and carries the seeds of incoherence and contradictions [9] [10].

In 1931 Albert Einstein rightfully proclaimed: "the belief in an external world independent of the perceiving subject is the basis of all natural science" [11]. The restoration of philosophical realism as the basis of quantum mechanics is hence worth being pursued. The corresponding change of formalism should be realized, however, keeping as much as possible the experimental predictions of OQM, a theory imposingly successful [12].

This is the main aim of the spontaneous projection approach (SPA), a version of quantum theory previously formulated for cases where the Hamiltonian does not depend explicitly on time. It achieved this goal to a certain degree: it does not modify the Schrödinger equation and recovers a version of Born's postulate where no reference to measurements is made [13] [14] [15]. But the fact that it cannot account for cases where the Hamiltonian depends explicitly on time was a flaw which became increasingly apparent during our critical review of time dependent perturbation theory (TDPT) and forced us to conclude that *OQM weirdness is not limited to the measurement problem* [9] [10].

The version of SPA introduced in the present paper is more general than the previous one for it includes cases where the Hamiltonian depends explicitly on time. It keeps, however, the essential traits of SPA first version and yields, as far as we can see, the same experimental predictions obtained from OQM.

2. Philosophical Realism, Quantum Measurements and Scientific Problems

We uphold philosophical realism. We did in the first version of SPA and adopt the same epistemology as the basis of our present, more elaborated and general formulation of SPA. Our philosophical starting point can be stated as follows: 1) the things physics is about are supposed to exist, whether they are observed or not; 2) every scientific theory represents things through conceptual models; and 3) the adequacy of a theory (and corresponding models) to the things it refers to must take experimental results into account. In agreement with the philosophical point of view we adopt, "*there are no definitive theories or models in* (*factual*) *science*, because scientific knowledge is always of a hypothetical and never of a final nature" [16] [17]. More on this subject in ([18], p. 86).

According to Mario Bunge, "the main epistemological problem about quantum theory is whether it represents real (autonomously existing) things, and

therefore whether it is compatible with epistemological realism. The latter is the family of epistemologies which assume that a) the world exists independently of the knowing subject, and b) the task of science is to produce maximally true conceptual models of reality…" ([19], pp. 191-192). He adds: "The main pillar of the non-realist interpretations of quantum theory is a certain view on measurement and on the projection (reduction) of the state function that is involved in measurement… [Sometimes] 'measurement' is misused to denote *any interaction* of an entity with the environment… However, the worst misconception of measurement is its identification with the subjective experience of *taking cognizance* of the outcome of measurement" ([19], pp. 192-193). For instance, in von Neumann's view, a complete measurement involves the consciousness of the observer ([1], pp. 481-482) ([20], pp. 418-421). "By assuming that observation escapes the laws of physics… the orthodox view treats measurement as an unphysical process…" ([19], p. 200).

In his answer to the question "what can be observed?" Bell quotes Einstein saying "it is theory which decides what is 'observable'. I think he was right—'observation' is a complicated and theory-laden business. Then *that notion should not appear in the formulation of fundamental theory*" ([21], p. 208; emphases added). Bell exposes to ridicule the supposedly necessary intervention of an observer to cause projections when he asks: "What exactly qualifies some physical system to play the role of 'measurer'? Was the wave function of the world waiting to jump for thousands of millions of years until a single-celled living creature appeared? Or did it have to wait a little longer, for some better qualified system... with a PhD? If the theory is to apply to anything but highly idealized laboratory operations, are we not obliged to admit that more or less 'measurement-like' processes are going on all the time, more or less everywhere? Do we have jumping all the time?" ([21], p. 209).

Some authors dealing with the measurement problem avoid reference to the observer, but assume that measuring devices are macroscopic. Concerning this hypothesis Max Jammer highlights: "as long as a quantum mechanical one-body or many-body system does not interact with a macroscopic object, as long as its motion is described by the deterministic Schrödinger time-dependent equation, no events could be considered to take place in the system… If the whole physical universe were composed only of microphysical entities, as it should be according to the atomic theory, it would be a universe of evolving potentialities (time-dependent ψ -functions) but not of real events" ([1], p. 474).

A few authors have considered the possibility that projections may happen at the microscopic level, that they are not necessarily the result of the interaction between a quantum system and a macroscopic object [22] [23]. We agree. Collapses are a kind of spontaneous processes occurring in nature. In order to take place, they require neither the intervention of observers nor the interaction of a microscopic (quantum) system with a macroscopic (classical) measuring device [13]. Reductions may also happen in tiny isolated systems.

According to Bunge *"the question of reality has nothing to do with scientific problems such as whether all properties have sharp values, and whether all behavior is causal"* ([19], p. 192; emphases added). He adds: "unfortunately the two main controversies, those over realism and determinism (or hidden variables), have often been mixed up—and this by scientists of the stature of Einstein and de Broglie, Bohm and d'Espagnat. Yet the two issues are quite different: whereas the problem of realism is epistemological, that of hidden variables is ontological…" ([19], p. 168). We agree. But the list of scientific problems which have nothing to do with the question of reality ought to include at least three additional issues not mentioned by Bunge: the kind of action-at-a-distance pointed out by Einstein in the Fifth Solvay Congress ([1], p. 116); the validity of conservation laws [8]; and OQM incoherence and contradictions introduced through TDPT [9] [10]. Let us briefly consider these three issues.

2.1. OQM Implies a Kind of Action-at-a-Distance

The contradiction between the individual interpretation of the wave function ψ and the postulate of relativity was first pointed out by Einstein in the Fifth Solvay Congress. In the case of a particle that, after diffraction in a slit arrives at a certain point of a scintillation-screen, he pointed out that the theory of quanta can be considered from two different viewpoints: I) The de Broglie-Schrödinger waves do not represent one individual particle but rather an ensemble of particles distributed in space. Accordingly, the theory provides information not on an individual process but rather on an ensemble of them… II) Quantum mechanics is considered a complete theory of individual processes. Hence, "each particle moving toward the screen is described as a wave packet which, after diffraction, arrives at a certain point P on the screen, and $|\psi(r)|^2$ expresses the probability (probability density) that at a given moment one and the same particle shows its presence at *r*…" ([1], pp. 115-116).

Einstein objected to the second possibility on the following grounds: "If $|\psi|^2$ is interpreted according to II, then, as long as no localization has been effected, the particle must be considered as potentially present with almost constant probability over the whole area of the screen; however, *as soon as it is localized, a peculiar action-at-a-distance must be assumed to take place which prevents the continuously distributed wave in space from producing an effect at two places in the screen*… 'It seems to me,' Einstein continued, 'that this difficulty cannot be overcome unless the description of the process in terms of the Schrödinger wave is supplemented by some detailed specification of the localization of the particle during its propagation… If one works only with Schrödinger waves, *the [individual] interpretation of* $|\psi|^2$, I think, *contradicts the postulate of relativity*'." ([1], p. 116; emphases added).

As early as 1927 (during the Fifth Solvay Congress) Einstein proved that the idea that quantum mechanics is a complete theory of individual processes renders inescapable the notion of instantaneous quantum jumps [15] [24]. His conclusion is the result neither of a sophisticated experiment nor of a cumbersome

argument. It comes from logical reasoning applied to a very simple though experiment. To our knowledge, nobody has shown him wrong.

Eight years later, Einstein *et al.* published their celebrated article *Can Quantum-Mechanical Description of Physical Reality Be Considered Complete?* [25]. In this paper, best known as the EPR paradox, they referred to a system of two particles in an entangled state. In 1964 John Bell proved that no theory of nature that obeys local realism (and so satisfies certain inequalities) can reproduce all the predictions of quantum theory [26]. The contradiction between Bell's inequalities and quantum mechanics was submitted to experimental test by Stuart Freedman and John Clauser in 1972 [27]. Many other experiments followed this pioneer contribution. In general they yielded results in agreement with quantum mechanics. We have addressed the EPR paradox and related contributions in previous papers [15] [16] [24].

OQM implies what Einstein named "a spooky action-at-a-distance." There was a time when this notion was rejected by the majority of physicists. Nowadays it is accepted by almost everybody. This change of attitude can be retraced to the series of experiments aiming to test Bell's inequalities, in particular that performed by Hensen *et al.* in 2015 [28] and quantum teleportation obtained quite recently [29]. Let us add that, even though non-locality has been mostly associated to systems of particles in an entangled state, non-locality has been proven to also be present in experiments performed with individual particles. *This can be easily verified with experimental techniques accessible to everybody* [24].

The experiment performed by Hensen *et al.* has prompted Howard Wiseman to claim *Death by experiment for local realism* [30]. Local realism has died. Let us stress, however, that neither realism implies locality nor locality implies realism. These two concepts have been unduly mixed up. Non-locality really happens; the notion that every process is local lacks justification. This does not imply, however, renouncing realism.

2.2. OQM Is at Variance with Determinism and Conservation Laws

OQM conflicts determinism. To sample the reaction generated a century ago by such a conflict, let us recall that during the general debate of the Fifth Solvay Congress, its chairman Hendrick Lorentz objected the rejection of determinism, as proposed by the majority of speakers. He concluded with a desperate remark: *"Je pourrais toujours garder ma foi déterministe pour les phénomènes fondamentaux… Est-ce qu'un esprit plus profond ne pourrait pas se rendre compte des mouvements de ces électrons? Ne pourrait-on pas garder le déterminisme en faisant l'objet d'une croyance? Faut-il nécessairement exiger l'indéterminisme en principe?"* [I could always keep my faith in the determinism of fundamental phenomena… A more powerful mind could not give an account for the motion of these electrons? Determinism could be not kept as believe? Is it necessary to renounce determinism by principle?] ([1], p. 114).

The relation between determinism and conservation laws was first pointed out by Henry Poincaré. Concerning the law of conservation of energy, he declared: *"[cette loi] ne peut avoir qu'une signification, c'est qu'il y a une propriété commune à tous les possibles; mais dans l'hypothèse déterministe il n'y a qu'un seul possible et alors la loi n'a plus de sens. Dans l'hypothèse indéterministe, au contraire, elle en prendrait un…"* [this law cannot have more than one meaning, it is that there is a property shared by every possible; but in the determinist hypothesis there is a unique possible, then the law has no sense any more. In the indeterminist hypothesis, by contrast, it would have a sense…] ([31], p. 161).

This remark is pertinent: since OQM explicitly states that quantum measurements are processes not ruled by deterministic laws, one should suspect that conservation laws are not necessarily valid in such processes [15]. We have dealt with this subject for some time and concluded that, in the framework of OQM, conservation laws are strictly valid in spontaneous processes (ruled by a deterministic law); but have only a statistical sense in measurement processes (ruled by probability laws) [4] [5] [6] [7] [8]. Taking into account Poincaré's remark, this should not be surprising: in the first case conservation laws are theorems which can be derived from an axiom which is not valid in the second case.

2.3. OQM Is Incoherent and Contradictory

OQM marvelous success in the area of experimental predictions requires, in general, the application of TDPT. It is agreed that the method provided by TDPT must be used in all problems involving a consideration of time, including *spontaneous* time dependent processes; see for instance ([2], p. 168). This is the case of absorption and emission of light and of processes occurring in semiconductors. *To give an account for such spontaneous processes*, however, *TDPT requires the application of a law which is not valid in spontaneous processes*. This is a flagrant incoherence we have not noticed in the literature [9].

Let us sketch our argument: Consider a system with Hamiltonian ε which does not depend explicitly on time. It will be called the *unperturbed Hamiltonian* of the system. Its eigenvalue equations are

$$\varepsilon\left|\phi_n\right\rangle = E_n\left|\phi_n\right\rangle \tag{1}$$

where $E_n\left(n=1,2,\cdots\right)$ are the eigenvalues of ε and $\left|\phi_n\right\rangle$ the corresponding eigenstates. For simplicity we assume ε spectrum to be entirely discrete and non-degenerate; all the states referred to in this study are normalized.

Let us suppose that at initial time $t = 0$ the system is in the stationary state $\left|\phi_j\right\rangle$. A system in a stationary state will remain in that state forever: if for $t \geq 0$ the Hamiltonian were ε, the state vector at time t would be

$$\left|\psi\left(t\right)\right\rangle = \mathrm{e}^{-iE_jt/\hbar}\left|\psi\left(0\right)\right\rangle = \mathrm{e}^{-iE_jt/\hbar}\left|\phi_j\right\rangle \tag{2}$$

Nevertheless, TDPT establishes that by applying a *time dependent perturbation*, transitions between different eigenstates of ε can be induced and determines the probability corresponding to every particular transition ([2], pp.

172-173).

If at $t = 0$ a time dependent perturbation $\mathcal{W}(t)$ is applied, for $t \geq 0$ the total, *perturbed Hamiltonian* will be

$$\mathcal{K}(t) = \varepsilon + \mathcal{W}(t) \tag{3}$$

The perturbation $\mathcal{W}(t)$ causes the state $|\psi(0)\rangle$ to change. According to TDPT, the Schrödinger evolution leads the initial state $|\psi(0)\rangle = |\phi_j\rangle$ to the state

$$|\psi(t)\rangle = \mathcal{U}(t,0)|\psi(0)\rangle = \mathcal{U}(t,0)|\phi_j\rangle \tag{4}$$

where $\mathcal{U}(t,0)$ is, by definition, the evolution operator corresponding to the Hamiltonian $\mathcal{K}(t)$. The probability of a transition taking place from state $|\phi_j\rangle$ to state $|\phi_k\rangle$ during the time interval $(0,t)$ is

$$\mathcal{P}_{0,t}(E_j E_k) = \left|\langle\phi_k|\mathcal{U}(t,0)|\phi_j\rangle\right|^2 \tag{5}$$

TDPT deals with processes having two clearly different stages. In the first—during the time interval $(0,t)$—a Schrödinger evolution leads the system's state from $|\psi(0)\rangle$ to $|\psi(t)\rangle$ given by Equation (4) with certitude; *this change is automatic*. In the second an instantaneous projection of $|\psi(t)\rangle$ to a stationary state $|\phi_k\rangle$ is ruled by *probability laws* [9]. According to OQM, the Schrödinger equation governs every spontaneous process; Born's postulate and/or the projection postulate apply only when measurements are performed, resulting in a quantum jump. "*The fact that TDPT requires the application of postulates concerning measurements to give an account for processes supposedly spontaneous* (*v.g. absorption and emission of light*) *is at the very heart of OQM incoherence*" [9].

A further critical review of TDPT unveiled a contradiction reminiscent of Zeno's paradoxes concerning motion [10]. The argument can be sketched as follows.

Referring to a system in the initial state $|\psi(0)\rangle = |\phi_j\rangle$, Dirac asserts: "at time t the ket corresponding to the state in Schrodinger's picture will be $|\psi(t)\rangle = \mathcal{U}(t,0)|\phi_j\rangle$ according to Equation (4). The probability of the E_n's then having the values E_k is $\mathcal{P}_{0,t}(E_j E_k)$ given by Equation (5). For $k \neq j$, $\mathcal{P}_{0,t}(E_j E_k)$ is the probability of a transition taking place from state $|\phi_j\rangle$ to state $|\phi_k\rangle$ during the time interval $(0,t)$, while $\mathcal{P}_{0,t}(E_j E_j)$ is the probability of no transition taking place at all. *The sum of* $\mathcal{P}_{0,t}(E_j E_k)$ *for all k is, of course, unity*" ([2], p. 172-173; emphases added).

The transition taking place from state $|\phi_j\rangle$ to state $|\phi_k\rangle$ during the interval $(0,t)$ involves an instantaneous jump, *i.e.* a discontinuous change at time *t*. Since the sum of probabilities corresponding to all possible discontinuous changes at time *t* is unity, *no room is left for a non-null probability corresponding to a process continuous at this instant* [10]. Dirac does not impose any particular condition on the instant *t*. Hence the process cannot be continuous at any instant, the state vector at time *t* cannot be $|\psi(t)\rangle = \mathcal{U}(t,0)|\phi_j\rangle$ *and transitions between stationary states during the time interval* $(0,t)$ as referred to in TDPT

cannot take place; the system remains stuck to its initial stationary state. "Paraphrasing Zeno, these kinds of transitions between stationary states are nothing but illusions" [10].

Except Albert Messiah, no other author known to us imposes any particular condition on the interval $(0,t)$. By contrast, Messiah explicitly assumes that an instantaneous measurement is performed at time t ([32], p. 621). In absence of measurement, the Schrodinger evolution follows and the probability of a transition taking place from $|\phi_j\rangle$ to $|\phi_k\rangle$ during the interval $(0,t)$ is null. To avoid the "quantum Zeno contradiction" Messiah pays the price of assuming that an instantaneous measurement is performed every time a transition between two stationary states takes place [10].

Quantum weirdness has been traditionally associated with the *measurement problem*. To solve it, different authors have suggested several strategies. Among them are *statistical interpretation of quantum mechanics* [33], *many worlds interpretation* [34], *decoherence* [12] and *continuous spontaneous localization theory* [22]. We have addressed these and other proposed solutions to the measurement problem in previous papers [13] [14] [15]. Despite their value, these contributions do not solve the measurement problem, let alone OQM incoherence and the quantum Zeno contradiction just mentioned.

OQM weirdness is certainly not limited to the *measurement problem*. It is much more serious and justifies a radical revision of the theory [9] [10]. An overview of such a task follows.

3. The Spontaneous Projection Approach

Two kinds of processes irreducible to one another occur in nature: the strictly continuous and causal ones, which are governed by a deterministic law and those implying discontinuities, which are ruled by probability laws. This is the main hypothesis of SPA [13] [14] [15].

We explicitly discard the observer intervention and the interaction between the quantum system with a macroscopic measuring device as a source of projections. So the question is: *what could then induce quantum jumps?* SPA answers: *the tendency the system's state has to jump to the eigenstates of operators representing conserved quantities*. Let us establish this hypothesis in a formal way.

Let α be the self-adjoint operator representing the physical quantity $\boldsymbol{\alpha}$ referred to the physical system ζ. We assume that *the Hamiltonian*, denoted by ε, *does not depend explicitly on time t*. Then, if the operator α fulfills the conditions

$$\frac{\partial \alpha}{\partial t} = 0 \tag{6}$$

and

$$[\alpha, \varepsilon] = 0 \tag{7}$$

the system's state $|\psi(t)\rangle$ has the tendency to jump to the eigenstates of α. We have shown, however, that this tendency is seldom realized [13] [14] [15].

Let us highlight the difference between this hypothesis and that adopted in *continuous spontaneous localization theory*. In the last approach collapses *localize* the wave function [22]. As a result, steady states cannot be attained [35]. By contrast, according to SPA in most cases projections lead the system to stationary states [13].

3.1. The Statistical Sense of Conservation Laws

We have previously asserted that the conflict of OQM with conservation laws has been largely ignored [4] [5] [6] [7] [8]. Let us briefly review this issue.

The mean value of the physical quantity $\boldsymbol{\alpha}$ is by definition

$$\langle\alpha\rangle(t)=\langle\psi(t)|\alpha|\psi(t)\rangle \tag{8}$$

In Schrödinger evolutions the validity of Equations (6) and (7) ensures that $\langle\alpha\rangle(t)$ remains a constant in time for every state $|\psi(t)\rangle$ of ζ. It is said that α is a constant of the motion and that $\boldsymbol{\alpha}$ is conserved. By contrast, in processes ruled by another, different law from Schrödinger equation, the validity of Equations (6) and (7) does not guarantee that $\langle\alpha\rangle(t)$ remains a constant in time: if the process starts at t_0 and ends at t_f, it can result $\langle\alpha\rangle(t_f)\neq\langle\alpha\rangle(t_0)$ [8]. Hence the assertions "α is a constant of the motion" and "$\boldsymbol{\alpha}$ is conserved" are not justified. However, the *average* of the changes $\delta\langle\alpha\rangle=\langle\alpha\rangle(t_f)-\langle\alpha\rangle(t_0)$ obtained by repeating the process many times, converges to zero [8].

Let us consider a set of N orthonormal vectors: $|u_1\rangle,|u_2\rangle,\cdots|u_N\rangle$ ($\{N_u\}$ for short) such that the system's state at time t can be written

$$|\psi(t)\rangle=\sum_j c_j(t)|u_j\rangle \tag{9}$$

where $c_j(t)=\langle u_j|\psi(t)\rangle$ and $j=1,2,\cdots,N$. The mean value of $\boldsymbol{\alpha}$ at time t is $\langle\alpha\rangle(t)$ given by Equation (8); in particular, if $|\psi(t)\rangle=|u_j\rangle$ this mean value is $\langle u_j|\alpha|u_j\rangle$. Then,

Postulate I: If Equations (6) and (7) are satisfied, the validity of

$$\langle\psi(t)|\alpha|\psi(t)\rangle=\sum_j|c_j(t)|^2\langle u_j|\alpha|u_j\rangle \tag{10}$$

is a necessary condition for the state $|\psi(t)\rangle$ given by Equation (9) may collapse to the vectors of the set $\{N_u\}$, *i.e.* for jumps like $|\psi(t)\rangle\to|u_1\rangle$, or $|\psi(t)\rangle\to|u_2\rangle$, $\cdots$ or $|\psi(t)\rangle\to|u_N\rangle$, may occur [13] [14] [15].

Postulate I recovers Poincaré's assertion: In the indeterminist hypothesis, conservation laws have a *statistical sense* [13] [14] [15].

3.2. The Concept of Preferential Set

If there is *a unique set* of $N\geq 2$ orthonormal vectors: $|\varphi_1\rangle,|\varphi_2\rangle,\cdots,|\varphi_N\rangle$ ($\{N_\varphi\}$ for short) such that 1) the state of the physical system ζ at time t can be

written

$$\left|\psi(t)\right\rangle = \sum_j \gamma_j(t)\left|\varphi_j\right\rangle \tag{11}$$

where 2) $\gamma_j(t) = \left\langle\varphi_j\middle|\psi(t)\right\rangle \neq 0$ for every $j = 1, 2, \cdots, N$; 3) at least $(N-1)$ vectors belonging to the set $\{N_\varphi\}$ are eigenstates of the Hamiltonian ε (*i.e.* stationary states); and 4) *every* self-adjoint operator α for which Equations (6) and (7) are valid satisfies the relation

$$\left\langle\psi(t)\middle|\alpha\middle|\psi(t)\right\rangle = \sum_j \left|\gamma_j(t)\right|^2 \left\langle\varphi_j\middle|\alpha\middle|\varphi_j\right\rangle \tag{12}$$

we shall say that $\{N_\varphi\}$ *is the preferential set* of ζ in the state $\left|\psi(t)\right\rangle$ and the members of $\{N_\varphi\}$ will be called *its preferential states*.

Comment 1: According to this definition, a system ζ in the state $\left|\psi(t)\right\rangle$ can either have a unique preferential set including at least two preferential states or not have a preferential set at all.

Comment 2: The concept of *the* preferential set of ζ in the state $\left|\psi(t)\right\rangle$ adopted here coincides with that introduced in [10] and *is different* from our original concept of *a* preferential set of ζ in the state $\left|\psi(t)\right\rangle$ [13] [14]; the difference being that in the original definition the set $\{N_\varphi\}$ was not supposed to be unique, and condition (2) was not assumed to be valid.

Comment 3: Besides the concept of *a* preferential set of ζ in the state $\left|\psi(t)\right\rangle$, in previous papers we introduced the concepts of preferential basis and of maximal preferential set [13] [14]. Taking into account the present definition of *the* preferential set of ζ in the state $\left|\psi(t)\right\rangle$, the concepts of preferential basis and of maximal preferential set become superfluous. Hence they will not be referred to in the following.

We have so far assumed that the system's Hamiltonian ε does not depend explicitly on time. Let us now consider cases where the system's Hamiltonian depends explicitly on time. It can be written

$$\mathcal{H}(t) = \varepsilon + \mathcal{V}(t) \tag{13}$$

where $\mathcal{V}(t)$ includes every term of the Hamiltonian which depends explicitly on time. Then we state

Postulate II: The preferential set (and its preferential states) of ζ in the state $\left|\psi(t)\right\rangle$ does not depend on the term $\mathcal{V}(t)$.

Examples of the determination of preferential states have been given elsewhere [10] [13] [14] [15].

3.3. The Formalism of SPA

SPA includes the primitive (undefined) notions: *system*, *state*, *physical quantity* (or dynamical variable) and *probability*. Note that except the last one, these primitive concepts coincide with those adopted in Jammer's axiomatic presentation of the formalism of quantum mechanics due to von Neumann ([1], p. 5).

Postulate A: To every system ζ corresponds a Hilbert space $\mathcal{S}$ whose vectors

(state vectors, wave functions) $|\psi(t)\rangle$ completely describe the states of the system.

Postulate B: To every physical quantity $\boldsymbol{\alpha}$ corresponds uniquely a self-adjoint operator α acting in $\mathbb{S}$. It has associated the eigenvalue equations

$$\alpha\left|a_k^{\nu}\right\rangle = a_k\left|a_k^{\nu}\right\rangle \tag{14}$$

(ν is introduced in order to distinguish between the different eigenvectors that may correspond to one eigenvalue a_k), and the closure relation

$$\sum_{k,\nu}\left|a_k^{\nu}\right\rangle\left\langle a_k^{\nu}\right| = \mathbb{S} \tag{15}$$

is fulfilled (here $\mathbb{S}$ is the identity operator). If k or ν iscontinuous, the respective sum has to be replaced by an integral.

Comment I: The correspondence postulates A and B associate the primitive notions system, physical quantity and state of the system with mathematical entities. The same is true of von Neumann's quantum mechanics version reported in ([1], p. 5).

Postulate C: *Continuous processes* are governed by the Schrödinger equation

$$i\hbar\frac{\mathrm{d}}{\mathrm{d}t}|\psi(t)\rangle = \mathcal{H}(t)|\psi(t)\rangle \tag{16}$$

where $\mathcal{H}(t)$ is the Hamiltonian of the system, $\hbar$ Planck's constant divided by 2π and i the imaginary unity.

Comment II: The Schrödinger equation is a deterministic law. The solution $|\psi(t)\rangle$ of Equation (16) which corresponds to the initial condition $|\psi(0)\rangle$ is *unique*. The system's state evolves in correspondence with the equation

$$|\psi(t)\rangle = \mathcal{U}(t,0)|\psi(0)\rangle \tag{17}$$

where $\mathcal{U}(t,0)$ is the *evolution operator* corresponding to the Hamiltonian $\mathcal{H}(t)$; more details in ([2], p. 109) ([36], p. 137) ([37], p. 308) ([38], p. 41).

Postulate D: *A discontinuous change* of the system's state occurs if and only if $|\psi(t)\rangle$ jumps to one of its preferential states. If the system ζ in the state $|\psi(t)\rangle$ does not have preferential states, the process is necessarily continuous and governed by the Schrödinger equation.

Let us assume that the system ζ in the state $|\psi(t)\rangle$ has the preferential set $\{N_{\varphi}\}$. So we can write

$$|\psi(t)\rangle = \sum_k \gamma_k(t)|\varphi_k\rangle \tag{18}$$

where $k = 1, 2, \cdots, N$. Under these conditions we state

Postulate E: In the small time interval $(t, t+\mathrm{d}t)$ the state $|\psi(t)\rangle$ can undergo the following changes

$$|\psi(t)\rangle \to |\psi(t+\mathrm{d}t)\rangle = |\varphi_k\rangle \tag{19}$$

with probability

$$\mathrm{d}\mathcal{P}_k(t) = \left|\gamma_k(t)\right|^2 \frac{\mathrm{d}t}{\tau(t)} \tag{20}$$

or

$$\left|\psi(t)\right\rangle \to \left|\psi_{\mathcal{U}}(t+\mathrm{d}t)\right\rangle = \mathcal{U}(t+\mathrm{d}t,t)\left|\psi(t)\right\rangle \tag{21}$$

with probability

$$\mathrm{d}\mathcal{P}_{\mathcal{U}}(t) = 1 - \frac{\mathrm{d}t}{\tau(t)} \tag{22}$$

Here

$$\tau(t)\Delta\varepsilon(t) = \frac{\hbar}{2} \tag{23}$$

and

$$\left[\Delta\varepsilon(t)\right]^2 = \left\langle\psi(t)\right|\varepsilon^2\left|\psi(t)\right\rangle - \left[\left\langle\psi(t)\right|\varepsilon\left|\psi(t)\right\rangle\right]^2 \tag{24}$$

Comment III: Since $\left|\psi(t)\right\rangle$ is normalized, during a small time interval $(t,t+\mathrm{d}t)$ the system in the state $\left|\psi(t)\right\rangle$ has a probability $\frac{\mathrm{d}t}{\tau(t)}$ to jump to *one* of its *N preferential states*. If $\mathrm{d}t \ll \tau(t)$, the dominant process is the Schrödinger evolution [13].

Comment IV: In general the parameter τ defined by Equation (23) depends on time *t*. But if τ is a constant, the state $\left|\psi(t)\right\rangle$ may be considered as an unstable state that can decay to *one* of its *N* preferential states [13] [14] [15]. Let $\mathcal{P}_{\mathcal{U}}(t)$ be the probability that the system's state has not jumped to any preferential state in the interval $(0,t)$. The well-known exponential decay law is then obtained:

$$\mathcal{P}_{\mathcal{U}}(t) = \mathrm{e}^{-t/\tau} \tag{25}$$

4. Concluding Remarks

Let us conclude with the following remarks.

On the one hand SPA and OQM share several traits:

1) Both theories refer to individual systems, not to ensembles of systems similarly prepared.

2) SPA does not modify OQM in a substantial way: It keeps without changes the Schrödinger equation and recovers a version of Born's postulate where no reference to measurement is made. So, in general its experimental predictions coincide with those of OQM [13] [14] [15].

3) Both theories imply a "spooky action-at-a-distance" which is a kind of action-at-a-distance easily verifiable with techniques accessible to everybody [24]. Since this effect actually happens, there is no reason to discard theories which imply it.

4) In SPA as in OQM conservation laws fail in individual processes involving

quantum jumps.

On the other hand, SPA and OQM exhibit remarkable differences:

1) Unlike OQM, SPA is compatible with philosophical realism. In SPA there is no room for observers placed above the laws of nature.

2) The conspicuous notions of measurement and observation in OQM are alien to SPA. Differing from OQM, SPA fulfills Bell's requirement: *"[the notion of observation] should not appear in the formulation of fundamental theory"* ([21], p. 208; emphases added).

3) In OQM spontaneous processes are necessarily continuous and ruled by the Schrödinger equation, a deterministic law which yields automatic changes. By contrast, in SPA spontaneous processes are not necessarily continuous and ruled by the Schrödinger equation. If the system in the state $|\psi(t)\rangle$ has the preferential set $\{|\varphi_1\rangle, |\varphi_2\rangle, \cdots, |\varphi_N\rangle\}$, it can either follow a Schrödinger evolution or instantaneously jump to one of its preferential states.

4) In OQM reductions are ad-hoc, in SPA they are not surreptitious but explicitly included in the formalism.

5) OQM is incoherent and exhibits a contradiction reminiscent of Zeno's paradoxes of motion. SPA escapes these issues thanks to the hypothesis that collapses are natural processes [10].

In sum: while yielding experimental predictions which in general coincide with those of OQM, SPA enjoys a coherence which is absent from OQM and overcomes its main flaws.

Acknowledgements

We are indebted to Professor J. C. Centeno for many fruitful discussions. We thank Carlos Valero for his assistance with the transcription of the manuscript.

Conflicts of Interest

The authors declare no conflicts of interest regarding the publication of this paper.

References

[1] Jammer, M. (1974) The Philosophy of Quantum Mechanics. John Wiley & Sons, New York.

[2] Dirac, P.A.M. (1958) The Principles of Quantum Mechanics. Clarendon Press Oxford, Oxford.

[3] von Neumann, J. (1932) Mathematische Grundlagen der Quantenmechanik. Springer, Berlin.

[4] Burgos, M.E. (1994) *Physics Essays*, **7**, 69-71. https://doi.org/10.4006/1.3029115

[5] Burgos, M.E. (1997) *Speculations in Science and Technology*, **20**, 183-187.

[6] Burgos, M.E., Criscuolo, F.G. and Etter, T. (1999) *Speculations in Science and Technology*, **21**, 227-233. https://doi.org/10.1023/A:1005552504638

[7] Criscuolo, F.G. and Burgos, M.E. (2000) *Physics Essays*, **13**, 80-84. https://doi.org/10.4006/1.3025430

[8] Burgos, M.E. (2010) *JMP*, **1**, 137-142. https://doi.org/10.4236/jmp.2010.12019

[9] Burgos, M.E. (2016) *JMP*, **7**, 1449-1454. https://doi.org/10.4236/jmp.2016.712132

[10] Burgos, M.E. (2017) *JMP*, **8**, 1382-1397. https://doi.org/10.4236/jmp.2017.88087

[11] Einstein, A. (1931) James Clerk Maxwell: A Commemoration Volume. Cambridge University Press, Cambridge.

[12] Tegmar, M. and Wheeler, J. (2001) *Scientific American*, **284**, 68-75. https://doi.org/10.1038/scientificamerican0201-68

[13] Burgos, M.E. (1998) *Foundations of Physics*, **28**, 1323-1346. https://doi.org/10.1023/A:1018826910348

[14] Burgos, M.E. (2008) *Foundations of Physics*, **38**, 883-907. https://doi.org/10.1007/s10701-008-9213-5

[15] Burgos, M.E. (2015) The Measurement Problem in Quantum Mechanics Revisited. In: Pahlavani, M., Ed., *Selected Topics in Applications of Quantum Mechanics*, INTECH, Croatia, 137-173. http://dx.doi.org/10.5772/59209

[16] Burgos, M.E. (1983) *Kinam*, **5**, 277-284.

[17] Burgos, M.E. (1987) *Foundations of Physics*, **17**, 809-812. https://doi.org/10.1007/BF00733269

[18] Bunge, M. (1973) Philosophy of Physics. Reidel Publishing Company, Dordrecht, Boston, Lancaster.

[19] Bunge, M. (1985) Treatise on Basic Philosophy, Vol. 7, Philosophy of Science & Technology. D. Reidel Publishing Company, Dordrecht, Boston, Lancaster.

[20] von Neumann, J. (1955) Mathematical Foundations of Quantum Mechanics. Princeton University Press, Princeton.

[21] Bell, M., Gottfried, K. and Veltman, M. (2001) John S. Bell on the Foundations of Quantum Mechanics. Word Scientific, Singapore.

[22] Ghirardi, G.C., Rimini, A. and Weber, T. (1986) *Physical Review D*, **34**, 470-490. https://doi.org/10.1103/PhysRevD.34.470

[23] Primas H. (1990) The Measuremnet Process in the Individual Interpretation of Quantum Mechanics. In: Cini, M. and Lévy-Leblond, J.M., Eds., *Quantum Theory Without Reduction*, Adam Hilger, Bristol, 49-68.

[24] Burgos, M.E. (2015) *JMP*, **6**, 1663-1670. https://doi.org/10.4236/jmp.2015.611168

[25] Einstein, A., Podolsky, B. and Rosen, N. (1935) *Physical Review*, **47**, 777-780. https://doi.org/10.1103/PhysRev.47.777

[26] Bell, J.S. (1964) *Physics*, **1**, 195-200. https://doi.org/10.1103/PhysicsPhysiqueFizika.1.195

[27] Freedman, S.J. and Clauser, J.F. (1972) *Physical Review Letters*, **28**, 938-941. https://doi.org/10.1103/PhysRevLett.28.938

[28] Hensen, B., Bernien, H. and Dréau, A.E. (2015) *Nature*, **526**, 682-686. https://doi.org/10.1038/nature15759

[29] Wikipedia. The Free Encyclopedia: Quantum Teleportation. https://en.wikipedia.org/wiki/Quantum_teleportation

[30] Wiseman, H. (2015) *Nature*, **526**, 649-650. https://doi.org/10.1038/nature15631

[31] Poincaré, H. (1906) La science et l'hypothèse. Flammarion, Paris.

[32] Messiah, A. (1965) Mécanique Quantique. Dunod, Paris.

[33] Ballentine, L.E. (1970) *Reviews of Modern Physics*, **42**, 358-381.

https://doi.org/10.1103/RevModPhys.42.358

[34] Wikipedia. The Free Encyclopedia: Many-Worlds Interpretation. https://en.wikipedia.org/wiki/Many-worlds_interpretation

[35] Ballentine, L.E. (1991) *Physical Review A*, **43**, 9-12. https://doi.org/10.1103/PhysRevA.43.9

[36] Bes, D.R. (2004) Quantum Mechanics. Springer, Berlin. https://doi.org/10.1007/978-3-662-05384-3

[37] Cohen-Tannoudji, C., Diu, B. and Laloë, F. (1977) Quantum Mechanics. John Wiley & Sons, New York, London, Sydney, Toronto.

[38] Yndurain Muñoz, F.J. (2003) Mecánica Cuántica. Editorial Ariel S.A., Barcelona.

Call for Papers

Journal of Modern Physics

ISSN: 2153-1196 (Print) ISSN: 2153-120X (Online)
http://www.scirp.org/journal/jmp

Journal of Modern Physics **(JMP)** is an international journal dedicated to the latest advancement of modern physics. The goal of this journal is to provide a platform for scientists and academicians all over the world to promote, share, and discuss various new issues and developments in different areas of modern physics.

Editor-in-Chief

Prof. Yang-Hui He City University, UK

Executive Editor-in-Chief

Prof. Marko Markov Research International, Buffalo Office, USA

Subject Coverage

Journal of Modern Physics publishes original papers including but not limited to the following fields:

Biophysics and Medical Physics
Complex Systems Physics
Computational Physics
Condensed Matter Physics
Cosmology and Early Universe
Earth and Planetary Sciences
General Relativity
High Energy Astrophysics
High Energy/Accelerator Physics
Instrumentation and Measurement
Interdisciplinary Physics
Materials Sciences and Technology
Mathematical Physics
Mechanical Response of Solids and Structures
New Materials: Micro and Nano-Mechanics and Homogeneization
Non-Equilibrium Thermodynamics and Statistical Mechanics
Nuclear Science and Engineering
Optics
Physics of Nanostructures
Plasma Physics
Quantum Mechanical Developments
Quantum Theory
Relativistic Astrophysics
String Theory
Superconducting Physics
Theoretical High Energy Physics
Thermology

We are also interested in: 1) Short Reports—2-5 page papers where an author can either present an idea with theoretical background but has not yet completed the research needed for a complete paper or preliminary data; 2) Book Reviews—Comments and critiques.

Notes for Intending Authors

Submitted papers should not have been previously published nor be currently under consideration for publication elsewhere. Paper submission will be handled electronically through the website. All papers are refereed through a peer review process. For more details about the submissions, please access the website.

Website and E-Mail

http://www.scirp.org/journal/jmp **E-mail: jmp@scirp.org**

What is SCIRP?

Scientific Research Publishing (SCIRP) is one of the largest Open Access journal publishers. It is currently publishing more than 200 open access, online, peer-reviewed journals covering a wide range of academic disciplines. SCIRP serves the worldwide academic communities and contributes to the progress and application of science with its publication.

What is Open Access?

All original research papers published by SCIRP are made freely and permanently accessible online immediately upon publication. To be able to provide open access journals, SCIRP defrays operation costs from authors and subscription charges only for its printed version. Open access publishing allows an immediate, worldwide, barrier-free, open access to the full text of research papers, which is in the best interests of the scientific community.

- High visibility for maximum global exposure with open access publishing model
- Rigorous peer review of research papers
- Prompt faster publication with less cost
- Guaranteed targeted, multidisciplinary audience

Scientific Research Publishing

Website: http://www.scirp.org

Subscription: sub@scirp.org

Advertisement: service@scirp.org